

**FAILURE MODE AVOIDANCE AND
RELIABILITY ANALYSIS OF
LAUNCH VEHICLE AND SATELLITE SYSTEMS**

A THESIS

Submitted by

MURUGESAN V.

for the award of the degree

of

DOCTOR OF PHILOSOPHY



MECHANICAL ENGINEERING DIVISION

SCHOOL OF ENGINEERING

COCHIN UNIVERSITY OF SCIENCE AND TECHNOLOGY, KOCHI

JULY 2018

**FAILURE MODE AVOIDANCE AND
RELIABILITY ANALYSIS OF
LAUNCH VEHICLE AND SATELLITE SYSTEMS**

A THESIS

Submitted by

MURUGESAN V.

for the award of the degree

of

DOCTOR OF PHILOSOPHY



MECHANICAL ENGINEERING DIVISION

SCHOOL OF ENGINEERING

COCHIN UNIVERSITY OF SCIENCE AND TECHNOLOGY, KOCHI

JULY 2018

THESIS CERTIFICATE

This is to certify that the thesis entitled “**FAILURE MODE AVOIDANCE AND RELIABILITY ANALYSIS OF LAUNCH VEHICLE AND SATELLITE SYSTEMS**” submitted by **Mr. Murugesan V.** to the Cochin University of Science and Technology, Kochi for the award of the degree of Doctor of Philosophy is a bonafide record of the research work carried out by him under our supervision and guidance at the division of Mechanical Engineering, School of Engineering, Cochin University of Science and Technology. The contents of this thesis, in full or in parts, have not been submitted to any other University or Institute for the award of any degree or diploma.

We further certify that the corrections and modifications suggested by the audience during the pre-synopsis seminar and recommended by the Doctoral Committee of **Mr. Murugesan V.** are incorporated in the thesis.

Kochi-682022

Date: 09-07-2018

Dr. P.S.Sreejith, Research Guide
Dean, Faculty of Engineering
Cochin University of
Science and Technology, Kochi

Dr. A.K.Anilkumar, Joint Guide
Head, Applied Mathematics Division
Vikram Sarabhai Space Centre
Thiruvananthapuram

DECLARATION

I hereby declare that the work presented in the thesis entitled **“FAILURE MODE AVOIDANCE AND RELIABILITY ANALYSIS OF LAUNCH VEHICLE AND SATELLITE SYSTEMS”** is based on the original research work carried out by me under the supervision and guidance of Dr. P.S. Sreejith, Dean (Faculty of Engineering), Cochin University of Science and Technology, Kochi and Dr. A.K. Anilkumar, Head, Applied Mathematics Division, Vikram Sarabhai Space Centre, Thiruvananthapuram for the award of the degree of Doctor of Philosophy with Cochin University of Science and Technology. I further declare that the contents of this thesis, in full or in parts, have not been submitted to any other University or Institute for the award of any degree or diploma.

Kochi – 682022

Murugesan V.

Date: 09-07-2018

Research Scholar

ACKNOWLEDGEMENTS

I gratefully acknowledge my sincere gratitude and appreciation to Dr. P.S. Sreejith, Dean (Faculty of Engineering), Cochin University of Science and Technology (CUSAT) for his immense knowledge, professional guidance and constant support. His able guidance has helped me at all stages of research and writing of this thesis.

I would like to express my sincere gratitude to Dr. A.K. Anilkumar, Head, Applied Mathematics Division, Vikram Sarabhai Space Centre (VSSC) for his patience, motivation, insightful comments and personal guidance.

I would like to express my sincere gratitude to my Doctoral Committee member Dr. P.S. Tide, Professor, Mechanical Engineering Division (MED), School of Engineering (SOE), CUSAT for sharing his expertise during various phases of work. I am grateful to Dr. G. Madhu, former Principal, SOE, CUSAT and Dr. M.N. Vinodkumar, Professor, SOE, CUSAT for their encouragement and advice.

Thankful appreciation is extended to and Dr. B.S. Gireesh Kumaran Thambi, Head, MED, SOE, CUSAT and Dr. A.B. Bhasi, Professor, MED, SOE, CUSAT for their valuable suggestions during the pre-synopsis seminar.

I am thankful to my colleagues in VSSC, Dr. Shashi Bhushan Tiwari, Dr. S.V.S. Narayana Murty, Mr. V.J. Saji, Mr. P.K.Sreekumar, Mr. Prashanthan Arayil, Mr. P.B. Sundaresan, Mr. R. Hutton, Mr. B. Sundar, Mr. P. Anoop, Mr. P. Ramesh Narayanan, Mr. S.S. Maruthi, Mr. V. Sajiv, Mr. K. Kumar, Mr. P. Renish, Mr. M.Ranjith, Dr. O. Vijayan, Mr. S. Govind, Mr. M. Kodeeswaran, Mr. Geogi George, Mr. Mathew Varghese, Mr. V. Ramachandran, Mr. N. Raghu, Mr. Sushant K. Manwatkar, Mr. S. Sankar Narayan, Mr. V. Ramasubramanian, Dr. M.J. Chacko, Mr. V. Kishorenath, Dr. R. Rameshkumar, Dr. T.J. Apren, Mr. C.K. Krishnadasan, Mr. M. Premdas, Mr. M. Gopakumar, and Mr. P. Damodaran, for their valuable help in my thesis work.

I am indebted to the staff of VSSC library for their whole hearted support in my literature survey.

I would like to thank the engineers of ISDTF and CADD facilities of VSSC for facilitating the experimentation.

I would like to express my sincere thanks and gratitude to Dr. B. Valsa, Deputy Director, VSSC and Mr. S. Saratchandran, Group Director, VSSC for their encouragement and continual support during the course of this work.

I would like to thank Dr. K. Sivan, Chairman, ISRO and Mr. S. Somanath, Director, VSSC for their interest and support for reliability activities, and permitting me to publish the work in international journals and conferences.

I am thankful to my parents for their encouragement and support towards my academic achievements. I am thankful to my wife Mrs. M. Bama and son Mr. M. Aravind for their support and encouragement towards my successful completion of Ph.D research work.

ABSTRACT

Key words: Reliability; Pedigree system; Weighting factor; Failure mode avoidance; Design robustness; Environments

Reliability is considered as one of the most critical design parameters for launch vehicles and satellites. Considering the high complexity of the space systems, and the severe launch and space environments, the probability of a failure mode getting into the flight system and causing a failure is high. The failure mode could be design, process or workmanship related. These failure modes have to be avoided to make the systems reliable. Accordingly, research is done on the failure modes through analysis and experimentation on selected space systems, and the Failure Mode Avoidance (FMA) concepts have been developed and validated. Accurate assessment of reliability of space systems is essential to finalise the technological and commercial aspects of a mission. The reliability demonstration through a large number of flights and tests is the ideal way to assess the reliability of complex space systems. However, the test data is limited in the case of a newly developed space system, due to many reasons including the cost, efforts required and lack of time. An analytical model for the reliability analysis of space systems with limited data is developed and validated.

The analytical model for reliability analysis captures systematically the similarities with the pedigree systems and the uncertainties of the new design. The similarities between the new and pedigree systems are analysed by comparing them for a number of factors influencing system reliability, by assigning a weighting index. The model also accounts for uncertainties due to various aspects of the system like the complexity of the system, and the limitations in design analysis and verification. The model is validated with test data of existing propulsion systems. The model is found to be efficient and capable of giving an accurate reliability estimate for the complex space systems. Since the method focuses on systematic technical evaluation of the system, the method is more objective, accurate, and overcomes the disadvantage of other existing methods.

The research on the failure modes and their investigation through extensive analysis and experiments on space systems has brought out various FMA concepts and forms the basis for a general FMA strategy. The failure of a double row angular contact ball bearing in a

control actuation system has been investigated through analysis and experiments. The cause of the failure is identified as overloading of the bearing caused by a combination of factors. The high stress testing carried out on the control actuation systems has brought out the marginalities in the design leading to design corrections. The fatigue failure mode of the hydraulic plumbing of a control actuator subjected to high vibration response has been investigated. The reason for higher vibration response has been identified as pump pulsation frequency coinciding with the fourth mode of the plumbing. The failure of an AISI 304 stainless steel sleeve in the swaged joint of a flexible hose of the control actuator is investigated by micro structural analysis of the material. The typical space environment induced failures and their prevention by proper qualification is highlighted with spacecraft related failures. A failure observed in an umbilical shutter mechanism in the vibration environment is analysed and design made robust by simple design changes. Research is done on failure modes and the failure mechanisms of different seals in the critical pressure monitoring system of a solid rocket motor, by high stress experimentation with noise factors. The significance of failure mode effect analysis and high stress testing to evaluate and improve the reliability of the systems are brought out.

The high stress tests simulating noise factors to induce intentional failures, illustrated in the gas motor system and solid rocket motor pressure sealing joints, lead to detection of failure mechanisms in the early design phase leading to optimal design corrections. The fatigue analysis of plumbing brings out the significance of identification of the potential failure modes and detailed experimentation to assess them. The requirement of having comprehensive guidelines for the selection and acceptance of materials, and the precautions to be followed in their usage for space applications are brought out through detailed analysis of the flexible hose failure. The analysis of the bearing failure modes brings out the FMA concepts such as configuration control of the systems addressing finer design details, manufacturing process review, detailed process documents, and imparting adequate training to the operation team to avoid failures. The experimental results stress the need for enhancing the testability of systems at all phases of integration till launch.

Thus the research thesis develops FMA concepts for space systems based on analysis of failure modes and failure mechanisms of selected space systems. An efficient analytical model is formulated for accurate determination of reliability of space systems. Limitations and scope for future work are addressed.

TABLE OF CONTENTS

ACKNOWLEDGEMENTS	i
ABSTRACT	iii
TABLE OF CONTENTS	v
LIST OF FIGURES	x
LIST OF TABLES	xiv
ABBREVIATIONS	xvi
NOTATION.....	xviii
1 INTRODUCTION	1
1.1 Introduction.....	1
1.2 Motivation and objectives.....	3
1.3 Thesis outline.....	5
2 LITERATURE REVIEW	9
2.1 Introduction.....	9
2.2 Reliability analysis.....	10
2.2.1 Back ground of reliability studies	10
2.2.2 Measure of reliability for launch vehicles	11
2.2.3 Reliability statistics for launch vehicles	11
2.2.4 Methods for reliability analysis of launch vehicles	12
2.2.5 Accounting failures in reliability analysis	17
2.2.6 Accounting changes in reliability analysis	17
2.2.7 Reliability growth	18
2.3 Failure Mode Avoidance	19
2.3.1 Failure, terminology and perceptions	19
2.3.2 Causes of failure	20

2.3.3	FMA concepts	21
2.3.4	Methods to achieve FMA.....	22
3	ANALYTICAL MODEL FOR RELIABILITY ANALYSIS OF SYSTEMS WITH LIMITED TEST DATA	29
3.1	Introduction.....	29
3.2	Reliability of a new liquid propulsion stage	31
3.3	Methodology of reliability assessment - a new analytical model.....	34
3.3.1	Prerequisites for application of the method	35
3.3.2	Identification of SRIFs.....	36
3.3.3	Weighting index of SRIFs	37
3.3.4	Analytical model for the weighting score	38
3.3.5	Weighting factor for the test data of pedigree system	45
3.4	Analysis of liquid propulsion stages and model validation	46
3.4.1	Reliability estimation of L110 stage	46
3.4.2	Validation of the analytical model	49
3.5	An over view of the analytical model for reliability analysis.....	51
4	FAILURE MODE AVOIDANCE OF CONTROL ACTUATION SYSTEMS.....	54
4.1	Introduction.....	54
4.2	Failure mode avoidance of gas motor bearing.....	56
4.2.1	Bearing selection and failure observed	57
4.2.2	Failure analysis	62
4.2.3	Failure cause and corrective actions	74
4.3	Design robustness testing of gas motor	79
4.3.1	Tests with hot gas at 315 °C	84
4.3.2	Tests with hot gas at 390 °C	86
4.3.3	Wet steam test:	87

4.3.4	High speed test:.....	88
4.3.5	Vibration test.....	89
4.4	FMA concepts based on the failure mode investigations	90
4.4.1	Configuration control and quality control.....	90
4.4.2	Design robustness	91
4.4.3	System hardware certification.....	92
5	FAILURE PREVENTION IN PLUMBING AND HOSES OF HYDRAULIC CONTROL ACTUATION SYSTEMS	94
5.1	Introduction.....	94
5.2	Fatigue life estimation and reliability analysis of hydraulic plumbing	94
5.2.1	System description and the failure mode study	96
5.2.2	Experimentation.....	98
5.2.3	Dynamic vibration response analysis.....	101
5.2.4	Stress analysis of plumbing flared joint.....	104
5.2.5	Strength distribution of plumbing and joints	108
5.2.6	Fatigue analysis of plumbing joint.....	108
5.2.7	Fatigue analysis results and improvement in system design	116
5.3	Failure analysis of a flexible hose.....	118
5.3.1	System description	118
5.3.2	Qualification procedure for flexible hose system	119
5.3.3	Background to failure	120
5.3.4	Failure analysis procedure	121
5.3.5	Results of the failure analysis	122
5.3.6	Failure analysis findings	130
5.4	FMA concepts based on the failure mode assessment.....	133

6	AVOIDANCE OF ENVIRONMENT INDUCED FAILURES IN SPACE SYSTEMS.....	136
6.1	Introduction.....	136
6.2	Qualification of space systems for environments	136
6.3	FMA of umbilical shutter mechanism	138
6.3.1	System description and failure observed	139
6.3.2	Experimentation.....	142
6.3.3	Failure analysis and numerical results	144
6.3.4	Design solution and margin demonstration	148
6.4	FMA concepts based on the analysis of failures	150
7	FAILURE AVOIDANCE IN SOLID ROCKET MOTOR PRESSURE MONITORING JOINT SEALS	152
7.1	Introduction.....	152
7.2	System description and design options.....	153
7.3	FMEA Procedure	154
7.4	FMEA - Design option 1	155
7.4.1	Threaded interface with PTFE tape (J1)	159
7.4.2	Metal to metal seal (J2 and J4)	159
7.4.3	Welded joints (J3).....	161
7.4.4	Total RPN for design option 1	161
7.5	FMEA - Design option 2	162
7.5.1	Design considerations	162
7.5.2	Study of failure modes and mechanisms	163
7.5.3	Total RPN for design option 2.....	167
7.6	FMA concepts and reliability analysis based on investigation of failure modes	167
7.6.1	Comparison of RPN for the design options	168

7.6.2	Reliability analysis.....	170
7.6.3	Significance of quality control checks	171
8	SUMMARY AND FUTURE SCOPE OF WORK.....	173
APPENDIX A	Computation of weighting factor for L37.5 stage for reliability assessment of L110 stage.....	177
APPENDIX B	Computation of weighting factor for L40 stage for reliability assessment of L110 stage.....	179
APPENDIX C	Computation of weighting factor for L37.5 for reliability assessment of L40 stage	181
APPENDIX D	Rationale for ratings for RPN	183
APPENDIX E	Functionally critical dimensions and parameters.....	184
REFERENCES.....		185
LIST OF PAPERS BASED ON THESIS.....		198
CURRICULAM VITAE.....		200

LIST OF FIGURES

Figure 3.1	LRE in different launch vehicles and the stage designations	32
Figure 3.2	Schematic of liquid engine operation	33
Figure 3.3	Basic analytical models considered for the weighting score and compared with ref. model $w_s = w_i$	38
Figure 3.4	Sensitivity of k_{1j} on weighting score, $c_j = 1$, $k_{2j} = 1$	42
Figure 3.5	Sensitivity of k_{2j} on weighting score, $c_j = 1$, $k_{1j} = 1$	44
Figure 3.6	Analytical model selected for the analysis with $k_{1j} = 0.8$ and $k_{2j} = 1.2$ in comparison with ref. $w_s = w_i$ and basic model with $c_j = 1$, $k_{1j} = 1$ and $k_{2j} = 1$	48
Figure 4.1	Schematic of electro hydraulic Actuation System.....	54
Figure 4.2	Schematic of gas motor system	55
Figure 4.3	Double row angular contact ball bearing.....	58
Figure 4.4	Digital photograph of the bearing after failure	59
Figure 4.5	Bearing parts after failure	60
Figure 4.6	The inner race, cage and balls of first row.....	60
Figure 4.7	Comparison of the of the two rows of bearing	61
Figure 4.8	Magnified view of outer race.....	61
Figure 4.9	Dynamic seal of the bearing in good condition.....	62
Figure 4.10	Finite element model of the ball bearing	64
Figure 4.11	Validation of thermal model: computed and test measured temperatures.....	66
Figure 4.12	Bearing clamping load path and the preload	70
Figure 4.13	Finite element mesh of the rotor shaft and the $10\ \mu\text{m}$ step at the shaft shoulder.....	72
Figure 4.14	FE mesh of the inner race (a), and the zoomed view of the $0.8\ \text{mm} \times$ 45° chamfer (b)	72

Figure 4.15	Interface gap of 0.15 mm (a) caused by the interface mismatch of shaft shoulder radius R1 (b) and the $0.8 \times 45^\circ$ chamfer of the inner race (c).....	73
Figure 4.16	Misalignment of 9 arc minutes, caused by the inner race clamping with a 0.15 mm gap, due to the interface mismatch at the shaft shoulder.....	74
Figure 4.17	Ball path pattern on the inner race	75
Figure 4.18	Low speed dynamometer test set up	78
Figure 4.19	Thermal regulator	80
Figure 4.20	Functioning of control actuation system	81
Figure 4.21	The process diagram of the gas motor.....	84
Figure 4.22	Bearing polyamide cage material damage during hot test at 315°C	85
Figure 4.23	Temperature data and observation on regulator O-rings during 390°C test.....	86
Figure 4.24	Observation on regulator O-rings during 390°C test.....	87
Figure 4.25	Performance of control actuation system during wetness tests	88
Figure 4.26	Performance of actuator during high speed test	89
Figure 5.1	Delivery line plumbing in the actuator assembly	97
Figure 5.2	Delivery line plumbing flared tube coupling joint with ferrule.....	97
Figure 5.3	Test set up for measurement of pressure pulsation at pump outlet.....	99
Figure 5.4	Pressure pulsation measured at pump outlet.....	99
Figure 5.5	Test setup of the actuator simulating the engine inertia	100
Figure 5.6	Peak response measured on the delivery plumbing	101
Figure 5.7	FE model of the plumbing	102
Figure 5.8	Fourth mode shape of the plumbing at 709 Hz (Analytical)	103
Figure 5.9	Comparison of vibration response - experimental vs analytical.....	104
Figure 5.10	Axisymmetric FE model of the delivery plumbing and the stress analysis	105
Figure 5.11	The rms stress distribution upto 2000 Hz	106

Figure 5.12	Microstructure of the flared tube	108
Figure 5.13	Goodman diagram with minimum strength and maximum stress	110
Figure 5.14	Goodman diagram with mean strength and mean stress	113
Figure 5.15	Schematic showing the swaged joint interface of hose assembly	118
Figure 5.16	Digital photograph showing the swaging process	119
Figure 5.17	Digital photograph showing the cracking of sleeve in hydraulic pressure set up (a), and after removal from the set up (b)	121
Figure 5.18	Photograph showing the circumferential crack on the sleeve.	122
Figure 5.19	SEM image of circumferential micro cracks near to the primary crack.....	123
Figure 5.20	SEM image showing a full view of fracture surface covering complete thickness of the sleeve.	123
Figure 5.21	SEM image showing isolated large size silicate inclusion (indicated by white arrows) and uniformly distributed sulphide inclusion stringers (indicated by black arrows) at the location of crack path deviation.	124
Figure 5.22	High magnification SEM images showing isolated large size silicate stringer on the fracture surface	124
Figure 5.23	High magnification SEM images showing sulphide inclusion stringers on the fracture surface	125
Figure 5.24	SEM images on the fracture surface showing inter granular mode of cracking.....	125
Figure 5.25	Optical micrographs in un etched condition showing (a) sulphide and oxide inclusions, (b) silicate inclusion stringer, (c & d) silicate inclusion stringers at high magnification.....	126
Figure 5.26	Optical micrographs showing very long silicate inclusions.	126
Figure 5.27	Optical micrographs showing (a) two micro cracks of size 250 μm and 400 μm indicated by arrows near to the primary crack and silicate inclusion stringer along the crack path, (b) little deviation of the crack at the intersection with silicate inclusion stringer, (c) numerous small size micro cracks of size 20-30 μm at outer edge of the sleeve.	127

Figure 5.28	Optical micrographs showing deformed and elongated grains at the outer diameter up to approximately 400 μm inside and equiaxed grains at interior of the sleeve.	128
Figure 5.29	Optical micrographs showing (a) cracking along the grain boundaries, (b & c) chromium carbide precipitation at the grain boundaries.....	128
Figure 5.30	EDS spectrum showing chemical composition of silicate inclusion.	129
Figure 5.31	EDS spectrum showing chemical composition of sulphide inclusion.....	129
Figure 5.32	EDS spectrum showing chemical composition of chromium carbide precipitation at grain boundaries.	130
Figure 6.1	Payload cooling umbilical with shutter	139
Figure 6.2	Payload cooling umbilical and its vibration test configuration	140
Figure 6.3	Measured vibration response in the acoustic test and extrapolated spectrum for qualification and acceptance vibration tests.....	142
Figure 6.4	Vibration response on the shutter, original design	143
Figure 6.5	First mode of the shutter assembly from the modal analysis.....	145
Figure 6.6	Free body diagram of the rocker clamp mechanism, original design.....	147
Figure 6.7	Free body diagram of the rocker clamp mechanism, modified design.....	148
Figure 6.8	Vibration response on the shutter with modified design and the transmissibility comparison with original design	149
Figure 7.1	A typical launch vehicle with more number of solid rocket motors	153
Figure 7.2	Schematic of design option 1 for pressure monitoring.....	156
Figure 7.3	System block diagram for the design option1	157
Figure 7.4	Metal to metal sealing joint	160
Figure 7.5	Design option 2 with O-ring interface	162
Figure 7.6	Thermo gravimetric analysis data of fluorocarbon O-ring	164
Figure 7.7	Vibration test set up for pressure monitoring system	165

LIST OF TABLES

Table 3.1 Usage history of the LRE in different launch vehicles and the stage designations	31
Table 3.2 Rationale for classifying similarity and assigning weighting index.....	37
Table 3.3 Guideline for assigning value for tuning parameter of sensitivity, c_j	40
Table 3.4 Guideline for finalizing the tuning parameter of complexity, k_{1j}	41
Table 3.5 Guideline for finalising the tuning parameter of design verification, k_{2j}	43
Table 3.6 Computation of the weighting score	45
Table 3.7 Reliability estimation of L110 stage	49
Table 3.8 Reliability of L40 Stage based on similarity with L37.5 Stage.....	50
Table 4.1 Flight acceptance test matrix for the gas motor	58
Table 4.2 Bearing Design load requirement and the Capability	63
Table 4.3 Clearance at the bearing interfaces.....	67
Table 4.4 Critical components, failure modes, and environments of the gas motor	82
Table 4.5 Qualification test requirements of gas motor system	83
Table 4.6 Temperature measured at critical locations during hot gas test at 315°C	85
Table 5.1 FE analysis results for plumbing, with and without oil.....	103
Table 5.2 Dynamic stress for different load cases.....	107
Table 5.3 Strength properties at the flared portion, from sample test results.....	107
Table 5.4 Statistical distribution of stress and strength	111
Table 5.5 Results of Kolmogorov-Smirnov test for normal distribution at a level of significance of $\alpha = 0.05$	112
Table 5.6 Flight number of cycles and fatigue life at different stress levels.....	115
Table 5.7 Details of the qualification tests for the flexible hose assembly	120
Table 7.1 Critical interface joints of design option 1	156

Table 7.2 Failure Modes Effects Analysis (FMEA) of design option 1.....	158
Table 7.3 Overall RPN index for design option 1	161
Table 7.4 Failure modes effects analysis (FMEA) of design option 2.....	166
Table 7.5 Overall RPN index for design Option 2	167
Table 7.6 Summary of RPN values for design option 2 as compared to design option 1	169
Table 7.7 Reliability comparison of design options 1 & 2.....	170

ABBREVIATIONS

CAS	Control Actuation System
cdf	cumulative density function
CFD	Computational Fluid Dynamics
CFP	Critical Functional Parameter
DQT:	Design Qualification Testing
EDS	Energy Dispersive X-ray Spectroscope
FCD	Functionally Critical Dimension
FE	Finite Element
FEA	Finite Element Analysis
FMA	Failure Mode Avoidance
FMEA	Failure Modes Effects Analysis
FN	False Negative
FORM	First Order Reliability Method
FP	False Positive
FR	Frequency Response
FRACAS	Failure Reporting Analysis and Corrective Action System
FTA	Fault Tree Analysis
GG	Gas Generator
HALT	Highly Accelerated Life Testing
HASS	Highly Accelerated Stress Screening
ID	Inner Diameter
LRE	Liquid propellant Rocket Engine
LSD	Low Speed Dynamometer
MCS	Monte Carlo Simulation

MEOP:	Maximum Expected Operating Pressure
MFMA	Manufacturing Failure Mode Avoidance
OASPL:	Overall Acoustic Sound Pressure Level
OD	Outer Diameter
pdf	probability density function
PLF:	Pay Load Fairing
PSD:	Power Spectral Density
PTFE:	Poly Tetra Fluoro Ethylene
QA	Quality Assurance
QC	Quality Control
rms	root mean square
RPN:	Risk Priority Number
RSM	Response Surface Method
SEM	Scanning Electron Microscope
SRB	Solid Rocket Booster
SRE	Space capsule Recovery Experiment
SRIF	System Reliability Influencing Factor
SRM:	Solid Rocket Motor
SSME	Space Shuttle Main Engine
UDMH	Unsymmetrical Di Methyl Hydrazine
UH25	Mixture of 75% UDMH and 25% hydrazine hydrate
UTS	Ultimate Tensile Strength
WCA	Worst Case Analysis
YS	Yield Strength

NOTATION

C	Confidence level
c_j	Tuning parameter of sensitivity for j^{th} SRIF
CMD	Command
f	Frequency
FB	Feedback
f_n	Natural frequency
$f_s(s)$	Probability density function of strength
$f_s(s)$	Probability density function of stress
Grms	Root mean square acceleration response
k_{1j}	Tuning parameter of complexity for for j^{th} SRIF
k_{2j}	Tuning parameter of design verification for j^{th} SRIF
L110	Liquid propellant rocket stage with 110 tons of liquid propellant
L37.5	Liquid propellant rocket stage with 37.5 tons of liquid propellant
L40	Liquid propellant rocket stage with 40 tons of liquid propellant
LVA	Launch Vehicle A
LVB	Launch Vehicle B
LVC	Launch Vehicle C
MPa	Mega Pascal
n_e	Equivalent number of tests for new system, based on tests on pedigree system
p	Probability of success
P_h	System high pressure of control system
P_r	System regulated pressure of control system
q	Probability of failure
Q	Amplification at resonance
R	Reliability

S_a	Alternating stress
S_e	Endurance strength
S_{ea}	Equivalent fully reversible alternating stress
S_m	Mean stress
S_u	Ultimate tensile strength
TGM	Gas motor inlet gas temperature
U	Unreliability
wf	Weighting factor
w_{ij}	Weighting index for j^{th} SRIF
ws_j	Weighting score for j^{th} SRIF
μ_s :	Mean of strength
μ_s :	Mean of stress
ζ :	Critical damping ratio
σ :	Standard deviation
σ_s :	Standard deviation of stress
σ_s :	Standard deviation of strength

CHAPTER 1

INTRODUCTION

1.1 Introduction

Space based satellite systems give a large number of services to common man and are instrumental in improving the quality of life for the mankind. Launch vehicles lift the satellites from the earth surface and put them in the specified orbits depending on the application. The successful accomplishment of a launch vehicle mission requires a flawless performance of its various systems such as the structures, propulsion systems, ignition systems, separation systems, avionics, software, navigation, guidance and control systems. It is also essential to have an accurate analysis and assessment of the flight dynamics and aerodynamics. A thorough understanding of all the above complex disciplines and their interdependencies is a great challenge facing the space agencies, for design, development and operation of a launch vehicle without any failures (Suresh and Sivan, 2015).

Space missions are very expensive, and the objectives are to get maximum returns at a minimum cost (Wiley Larson and James Wertz, 2005). A failure of a launch vehicle or a satellite has many implications such as: non accomplishment of the mission objectives; delay in the committed programs; destruction of the launch pad and the surrounding structures; inconveniences or danger to the general public; and the loss of human life in case of manned missions. Also, the cost of failure increases manifolds with every subsequent phases of realisation of a system. In addition, finding the root cause and arriving at optimum solution become very difficult, when the failures occur at the later stages of the system realisation (Carlson, 2012).

Considering the challenges in avoiding the failures and the very high cost of failures, reliability is considered as one of the most important design drivers for aerospace systems (Zhaogfeng Huang, 2014). Reliability has two connotations, probabilistic and deterministic. In the probabilistic point of view, reliability is defined as the probability that a system will perform its function without failure for the specified mission duration under stated conditions of use (Kapur and Lamberson, 1977; Patrick

O’Conner and Andre Kleyner, 2012). It is concerned with quantitative assessment of the probability of successful functioning of the system, using the test data and application of statistics. The assessment is used to finalise the system configuration and design options, and to optimise the technological and commercial aspects of the mission (Bernard, 2004; Seth Guikema and Elisabeth Pate-Cornell, 2004). A large number of test data is essential, to get adequate confidence in such assessments. Therefore, reliability quantification for any newly developed space system is a challenging job considering that the systems at this stage do not have a large number of test data owing to many factors like technological considerations, cost and schedule.

In the deterministic sense, reliability is defined as the ability of a system to do its intended function under the specified environmental conditions for the specified period of time (Mohammed Modarres et al., 2010). It is concerned with the failure modes of the system and the ways to avoid them, and can be defined as ‘Failure Mode Avoidance (FMA)’. FMA is a design activity to make systems work under a wide range of harsh environments. This is a very important aspect, since there are lot of uncertainties regarding the flight environments when the launch vehicle is flown for the first time, in spite of the state of art design and analysis tools (Don Clausing and Daniel Frey, 2005). FMA also depends on the realisation of the flight systems as designed, with respect to quality of materials, manufacturing, inspection and testing. Many launch vehicle failures are reported in literature, as due to minor non-conformances or simple mistakes committed during the realisation process. Hence realising and integrating the system hardware as designed is an equally important prerequisite for the failure mode avoidance of a launch vehicle mission. The system design robustness and the realisation of systems with zero defects, together lead to FMA. However, achieving this is not an easy task and the history of spaceflight failures stress the need for evolving comprehensive FMA strategies for the launch vehicle systems.

Thus, there are two important challenges, in the reliability analysis of space systems namely probabilistic quantification of reliability and improving the reliability by failure mode avoidance.

1.2 Motivation and objectives

Failure mechanisms of passive mechanical systems are concerned with the stress exceeding the strength. Reliability of these systems is assessed by stress-strength interference theory, using the design margin and the dispersion in the stress values and strength properties (Mohammed Modarres et al., 2010, William Wessels. 2010). The failure mechanisms of the electrical devices are electrical over stresses, intrinsic failure mechanism of the device itself such as oxide layer that separate gate metal from semiconductor getting damaged because of poor manufacturing process or electrostatic discharge, and extrinsic failure mechanisms due to poor packaging and interconnections (Mohammed Modarres et al., 2010). The reliability of electrical devices is well addressed in literature and enough data is available for the reliability of the standard electrical parts in hand books (MIL HDBK 338 B, 1998). The avionics systems are tested at package level and system level for long durations to screen for extrinsic failure mechanisms. These test data can be used for the reliability assessment of the avionics. But for most of the other launch vehicle systems, with complex dynamic systems and ballistic performance requirements like propulsion systems, control actuation systems and pyro systems, reliability is assessed based on the number of tests carried out and the failure statistics. The binomial model is an elegant statistical tool for reliability analysis of such systems. However, reliability testing is very costly and difficult, as they require huge infrastructure, tests are destructive (as in the case of a solid rocket motor) and the number of tests to be done for meeting system reliability goal are very large (Kenan Bozkaya et al., 2009). So, only limited test data will be available for systems of a new launch vehicle. It poses a great challenge to the system engineer, to make a pragmatic assessment of quantitative reliability of such systems. The reliability assessed with the limited data would be inaccurate and in most cases would be too low. However, the system engineer based on the data, experience and knowledge with similar systems, intuitively knows that the reliability of the new system is higher. The Bayesian approach is generally used for reliability assessments in such situations. But the method has the problem of choosing a prior distribution based on subjective judgement (Patrick O’Conner and Andre Kleyner, 2012; Seth D. Guikema and Elisabeth Pate-Cornell, 2004). This necessitates the need for development of an

innovative methodology for the reliability analysis of space systems with limited test data.

A mechanical system failure occurs when the stress exceeds the strength, when the cumulative damage exceeds the endurance limit, or due to the performance degradation with time (Mohammed Modarres et al., 2010). Human errors also cause failures of systems. A system can be made reliable if these failure modes are avoided. However, in practice, the launch vehicle systems are very complex and multi disciplinary with large number of parts, systems and associated interfaces. The systems are also subjected to a number of environmental conditions. Therefore, it has a large number of failure modes and the associated inter dependent failure mechanisms that cannot be comprehensively assessed in the early design phase. Although, enough efforts are taken by the system designers through detailed failure mode and effect analysis (FMEA) studies, stringent design review mechanisms, and procedures for controlling the manufacturing processes, there could still be some un-contemplated failure modes present in the systems. Although, a few literatures (Dennis Moore and Willie Phelps, 2011; Don Clausing and Daniel Frey, 2005; Rosa Lynn Pinkus et al., 1997) address a few specific concepts and strategies for failure mode avoidance, their use is limited to certain specific cases and situations. Therefore, there is a need to develop comprehensive failure mode avoidance concepts and strategies for space systems.

In accordance with the above challenges identified in the area of reliability analysis and failure mode avoidance of launch vehicle and satellite systems, the main objectives covered in this thesis are as follows:

- To develop an efficient analytical model for the reliability analysis of launch vehicle systems with limited data, systematically capturing the similarities with the pedigree system and also uncertainties associated with the limited testing of the new system
- Developing comprehensive failure mode avoidance concepts, strategies and procedures for the launch vehicle systems through research on failure modes and failure mechanisms of space systems, with focus on making the design robust by widening the range of system operation environments in the design

phase, and ensuring zero defects during the manufacturing, assembly and testing phases.

1.3 Thesis outline

The primary objectives of the thesis are to formulate an efficient analytical model for the reliability analysis, and develop comprehensive failure mode avoidance strategies for launch vehicle and satellite systems. Chapter three presents a newly formulated analytical model for reliability analysis of launch vehicle systems with limited data, which considers effectively the confidence on the new system derived from the successful development and operation of similar systems, and also the uncertainties associated with limited testing of the new system.

Chapters four to seven presents the research carried out on the failure modes and failure mechanisms on selected space systems with different physics of failures, through analysis and experimentation. Based on this research and analysis, the failure mode avoidance concepts have been developed and validated. The problem specific solutions in each analysis address two aspects: making the design robust by widening the range of system operation environments; and evolving the quality systems and procedures for ensuring zero defect systems during the manufacturing, assembly and testing. The ensemble of the case-specific solutions evolved forms the basis for the general failure mode avoidance concepts and strategies for the space systems.

Chapter 2: Literature review

In this chapter, a detailed review of literature related to the failure mode avoidance and reliability analysis of launch vehicle and satellite systems is presented. A comprehensive survey of the technical papers, reports, and standards on the subject of reliability is made and the current methodologies available for the reliability analysis and their limitations are brought out, which leads to the challenging requirement of reliability analysis of new systems with limited data. The chapter also addresses literature on the failure modes and failure mechanisms of space systems, and the measures for mitigation of the failure modes. Thus, the literature review forms the basis for this research thesis on reliability analysis and failure mode avoidance of launch vehicle and satellite systems.

Chapter 3: Analytical model for reliability analysis with limited test data

In this chapter, a new analytical model is formulated and developed for the reliability assessment of space systems with limited test data, giving an accurate weighting for the tests and flight experiences with similar systems. The model captures systematically the quantum of similarities with the proven systems and also accounts for the uncertainties arising from various aspects of the new design. The method is illustrated and validated with test data of three liquid propellant rocket systems. The method has given a pragmatic reliability estimate of 0.978 for a new liquid propellant stage as compared to a reliability estimate of 0.877 with conventional method.

Chapter 4: Failure mode avoidance (FMA) of control actuation systems

In this chapter, the FMA concepts and strategies of launch vehicle systems are developed through two failure mode investigations on the gas motor subsystem of a launch vehicle Control Actuation Systems (CAS). The first analysis presents a detailed step by step investigation, through analysis and experimentation, on a failure observed in the double row angular contact ball bearing of the gas motor system during the qualification program. The analysis identified the root cause of the failure as overheating of the bearing, by a combination of errors in design, manufacturing, inspection and assembly processes. FMA concepts have been evolved to prevent identified failure mechanisms.

The second analysis of the chapter presents severe environmental stress testing carried out on the gas motor at system level. The environmental test levels and the value of noise factors have been deliberately increased, through high stress testing beyond the qualification levels. The tests included testing of the gas motor with hot air and with wet steam, high speed test, speed oscillation test, and vibration test. The tests induced failures of materials and parts, which has given a better understanding of the failure mechanisms, leading to design solutions that make the design robust. The experimentation also brought out the criticalities with respect to manufacturing and assembly processes, operating parameters, and system hardware dimensions. Based on the identified criticalities, comprehensive FMA concepts have been formulated in design, manufacture, inspection and testing phases of system realisation.

Chapter 5: Failure prevention in plumbing and hoses of hydraulic CAS

In this chapter, the failure modes of the hydraulic plumbing, flexible hoses and the associated joints used in the CAS, which can lead to catastrophic mission failures, are investigated through two systems of CAS. The fatigue analysis of a hydraulic plumbing and the metallurgical investigation of a failure in the flexible hose are presented. The identification of critical failure modes, detailed experimentation to understand the failure mechanisms, and finding optimal design solutions arising from the physics of failures emerge as the effective strategies for FMA. The study brings out the requirement of having comprehensive guidelines for the material selection, acceptance and usage to prevent failures.

Chapter 6: Avoidance of environment induced failures in space systems

This chapter presents the strategies for prevention of failures in the systems due to harsh launch and space environments during space flight. The typical space environment induced failures and their avoidance through proper qualification is highlighted with satellite and space capsule related failures. The second part of the chapter presents a detailed study of a failure observed on the payload cooling umbilical shutter system mounted on the cylindrical portion of the PayLoad Fairing (PLF) structure, during its design qualification vibration testing. The vibration responses on the shutter, the dynamic behaviour of the system, and the forces and moments on the mechanism are analysed, and the physics of failure due to the vibratory forces have been brought out. The design marginality is identified and the shutter locking mechanism reconfigured to achieve the desired level of robustness in the system. Based on the physics of failure, FMA concepts have been evolved including the design control requirement of flight acceptance testing the mechanisms for flight certification.

Chapter 7: Failure avoidance in solid rocket motor pressure monitoring joint seals

In this chapter, the failure modes and the failure mechanisms of different seals in the pressure monitoring system of Solid propellant Rocket Motors (SRMs) of launch vehicles are studied through investigative tests with deliberately induced variations in the design parameters and non conformances. Systematic analysis is carried out for

the designs through a Failure Mode Effect Analysis (FMEA), failure modes ranked in accordance with Risk Priority Number (RPN) and reliability of the joints worked out from the data. Design concerns are analyzed, alternate designs explored and innovative solutions evolved. The effectiveness of the final design is brought out quantitatively by reduced RPN ratings and quantum jump in the reliability. Critical design, process and quality control parameters have been identified and procedures to ensure them evolved as part of FMA.

Chapter 8: Summary and future scope of works

In the concluding chapter, the whole research work is summarised and salient features and importance of the work to launch vehicle and satellite systems are brought out. A new analytical model for reliability analysis has been formulated, developed and validated. The model has been found to give accurate results, is generic in nature and can be applied for reliability analysis of any system which has considerable similarities with a pedigree system. The failure mode avoidance concepts and strategies have been developed and validated for space systems through analysis and experimentation of failure modes and failure mechanisms of selected systems with different physics of failures.

A thought for the scope of further research in the area of reliability analysis and failure mode avoidance is presented.

CHAPTER 2

LITERATURE REVIEW

2.1 Introduction

Space based satellite systems provide a large number of services to mankind. Launch vehicles lift the satellites from the surface of the earth and inject into the specified orbit. Any launch vehicle along with state of art satellite costs hundreds of millions of dollars. Hence, a launch failure is one of the most expensive losses. Further, the time and effort required for identifying the failure cause, finding the technical solution to the problem, and putting the space program back on track are enormous.

Design and operation of a launch vehicle and satellite systems are unique for many reasons. The mission is considered to be a success only when the satellite is precisely injected into its designated orbit and the satellite performs satisfactorily for the specified operational life. A defect in any of the launch vehicle or satellite systems cannot be rectified, once the launch vehicle lifts off from the launch pad. Another feature of space systems is that they are multi disciplinary in nature, and all the systems have to function in a synchronised manner for the mission success (Suresh and Sivan, 2015). Predicting the flight environments are very difficult, even with the current state of art analytical tools and test methods. Identifying the failure mechanisms induced by these environments and their interactions are even more difficult. These uncertainties pose a great challenge for the designers to ensure a reliable performance of the launch vehicle systems. The implication of lower reliability is higher probability of space related failures, putting millions of dollars at risk (Shih Chang, 1996).

In view of the above challenges in ensuring the success of space missions and the cost of failures, reliability is considered as one of the most important design requirements for space systems (Zhaogfeng Huang, 2014).

Reliability is defined as the probability that an item can perform its intended function successfully for a specified period under stated conditions (MIL HDBK 338B, 1998; Mohammed Modarres et al., 2010). Reliability of an item at time t or cycle t can also

be defined as $R(t) = \Pr(T \geq T' | c_1, c_2, \dots)$, where T is the time or cycle to failure, T' is designated period of time or number of cycles of an item's operation like mission time, and c_1, c_2, \dots are the designated conditions (Mohammed Modarees et al., 2010).

A simple definition of reliability is absence of failures (Patrick O' Conner, 1995). Reliability can also be stated as Quality in time dimension (Levin and Kalal, 2003; Patrick O' Conner, 2000). Don Clausing and Daniel Frey (2005) define reliability in a deterministic sense as 'Failure Mode Avoidance'.

2.2 Reliability analysis

2.2.1 Back ground of reliability studies

Way back to the history, reliability was first used as a measure of safety of engineering systems in aeronautical industry. This led to the specification of acceptable accident rates, number of accidents per flying hour of an aircraft. The mathematical models of reliability have evolved during the Second World War, with the German mathematician Robert Lusser applying the simple product rule for a non-redundant system that gives system reliability as a function of the reliability of its components (Andrews, 2009). In the course of time, reliability had been used to finalise the warranty costs and the need for spares and test equipments of the products (Patrick O' Conner, 1995). In the case of launch vehicles, accurate determination of reliability is required for the selection of a launch vehicle for specific mission, and determination of the insurance coverage and premiums for a given launch (Seth Guikema and Elisabeth Pate-Cornell, 2004). The quantification of reliability is done by appropriate application of statistics to engineering (Bernard, 2004).

The reliability requirements of a launch vehicle have to be firmed up on the basis of the statistical data of operational launch vehicles that were developed with similar procedures. The requirements are then apportioned to the subsystems with appropriate allocation models (Federal Aviation Administration, 2005a). The system qualification plans have to be evolved to demonstrate the reliability goal of the systems. The complex systems of space missions have a large number of failure mechanisms related to errors due to design, process and workmanship. Failures are also caused by the random failures of components. All these aspects have to be considered while

assessing the reliability. This is a hard task, as reliability is not a simple concept like mass or power which can be measured by an instrument (Bernard, 2004; Patrick O'Conner, 2000). There is no single straight forward method to assess the reliability of systems, and the method to be applied depends on the system and available data.

2.2.2 Measure of reliability for launch vehicles

When a launch vehicle has sufficient test data, a simple measure of reliability is success rate, which is the ratio of the number of successful flights with the total number of flights (Lisa Bloomer, 2004). But this is a point estimate and can mislead in many situations. The system reliability estimated by this method, when all the tests are successful is 1. However, practically this is not correct, as no system is 100 percent reliable considering the variations in the technical parameters of the engineering systems and the flight environments (Lisa Bloomer, 2004). Hence, lower bound reliability at certain confidence level is more appropriate way of representing reliability of systems.

The binomial distribution is applicable to situations where the outcome a test is either a success or a failure. Such trials are called Bernoulli trials. The probability density function (pdf) for the binomial distribution presents the probability of obtaining 'x' number of successes in 'n' number of trials. The cumulative distribution function (cdf) of the binomial distribution gives the probability of obtaining a certain number say 'r' or fewer successes. Based on the binomial cdf, reliability can be computed as a function of number of tests, number of failures and confidence level (Huairui Guo et al., 2010; Patrick O'Connor and Andre Kleyner, 2012). When a system is tested 1000 times without any failure, the lower bound for the reliability obtained from the above method is 0.997 with 95% confidence. This means that there is a 95% chance that the reliability value is between 0.997 to 1. The guide to probability of failure analysis (Federal Aviation Administration, 2005b) for suggests using a confidence level of 60%, when assessing the reliability of expendable launch vehicles.

2.2.3 Reliability statistics for launch vehicles

The launch vehicle success rate of US launch vehicles up to the year 2000, shows that the reliability had been very low in the initial period of rocketry from 1957 to 1964. The reliability of launch vehicles improved with time substantially after 1964, and had

been in the range of 0.91 to 0.95. In the period from 1964 to 2000, 67% of the total failures were due to propulsion systems and half of the remaining 33% failures were attributed to guidance and control systems. The success rate of the solid propulsion systems was higher at 0.995 as compared to 0.981 for liquid propulsion systems. The reliability had grown over time and the data from 1991 to 2000 show that the reliability of solid stages was higher at 0.9971 and that of liquid stages was 0.9917 (Brian Allan, 2001). The reliability of the solid rocket motors (SRMs) have steadily increased over last 17 years, and the statistics indicate that from the year 1998 to 2015, more than 900 SRMs were tested without even a single failure with 100 percent success rate (Sojourner et al., 2015).

Interestingly, the study of US launch vehicles reliability from 1980 to 2015 (Susie Go et al., 2017) shows that about half of all the historical launch vehicle errors can be attributed to process error, one third due to design error and for most of the remaining failures, the cause was not known. However, the cumulative number of anomalies though had a constant slope, the unknown failures reached a plateau after 2002 as cause for most failures were localised due to better failure investigation and documentation. The liquid propulsion stages failure rates had been higher at 2.1×10^{-2} failures per liquid stage followed by solid stage failure rate of 1.2×10^{-2} failures per stage and 5.0×10^{-3} failures per staging event (Susie Go et al., 2017).

Michael Lutomski and Joel Garza (2012) had analysed the reliability of a human-rated Soyuz launch vehicle with two different approaches. When all the Soyuz rocket statistics up to the year 2011 is considered without considering their mission objectives or the launch vehicle system changes, the success rate was found to be 0.973 (24 failures in 896 launches, ie., 1 in 37). When only the human rated launches bound to space stations were considered for the analysis, the success rate was substantially higher at 0.987 (failure rate was considerably low with 3 failures in 235 launches, ie., 1 in 78).

2.2.4 Methods for reliability analysis of launch vehicles

Based on large amount of test data

The best method for accurate determination of reliability and its uncertainty is to test large number of systems at the highest level of integration until a failure occurs. The

method is suitable for example, when assessing the reliability of a launch vehicle with sufficient launch attempts like Soyuz launch vehicle. However, this method cannot be applied with a new launch vehicle with scarce data (Seth Guikema and Elisabeth Pate-Cornell, 2004). Testing of a large number of integrated systems is not a practical solution considering huge efforts and high costs involved. Also, subsystems of complex space systems are designed and realised by different teams and at different geographical locations (Jose Emmanuel et al., 2006; Yung Li Lee et al., 2015). When it comes to the human rated launch vehicle, the reliability requirement is a highly demanding value of 0.999 with 95% confidence (Lisa Bloomer, 2004). The demonstration of this level of reliability requires 2996 flight tests without any failure, and for the launch vehicle systems the requirement will be much higher. This shows that the binomial model will not suffice as a sole basis of reliability demonstration of systems like an integrated solid rocket motor (SRM) or a liquid propulsion stage. This poses a great challenge to system reliability engineers to develop new models to pragmatically assess the reliability of systems when the test data is limited.

Technical judgment of experts

When there is scarce test data at system level, the reliability is often assessed based on technical judgement by the experts in the field, considering the level of maturity of the systems, and experience with similar systems (Federal Aviation Administration, 2005b). But the method is very subjective and the reliability assessments vary widely depending on the position of the experts in the organisation. The reliability engineers who have analysed all the failure modes assess the reliability more conservatively while those in the development or management side may assess with higher level of confidence and give a more positive reliability figure. For example, the probability estimate of a catastrophic failure of Space Shuttle was found to vary from 1 in 100 to 1 in 100,000 (Richard Feynman, 1986, Rosa Lynn Pinkus et al., 1997). Considering that the method is vague and person dependent, the method is not preferred.

Prediction based on subsystem data

An alternate method is to make use of the component or subsystem reliability data and assess the system level reliability with the aid of system reliability block diagrams and fault tree analysis. Reliability assessed using this method is known as the predicted reliability. Reliability prediction is a bottom-up approach, based on the component

reliabilities from the standards and handbooks, and gives the design reliability (Lisa Bloomer, 2004; Sergio Guarro, 2015). Such assessments are made using the failure rate data base provided in MIL-HDBK-217 F (1998) for electronic equipments, and NPRD-1995 (1995) and NSWC-2010 (2010) for non electronic parts (Vintr, 2007). IEEE standard 1413-2003 presents a frame work for the prediction of reliability for electronic parts, but can be applied to other systems also when followed meticulously, gives consistent predictions. It also results in complete documentation of the reliability prediction process that gives a more vivid picture of the system reliability (John Elerath and Micheal Pecht, 2012).

The disadvantage of reliability prediction is that it is solely based on design and the selection of parts and does not account for the process related failures which could be caused by manufacturing, assembly and testing. The large gap between the actual reliability and the predicted reliability is explained by the data on the cause of US launch vehicle failures. For example, Titan IV launch vehicle had a success rate of only 0.875 as compared to the published design reliability value of 0.9975. Most launch failures were due to errors caused by design, workmanship and process (Sergio Guarro, 2015). The study of US launch vehicle failures from 1985 (Susie Go et al., 2017) has brought out that 48% of the total failures were due to process errors and 35% had been due to the design errors. The predicted reliability capture only random failures of parts and components based on their failure rates. Even the design errors which have been missed by the scrutiny of design reviews and the test program cannot be accounted by reliability prediction. Therefore, reliability demonstrated through tests is a more practical and useful measure when sufficient system level test data is available, while the predicted reliability assumes significance in the initial design phase when system level test data are not available (Lisa Bloomer, 2004).

Margin based approach

In the design of structures, a deterministic approach can be adopted by estimating the absolute upper bound for the load and lower bound for the strength and separating them by a very high safety factor. However, such an approach results in either an overdesign, or a failure because of not statistically accounting the dispersions in the load and properties of material. This necessitated the use of probabilistic methods. With the increasing computational capability, many probabilistic methods have been

developed such as Monte Carlo Simulation method (MCS), First Order Reliability Method (FORM), and Response Surface Method (RSM) (Bin Wu, 2013). The MCS method performs a repetitive simulation process through random sampling to simulate a large number of experiments and observe the results (Andrews, 2009; Bin Wu, 2013). The experiments have to be conducted on the system performance, with randomly sampled event times from the appropriate distributions. In the FORM method, if the strength 'S' and load 's' are variables following normal distribution, the margin '(S-s)' is also a normally distributed variable denoted by 'M'. The mean and standard deviation of M can be determined from the mean and standard deviation of the variables S and s, and the probability of failure is the probability that M is less than zero. When the system is working under harsh environments with higher dispersions, the load and strength distributions will have significant overlap (Moss and Andrews, 1996). The RSM brings out an analytical model for the output or the response as a function of several inputs (independent variables). Such a relationship expressed as a first order or second order polynomial function is called a response surface model. The model can then be used to estimate the reliability using the FORM or MCS methods (Bin Wu, 2013).

Thiokol Corporation developed a method known as statistical approach for engineering reliability (SAFER). The method is based on the stress-strength interference theory to estimate the one sided lower bound of reliability at the prescribed confidence level for a composite motor case. The method balances the principles of sound engineering design, understanding failure modes, failure mechanisms, process control and material characterisation (James Ekstrom and Alan Allred, 1991). This method can be successfully applied to the rocket motor case as a structure, but cannot be applied to the solid rocket motor as a whole system that comprises of many subsystems like propellant system, insulation, inhibition, nozzle and their interfaces which have to function together as an entity to give the required ballistic performance.

Ideally, all the flight systems manufactured as per a design drawing shall be identical with respect to all the engineering parameters such as its material properties and geometrical features. The environments shall be well controlled within a narrow band. However, in practice the engineering parameters of a system as well as the environments encountered by them have inherent variations. The part stress exceeding

the strength could cause a mechanical system failure. An electrical parameter going beyond specifications due to higher temperature variation can cause an electronic system failure. These variations are mathematically modelled using different distributions like Gaussian, lognormal and Weibull, but they are only approximations to the true variations. The tail regions of these distributions like high stresses, low strengths, low and high temperatures etc., are the areas to be studied in detail for the reliability assessment (Patrick O' Conner, 2000). The variations shall be minimised to get higher reliability. When the process is controlled to get $\pm 3\sigma$ of the variable's distribution within the acceptable bounds, then 2.7 components out of 1000 will fail. This level of reliability is not acceptable in many instances. The $\pm 6\sigma$ sigma quality results in a rejection rate of 1 in 1e 9 rejections (Patrick O' Conner, 2000).

Bayesian Approach

The pragmatic reliability analysis of launch vehicles with limited test data is a very challenging task. One of the most common methods used in such situations is the Bayesian approach based on the subjective view of probability. The prior probability distribution of the reliability (future success rate) of the launch vehicle is subjectively assessed based on the information and knowledge about the launch vehicle before any of the launch attempt. The prior distribution is finalised on the basis of expert assessment or from the performance of similar system. If there is no opinion on the reliability of the system, it can be reflected by a uniform distribution over [0, 1]. When new evidence or data is available, an update is obtained using the mathematical formulation of Bayes theorem. The updated probability distribution represents the reliability estimate of the launch vehicle posterior to seeing the data and hence is called posterior distribution (Fox, 1966; Huairui Guo et al., 2010; Michael Stamatelatos and Homayoon Dezfuli, 2011; Seth Guikema and Elisabeth Pate-Cornell, 2004). Different reliability estimates can be obtained from the posterior reliability distribution such as the mean value estimate and the percentile values that gives the reliability estimate at any desired confidence level. Thus, the method has the advantage of giving not only an estimate of the reliability but also an estimate of the uncertainty in the reliability assessed (Michael et al., 2008; Sergio Guarro, 2013; Seth Guikema and Elisabeth Pate-Cornell, 2004). However, the method is considered subjectivist, considering the subjective judgment associated with the determination of the prior distribution (Mohammed Modarres et al., 2010). The Bayesian method is

also very difficult to comprehend with, and the results are influenced by the subjective prior distributions (Huairui Guo et al., 2010).

Integrated stage reliability

When the launch vehicle has lesser number of flight data, an alternate method for reliability analysis based on the individual stage reliability is employed. This is a practical solution, as in many instances, in new vehicle the propulsion stages could be with pedigree, flown in earlier launch vehicles. Therefore, it is prudent in such instances to assess the reliability of the launch vehicle as the composite reliability of all the stages. The reliability computed on the basis of ground and flight testing of integrated propulsion stage can also be considered as demonstrated reliability, as it is based on performance of the stage along with its avionics and control systems. The demonstrated reliability is more useful as it comprises of both the design and the process reliabilities (Sergio Guarro, 2015).

2.2.5 Accounting failures in reliability analysis

The in-flight failure of a launch vehicle is taken very seriously by the space agencies and the root cause of failure in most cases are identified by in depth analysis of flight data, and recreating the failure by simulations and testing. On the basis of identified failure modes, design and process improvements are made to avoid the failures. When such actions are taken to mitigate the failure modes, failure is discounted by a factor in the reliability analysis. The factor depends on the certainty with which the root cause is identified and the confidence level in the corrective actions. With proper justification, the failure can be discounted by 67% or more, but never by 100% as the improvements made could introduce additional failure modes (Michael Lutomski and Joel Garza, 2011).

2.2.6 Accounting changes in reliability analysis

The objective of a reliability program is to lower the risk for the mission and maximize the probability of success. This can be achieved through focused efforts to avoid significant launch vehicle issues that could lead to a mission failure and satellite problems that could degrade mission capability (John Buzzatto, 2015). The mission risk assessment is of paramount interest for human spaceflight programs (Hamlin et al., 2013). The risk is the probability that a system will fail and so is closely related to

reliability (Lisa Bloomer, 2004). The design, process and operational changes have significant influence in the risk associated with the specific mission. The risk assessment of the Space Shuttle was made with the knowledge gained over 30 years of its operation. The risk did not decrease monotonically in accordance with the conventional reliability growth pattern, but showed a step like pattern with both increase and decrease of risks at different stages. The decrease in the risk is due to the redesigns, and changes in the quality procedures that were enforced after Challenger and Columbia accidents. The increase in risks is attributed to the changes made to improve the performance of systems at the cost of safety factors, like in the case of increasing the power level of the space shuttle main engine (SSME) compromising the safety margins (Hamlin et al., 2013).

2.2.7 Reliability growth

The system design gets matured with time through iterative design process, by the corrective actions implemented to solve the problems and marginalities observed during the extensive ground and flight testing. Hence, initially the reliability is low and improves with operational life of the launch vehicles. The reliability grows asymptotically and reaches a plateau (Elisabeth et al., 2010). When a failure occurs there is a sharp drop in the reliability, necessitating design corrections. After the right corrections are made, the reliability improves. When sufficient data is available the drop in reliability due to a failure becomes lesser. After a large number of launches the demonstrated reliability reflects the true reliability of the system. The reliability growth is possible, when the design and process changes made to mitigate failures do not introduce additional failure modes. Since the space agencies view failures critically and carry out a comprehensive analysis of the failure with due impact analysis of the corrective actions, such a possibility is remote. However, the changes in launch vehicle systems for improving the payload capability, increasing the performance level of systems, changing mission requirements or the technology obsolescence often introduce new failure modes.

The statistical data of SOYUZ launch vehicle clearly shows that the human rated missions had significantly higher reliability as compared to the reliability computed based on all the SOYUZ vehicles. This proves that with the special design,

manufacturing and quality procedures, it is possible to avoid failures (Michael Lutomski and Joel Garza, 2012)

2.3 Failure Mode Avoidance

2.3.1 Failure, terminology and perceptions

Failure can be defined as the inability of a component, machine, or process to function properly. The failure can be a functional failure where the component, machine, or process fails in totality and stops functioning as in the case of a bearing failure, or a failure to deliver the expected performance such as a deviation in the flow through a valve (Howard Boyer, 1975).

The way in which a failure gets revealed in a system is known as failure mode. It could be a leak in the hydraulic hose or a crack in a structural assembly. Every failure has a cause and effect. The failure cause or the failure mechanism reflects the cause of a particular failure mode, and the failure stresses activate these failure mechanisms (Ahsan Qamar et al., 2017; Vincent Lalli, 1994). The failure modes have become unavoidable consequence of product development processes, with the increasing complexity of the products which are designed and manufactured by different organisations at different times and places. As the identification of these failure modes and fixing them are delayed to the subsequent phase of the product life cycle, the cost shoots up by 10 times (Saxena et al., 2005; Carlson, 2012).

The perception of a failure can differ among individuals, and over time. It is subjective in many instances to assess whether a leaking hydraulic hose is a failure or not. It has to be assessed based on the application. The damage to O-ring seals in the solid rocket booster (SRB) joints of Space Shuttles was not considered a failure until the space shuttle STS-51L Challenger accident took place (Patrick O' Conner, 2000). The launch management team cleared for launching challenger at 3.3°C as compared to the temperature dependent launch criteria of minimum 11.7°C. This resulted in the loss of resilience properties of the O-rings in the segment joints of SRB, causing the leak of the combustion gases which struck the aft strut joints and the external tank. The flame from the joint breached through the bottom segment of the external tank causing liquid hydrogen to leak, and also burned through the two aft struts connecting the solid motor to external tank. This caused the SRB to tilt with top strut as pivot and

the booster fore end collided with the bottom of liquid oxygen tank causing its structural failure. The burning of leaking hydrogen and oxygen resulted in an explosion (Shih Chang, 1996; Ben Evans, 2007; Susie Go, 2017). The O-ring damage which was not considered a failure till then, became one of the most discussed topics under the heading of failures after the Challenger accident.

2.3.2 Causes of failure

Failures could be caused by many aspects of design, material selection, manufacturing, assembly, or service conditions (Howard Boyer, 1975). Defects or faults in the parts could be a cause of failure, but it need not always cause a failure (Patrick O' Conner, 2000). If a part fails because of the fault in the part, it is a primary failure. If a part fails due to failure of another system failure or any other reason it is a secondary failure. For example, a transistor failure due to a fault in it is a primary failure whereas its failure due to an over stress caused by power supply voltage rise is a secondary failure. Secondary failures are sometimes more important than even the primary failures and has to be given special attention. Also, all failures need not be the result of a fault. The O-ring assembled in the segment joints of Solid Rocket Booster (SRB) of the Space Shuttle Challenger was not faulty, but the O-ring failed in the service environments and resulted in a catastrophic failure (Patrick O' Conner, 2000). Assembly, testing, in-service operations, poor storage or improper maintenance could be a cause for the failure. Failure avoidance is therefore also concerned with employing the right people, skills, teams and resources for every activity. From this, it is evident that the failure avoidance is the job not limited to quality and reliability professionals alone, but is the responsibility and duty of all the concerned stake holders like designers, manufacturers, and assembly, test and maintenance engineers (Patrick O' Conner, 2000).

The systems often fail due to lack of comprehensive technical knowhow and considerations related to cost and schedules (Mohammed Modarres et al., 2010). When systems fail, it gives very valuable information about the system and opportunity to learn and understand more about the system functioning and their failure modes. Failure analysis helps in identifying the root cause and the corrective action ensures that the cause is addressed (Vincent Lalli, 1994). However, prevention of failures in the early design stage through a proactive approach is more effective

than reacting to failures. The designers should have the complete understanding of the failure mechanism which can be caused by incorrect design, manufacturing or an external environment to design a reliable system (Daniele Regazzoni and Davide Russo, 2010; Vincent Lalli, 1994).

Launch vehicle failures are primarily attributed to the problems associated with propulsion, structural, avionics, separation and electrical systems (Shi Chang, 1996). In order to make the system reliable, failures have to be avoided and this requires comprehensive understanding of the way its parts can fail and the type and magnitude of stresses that cause such failures. In this perspective, reliability can be defined as the probability that the critical failure modes of a system will not occur during a specified period of time and under specified conditions when used in a manner and for the purpose intended. The words ‘critical failure modes will not occur’ replaces the words ‘system functions successfully’ in the original definition (Vincent Lalli, 1994). When the potential failure modes and failure mechanisms are removed from the system, significant reliability growth takes place (Elisabeth et al., 2015). This leads to the Don Clausing’s pragmatic definition “Reliability is Failure Mode Avoidance (FMA)”.

2.3.3 FMA concepts

A system design has to be robust for it to be reliable. The system shall have the ability to function satisfactorily under the full range of conditions experienced in the field. (Don Clausing and Daniel Frey, 2005). Reliability is dependent on two important features related to the design and manufacturing: (i) Design robustness, the ability of the system to function throughout its life cycle under wide range of harsh operating conditions; and (ii) Mistake proofing, which avoids faults in design, manufacture, assembly and testing. Incorporating the robustness in the design is the major challenge for effective systems engineering. Reliability can be conceived as “Failure mode avoidance”. It is achieved by removing the physical failure modes (Don Clausing and Daniel Frey, 2005). FMA has its roots in Taguchi (Roger Rivett et al., 2015). Taguchi defines robustness as the “state where the technology, product, or process performance is minimally sensitive to factors causing variability either in the manufacturing or user’s environment”. Taguchi introduced the parametric design which aims at reducing the effect of the uncontrolled variation due to noise factors on

the performance of the system, by controlling the settings of the design parameters known as control factors (Tapan Bagchi, 1993; Roger Rivett et al., 2015). In reducing variability in this way, the robustness approach has some similarities with the Six Sigma approach (Roger Rivett et al., 2015). When several factors influence the performance of a system, statistically designed experiments could separate the vital factors from many trivial factors (Tapan Bagchi, 1993).

In the complex space systems, it is very difficult to define the complete set of combination of loads and its magnitude in the early design phase. The design robustness is the key requirement for such systems and can be achieved by widening the set of conditions known as "operating windows", under which the system can function satisfactorily (Don Clausing and Daniel Frey, 2005). The authors propose and illustrate four concepts that can be attempted in the designs to avoid the failure modes namely, (i) relaxing a constraint limit on a control factor, (ii) use of physics of incipient failure to avoid failure, (iii) creating two different operating modes for two different demand conditions, and (iv) exploiting interdependence between two operating window system variables. "Operating window methods" developed by Xerox Corporation in the 1970s is another method for making the operating window larger. In this method, the value of the noise factors are increased which makes the system to fail at increased rate. Understanding the physics of failures, improvements could be made by appropriately changing the settings of control factors.

2.3.4 Methods to achieve FMA

It is important to understand when and why potential failure modes are created, for creating an effective FMA strategy. Several failure modes are created right at the concept development and selection phase. It continues in the system design phase, process design phase and at start of production. The process of quality and reliability enhancing efforts has to be applied early to reduce the time gap between the creation and detection of the failure mode (Ake Lonnqvist and Ida Gremyr, 2008).

Design

FMA is the methodology for the early detection and mitigation of the failure modes, with emphasis on enabling the designers to have sufficient knowledge of the failure modes and take robust corrective measures (Saxena et al., 2005). The FMA frame

work developed by the University of Bradford Engineering Quality Improvement Centre is on the basis of the function analysis of the system which captures both main functions and interface functions of the system design. By developing a functional understanding of the system through existing Quality Assurance (QA) tools such as failure mode effect analysis (FMEA) and process diagrams. FMA focuses on systematic identification of all the failure mechanisms, development and implementation of robust counter measures for mitigation of failure modes, and finally verification of the effectiveness of the counter measures (Ed Henshalla et al., 2017; Goodland et al., 2013).

The complimentary top-down approach of fault tree analysis (FTA) and the bottom-up FMEA are still very tools to identify the failure modes and take actions for prevention of failures. FMEA is a systematic analytical tool widely used in many industries such as automotive, aerospace and electronics industries to identify, prioritize and eliminate the failure modes. FTA is the most commonly used tool for causal analysis in risk and reliability studies (Daniele Regazzoni and Davide Russo, 2011; Samira Abbasgholizadeh Rahimi et al., 2015; Saxena et al., 2005). In the preparation of an FMEA, the engineers brainstorm about the failure modes of parts, components and subsystems and keep adding a large number of failure modes, but it is difficult to judge whether the list is comprehensive. The FMEAs have to be carried out with a structured frame work addressing design parameters, materials used, noise factors and adherence to design rules for all the components. The most important role of FMEA is to address the counter measures to make the design robust (Saxena et al., 2005).

Prevention of failures in systems can be accomplished by (i) use of intrinsically reliable components that have high margins of safety, (ii) avoiding wear out failures by safe life design and proper maintenance, and (iii) avoiding failure modes related to system interfaces and interactions. However, addressing all these aspects in the initial design is a great challenge even for the most expert engineering team. So, the design has to undergo rigorous analysis and testing to bring out the weakness in the design (Patrick O' Conner, 2000). Reliable performance of launch vehicle systems can be ensured by fault avoidance and fault tolerance. Fault avoidance is achieved by making the system design simple with minimum number of subsystems, ensuring adequate margins of safety and health check of systems prior to launch. The fault tolerance is achieved by ensuring that system functions even in the presence of faults by providing

redundant subsystems, like a redundant power source or a redundant control system (Frank Corl et al., 2014). Fault tolerance takes care of random failures in components due to manufacturing defects that are missed during the screening process. The design defects also manifest only on one of the many redundant units because of the variations in environmental conditions encountered by these units. Therefore, redundancy helps in the isolation of such defects. In several missions of the space shuttle, redundant systems have helped in salvaging even the design defects (Elisabeth, 2015). However, the redundancy fails when the systems have a common failure mode, like susceptibility to a particular environment.

The design robustness has to be incorporated in the basic design, and there are no limits for designing and building reliability in products (Patrick O' Conner, 2000). In the case of the SRB segment joint, after the challenger accident, the capture feature to improve joint stiffness and reduce the relaxation in O-ring compression was the straight forward solution that emerged from the physics of failure. But a number of other design features emerged to make the design robust and were implemented. These include a J-leg insulator to provide an additional thermal barrier and act as an effective seal, an interference fit with capture feature, a third O-ring in the capture feature to prevent the gas leak, increasing the O-ring diameter to have higher compression, widening of the O-ring groove to avoid four wall contact thereby enhancing pressure actuation feature, modification of the segment joint pin and the pin holding band to improve reliability, introduction of metal shims between the tang and outer clevis arm to reduce the relaxation in O-ring compression, introduction of leak check port to verify the primary seal effectiveness and vent port to vent the air between capture feature and primary O-ring, and introduction of heaters for the field joint to ensure that the O-rings follow the dynamic movements of the casing even under cold conditions (Marshall Space Flight Center, Practice No. PD-ED-1257; Dennis Moore and Willie Phelps, 2011; Mohammed Gharouni et al., 2014).

The system reliability activities pertaining to failure prevention are risk mitigation, design/ process FMEA, Worst Case Analysis (WCA) and HALT before the manufacturing process, while HASS and Failure Reporting, Analysis and Corrective Action System (FRACAS) are the methods to be applied after manufacturing (Bernard, 2003).

Manufacturing

The historical data of US launch vehicle failures show that most liquid engine failures were associated with interactions between systems, and were dominated by process control issues. The increasing process related errors may be due to the higher complexity of the liquid engines or because the liquid stages are used to meet the more challenging mission needs (Susie Go et al., 2017). This emphasises the need for stringent process control during manufacture, assembly and testing of such complex space systems. The manufacturing of highly intricate aerospace components relies on various factors like the material control, complex and accurate machining centres, and experience of the skilled operators. In order to achieve consistently zero defect products, factors affecting the variations in process have to be identified and counter measures taken through a structured manufacturing failure mode avoidance framework (MFMA). The frame work comprises of functional analysis of the process, failure mode identification, process improvement, and process control and validation. These are accomplished using tools like process mapping, process FMEA, process capability studies and process control. Goodland (2013) explains and illustrates the application of the above frame work with a case study of heat treatment process of aluminium rivets for aerospace applications.

Testing

If the failure modes and failure mechanisms causing them are understood and actions are taken to avoid these failure modes, failures do not occur. Although designing reliable products appears very simple from this view point, getting to know all the different failure modes and controlling their failure mechanisms are a hard task (Patrick O' Conner, 2000). The failure mechanisms are initially unknown, either because they are beyond the imagination of the concerned engineers and the failure modes remain 'unknown unknowns', or because the failure modes are known but happens to be much more probable than expected. Therefore, designs must be rigorously analysed and tested to avoid failures (Elisabeth et al., 2015; Patrick O' Conner, 2000). The engine failures in the Ariane launch vehicle were solved only after testing the engine in high stress conditions and in variable / transient conditions (Elisabeth et al., 2015). The re designed SRM segment joint of the space shuttle was evolved through a large number of analysis, simulations, characterisation studies and

an iterative design process. Six number of static tests were done to identify the cause and qualify the redesigned motor. The tests include testing at cold and hot temperatures, and to failure mode simulation tests to verify the redundant features of the seal (Dennis Moore and Willie Phelps, 2011). The philosophy of “test like you fly, fly like you test” emerges from the necessity to simulate defect trigger conditions. It is also important to review all the lessons learned from the earlier failures and implement corrective actions to avoid recurrence of failures (Elisabeth et al., 2015).

The effectiveness of testing depends on its ability to detect the defects. Some defects, like the software error which caused Ariane 5 failure, are detected early as they affect all the mission scenarios. Some defects are latent, but are triggered in an unfavourable environmental condition such as the SRB O-ring seal failure in Challenger. The operating window method of high stress testing simulating the noise factors can bring out these defects. The high stress tests are possible with Liquid Rocket Engines (LRE), and such tests done on ground for the LRE of the Space Shuttle Main Engine (SSME) have contributed significantly for its excellent flight reliability (Elisabeth et al., 2010). These tests are similar to Highly Accelerated Life Testing (HALT). In the HALT, in the early phase of design, the failures are created quickly by subjecting the systems to the highest stresses within the limits of technology, thereby throwing light on the failure causes and making opportunities for design improvements (IEEE 1413.1, 2002). In the HALT, often the failures are created by different type of an environment, say vibration, instead of the actual service environment which triggers the failure in the field like thermal or vacuum. The focus is mainly in identifying the failure mechanism and taking the actions to mitigate them and not in simulating the service environments. This results in achieving design robustness with simple design solutions without much impact on the cost. The issue of a loosened screw, which can cause a catastrophic failure, can be solved by a thread sealant or by using a nut with locking provision. Highly accelerated stress screening (HASS) is used in the screening of production items with stresses much higher than those experienced in normal use including shipping and storage. The HALT and HASS are not limited to avionics packages, but to other systems like mechanical systems and propulsion systems. HALT address design and production weaknesses whereas HASS may expose design weaknesses if any remaining and also problems related to production (Hobbs, 2000; Patrick O' Conner, 2000).

Instrumentation and data analysis

The study of failure mode avoidance assumes greater significance in human rated launch vehicles. Health management system is one of the key reliability and safety design feature in the human rated launch vehicles. For example, in the liquid engine, critical engine operating parameters are monitored and when it crosses the acceptable bounds called the red line limits, the engine can be shut down safely. Although this may ensure crew safety, the overall objectives of mission may not be achieved. The reliability measures of the health management systems are false positive (FP) where the engine is erroneously shut down, whereas false negative (FN) refers to the case when the engine needs to be shut down, but the system does not do so (Zhaofeng Huang, 2015). Another essential feature in crewed launch vehicle is the crew escape system for the crew to quickly escape from the failing vehicle. In this case, FP means erroneous abort and FN refers to the case where abort is needed but either sensor did not work or the fault detection did not take place. The bottom line is to create abort triggers in such a manner that it avoids false aborts and at the same time allows sufficient time for the crew to depart from the vehicle (Hanson et al., 2013).

While successful performance data is an important input to the designer, it is equally important to have in depth knowledge of the failures that have occurred and their root causes (Marshall Space Flight Center, PD-ED-1257). The comprehensive test and evaluation of the space systems, to envelope the space environments such as thermal-vacuum, vibro-acoustics, electromagnetic and radiation, gives adequate confidence on the flight systems (Nanjundaswamy and Rajangam, 2018).

It is of paramount importance not only to have sufficient instrumentation during the ground testing and flight but also have an in depth analysis of all the data, to identify design marginalities and near misses. Unfortunately, though systems give early warnings through these measured data, in many cases either the data is not seen meticulously, or it is taken lightly and short cuts taken in the root cause analysis. When the flights are successful, complacency sets in and these details are revisited only when a failure occurs (Elisabeth et al., 2010). It is also equally important to use the statistical tools for the analysis of data in the right perspective when taking critical decisions about the implications of a non-conformance. In the case of SPACE shuttle Challenger, the ambient temperature on the day before launch was minus 13°C which

was the lowest for a shuttle launch, and at the time of launch it was 3.3°C. The wind from the west blowing around the super cold external tank had chilled the downstream motor case surface to minus 13.3°C. When the concerns were raised to launch the shuttle at low temperature, the inspection data of field joints of SRM recovered from previous 23 launches were looked into. However, only seven cases where the O-ring damages observed have been considered for the decision making. Based on the fact that failures were observed at both high end and at low end of temperatures (11.7, 13.9, 14.4, 17.2, 21.1 and 22.8°C), it was concluded that the O-ring damages had occurred irrespective of the temperature and clearance was given for launch. However, in the 23 data points that were available, 19 were launched at temperatures greater than 18.9°C, and only in three cases of O-ring damages were observed. However, in the four launches where temperature was below 17.8°C, the O-ring damage was observed in all the four cases, which clearly establishes that the low temperature is a sensitive parameter affecting the O-ring resilience. If a simple linear regression analysis of all 23 points had been done, a correlation of -0.56 would have been observed which is statistically significant at 0.05 probability level, establishing the O-ring erosion to temperature relation. The concerned engineers lacked the statistical knowledge critical for the decision making process (Rosa Lynn Pinkus et al., 1997; Ben Evans, 2007).

The detailed literature survey on reliability analysis has been carried out, and the current methods for determination of reliability of launch vehicle systems, their applicability, and the limitations are brought out. The need for developing new methods for accurate determination of reliability of launch vehicles and its major systems with limited test data is identified. A comprehensive review of literature on the concepts of failure mode avoidance of complex systems has been carried out, highlighting their applicability for space systems. The literature review forms the basis for this research thesis on reliability analysis and failure mode avoidance of launch vehicle and satellite systems.

CHAPTER 3

ANALYTICAL MODEL FOR RELIABILITY ANALYSIS OF SYSTEMS WITH LIMITED TEST DATA

3.1 Introduction

Reliability is one of the critical design parameters for the launch vehicles and its systems considering the high cost of space missions, the safety of crew as well as public, and the implications associated with committed programs. It is also used to finalise the configuration and design options depending on the mission requirements. Hence, an accurate estimation of the reliability of the launch vehicle systems is necessary, to optimise the technological and commercial aspects of the mission (Seth Guikema and Elisabeth Pate-Cornell, 2004; Steven Lee, 2001; Zhaogfeng Huang, 2014).

System reliability can be assessed by two approaches namely reliability prediction and reliability demonstration. Reliability prediction is a bottom-up approach, based on the component reliabilities from the handbooks and the system reliability block diagram. It gives the design reliability. The demonstrated reliability is computed using the system level test data. The demonstrated reliability is more useful as it accounts for the design, process and human reliability (Sergio Guarro, 2015). If the system is already tested and flown many times, the reliability can be estimated in terms of the success rate, as a ratio of the number of successful trials to the total number of trials. However, success rate as a measure of reliability can mislead when the number of trials is limited (Lisa Bloomer, 2004). In such situations, the use of a model with the number of successes following a binomial distribution will be a more pragmatic approach. The probability density function (pdf) of a binomial distribution is used to get the probability of obtaining x successes in n tests, when the outcome of tests is only a success or a failure known as Bernoulli trials. The probability of obtaining ' x ' successes and ' $(n-x)$ ' failures, in ' n ' tests, is given by

$$f(x) = \binom{n}{x} p^x q^{(n-x)} \quad (3.1)$$

where ‘p’ is the probability of success and ‘q’ is the probability of failure. The cumulative distribution function (cdf) of the binomial distribution, i.e., the probability of obtaining r or fewer successes is given by

$$F(r) = \sum_{x=0}^r \binom{n}{x} p^x q^{(n-x)} \quad (3.2)$$

Therefore assuming that reliability $R = p$ in the Equations (3.1) and (3.2), the probability of a product to survive based on the binomial cdf can be presented in the form of:

$$C = 1 - \sum_{x=0}^r \binom{n}{x} R^{n-x} (1 - R)^x \quad (3.3)$$

where n is the number of tests carried out, r is the number of failures, R is the one sided lower bound for the reliability, and C is the confidence level (Huairui Guo et al., 2010; Patrick O'Connor and Andre Kleyner, 2012). In this paper, reliability assessment is made at a confidence level of 60% with $C = 0.6$, in accordance with the ‘guide to the probability of failure analysis for expendable launch vehicles’ (Federal Aviation Administration, 2005b), which acts as a standard reference when comparing the reliability of different launch vehicle systems. Assessment can be made at a higher confidence level, when the number of test data available is large, as in the case of manned missions. The binomial model is an elegant statistical tool for reliability analysis of systems but has limitations when assessing the reliability of new systems with scarce data.

Reliability of propulsion systems is a major concern area for launch vehicle community. Liquid propellant Rocket Engines (LRE) are widely used in launch vehicles world over, as main propulsion systems, because of their high specific impulse, relatively clean exhaust gases and provision for commanded cut off. The thrust can also be up-rated when demanded (George Sutton and Oscar Biblarz, 2010). Testing of propulsion systems can be treated as an event resulting in success or failure as in the case of a one shot device. The number of tests in the integrated stage level is limited considering the cost and schedule aspects, and hence system reliability estimate based on these tests alone does not truly reflect the inherent reliability of the system. Therefore, estimation of reliability for new launch vehicle systems with limited test data is a challenging task for the system engineers

This chapter presents a new analytical model for the reliability assessment of systems with limited test data, taking into account of the previous experience, knowledge, and data gained from the design and operation of similar systems. The analytical model gives an accurate weighting for the tests carried out on the pedigree systems which has demonstrated a large portion of the new design.

3.2 Reliability of a new liquid propulsion stage

A new liquid propellant rocket stage designated as L110 stage, with 110 tons of propellant stored in separate fuel and oxidiser tanks and configured with twin LREs, is developed as a core booster stage for a new launch vehicle, LVC. Similar LRE has been used in the L37.5 stage which is the second stage of the earlier flown launch vehicles LVA and LVB. The stage is filled with 37.5 tons of propellant in a common bulkhead type propellant tank. In the launch vehicle LVB, it is also used as four strapon booster stages and is designated as L40 stage with 40 tons of liquid propellant stored in separate fuel and oxidiser tanks. Table 3.1 and Figure 3.1 give the actual data of usage of the LREs in each launch vehicle, and flight history. The total number of LRE tests in ground and flight is also tabulated in Table 3.1.

Table 3.1 Usage history of the LRE in different launch vehicles and the stage designations

Sl.No.	Launch Vehicle	No. of launches	Liquid Stage Nomenclature	Stage of the launch vehicle	Total No. of LRE tests
1	LVA	38	L37.5	Second stage	61
2	LVB	10	L37.5	Second stage	
3			L40	Strapon Booster	46
4	LVC	-	L110	Core Booster	14

All the three liquid stages employ the pump fed earth storable engine with UH25 (Mixture of 75% Unsymmetrical Di-Methyl Hydrazine (UDMH) and 25% hydrazine hydrate by mass) as fuel and N_2O_4 (nitrogen tetra oxide) as the oxidiser, with fine tuning for particular stage configuration and burn duration. This approach of using the pedigree engine in a new stage is preferred to a totally new advanced design which may offer promising performance on paper. This is because new systems have more

uncertainties due to hidden failure modes that can come out only with a large number of tests over a longer period of time. Also, for an advanced design, the maturity can be attained only through corrections based on the experience of a large number of testing (Gaspare Maggio and Dennis Pelaccio, 2000).

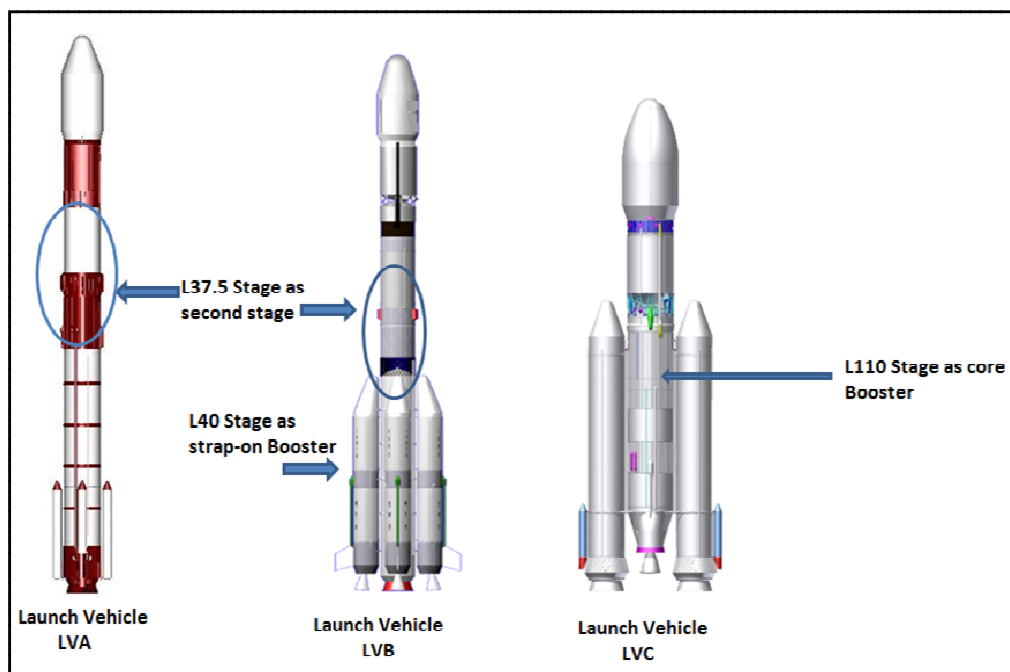


Figure 3.1 LRE in different launch vehicles and the stage designations

The basic LRE is a pump fed engine. The engine chamber pressure developed is 5.85 MPa to generate a thrust of 800 kN. Operating mixture ratio, the ratio of mass flow rate of N_2O_4 to mass flow rate of UH_2 , is 1.7 nominal. The specific impulse generated is 293 s. The operating principle of an LRE is explained in Figure 3.2. There are three centrifugal type pumps, driven by a common turbine, for pumping N_2O_4 , UH_2 and water. The hot pressurized gas required for running the turbine is generated in a Gas Generator (GG). The command module pneumatically opens the main engine valves with gaseous nitrogen. The propellant stored in the propellant tank and water in the water tank are admitted to the suction side of the respective pumps.

The pump pressurizes the propellants and discharges them at a higher volumetric flow rate to the thrust chamber through an injector. The fuel and oxidiser injected into the thrust chamber of the nozzle are atomized, mixed and burned together to form the high pressure gas (Thomas Ward, 2010). The pressure developed in the thrust chamber results in thrust generation. At the same time, the required quantities of

propellants are branched from the pump outlets and admitted into the combustion chamber of the GG through the respective regulators. The water discharged from the water pump enters the gas generator, mixes with the combustion gasses thus maintaining the hot gas temperature within acceptable limits. The high temperature gas operates the turbine and as the turbine speeds up, the three pumps also speed up and start discharging fluids at higher pressure thus feeding to the main thrust chamber. The engine works as a closed loop system using the reference pressures, controlled by the command module, and maintains the required chamber pressure.

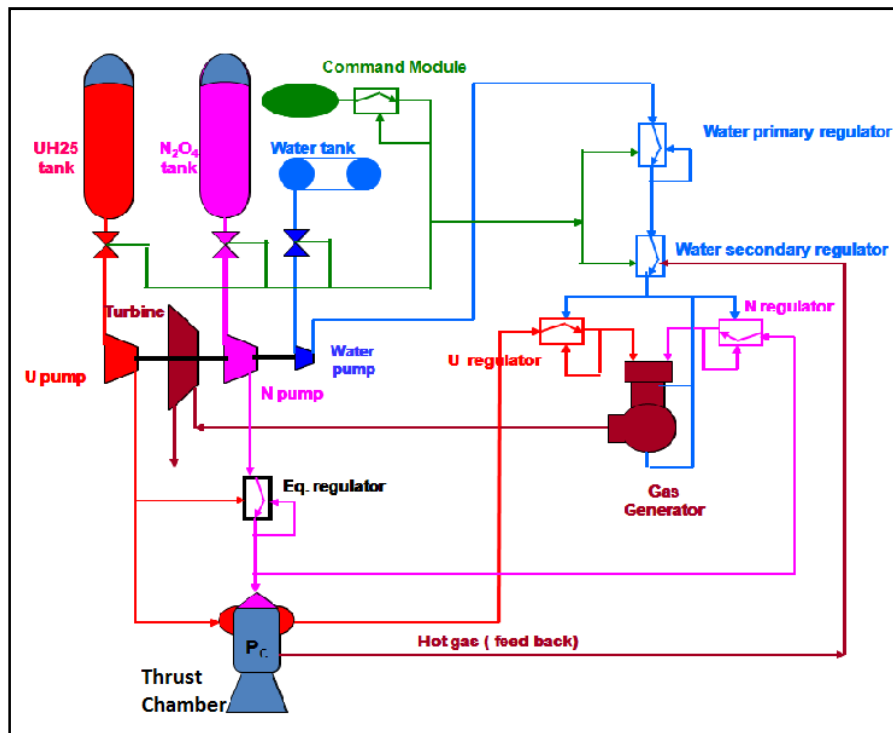


Figure 3.2 Schematic of liquid engine operation

The L110 stage has been qualified through three successful stage level hot tests and eight engine level tests, which is very limited, considering various factors such as the technical assessment of the system functioning, resources, and launch vehicle program schedule. With three stage level hot tests, the reliability of the L110 stage with twin engines from Equation (3.3) is only 0.736. However, the new stage and its systems are derived from the flight-proven L37.5 and L40 stages, which give good confidence on the reliable performance of the stage. Such instances are common in space systems and there is a need to develop an analytical model to correctly assess the reliability of the new system considering the space agency's past record of successfully developing and operating similar systems.

3.3 Methodology of reliability assessment - a new analytical model

When a new system is inducted for a launch vehicle which is derived from a proven design, many of its subsystems and its interfaces are already proven in the pedigree system through testing at highest levels of system integration and the flight performance. Therefore, a weighting can be given for the tests carried out on pedigree systems based on the percentage of similarity of the new system with the pedigree system, to get an equivalent number of tests of the new system. This along with the tests on the new system can be used to get the reliability estimate of the new system.

When the test data is limited, an approach for finalising the weighting factor is to make a combined engineering judgment by all the stakeholders like the project engineers, design engineers, and quality assurance engineers. However, this method has the drawback of subjectivity. A system reliability person looks every system incredulously and assigns a very low weighting factor, while the design and project engineers look at systems more optimistically and tend to give very high weighting factors. A person working on the shop floor knows the ways in which things can go wrong and is aware of the near misses and so, is not as optimistic as a higher level manager. The managers with an overall perspective look things in a more general way and are very optimistic as long as things go well (Richard Feynmann, 1986). Another approach is to use the Bayesian method based on the subjective view of probability, the results of which are influenced by the subjective prior distributions.

In the proposed analytical model, the similarities of a new system are assessed with respect to the existing systems, for different factors that influence the system performance and its reliability, addressed henceforth as System Reliability Influencing Factors (SRIFs). The SRIFs are identified, and for each factor the similarity of the new system with the pedigree system is quantified based on the design, functionalities, and configuration. Appropriate de-rating is given for the uncertainties introduced due to design changes, and an overall weighting factor to be applied to the test data of the pedigree system is computed. The procedure for arriving at the weighting factor comprises of following steps:

- Verification of compliance to the prerequisites
- Identification of SRIFs

- Assignment of the similarity class and fixation of weighting index 'wi' for each SRIF; wi of the jth SRIF is designated as 'wi_j', where j varies from 1 to N when there are N SRIFs.
- Computation of weighting Score 'ws' for each SRIF; ws of the jth SRIF is designated as 'ws_j'
- Computation of weighting Factor 'wf'

The approach of the new model is similar to the Bayesian approach as it can provide the justification for the lesser amount of reliability demonstration testing (Patrick O' Connor and Andre Kleyner, 2012). The main disadvantage of the Bayesian approach lies in the problem of choosing the right prior statistical distribution for the reliability of the system based on subjective judgment or expert opinion. In fact, an unfavourable prior can actually have an opposite effect on the reliability demonstration (Patrick O' Connor and Andre Kleyner, 2012). It neither considers the evolution of different systems and the associated reliability improvements nor the similarities of the new system with the pedigree system (Seth Guikema and Elisabeth Pate-Cornell, 2004). The subject experts find it difficult to define the prior distribution which needs in-depth statistical knowledge. The proposed analytical model reduces the subjectivity in the Bayesian approach, since the experts find it more convenient to technically assess the similarities and uncertainties of the new system.

3.3.1 Prerequisites for application of the method

Design verification

In order to apply this method based on pedigree, qualification at subsystem level and integrated stage level have to be completed in the new system, demonstrating the structural and functional capability of the stage. Integrated level tests on systems demonstrate various aspects of the system functioning, like the subsystems functioning, interdependencies of subsystems, the system interfaces, fault tolerance, and the capability to function as an integrated system under different service environments like pressure, temperature and vibration. When this is not done, even in systems derived from proven systems unexpected failures can happen. Hence, the satisfactory qualification at different levels is an essential requirement for the application of the method.

Manufacturing

Stabilized production processes and established quality systems are the keys to the success of any launch vehicle program. Flight stage has to be realized strictly adhering to the best practices of process and quality control, and the quality of the hardware has to be equivalent to or better than the qualification hardware.

Design team

The new and the pedigree systems shall have been developed under identical circumstances by the same design team or a team of similar expertise level. When a new team is developing a launch vehicle system, the experience with a similar system developed by a reputed team cannot be given any weighting. This is because, the new team lacks the knowledge, experience and competence gained during the development and operation of the pedigree system.

3.3.2 Identification of SRIFs

The key factors influencing the system functioning are identified as SRIFs. The outcome of the FMEA and the studies carried out to assess the sensitivity of various factors on system performance can be used to identify the SRIFs. The key factors influencing the reliability of a system related to design are the design simplicity, design robustness, interaction among the subsystems and selection of the materials to meet the system requirements. In the case of an LRE system, the reliability is dependent on a large number of system and sub system reliability drivers like engine combustion cycle, engine operation duration, number of engines, engine thrust, reusability, engine de-rating or up-rating, and engine-out capability. Other key factors are propellant specific hazards, vehicle to engine interfacing and their interaction hazards, engine health management system, engine start hold down with launch commit criteria, number of planned engine starts and system design approach (Zhaofeng Huang et al., 2005).

The manufacturing process capability to meet the design specifications with respect to geometrical as well as the form tolerances and the quality systems in place for the realization of the systems are also critical for achieving the desired reliability levels. The quality systems for system hardware ensure aspects such as, robust manufacturing processes, compliance to wide-ranging qualification and acceptance

test programs, inspection and test procedures, non conformance management procedures, and certification procedures. These factors also have to be included as SRIFs as they are decisive for realization of systems as per the design specifications. The SRIFs have to be selected prudently without any bias giving the right level of representation to all disciplines such as design, materials, manufacture, inspection, assembly and testing.

3.3.3 Weighting index of SRIFs

Depending on the degree of similarity of the newly developed system with the proven system, for each of the identified SRIFs, a similarity class from I to IV is assigned. This decides the weighting to be given for the pedigree system, in the assessment of reliability of the new system and is designated as 'wi'. When the new system is same in all respects to the heritage system for an SRIF, it is assigned a similarity class I with a wi value of 1. A judgment is made that when there are some minor differences, but the similarities are more than 80%, a similarity class II is assigned with a wi of 0.8. When the similarity level is less than 80% but more than 40%, the difference is considered as major, and so a similarity class III is assigned with a wi of 0.4. When the systems have less than 40% similarity, the systems are considered totally different and hence assigned with a similarity class IV with no weighting, i.e., $w_i = 0$. The classification is explained in Table 3.2.

Table 3.2 Rationale for classifying similarity and assigning weighting index

Sl. No.	Similarity of new system relative to proven system for identified SRIF	Similarity class	Weighting index , 'wi'
1	Identical or better	Class I	1 (ie., 10 out of 10)
2	Minor difference	Class II	0.8 (ie., 8 out of 10)
3	Major difference	Class III	0.4 (ie., 4 out of 10)
4	Large difference	Class IV	0 (ie., less than 4 out of 10)

The classification quantifies the similarity of the new system with the heritage system for each SRIF. In most cases, the similarity level can be quantified without ambiguity. For example in the case of a liquid engine, for the SRIF 'combustion cycle', the

similarity level can be either I or IV and it is deterministic. Every SRIF can be assessed by a team of experts independently. If needed, w_i can be assigned any value based on the percentage of similarity. However, the above classification approach is simple and elegant, as it becomes easier to operate when getting feedbacks from experts and also make the assessments convergent and conservative.

3.3.4 Analytical model for the weighting score

The weighting index is finalised based on the percentage of similarity with the proven system. In practice, it is observed that though the changes or differences from the proven system are smaller, it affects the performance of the system in a relatively larger proportion. So, there is a need to further de-rate the weighting index w_i , to obtain a conservative weighting, given by weighting score ws for each SRIF. The de-rating shall be higher when the differences become more (with decreasing w_i), as uncertainties become much higher with increasing level of changes.

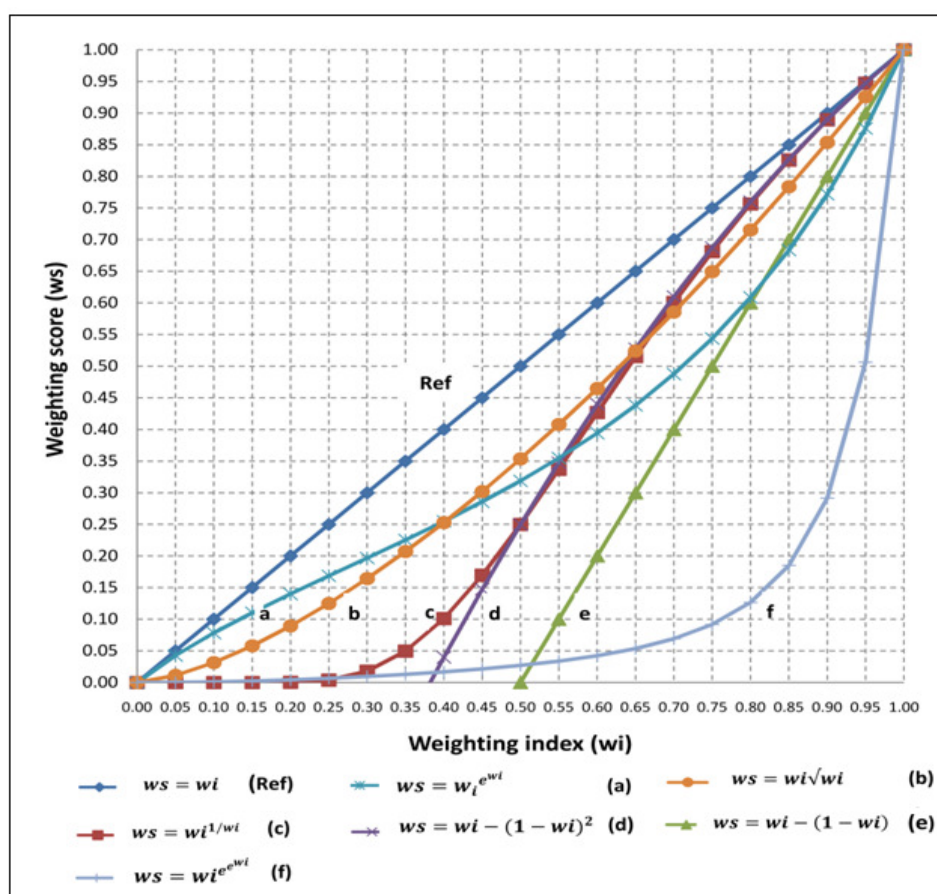


Figure 3.3 Basic analytical models considered for the weighting score and compared with ref. model $ws = w_i$

A number of mathematical formulations have been formulated for meeting the above criteria and following equations have been shortlisted and analysed further:

(a) $ws = wi^{e^{wi}}$; (b) $ws = wi\sqrt{wi}$; (c) $ws = wi^{1/wi}$;
 (d) $ws = wi - (1 - wi)^2$; (e) $ws = wi - (1 - wi)$; and (f) $ws = wi^{e^{wi}}$. The weighting score ws variation with respect to weighting index wi for these models are compared with respect to the basic reference of $ws = wi$, in Figure 3.3.

The models 'a', 'e' and 'f' have been eliminated as the quantum of de-rating is very high even when the similarity between the systems are very high with higher values of wi . The model 'b' is not considered as there is not adequate de-rating at lower values of wi . In the model 'd', ws is negative for low values of wi . Considering all the above aspects, the model 'c', $ws = wi^{1/wi}$ is found more suitable and has been finalized as the basic model, with an optimal de-rating (80% similarity de-rated to 76%, 60% de-rated to 43% and 40% de-rated to 10%). Thus, the basic model selected for the weighting score is,

$$\text{Weighting score, } (ws)_{\text{basic}} = wi^{(1/wi)} \quad (3.4)$$

However, the effect of changes made in the new system from the pedigree system cannot be captured by the above rigid model alone, which is based only on the proportion of changes. The system performance is dependent upon many other factors beyond the similarity in the design characteristics of the systems (Zhaofeng Huang, 2005). It is also dependent on the complexity of the systems, the experience of the design team, the rigor of design analysis, and the extent of design verification carried out. Also, all SRIF's may not be of equal importance for reliable system functioning. All these aspects are taken care by introducing three tuning parameters: parameter for sensitivity of the SRIF on system performance ' c_j ', parameter for complexity of the system ' k_{1j} ' and parameter for design verification ' k_{2j} '.

Depending on the relative criticality of SRIF in the problem under consideration, c_j can be fixed to give higher priority for the more important SRIFs. Based on the experience level of the space agency and maturity level of the systems, the tuning parameters k_{1j} and k_{2j} can be modified to get a more accurate assessment of reliability. Accordingly, the weighting score for the j^{th} SRIF is modified incorporating these tuning parameters as follows:

$$\text{Weighting score for the } j^{\text{th}} \text{ SRIF, } wS_j = c_j k_{1j} \left\{ w_{ij} \left(\frac{k_{2j}}{w_{ij}} \right) \right\} \quad (3.5)$$

where w_{ij} is the weighting index for the j^{th} SRIF, c_j is the tuning parameter for accounting the relative sensitivity of the SRIF on system performance, k_{1j} is for accounting uncertainties caused by the complexity of the system, and k_{2j} is for the deleterious effects the changes can have on the system behaviour because of possible inadequate design analysis and verification. The guidelines for finalising the values for tuning parameters are addressed in following sections.

Tuning parameter of sensitivity of SRIF, c_j

In many systems, a few SRIFs may influence the system performance more significantly in comparison with the other SRIFs. To give a higher weighting depending on the relative sensitivity of an SRIF in comparison with others, a tuning parameter of sensitivity for the j^{th} SRIF ' c_j ' is introduced to give an appropriate weighting for each SRIF. The criteria for assigning a value for this parameter is dependent on the many aspects such as prior knowledge and experience with the system; the sensitivity of various factors on system performance assessed through design analysis and understood from the test data; and engineering judgment. The rationale for assigning values of c_j is given in Table 3.3.

Table 3.3 Guideline for assigning value for tuning parameter of sensitivity, c_j

Sl. No.	Influence of the j^{th} SRIF as compared to other SRIFs	Assigned value of c_j	Remarks
1	Equal influence as other SRIFs	1	Assigned to most of the SRIFs
2	Marginally higher influence on the system performance as compared to other identified SRIFs	2	Assigned to a few SRIFs depending on their relative sensitivity on the system performance.
3	Higher influence on the system performance as compared to other identified SRIFs	3	
4	Large influence on the system performance as compared to other identified SRIFs	4	

Tuning parameter of complexity, k_{1j} and sensitivity analysis.

In complex systems, assessment of the changes becomes more difficult. For example, in a simple system where a change in an SRIF is not expected to affect other SRIFs, it is amenable to easy and better assessment of system performance. Interdependencies of one SRIF on others are difficult to assess for complex systems, particularly if the design team is not well experienced.

A change in one SRIF may seem to be minor in nature but can have an effect on other SRIFs. A change made in the type of pressure pick up, for example, though made for improvement in pressure monitoring system, could cause envelope (interface) related or vibration related issues because of the higher length and mass. The number of non-conformance may be lower, but this could be due to the reduction in the number of tests rather than improvement in the system hardware quality. Therefore, a de-rating is given considering the complexity of the system and experience level of the design team, by the tuning parameter k_{1j} . The guidelines for finalising the values are given in Table 3.4, considering different combinations of system complexity and experience of the design team.

Table 3.4 Guideline for finalizing the tuning parameter of complexity, k_{1j}

Sl. No.	Complexity of the system	Experience of the design team	k_{1j}
1	Low	High	0.9-0.95
2	High	High	0.8-0.9
3	Low	Low	0.8-0.9
4	High	Low	0.6-0.8

A system developing team is considered to have a high level of experience if a similar system developed by the team has a demonstrated reliability of more than 0.67 with 60% confidence level (Paul Wilde et al., 2013). The system can be considered highly complex if the number of subsystems is more; the subsystems are dynamic with parts having relative and rotary motions; or when the systems are of interdisciplinary in nature. In such systems, a change in one SRIF can have an impact on other SRIFs. The sensitivity of k_{1j} on the weighting score is assessed in Figure 3.4, with k_{2j} and c_j kept constant at a nominal value of 1.

Figure 3.4 shows the ws - wi relationship for k_{1j} values of 1, 0.8 and 0.5. If the k_{1j} value is 1, then no de-rating is implemented for system complexity aspects. Hence to give a minimum level of de-rating, an upper limit of 0.95 is finalised. The value of 0.95 can be assigned when a simple system is designed by an experienced team resulting in lesser uncertainties.

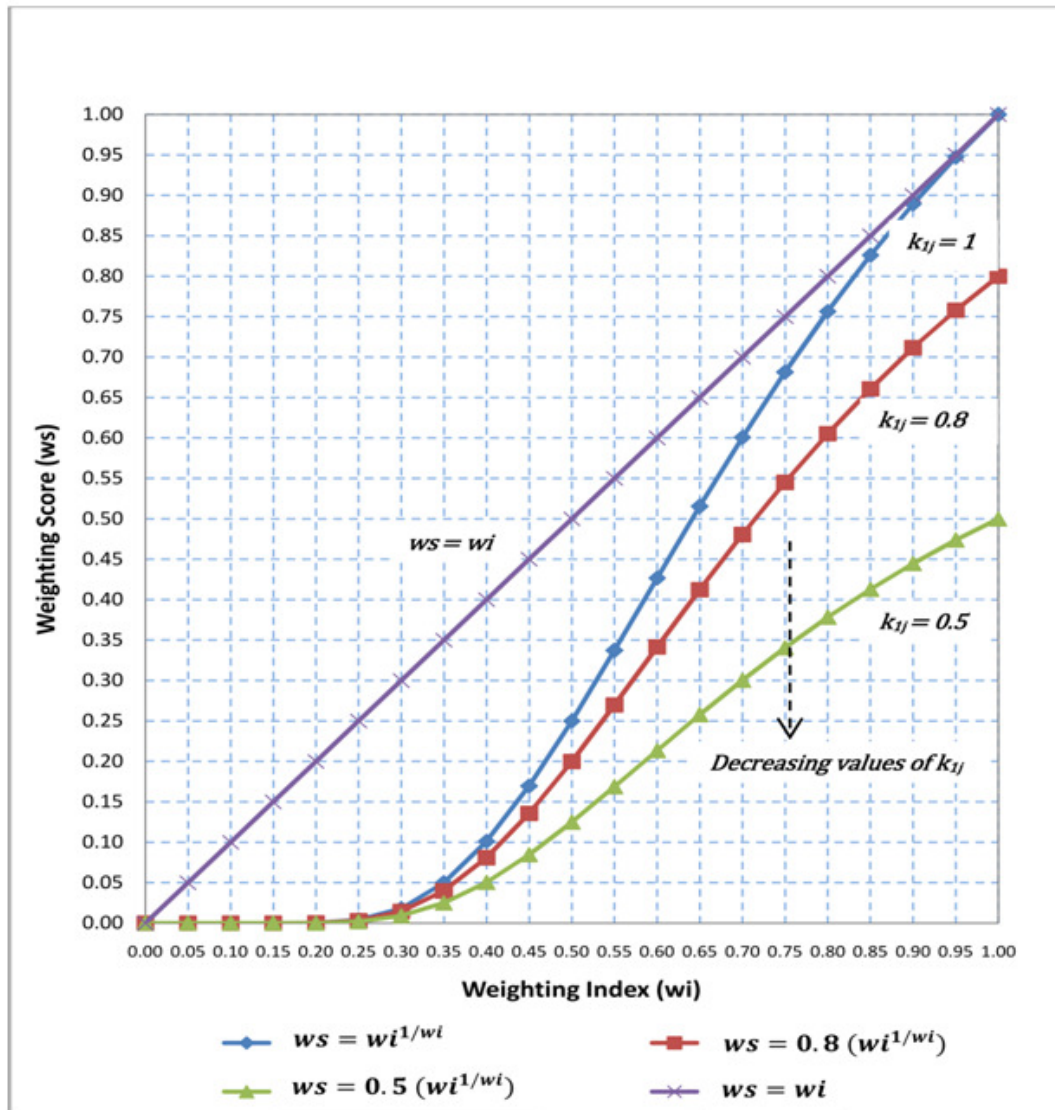


Figure 3.4 Sensitivity of k_{1j} on weighting score, $c_j=1$, $k_{2j}=1$

The tuning parameter k_{1j} is assigned a value of 0.6 to 0.8, when the experience level of the design team is considered low, and the complexity of the system is high. As discussed earlier, the value if wi is 0.8 when the difference from the pedigree system is minor. Even for such cases the weighting score approaches 0.4, and is considered as a threshold value, when k_{1j} is less than 0.6. Hence, minimum limit of k_{1j} value is fixed

at 0.6. Thus k_{1j} value can be assigned from 0.6 to 0.95, in accordance with guideline given in Table 3.4.

Tuning parameter of design verification k_{2j} and sensitivity analysis

The designer makes changes in systems with good intentions and expects the system to behave as planned, but it performs only as designed. Whenever a change is made on an SRIF, however minor the changes may be, a matured system design is disturbed and unforeseen failures are possible. In operational launch vehicles, for this reason, changes are not encouraged in the working systems unless they are of essential class, for want of improved performance. As the changes from existing system become more, there are risks of changing original design characteristics of the system and this may introduce new failure modes and hazards (Zhaofeng Huang et al., 2005).

A comprehensive design analysis and design verification program, at the highest level of integration simulating the harsh environments and longer durations bring out technical issues related to system performance caused by the changes. This enables timely action for prevention and mitigation of the failure modes. The factor k_{2j} is introduced to provide the de-rating for inadequate design analysis and test program. The guideline for finalising the values of k_{2j} is given in Table 3.5.

Table 3.5 Guideline for finalising the tuning parameter of design verification, k_{2j}

Sl. No.	Rigor of		k_{2j}
	Design analysis	Testing	
1	High	High	1 – 1.2
2	High	Low	1.3-1.5
3	Low	High	1.3-1.5
4	Low	Low	1.5-3

The rigor of design analysis is considered high when the state of art tools are used and comprehensive design analysis and simulations are carried out to ensure adequate margin and system performance (Paul Wilde et al., 2013). The rigor of testing is considered high when apart from subsystem qualification, integrated system level

qualification testing comprehensively covering all the aspects of system performance are carried out.

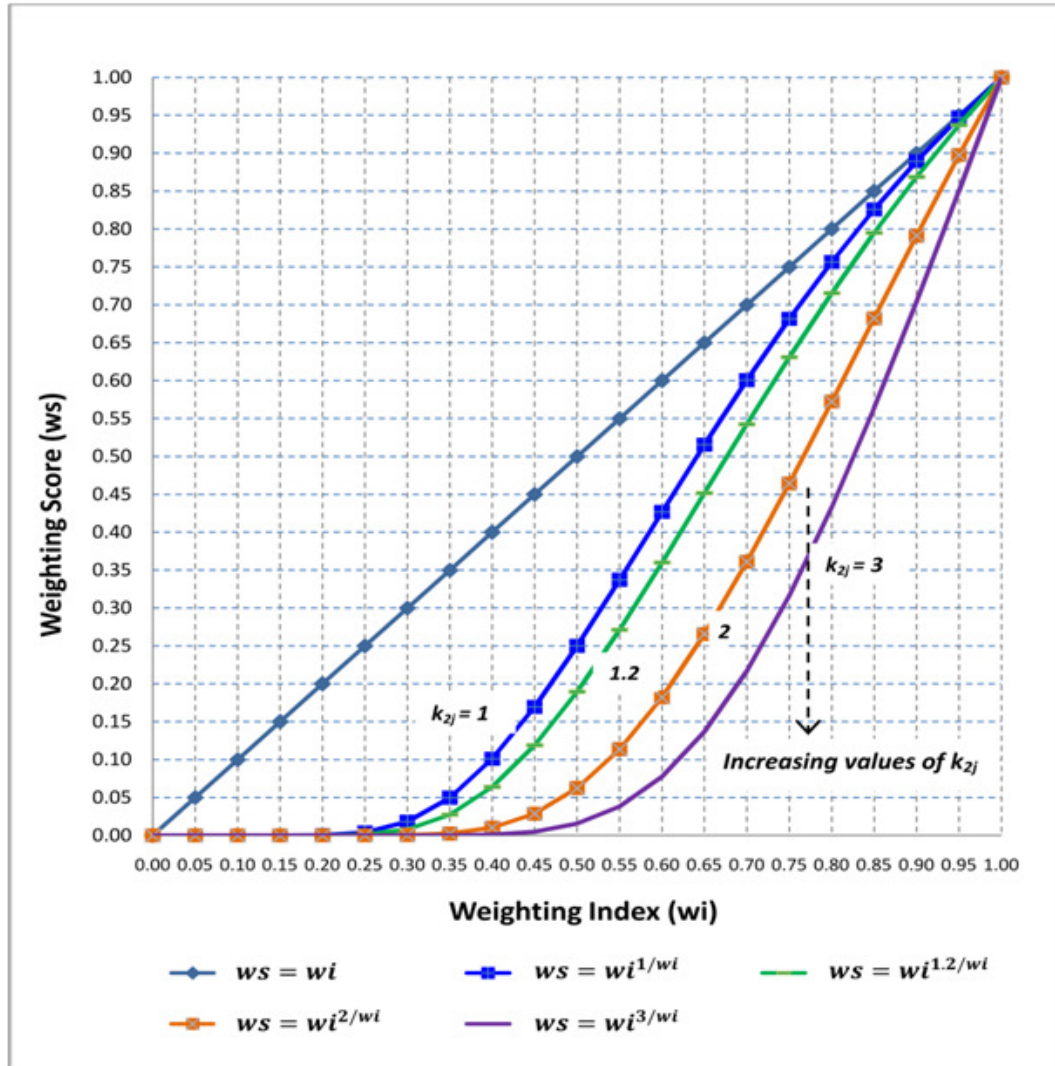


Figure 3.5 Sensitivity of k_{2j} on weighting score, $c_j = 1$, $k_{1j} = 1$

The tuning parameter k_{2j} alters the slope of the ws_j versus wi_j curve so as to increase the quantum of reduction in ws_j with decreasing values of similarity wi_j . To meet this criterion, k_{2j} shall be greater than or equal to 1. This criterion is not met for very low values of wi_j in the analytical model, but is acceptable as the weighting score values are negligibly small in this regime. Sensitivity analysis of the weighting score for different values of k_{2j} , with c_j and k_{1j} kept constant at 1 is carried out and plotted in Figure 3.5.

A k_{2j} value of 1 is applied to give a minimum level of derating. When the k_{2j} value is more than 3, the weighting score ws becomes less than the threshold value of 0.4 even

when the difference is minor, i.e., $w_i=0.8$. This only reiterates the fact that when the design verification is not adequate, the method should not be applied.

3.3.5 Weighting factor for the test data of pedigree system

The weighting factor w_f is used to compute the equivalent number of tests that can be considered as the tests done on the new system, based on the number of tests done on the proven system. The w_f to be applied on the test data of the pedigree system is obtained from the weighting index w_{ij} , weighting score ws_j , and the tuning parameter c_j , k_{1j} , and k_{2j} of each SRIF from Equation (3.6).

$$\text{Weighting factor } w_f = \frac{\sum c_j k_{1j} \{w_{ij}^{(k_{2j}/w_{ij})}\}}{\sum c_j} = \frac{\sum ws_j}{\sum c_j} \quad (3.6)$$

The equivalent number of tests, n_e for the new system based on the pedigree system is computed using Equation (3.7).

$$\text{Equivalent number of tests of new system, } n_e = n (w_f) \quad (3.7)$$

where n is the number of tests done on heritage system and w_f is the weighting factor.

The method of computing the weighting score for a new system 'B' based on similarity with heritage system 'A' is illustrated by considering three SRIFs in Table 3.6. Similarity class, w_{ij} , c_j , k_{1j} and k_{2j} are identified for three SRIFs. The SRIF, design methodology is assigned a higher c_j value of 2, as it is considered a key factor for reliable system performance as compared to other SRIFs. The ws_j is computed from Equation (3.5) and the w_f is computed from Equation (3.6).

Table 3.6 Computation of the weighting score

Sl. No.	SRIFs	Similarity Class	w_{ij}	c_j	k_{1j}	k_{2j}	ws_j , from Eqn. (5)
1	Design methodology	I	1	2	0.8	1.2	1.6
2	Materials and Manufacture	II	0.8	1	0.8	1.2	0.572
3	Inspection and test procedures	III	0.4	1	0.8	1.2	0.051
Total (for c_j and ws_j)				4			2.223

$$\text{Weighting factor wf} = \frac{\sum w_{sj}}{\sum c_j} = \frac{2.223}{4} = 0.55575 \quad (3.8)$$

If the number of tests done on the heritage system A is 100 and the number of tests done on the new system is 5, the total number of equivalent test on new system B is given by

$$(n_e)_B = (n)_B + (n_e)_A = 5 + (100 \times 0.55575) = 60.575 \quad (3.9)$$

Hence, though only 5 tests are done on the system B, based on its similarity with the heritage system A, the reliability can be computed considering that 61 tests are done on system B. The systematic procedure and guidelines identified by the analytical model for identifying the SRIFs, and fixing the values of c_j , k_{1j} and k_{2j} , results in the computation of weighting factors that are consistent among different experts and give accurate results.

3.4 Analysis of liquid propulsion stages and model validation

The analytical model is demonstrated and validated with the test data of the three liquid propulsion stages L110, L37.5 and L40 described in Section 3.2.

3.4.1 Reliability estimation of L110 stage

The reliability analysis of L110 stage with limited test data is used to demonstrate the effectiveness of the analytical model. The model is used to compute the weighting factor to be applied to the test data of L37.5 and L40, and the number of equivalent tests for the L110 stage. Based on the degree of similarity and weighting index assigned, the weighting score and weighting factor computation are illustrated in Appendices A and B. The rationale for finalising the similarity class is explained as follows:

The design related SRIFs are given adequate weighting as per the guidelines discussed in the earlier section. The engine combustion cycle is a key reliability driver. The GG combustion cycle is relatively simple with lower pressures, lower inert mass, but has the disadvantage of lower specific impulse. In contrast, the staged combustion cycles offer much higher performance, but the engines are more complex with its impact on reliability (Zhaofeng Huang, et al., 2005). So, the engine combustion cycle becomes an SRIF. The LRE, in all three stages, work in the GG

combustion cycle wherein operating stresses are benign and so a similarity class of I is assigned. The second key factor for the overall launch vehicle mission is the engine start/shut down transients which are same for all engines as the system is designed either for UH25 depletion or command cut off. Hence, a similarity of Class I is assigned to these factors.

Regarding the engine design methodology, though the engine is same since the stage is engineered with a twin-engine configuration, with two independent propellant tanks and a modified throat insert, a similarity class II is assigned. Being the core stage, L110 engine is subjected to a much higher lift off acoustics compared to L37.5 engines, and hence the SRIF environment level is assigned a Class III. In the case of L40, the environments are comparable with L110 and hence class I is assigned. Traditional reliability enhancement method attempts to reduce the number of components and subsystems by incorporating the state of art design and manufacturing methods. These actions result in a reduction of failure modes related to welds, seals, propellant lines, valves and engine system instrumentation (Aviation Administration, 2005b). Since the number of components in L110 is marginally higher, a similarity class of II is assigned to this factor. In most of the SRIFs related to materials, manufacture, inspection and testing areas, L37.5, L40 and L110 stages have been found to be identical and similarity class of I is assigned.

Many interface and interaction related failure modes such as POGO oscillations, contamination passing from the vehicle to engine, power supply failure, propellant feed line blockage, etc., are major issues in liquid propelled rockets. For example, failure of a liquid rocket stage because of a blockage by a piece of cloth in the liquid engine water cooling system is reported in the literature. Though such failure modes are addressed in the L110 stage by design and process, considering the overall changes in the stage, the similarity for the SRIF, vehicle and engine interfaces is regarded as class II. The materials used, manufacturing processes and the quality systems followed are almost identical for the two stages.

In this case study, the tuning parameter of complexity k_{ij} is assigned a value of 0.8 as per guideline in Table 3.4, since the level of experience of a team is high and the system complexity level is also high. As the new system has undergone comprehensive analysis, testing and evaluation, the tuning parameter of design

verification k_{2j} is assigned a value of 1.2, as per the guideline given in Table 3.5. All the SRIFs have been considered equally important and assigned a c_j value of 1. The w_s variation with w_i , for the finalised values of $c_j = 1$, $k_{1j} = 0.8$ and $k_{2j} = 1.2$ is given in Figure 3.6, and is compared with the reference $w_s = w_i$ model, and the basic w_s model where all the parameters c_j , k_{1j} and k_{2j} are assigned a value of 1.

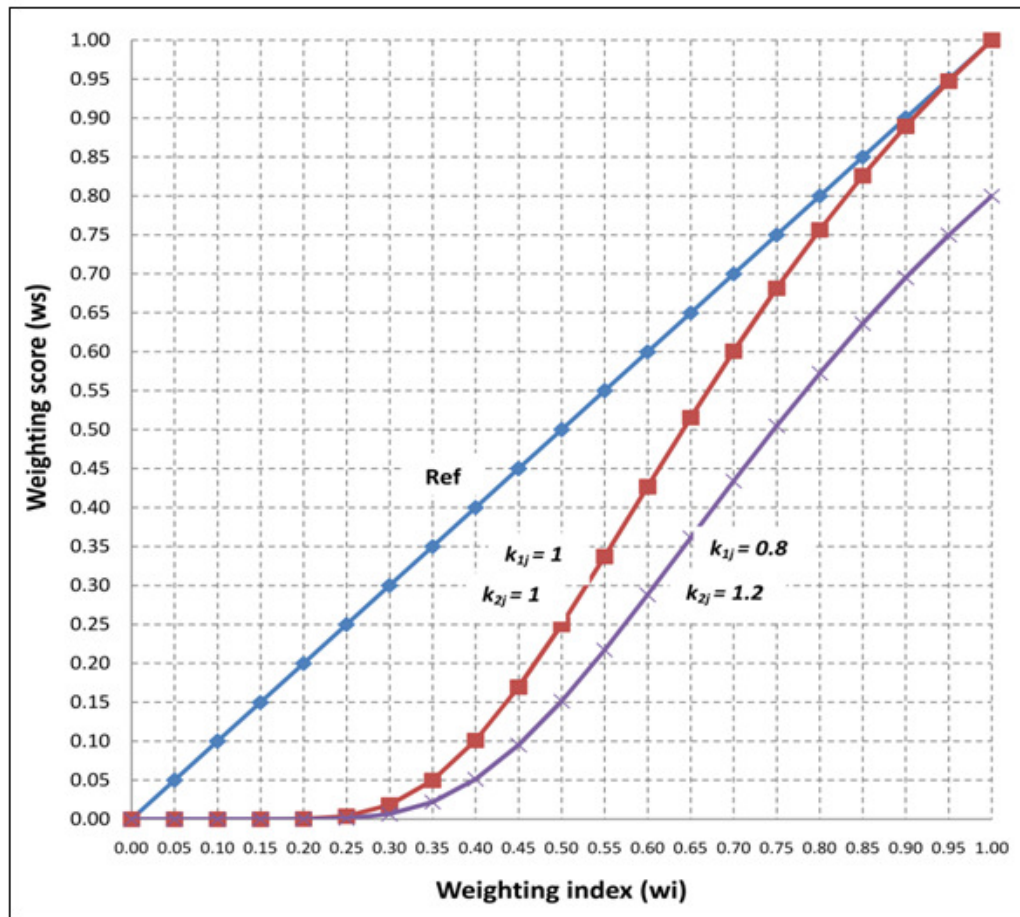


Figure 3.6 Analytical model selected for the analysis with $k_{1j} = 0.8$ and $k_{2j} = 1.2$ in comparison with ref. $w_s = w_i$ and basic model with $c_j = 1$, $k_{1j} = 1$ and $k_{2j} = 1$.

Appendices A and B give the details of the SRIFs selected for study, similarity class between the L110 stage as compared with pedigree systems L 37.5 and L40, weighting index w_i , and the weighting score computed for each SRIFs. The tuning parameter values of $c_j = 1$, $k_{1j} = 0.8$ and $k_{2j} = 1.2$ are used for weighting score computation. The weighting factor computations also are illustrated in the appendices A and B. The computation of the equivalent number of tests of L110 stage, using the test data of the propulsion stages L110, L37.5, and L40, and the weighting factor are explained in Table 3.7.

Table 3.7 Reliability estimation of L110 stage

Sl No.	Stages (Launch Vehicle)	No. of tests (n)	Weighting factor (wf)	No. of equivalent tests
1	LRE of L110 Stage (LVC)	^a (3×2)+8= 14	1	14
2	L37.5 Stage (LVA& LVB)	$n_{L37.5} = 61$	0.605 ^b	36.905
3	L40 Stage (LVB)	$n_{L40} = 46$	0.68 ^c	31.28
4	Total no. of equivalent tests for an LRE of L110 stage {Total (n_e) _{L110} }	81.185		

^a Stage level: 3 tests, equivalent to 6 engine tests + 8 engine level hot tests;

^b Refer Appendix A; ^c Refer Appendix B

In the Table 3.7, the total number of equivalent tests is computed as follows:

$$\begin{aligned}
 \text{Total } (n_e)_{L110} &= n_{L110} + \{(wf_{L37.5}) \times (n_{L37.5})\} + \{(wf_{L40}) \times (n_{L40})\} \\
 &= 14 + (0.605 \times 61) + (0.68 \times 46) = 81.185
 \end{aligned} \tag{3.10}$$

Since there are no failures, $r = 0$, Equation (3.3) becomes

$$R^n = 1 - C \tag{3.11}$$

Putting $n = 81$ and $C = 0.6$ in the above equation, the reliability of one LRE of L110 stage becomes 0.989. Since both engines have to function successfully for mission success, the reliability of the L110 stage with two LREs in series is (0.989×0.989) , ie., 0.978.

3.4.2 Validation of the analytical model

The validation of the analytical model is carried out with a case study of the L40 stage of launch vehicle LVB, for which only limited test data were available when it was newly introduced, but subsequently had sufficient flight data. The number of successful tests for L40 was only 7 before the first flight, which gave only a reliability of 0.877. On the available limited test data of the L40, test data of L37.5, a pedigree

system existing then, is added after applying the wf arrived using the proposed method. The rationale for assigning w_i and weighting factor computation is explained in Appendix C. The value of c_j , k_{1j} and k_{2j} are assigned 1, 0.8 and 1.2 respectively, as followed for the L110 stage case study. The wf is applied to the available number of tests of the L37.5 stage when L40 stage was newly introduced, and an equivalent number of tests for the L40 are found out. Reliability is assessed based on the equivalent number of tests and the details are given in Table 3.8.

Table 3.8 Reliability of L40 Stage based on similarity with L37.5 Stage

Sl. No.	Stages	No. of tests	weighting factor, w_f	Number of equivalent tests
	Assessment for L40 Stage, when it was newly introduced for launch vehicle LVB			
1	L40 Stage	7[when L40 was newly introduced]	1	7
2	L37.5 Stage	16[when L40 was newly introduced]	0.654 ^a	10.464
3	Total no. of equivalent tests for L40 Stage		17.464	
4	Estimated Reliability of L40 (LVB) Stage when newly introduced		0.949 ^b	
Assessment on L40 Stage now (after 10 LVB flights)				
1	L40 Stage	46[Available test data till date]	0.980 ^b	

^aRefer Appendix C

^bReliability computed using Equation (3.11) with $C=0.6$

With the weighting factor of 0.654, the number of equivalent tests of L40 based on 16 number of L37.5 tests is 10.464. This is added to 7 number of qualification tests done on L40 and with a total of 17.464 tests, the computed reliability for the stage is 0.949. The total number of tests available now on L40 stage, after an adequate flight experience, is 46 which give a demonstrated reliability of 0.980. Without considering the pedigree aspects the reliability estimate based on L40 stage tests alone would have been only 0.877, whereas with the new analytical model the predicted reliability is

higher at 0.949 which is closer to the reliability of 0.98 attained after adequate flight experience.

3.5 An over view of the analytical model for reliability analysis

A new analytical model has been formulated for the pragmatic assessment of the launch vehicle systems with limited test data. The proposed analytical model provides a general formalised methodology for the reliability estimation of complex systems with limited data. The model transforms the confidence derived from the operation of similar proven systems, into a quantitative reliability for the new system. The weighting score model is arrived in two steps:

Step 1: Even when systems are designed by an expert team and comprehensive design verification is done, still there could be certain un-contemplated failure modes caused by the changes made from the pedigree system. This aspect is considered in the basic weighting score given by Equation (3.4).

Step 2: When the expertise level of the team is not very high, there are chances of missing some finer aspects of design, particularly when systems are complex. The tuning parameter k_{1j} is used to derate for this uncertainty. In addition, there could be uncertainties because of inadequate design analysis and verification. Derating for this uncertainty is given by k_{2j} . The guidelines set for the identification of SRIFs, and the tuning parameters c_j , k_{1j} and k_{2j} are based on systematic technical evaluation of the systems, thus reducing the subjectivity in assessment.

The reliability of the newly developed L110 stage using three stage level hot tests is found to be only 0.736. The stage elements such as structures and pipelines are comparatively simpler and very high reliability can be ensured by adequate design margins, demonstrating the functional capability and controlling the manufacturing processes to limit the variability in the system realisation. So, the reliability of a liquid propellant stage is predominantly determined by the complex liquid engine with dynamic subsystems. So, with 14 number of engine tests (8 engine level tests and 3 stage hot tests with twin engines) the reliability of the stage is 0.877.

When the assessment is made with the new analytical model considering, in addition to the limited number of test data of L110 engines, the test data available for the flight

proven liquid L37.5 and L40 engines accounting for their similarity with the new stage, the total number of equivalent tests for the L110 engine is 81. The stage reliability computed with this data is 0.978 which truly represented the confidence of the system design team based on qualification of the L110 stage and the experience in the design and operation of L37.5 and L40 stages. Thus, the reliability is assessed pragmatically at 0.978 as compared to the traditional analysis method with test done on new system alone. The L110 stage flawlessly performed in the first two missions of LVC launch vehicle, giving additional confidence in the analytical model.

In the reliability study carried out for the validation of the model, the L40 stage reliability based on its similarity with L37.5 stage has been found to be 0.949 as compared to the reliability of 0.877 computed using the conventional method of reliability assessment. The reason for the marginally lower reliability estimate as compared to the stabilised reliability of 0.98 is due to the fact that L37.5 stage which is the pedigree system also had only 16 number of tests when L40 was introduced. In cases, where the pedigree system has a large number of test data, the assessment has given more accurate results giving adequate confidence in the new system.

The step by step procedure of the new analytical model has been found to act as a checklist for the experts, to think and consider in a systematic manner various aspects of the two systems such as the degree of similarity between the systems, complexity of the systems, the experience of the design team, the rigor of design analysis and testing carried out pertaining to each of the finalized SRIF. Though the overall confidence in the system varies among the experts, their assessment on technical parameters is found to be consistent and convergent. Thus, the method reduces considerably the subjectivity of assessment found with the expert opinion method and the Bayesian approach, resulting in a more accurate assessment of the reliability of the system. The method facilitates proper understanding of the practical aspects of the engineering problem, and hence is easy to comprehend by all the concerned engineers. Therefore, the model generates accurate data for the new system based on tests done on the proven systems. The data is used in the statistical formula for computing the binomial one-sided lower bound for reliability. Thus the analytical model complements the statistical method of computing the minimum bound on reliability to get an accurate reliability estimate. Such physics based approach, when

combined with statistical models give more confidence in the outcome of the statistical analysis.

The method has also the advantage of being generic in nature. In the present problem, it is applied to assess the reliability of liquid propulsion stage, but can be applied to any other aerospace systems like solid propulsion system, control system or a pyro system. Though the problem of reliability analysis with limited data is critical for space systems, it is a generic issue prevalent in many industries, and the analytical model is quite useful for assessing reliability for such systems also. The method though is very helpful when the test data is limited, it can be applied to systems with a large number of test data also, with more optimistic values assigned to the tuning parameters.

It is similar to the Bayesian approach as it can provide a justification for the lesser amount of reliability testing, but satisfactorily overcomes the disadvantages of Bayesian approach, viz., the subjective assessment of the prior statistical distribution, and not accounting the evolution of different systems and similarities of the system with the proven systems. The method contributes to cost saving and meeting the schedules, by pragmatically assessing the reliability test requirements by giving accurate weighting given for tests done on the proven system.

CHAPTER 4

FAILURE MODE AVOIDANCE OF CONTROL ACTUATION SYSTEMS

4.1 Introduction

Control actuation systems are used for attitude control of launch vehicles. They are closed loop position servo systems, vectoring the engine or nozzle of the rocket based on commands from the onboard computer (Jaya Balakrishnan et al., 2010). Electro hydraulic actuators are used for launch vehicle control actuation systems worldwide because of high power and mass savings. The schematic of the actuation system is given in Figure 4.1. The major subsystems are gas motor, pump, reservoir, accumulator, servo valve and hydraulic actuator. The hot gas from the gas generator of the liquid engine is used to drive the gas motor which in turn runs the pump. The hydraulic pump delivers the oil stored at a low pressure of 11 bar to the high pressure side of the hydraulic circuit at 210 bar. The hydraulic pump is an axial reciprocating piston pump with rotating pistons. It draws the oil during the pull (retraction) stroke and expels oil during the push (forward) stroke.

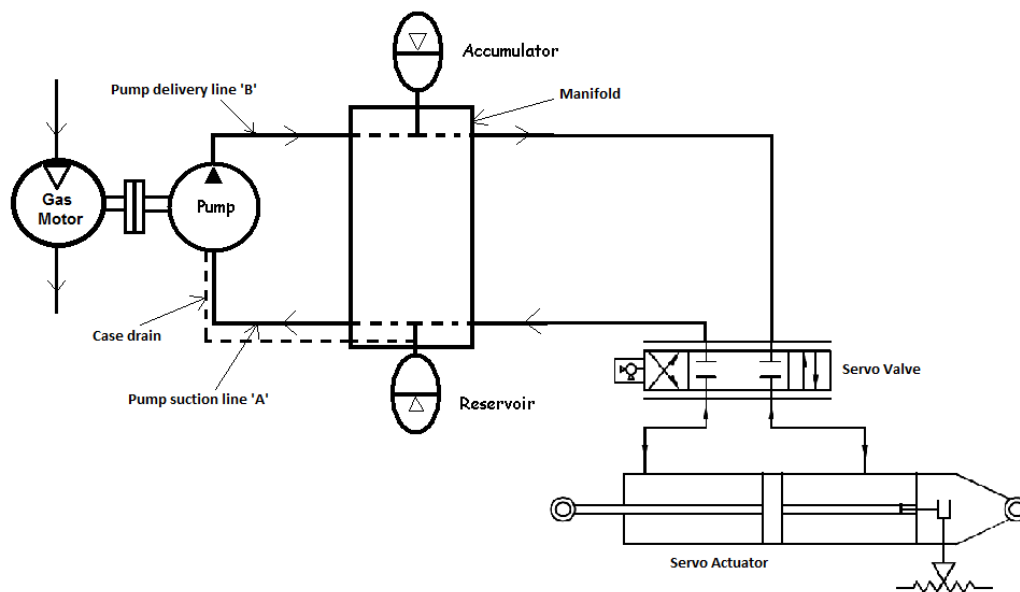


Figure 4.1 Schematic of electro hydraulic Actuation System

The subsystems in the control actuation systems such as the gas motor, pump, servo valve, accumulator, reservoir, and servo actuator are dynamic subsystems with a large number of critical failure modes and failure mechanisms. Therefore, it is of paramount importance to avoid these failure modes by appropriate measures of correction and mitigation during the design, manufacturing, qualification and acceptance testing phases of the system.

Failure mode avoidance comprises of making the design robust and realising the flight systems as designed without any mistakes. Design robustness can be built in the systems, by understanding the failure mechanisms under various environments, and by widening the operating range of systems through design solutions (Don Clausing and Daniel Frey, 2005). Flawless realisation of flight systems as designed requires dedicated efforts towards ensuring zero defect through implementation of stringent quality systems in each phase of realisation like manufacturing, inspection, testing and certification. This chapter, organised in two sections, presents the failure mode avoidance strategies of a control actuation system with a case study of the gas motor subsystem.

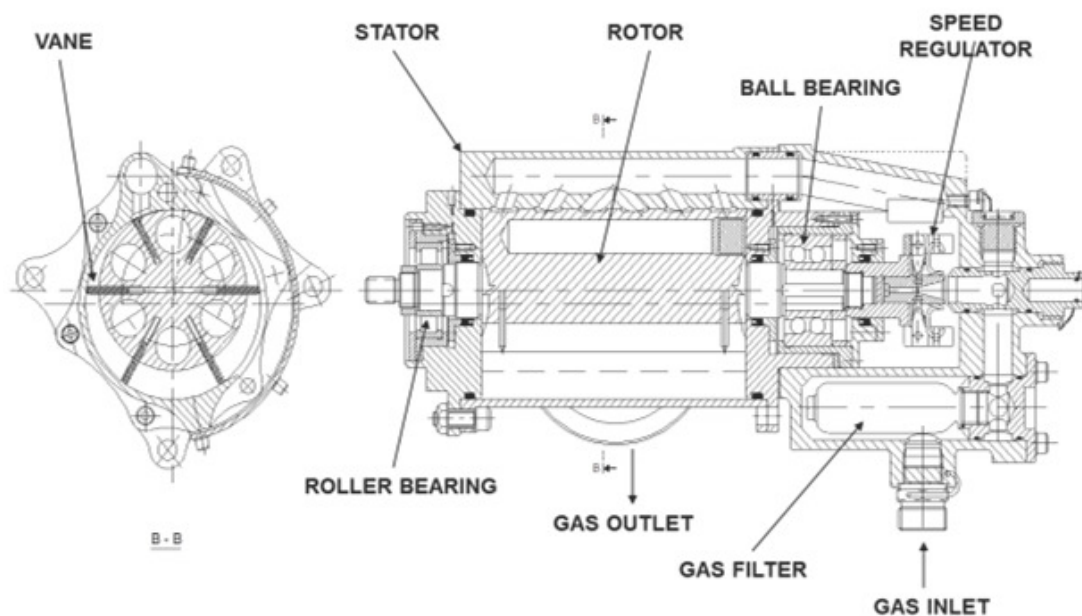


Figure 4.2 Schematic of gas motor system

The schematic of the gas motor is shown in Figure 4.2. The gas motor is of vane type with speed regulation by a centrifugal governor. The gas motor comprises of a

circular rotor, with six slots for vanes, positioned with an offset on the stator. The hot gas at 36 bar and 630°C is drawn from the liquid engine turbine inlet manifold, and the temperature is reduced to the required level of 225°C in a thermal regulator, with a maximum allowable temperature of 275°C. The gas at 225°C enters the vane chamber through a speed regulator. The vane chamber is enclosed by adjacent vanes, rotor and stator. The difference in pressure between the adjacent vane chambers exerts a net force on the vane which acts about the rotor centre to generate a torque causing the rotor to rotate. As the rotor rotates the hot gas expands, and after the required level of expansion, the gas exits through the gas outlet. The speed of the motor is regulated by a spring type centrifugal governor. As the speed increases, due to centrifugal action, the plunger moves towards the gas inlet nozzle and causes the gap to reduce. This reduces the flow of the gas into the chamber of vanes, thereby controlling the speed. The rotor is supported by a double row angular contact ball bearing at the regulator side and a cylindrical roller bearing at the pump coupling side. The gas motor runs at a speed of 4800 rpm and drives the pump, which sustains high oil pressure of 210 bar at the inlet of the servo actuator.

Section 4.2, presents a detailed investigation, through analysis and experimentation, of a failure in one of the critical parts of the gas motor system namely the double row angular contact ball bearing. Through the failure analysis, this section brings out the strategies to be adopted to avoid the failure modes of the bearing in the design, manufacturing, inspection, assembly and testing phases of the product life cycle. Section 4.3 presents severe environmental stress testing carried out on the gas motor at system level, inducing the failures which led to better understanding of the physics of failures. Consequently, pertinent design and process solutions could be taken in the early design phase to make the design robust.

4.2 Failure mode avoidance of gas motor bearing

The gas motor is a rotating machinery with a number of dynamic parts. In rotating machinery, rolling element bearings are employed to allow the relative motion and support the rotor shafts on the housings considering their load carrying capacity and friction characteristics (Upadhyay et al., 2013). The rolling element bearing faults are one of the primary causes of breakdown in rotating machinery (Feiyun Cong et al., 2013). The bearings will survive the predicted fatigue life, under ideal operating

conditions. However, in service, bearings are subjected to harsh environments such as thermal, vibration and impact loading. The bearing can fail due to various reasons such as wrong selection of bearing with respect to the type and load rating, inadequate lubrication, and the environmental conditions (Gurumoorthy et al., 2013). In most cases, bearing failures are encountered because of noncompliance with recommended practices. So, an accurate definition of the bearing loads, environments, design and selection of suitable bearing for the application, and proper installation in the field are critical to prevent failures in bearings.

The rotational speed of rotor at no load condition is 4800 rpm and because of the oscillations due to hot air dynamics it can go up to 5000 rpm. The rotor is supported on two bearings, as shown in Figure 4.2. A double row angular contact ball bearing is used as a locating bearing on the regulator side, and a roller bearing is used at the other side to allow for the thermal expansion of the rotor. Angular contact ball bearing has the ability to support combined axial and radial loads, by incorporating a contact angle between the balls and races. It also has high durability and low friction. Considering these special features it is widely used in aerospace applications (Bugra Ertas and Hohn Vance, 2014; Ronald Widener, 1986; Tedric Harris and Michael Kotzalas, 2007b). Dynamic seals are provided on the sides of the bearing to prevent hot gas entry into the bearing area. Operating conditions such as higher speeds, heavy and complex loading and extremely low and high temperatures, along with inappropriate assembly or operation of the machinery are identified as the potential failure causes of premature bearing failures (Tedric Harris and Michael Kotzalas, 2007a). In this section, a failure observed in the double row angular contact ball bearing during the acceptance test program is analysed for the above failure modes, the root cause of the failure is identified and the failure avoidance strategies to prevent such occurrences are addressed.

4.2.1 Bearing selection and failure observed

The double row angular contact ball bearing, with a split inner race, an integral outer race, the rolling element namely the balls, and the cages for retaining the rolling elements as shown in Figure 4.3a, has been selected to precisely locate the bearing on the shaft. The bearing is a standard product from a reputed manufacturer. The duplex bearing in back to back arrangement has a gap between the inner races known as

preload gap. When clamped axially the gap is closed developing a preload on the bearing. The preloaded bearings provide a higher bearing stiffness, better positioning accuracy and lower torque variability (Videira et al., 2013). With higher contact angle, the bearing can take heavier axial loads. The selected bearing has a contact angle of 15° .

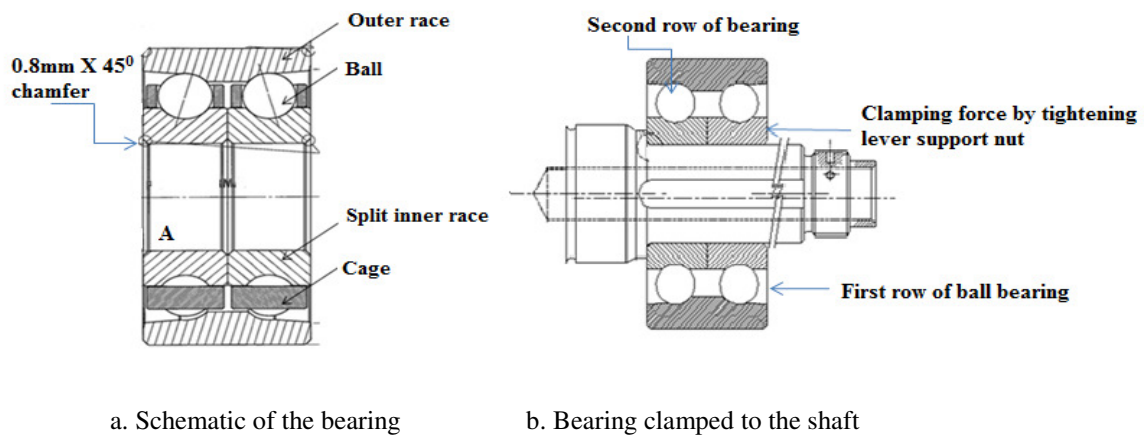


Figure 4.3 Double row angular contact ball bearing

The adequacy of the design has to be verified by system level bearing tests in the flight configuration simulating the flight environmental conditions on a number of system hardware covering a full range of tolerances, especially the diametral clearances (Ronald Widener, 1986). The test matrix is given in Table 4.1.

Table 4.1 Flight acceptance test matrix for the gas motor

Sl. No.	Test	Duration	Remarks
1	Performance test in cold gas	10 minutes	Performance test is done to evaluate the Speed-Torque characteristics
2	Cold gas Run-in test	2 hrs	
3	Performance test in cold gas	10 minutes	
4	Performance test with hot gas	3 minutes	
5	Performance test in cold gas	10 minutes	

The qualification tests include tests with ambient air and hot air. The gas motor performed normally till the performance test with hot air (Table 4.1, Sl. No. 4). During the final cold gas run after the hot test, the motor indicated large variations in speed and suspecting a failure, the test has been aborted. The gas motor has been disassembled from the test setup to make detailed observations. The rotor is verified for its free rotation by hand. The rotor is found to have an intermittent rotation, indicative of a malfunction of one of the bearings.

The system has been disassembled to have access to the angular contact ball bearing. During the bearing assembly over the shaft, the tightening of the interface nut known as lever support nut, develops a clamping force of 20 kN at the inner race and keeps the bearing in place with the rotor shoulder as shown in Figure 4.3b. The bearing row closer to the lever support nut which applies the clamping force on the inner race is henceforth referred as the first row and the row closer to the shaft shoulder is referred as the second row of the bearing, as shown in Figure 4.3b, in further discussions. The lever support required a higher torque for disassembly, but no damage is observed in the thread. On disassembly, failure has been observed in the angular contact ball bearing as shown in Figure 4.4.

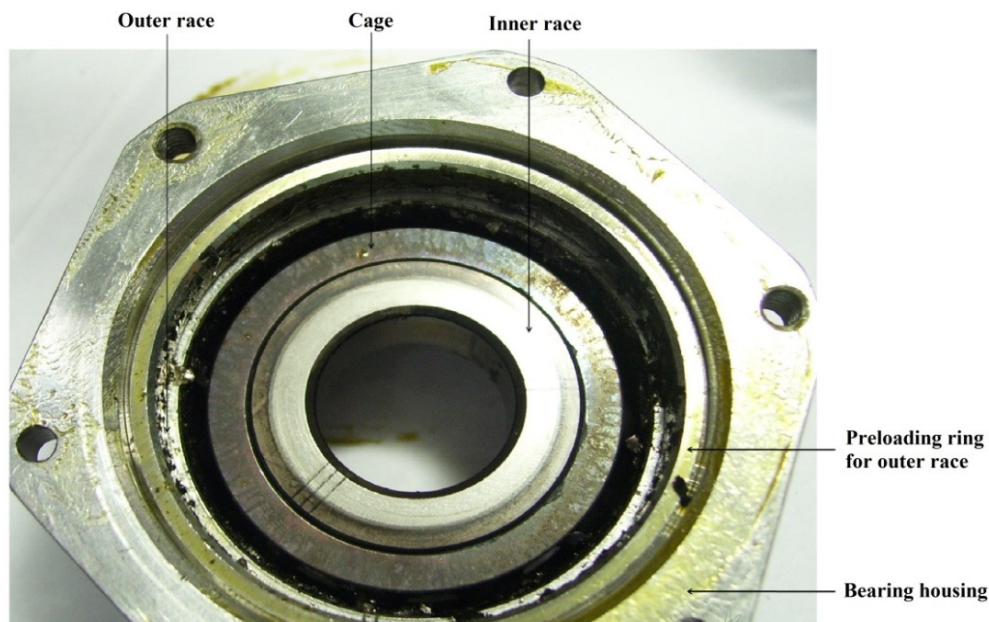


Figure 4.4 Digital photograph of the bearing after failure

The failed bearing has been inspected visually and the observations have been recorded using a digital camera. The parts of the bearing are captured in Figure 4.5. The inner race, cage and balls of the second row of bearings have been found in good condition without any discolouration. The degraded grease and a little metallic debris during disassembly are kept on the bearing holder, and shown in Figure 4.5.

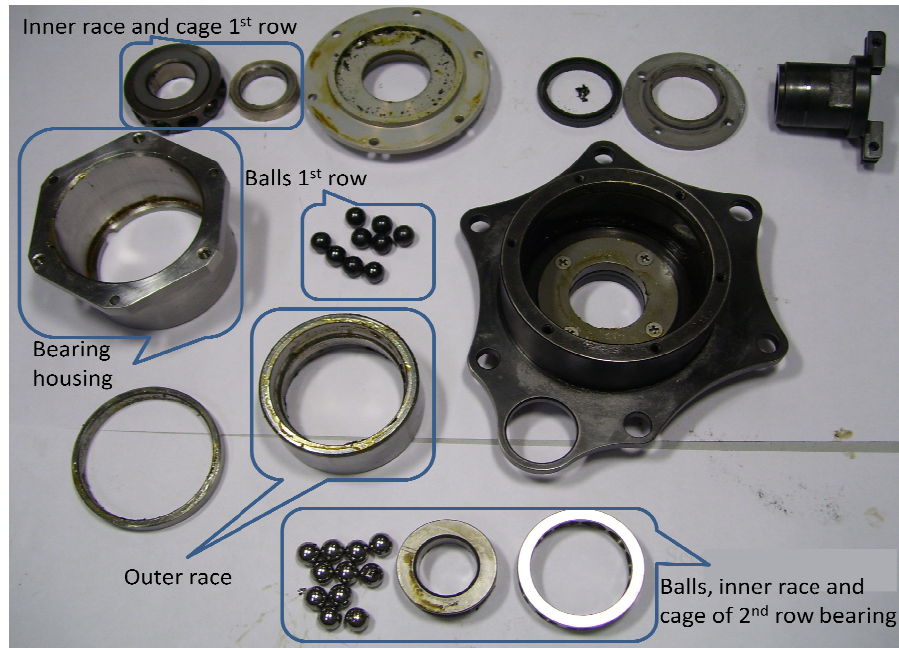


Figure 4.5 Bearing parts after failure

The inner race, cage, and the balls of the first row of the bearing are found in the discoloured condition as shown in Figure 4.6. The cage could not be separated from the inner race.



Figure 4.6 The inner race, cage and balls of first row

The two rows of bearing are compared in Figure 4.7. Figure 4.7a shows the clean second row of balls, 4.7b shows discoloured first row of balls and 4.7c shows the comparison of inner race and cage of two rows of bearing. The discoloured race and cage belongs to the first row of the bearing.

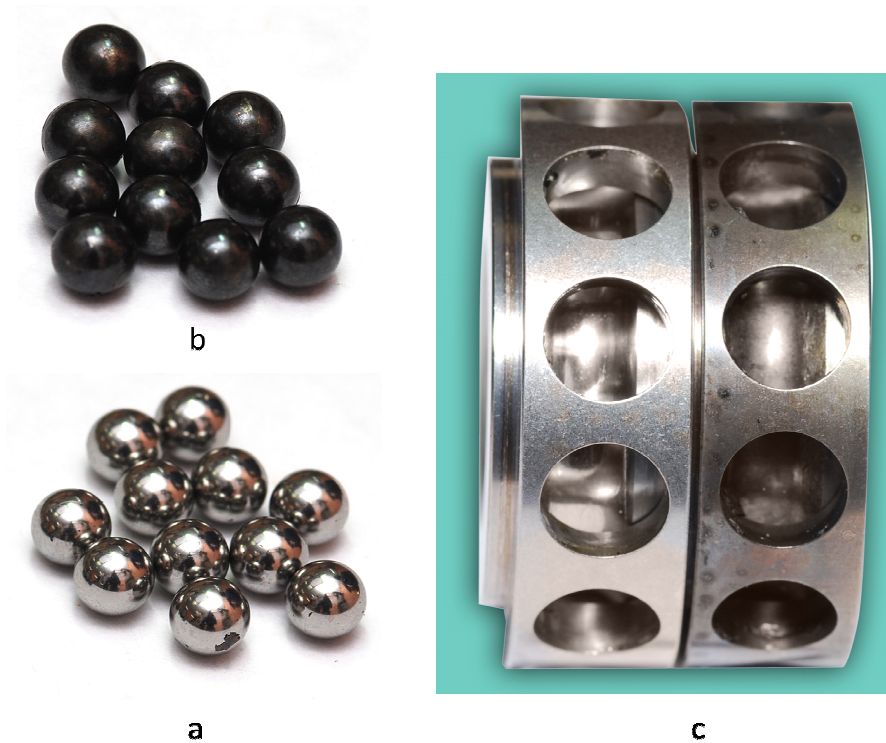


Figure 4.7 Comparison of the of the two rows of bearing

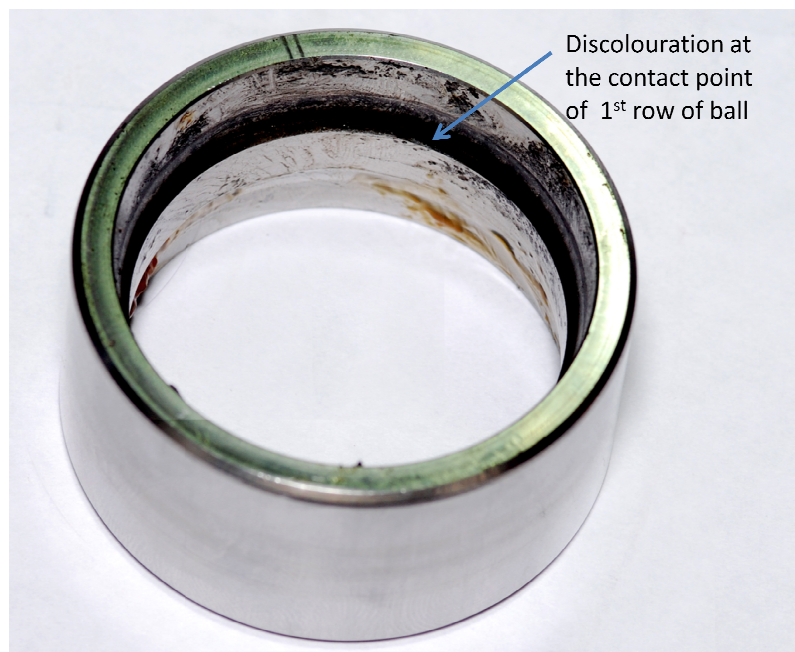


Figure 4.8 Magnified view of outer race

The photograph of the outer race is shown in Figure 4.8. The discolouration is observed circumferentially in the outer race where the first row of balls contacts with the outer race. Patches of discoloured grease is seen in this location. Portions of the outer race in contact with the second row of balls have been found to be normal. The dynamic seals provided in the assembly to prevent hot gas entry into the bearing have been found in good condition as shown in Figure 4.9. All other parts of the gas motor are found to be in normal condition.



Figure 4.9 Dynamic seal of the bearing in good condition

4.2.2 Failure analysis

The duplex bearing with split inner race has been selected as they have better stiffness and can withstand higher vibrations experienced by launch vehicle systems without any damage to its parts. The preload of 200 N developed in the bearing during its assembly with shaft eliminates both radial and axial internal play. Therefore, after assembly the radial and axial clearances become zero. However, this has a negative aspect also. As there is no axial or radial clearance, they are more rigid and any variation in dimensions and the consequent fit at the interface can directly influence the contact stresses. The radial force due to the circumferentially varying gas pressure acts on the rotor and is reacted by the ball and roller bearings. The axial force due to the gas pressure is resisted by the ball bearing alone. The failure modes and the mechanisms of failure that can lead to the observed failure are studied through detailed investigations and the failure causes have been eliminated one by one by

technical reasoning to finally converge on the root cause as explained in the following sections.

Improper design and selection of bearing

The bearing selected for the application shall have adequate margins with respect to load rating and the materials of construction shall be capable of withstanding the operating environments. The bearing shall also be properly mounted in the shaft and housing. The gas motor is run by the hot gases from the gas generator of the liquid engine. The temperature of the hot gas fed to the gas motor vary from 225°C to 275°C. Considering the thermal loading, one of the bearings has to be non-locating and for this purpose, cylindrical roller bearing is selected at one end and it takes only the radial loads. Angular contact ball bearing is selected for supporting the rotor at regulator end to carry both the axial and radial forces caused by the vehicle acceleration and the varying pressure distribution around the circumference of the rotor. The load computation and the load rating have been revisited and the bearing is found having sufficient margins with respect to the load rating, as shown in Table 4.2.

Table 4.2 Bearing Design load requirement and the Capability

Load	Requirement	Load rating
Dynamic (kN)	14	22
Static (kN)	5	18

The selection of ball bearings with pre loadable split inner race is found to satisfy geometric and load requirements of gas motor assembly. The selection is also found to be a good choice considering the high vibrations experienced by the control actuator at lift off and during the launch. The bearing material has to meet stringent requirements such as high strength, resistance to wear, high-temperature hardness, dimensional stability and corrosion resistance (Feiyun Cong et al., 2013). The bearing material used namely X40CrMoVN16.2 (XD15 NW) have been found meeting the requirements. Considering the heating due to high temperature gases, the bearing cage should have the capability to withstand higher temperatures. The bearing cage

material is made of AISI 440C. Considering all the above aspects, the bearing selection is found to be satisfactory for the application.

Thermal imbalance

During the operation of machinery, the bearing temperature has to be limited within the constraints of the materials of the bearing parts. Furthermore, the temperature gradient between the bearing races, has to be maintained in such a way that radial preloading does not happen (Tedric Harris and Michael Kotzalas, 2007a). During the functioning of the gas motor, the bearings get heated by the combined effect of the rolling friction between the inner race and the balls, convective heating of the rotor by the hot gases, and the radiative coupling between the hot stator and the rotor. Correct assessment of the temperature of various parts of the system by detailed modelling and experimentation is essential to study the effects of thermal load on the system (Keiji Mizuta et al., 2003). The thermal analysis is carried out using an axisymmetric model of the ball bearing, to assess the temperature at different locations of the bearing. The Finite Element (FE) model of the rotor assembly with bearing is shown in Figure 4.10.

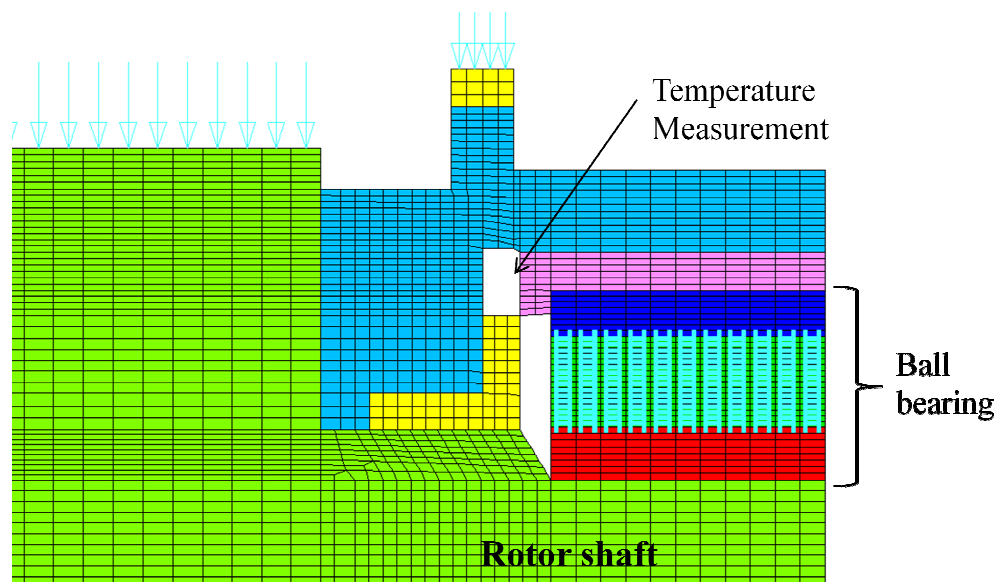


Figure 4.10 Finite element model of the ball bearing

Three levels of experiments have been carried for generating inputs for thermal analysis and validating the thermal model. The validated model is then used to predict the temperature at different locations for various operating conditions. First, the

bearing with the lubricant, with ends closed by the insulating tiles, has been heated with heater tape at the outer race and the temperature has been monitored on both the races. Thermal conductivity value obtained from the test is 1.07 W/mK which is used in the thermal model. Second, the bearing is run at 5000 rpm by an external source for a duration of 200 s and a temperature difference of 1.1°C has been observed between the inner and outer race. The thermal model could capture the difference in temperature, validating the model. Further, the gas motor level test has been carried out with the inlet hot air at 300°C with temperature monitoring at stator and a location close to bearing as shown in Figure 4.10. As the test is carried out at the gas motor level, the inner and outer races could not be accessed for instrumentation and wire harnessing. The pressure of air after the expansion is about 11 bar and the gas temperature after speed regulation is 258°C. This has been then compared with the results of analytical model.

The following empirical relation is used to estimate the heat generated due to the rolling friction between the balls and the races (Keiji Mizuta et al., 2003).

$$Q_b = 0.126 (4.5N^{0.1} + 33 \cdot 10^{-6} N^{5/3}) F_a^{0.3} \quad (4.1)$$

The ball bearing frictional heat (Q_b) generated is assessed for a rotor speed of 5000 rpm (N), which includes the speed oscillation of 200 rpm about the mean no load speed of 4800 rpm, and an axial load of 5 kN (F_a) corresponding to the test condition. The heat load is found to be 96 W. The heat transfer rates on the rotor are estimated using engineering correlation for a rotating cylinder.

The initial temperature is 30°C and the pressure of air after the expansion is about 11bar. The gas temperature after speed regulation is 258°C corresponding to an inlet gas temperature of 300°C. Convective heat transfer coefficient computed on the rotor at 30°C at 11bar is 1847.4 W/m²K and at 258°C is 1381 W/m²K using air properties. As the temperature of gases has approximately a linear variation with time, an average heat transfer rate of 1614.2 W/m²K is considered. Heat transfer coefficient is high, as it is a rotating cylinder and heat transfer will be through forced convection. The predicted temperature at the thermocouple location using the model and the measured temperature in the gas motor level test at this location are found having a good match as shown in Figure 4.11.

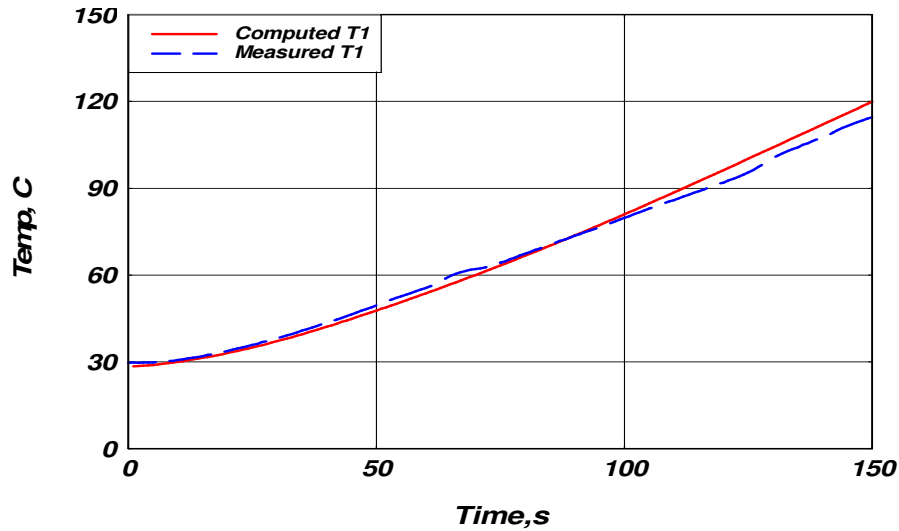


Figure 4.11 Validation of thermal model: computed and test measured temperatures

The thermal model validated with experimentation has been used for the analysis and temperatures at the shaft centre, bearing inner race, outer race and housings are computed, and given in Table 4.3.

The maximum temperature in the bearing is only 160°C for the period of operation of the failed bearing, and the temperature gradient between the inner race and the outer race is only 3°C, all within the specifications of the temperature constraints of bearing materials. The dynamic seals provided in the assembly to prevent hot gas entry from regulator side as well as from the vane chamber side have been found intact (Figure 4.9), indicating that there is no direct convective heating by the hot gases on the bearing. From all the above observations and the predicted temperature on the bearing parts, it is concluded that the heating due to the gas motor operation during the tests is not the cause for the failure.

Differential thermal expansion at the bearing interfaces

The differential thermal expansion at the bearing interfaces can cause increased loading of the rolling contact elements, resulting in increased friction leading to higher temperatures and bearing seizure (Tedric Harris and Michael Kotzalas, 2007b; Gurumoorthy et al., 2013). Differential thermal expansion of the rotor, the bearing races, and the housings, during the operating conditions of the gas motor can affect the fit at the interfaces, and could cause additional radial loads on the rolling elements. The clearances after thermal expansion have been assessed, considering the

actual hardware dimensions. The materials used for bearings and rotor, their coefficient of thermal expansion, the temperature of these parts from the thermal analysis, and the computed interface clearances are given in Table 4.3.

Table 4.3 Clearance at the bearing interfaces

Parameter	Shaft	Inner Race	Outer Race	Housing
Material (AFNOR)	Z15CN1703 (AISI 431)	X40CrMoVN16.2 (XD15 NW)	X40CrMoVN16.2 (XD15 NW)	Z15CN1703 (AISI 431)
Interface dia. D, mm	17.002	16.995	46.996	47.004
Temp, (T) , °C	159	160	157	155.8
$\Delta T = T - T_a$, T_a : Initial temperature	129	130	127	125.8
Coefficient of thermal expansion α mm/mm/°C	10.8×10^{-6}	10.4×10^{-6}	10.4×10^{-6}	10.8×10^{-6}
Dia. mm, after thermal expansion, $D(1 + \alpha \Delta T)$	17.0257	17.018	47.0581	47.0678
Clearance, mm	-0.0077 ^a		+0.0097 ^b	

a) Negative sign indicates interference of 7.7 μm shaft-inner race interface

b) Positive sign indicates clearance of 9.7 μm at outer race - housing interface

The measured Outer Diameter (OD) of the rotor shaft is 17.002 mm and the Inner Diameter (ID) of the bearing inner race is 16.995 mm, leading to 7 μm interference in this interface at standard room conditions. The interference at the interface is found to increase from 7 to 7.7 μm due to thermal expansion. The clearance at the outer race to housing interface is found to increase from 8 μm to 9.7 μm which is normal. The difference in the coefficients of thermal expansion of the materials is very small in the operating temperature range. Therefore, the observed increase in the interference at

the shaft outer diameter to bearing inner race interface, due to the increase in temperature caused by the normal operation of the bearing, is only 0.7 μm . Hence, the thermal expansion at the interface can be ruled out as the cause of failure.

Improper bearing lubrication

The rolling contact surfaces of a bearing are separated by a thin fluid layer of lubricating film or grease, which enhances the bearing life (Tedric Harris and Michael Kotzalas, 2007a; Gurumoorthy et al., 2013). The separation of the contacting surfaces by a thin oil film reduces the metal to metal contact and prevents excessive heating, acting as a lubricant (Ronald Widener, 1986). The major cause of failure of the lubricating oil or grease is the thermal environment. Bearing grease is synthetic hydrocarbon oil thickened with Microgel[®], qualified as per MIL-PRF-81322 F (1998), with an operating temperature range of -65°C to 204°C. The selected oil is useful for applications with high bearing loads and wider operating speeds and temperatures. In a hot gas test with normal assembly, the bearing temperature after 180 s duration is about 160°C, which is well within the grease capacity. Also, quality of grease after 200 s duration hot test with a normal bearing assembly has been found satisfactory. Hence, the bearing failure cannot be attributed to the wrong selection of the bearing lubricant.

Fatigue and corrosion

A rolling element bearing has a limited service life. Even when the bearings are operated under the recommended conditions of load, speed and lubrication, failure will ultimately result by some process such as fatigue or corrosion. The bearings used have been new, protected with grease and free from any corrosion when taken up for qualification. The number of cycles of operation has been much less than the designed life. Failure signatures indicative of fatigue or corrosion have not been found in the failed bearing. Considering these aspects, fatigue or corrosion are ruled out as the failure cause.

Fretting and wear

The incomplete contact and slight movement due to vibration between bearing rings and seat, and movement due to shaft bending can cause a chemical reaction on the surfaces in relative motion known as Fretting (Tedric Harris and Michael Kotzalas,

2007a; Ronald Widener, 1986). In this case, as the bearing inner rings are assembled with the rotor with the interference and adequate preload is given for clamping, the movements are not feasible. Though the bearing housing hardness is only 34 HRC as compared to the minimum requirement of 40 HRC as per NASA-SP-8048 (1971), this is acceptable as the maximum gas motor speed is only 5000 rpm while the NASA standard is meant for bearings running up to 50000 rpm. The bearing outer race, inner race and their interfacing elements have been found to be free from the rubbing marks typical of fretting.

The wear can be due to the rubbing contact between the contact surfaces or can be caused by extraneous hard particles. The severe wear or galling results in a phenomenon known as smearing due to the transfer of material from one surface to its contacting surface because of the high friction shearing forces. The smearing damage typical of the wear process is not reflected in the races of the failed bearing. Also, the rolling element bearings can withstand considerable wear before they become unsuitable for operation (Tedric Harris and Michael Kotzalas, 2007a; Ronald Widener, 1986). Considering the above points wear is ruled out as a failure cause.

Higher vibration and resonance

When the excitation frequency from the gas motor assembly coincides with the natural frequency of the bearing, it could cause resonance, resulting in high dynamic load on bearings. To study this gas motor has been operated at different speeds from 2000 to 5000 rpm with vibration monitoring at both the bearing location. There have been no significant vibration responses seen at the bearing frequency of 525Hz, which is indicative of absence of any resonance, thereby ruling out vibration as the cause of failure.

Contamination

Contamination is always a source of failure in a rolling element bearing. A contaminant getting entrapped between the surfaces of rolling contact can cause severe indentations on the surfaces and hard contaminants can cause plastic deformation around these indentations affecting the life of the bearings (Feiyun Cong et al., 2013). As the bearings have been fresh and assembly is carried out with care in a clean room, this possibility is very remote. Also, the assembly has undergone a

majority of the acceptance tests satisfactorily before the failure. Further, indentation marks, an indication of contamination, are not seen on the rolling elements. Hence, contamination as a cause is ruled out.

Impact due to higher preload

The angular contact ball bearings are preloaded to remove the play between the balls and the rings. This is essential in the bearing for space applications to withstand the flight vibrations. However, a very high preload stresses the balls and can cause premature failure. In the case of the angular contact ball bearing with the split inner ring, the bearings are matched pairs with built-in preload. The outer race being integral element the bearing clamping load F_{CB} is reacted by the bearing housing and no load gets transferred to the balls as shown in Figure 4.12. Hence, The load path is F_{CB} - R_1 , as shown in Figure 4.12a and Figure 4.12b.

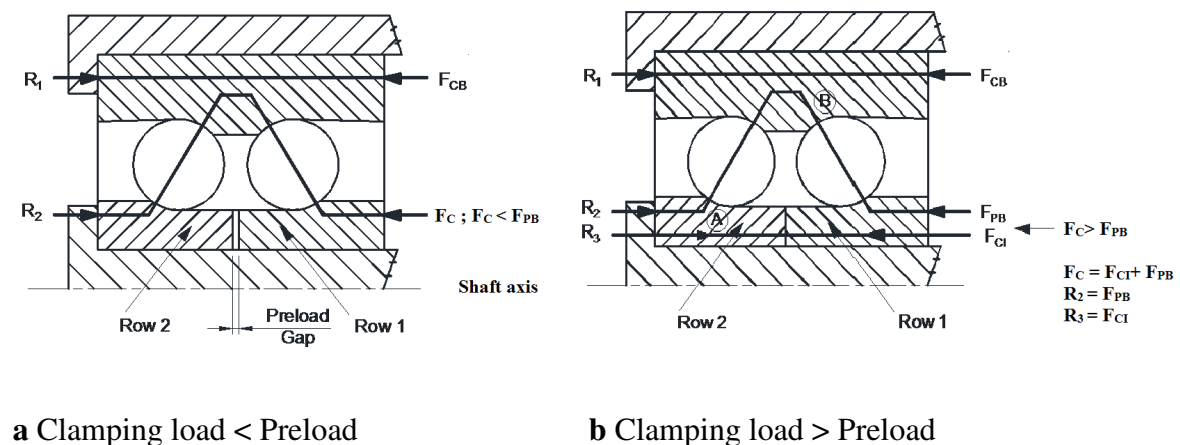


Figure 4.12 Bearing clamping load path and the preload

Inner races are ground to precision to maintain a preload gap as shown in Figure 4.12 a. The bearing inner race, after assembly over the shaft shoulder, is clamped by tightening the lever support nut to 47 Nm torque and this generates an axial force F_C of 20 kN at the inner race interface, as shown in Figure 4.12 a. The bearing preload F_{PB} is 200 N. When the inner race is tightened with a clamping load of F_C less than F_{PB} the load is transferred through the balls and outer race, and then to the inner race, along the load path F_C - R_2 , as shown in Figure 4.12 a. The additional clamping loads more than the preload F_{PB} , must pass through the bearing interfaces and not the balls (Videira, 2013). When the clamping load F_C becomes equal to the preset bearing preload F_{PB} of 200 N, the preload gap in Figure 4.12 a. becomes zero and the rest of

the load passes through the load path $F_{CI} - R_3$, as shown in Figure 4.12b. As the bearing is designed for the preload and is calibrated for the same, failure due to higher preload by the normal assembly process is not expected.

Improper fit, rotor misalignment

An oversize shaft or undersize bore results in an excessive press fit, and causes substantial reduction of bearing internal clearances. This leads to bearing tightness and radial preloading. This can cause higher rolling element raceway loading, higher friction and high temperatures (Tedric Harris and Michael Kotzalas, 2007a; Franz Josef Ebert, 2010). The shaft diameter $\Phi 17$ (-0.004,-0.014) with the inner diameter of the bearing inner race of $\Phi 17$ (-0.005) causes a maximum of 1 μm interference. The measured diameter of the shaft after machining and final grinding operation is found to be 17.002 mm. This causes an interference of 7 μm with bearing ID of 16.995 mm. Another problem in the acceptance procedure of the shaft has been that the shaft is machined and ground, the dimensional measurements are made, conformed to specifications and subsequently a case hardening treatment is done to increase the surface hardness. The case hardening process adds a thickness of 5 μm on the shaft outer diameter leading to additional 10 μm diametral interference, which is not considered in the design and the acceptance procedure of the shaft. Therefore, the diametral interference of 7 μm observed based on the measurements made at the machining stage has increased to 17 μm due to the case hardening treatment. The interference caused due to differential thermal expansion by virtue of the normal gas motor system operation is 0.7 μm as discussed in Table 4.3. Thus, there is a total diametral interference of 17.7 μm during gas motor operation with hot air.

The shaft shoulder is given an undercut or a fillet, at the bearing seating surface, for proper seating of the bearing. The fillet radius at the shaft shoulder should be less than the bearing corner radius to ensure proper seating (Bugra Ertas and Hohn Vance, 2014). However, in this assembly, the fillet radius is R1 in the shaft shoulder, and the corresponding chamfer in bearing is $0.8 \times 45^\circ$. This leads to an improper seating of bearing inner race on the rotor. The fillet radius on the rotor has been finalized based on the dimensions of an earlier selected bearing, which is not updated subsequently corresponding to the chamfer in the new bearing. A small step of 10 μm is also observed at the end of R1 fillet of the failed rotor. The effect of the dimensional

mismatch due to the R1 fillet radius and the fault of 10 μm step has been studied by generating a 3D model of the shaft and the bearings taking into account all the geometric features. The 3D model has been then converted to a Finite Element model through Hypermesh. The photograph of the shaft, its FE model and the zoom of the model with shaft fillet radius and the fault of 10 μm step are shown in Figure 4.13.

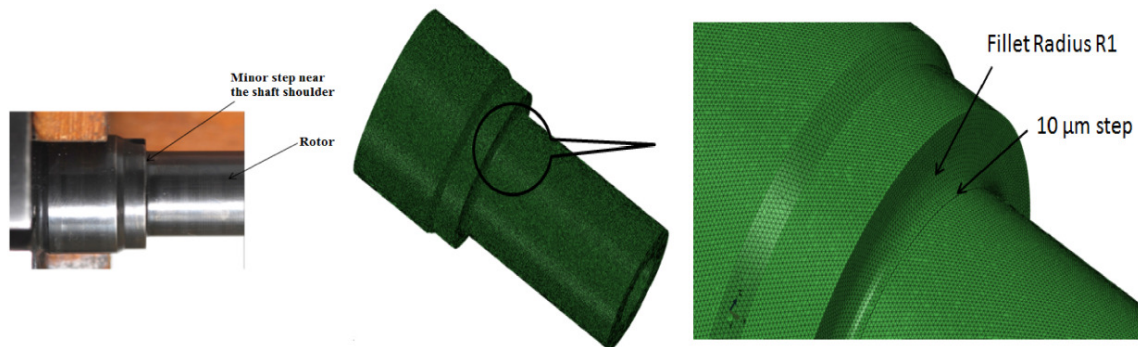


Figure 4.13 Finite element mesh of the rotor shaft and the 10 μm step at the shaft shoulder

The shaft has been modelled using tetrahedral element of 10 μm mesh size to capture the effect of the 10 μm step. The inner race has been modelled by an eight noded linear brick element of mesh size 0.2 mm to capture the effect of the $0.8 \times 45^\circ$ chamfer. The inner race model and the zoomed view of the $0.8 \times 45^\circ$ chamfer are shown in Figure 4.14.

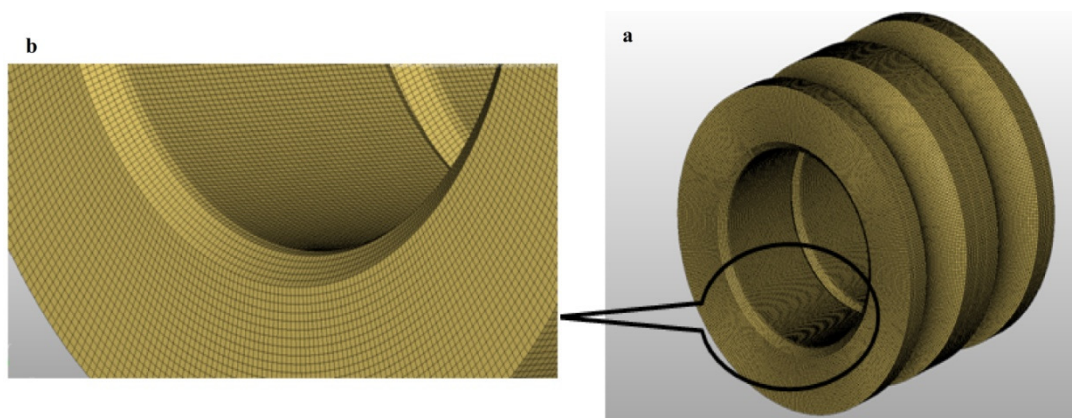


Figure 4.14 FE mesh of the inner race (a), and the zoomed view of the 0.8 mm \times 45° chamfer (b)

The shaft OD and the bearing ID, both have been made 17.002 mm, making the interface diametral clearance zero to enable the assembly in the model. The assembly

resulted in a uniform gap of 0.20 mm at the bearing inner race to shaft shoulder, due to the interference of the bearing chamfer with the shaft fillet radius and the 10 μm fault. During the bearing assembly, as the inner race is assembled with extra force to overcome the interference fit at the interface, the inner race is likely to have rode over the 10 μm step and got seated with a gap less than 0.2 mm caused by the interface mismatch due to higher shaft shoulder fillet radius of R1.

Considering the above aspects, to study the effect of this, the shaft has been modelled in Hypermesh by the eight noded brick element with the shaft fillet radius of R1 but without the fault of 10 μm step. The assembly resulted in a uniform gap of 0.15 mm at the bearing inner race to shaft shoulder, due to the interference of the bearing chamfer with the shaft fillet radius R1, as shown in Figure 4.15.

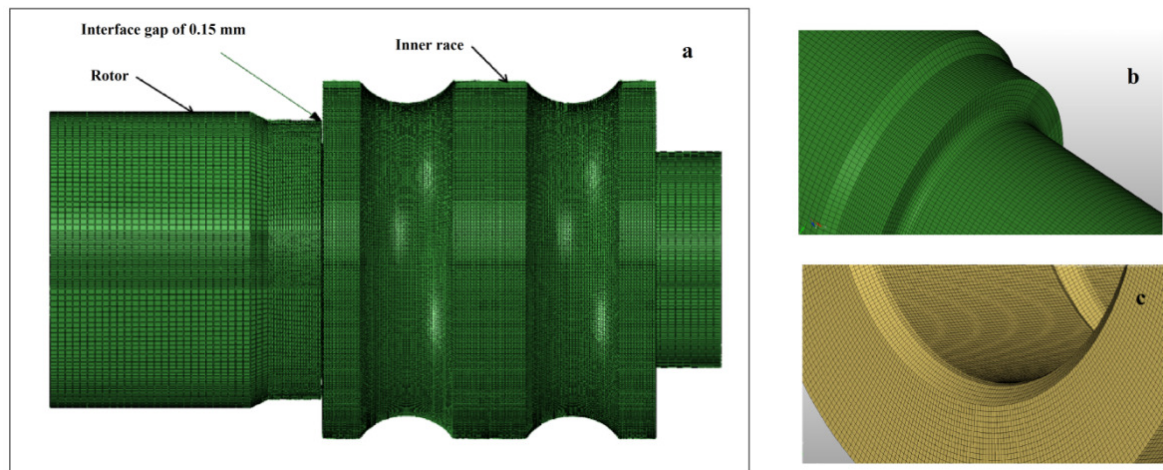


Figure 4.15 Interface gap of 0.15 mm (a) caused by the interface mismatch of shaft shoulder radius R1 (b) and the $0.8 \times 45^\circ$ chamfer of the inner race (c)

To capture the deformation pattern, the FE model is then imported into the Abaqus software and the boundary conditions are applied. The left side of the shaft and external surface of the outer race have been constrained from moving in the axial and radial directions. A uniformly distributed force of 20 kN is applied to the bearing inner race towards left, simulating the assembly preloading of the inner race. A linear static analysis is carried out to analyse the deformation pattern of the total assembly. With the application of the preload of 20 kN, the gap of 0.15 mm did not close fully and a residual gap of 0.02 mm gap is found at the outer diameter of the inner race.

The misalignment of the inner race with this interface mismatch is captured as 9 arc minutes from the analysis, as shown in Figure 4.16.

As the inner race gap of 0.15 mm did not close fully, and a residual gap of 0.02 mm is found after applying the clamping force, the effect of the 10 μm step on the misalignment would not be significantly different. Hence the significant contribution to the misalignment would be from the shaft shoulder mismatch, which is found to be 9 arc minutes from the finite element analysis.

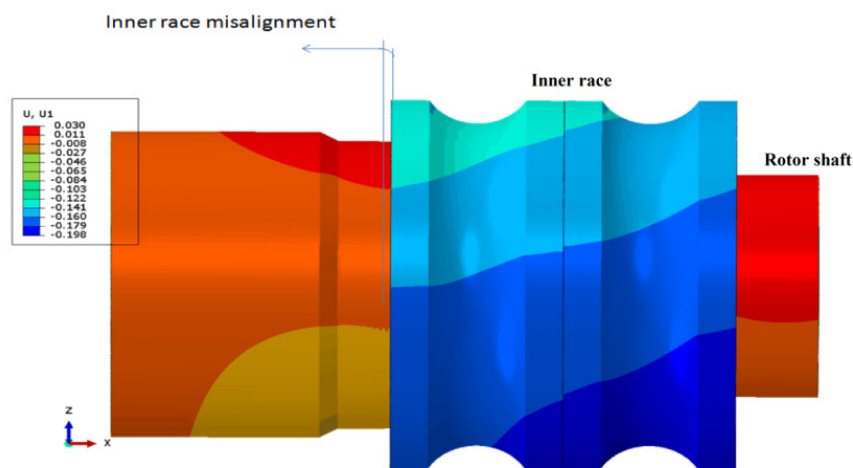


Figure 4.16 Misalignment of 9 arc minutes, caused by the inner race clamping with a 0.15 mm gap, due to the interface mismatch at the shaft shoulder

The effect of the 17.7 μm interference and the misalignment of 9 arc minutes on the performance of the bearing are addressed, through the impact analysis of these nonconformances in bearing performance, in Section 4.2.3 on failure causes and corrective actions.

4.2.3 Failure cause and corrective actions

The discolourations observed in the inner race, cage, and balls of the first row of bearing clearly indicate that the bearing failed due to excessive heating. The shaft fillet radius R1 is found to be more than the inner race chamfer of $0.8 \times 45^\circ$. The mismatch in the shaft shoulder radius with bearing inner race chamfer has resulted in an interface gap of 0.15 mm which has been captured in the FE model. The linear static analysis has been carried out in Abaqus software with appropriate boundary conditions and an assembly force of 20 kN applied on the bearing inner race as a uniform pressure. The analysis showed an inner race misalignment of 9 arc minutes.

The misalignment is also corroborated by the ball path pattern on the inner race of first row, which is inclined to the edge of the race as shown in Figure 4.17.

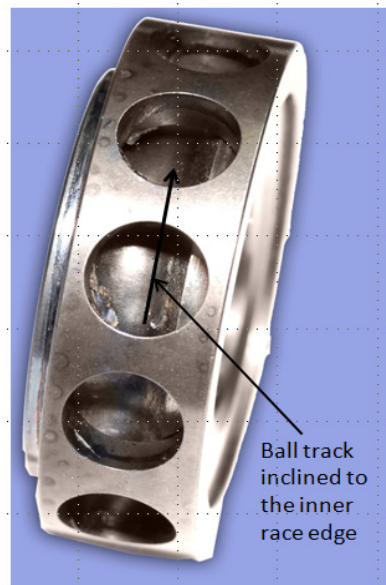


Figure 4.17 Ball path pattern on the inner race

The misalignment of the bearing in the application shall be within the misalignment capabilities of the bearing design. Bearing misalignment tolerance for angular contact ball bearing with split inner race is only 2 arc minutes (NASA-SP-8048, 1971). The inner race misalignment of 9 arc minutes in the case study is found to exceed the specified misalignment tolerance of 2 arc minutes. Ronald Widener (1986) suggests that, with a large fillet radius at the shaft shoulder, the face of the bearing will not seat properly with the shaft shoulder and this can result in misalignment of the bearing, bending of the shaft or cocking of the bearing which can cause the overheating of the bearing (Bugra Ertas and Hohn Vance, 2014).

When the inner race deforms more without the support, the row of the bearing close to the load application will get unloaded and the other row might get offloaded in the limiting case (Videira, 2013). Another effect of the clamping force on the inner race with the deviated assembly with 0.15 mm axial gap is that, because of the higher deformation, it causes the second row of balls getting unseated at the contact point 'A' in Figure 4.12b which causes the offloading of these balls and excessive loading of the first row of balls. This clearly explains the near virgin condition of the second row of inner race and balls, and the severe discoloration observed in the first row of inner race and balls. The theory is supported also by the discolouration observed in the

outer race at the point of contact of the first row of balls, the point 'B' in Figure 4.12b, and the normalcy at the contact point of second row.

The failed bearing assembly had a diametral interference of $7\text{ }\mu\text{m}$ in the rotor-bearing interface when measurements were made after machining. Due to case hardening treatment of $5\text{ }\mu\text{m}$ thickness, the diametral interference increased by an additional $10\text{ }\mu\text{m}$ to $17\text{ }\mu\text{m}$. Due to the thermal environments discussed in Section 3.3, the diametral clearance further increased to $17.7\text{ }\mu\text{m}$. The double row angular contact ball bearings have zero radial and axial clearances after preloading. Hence, higher interference could cause the expansion of the inner raceway resulting in undue preload and reduced life (Houghton, 1976). The hard preloaded bearings, for this reason, are more sensitive to the interface fits and thermal loading.

Considering the above points, the discolorations observed in the inner race, cage and balls of the first row of bearing, and the discoloration observed in the outer race at specific locations, the bearing failure mode is localised to the overheating of the bearing, due to the combination of following failure mechanisms:

- The $7\text{ }\mu\text{m}$ diametral interference, observed at the machining stage has increased to $17\text{ }\mu\text{m}$ due to $5\text{ }\mu\text{m}$ thickness build up during case hardening. The bearing inner race has been forced in to assemble with the shaft shoulder. The thermal expansion causes additional $0.7\text{ }\mu\text{m}$ interference making the net interference $17.7\text{ }\mu\text{m}$.
- As the preloaded bearings have zero axial and radial play (due to the 200 N preload designed at assembly level by the manufacturer) the interference directly contributes to additional radial loading on the balls and also heating of the balls during operation.
- There is an interface mismatch due to the shaft shoulder fillet radius R1 being more than the chamfer of 0.8 mm in the inner race. The clamping force of inner race in this condition causes a misalignment of 9 arc minutes as compared to the acceptable value of 2 arc minutes as per the standards. The ball path pattern on the failed inner race gives the evidence for the misalignment theory. The effect of this is clearly brought out in literature as overheating.
- The clamping load of the inner race with the interface gap of 0.15 mm at assembly causes the gapping at the second row of balls offloading them.

Therefore, the first row of balls take higher loads (onloading), causing the rolling surfaces of the first row getting heated up and discoloured.

Thus, failure cause is identified as the excessive loading on the balls and the overheating of the bearing, because of the misalignment of the bearing inner race due to the mismatch of the shaft shoulder radius with the bearing chamfer, and also the higher interference in the interface between the inner race and the shaft. The failure theory explains all the observations of the failure like the total failure of the first row of bearing, near fresh condition of the second row of the bearing and also the ball path pattern observed on the inner race. The selection of the hard preloaded bearing has been a very good choice for aerospace application with high vibrations, but is very sensitive to the misalignment of inner race, the bearing to shaft interface fit and thermal loading. Following design and process improvements have been made to avoid the failure modes:

- The fillet provided in the shaft has been replaced by an undercut R0.5 (max) to ensure proper seating of the bearing on the shaft shoulder.
- Though a minimum possible interference fit is recommended at the operating temperature to avoid relative motion as per standards (Franz Josef Ebert, 2010) a close running clearance fit is preferred for aerospace bearings to enable testing, disassembly and inspection requirements (Videira et al., 2013).
The shaft diameter tolerance has been accordingly specified as dia 17 (-0.008/-0.014) corresponding to the bearing ID of dia 17 (-0.005), resulting in a diametral clearance of 3 to 14 μm .
- The manufacturing process also has been modified with cylindrical grinding as the final operation, after case hardening treatment to ensure the correct fit during the final assembly.
- The rotor shaft and bearing housing dimensions have been identified as functionally critical and quality control procedures strengthened by re-measuring them on receipt of hardware from the industry.
- Assembly procedure has been modified with specific checks to ensure free assembly of the bearings.

The potential origin of the 10 μm step, though not a cause of failure, has been investigated. The shaft outer diameter of 17 mm is manufactured by precision turning in a CNC machine and subsequently, the required surface finish and the tight

tolerances in the shaft are achieved by the cylindrical grinding operation. During the final finishing of the shaft outer diameter by grinding the operator takes extra care not to damage the shaft shoulder face and has stopped the grinding process without smoothly merging the shaft outer diameter with the step. As only the parameters like geometric and form tolerances have been inspected as per the quality control plan, this step has not been highlighted in the inspection report. To avoid the improper seating that resulted because of the higher shaft shoulder radius of R, it is modified to an undercut of R0.5 mm. Since the relief is provided by the undercut, the operator can easily confirm the satisfactory completion of operation when the grinding wheel comes to the undercut location. An undercut is the simplest solution at the corner, if the strength and fatigue life requirements are met (Ronald Widener, 1986).

To ensure the health of the bearing system, screening tests have been introduced at two levels. The low speed dynamometer test to ensure that the bearing level friction is within the acceptable range has been introduced for acceptance of each bearing. The set up for test is shown in Figure 4.18. The bearing and flywheel are positioned over the shaft of the torque transducer. The flywheel is given a slow rotation and torque is read out from the torque reader. The measured torque is used to indirectly assess the condition of the metallic contact surfaces of the bearing.

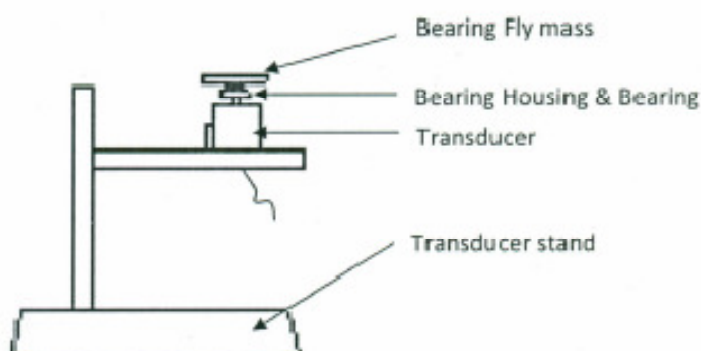


Figure 4.18 Low speed dynamometer test set up

The bearings additionally undergo acceptance run down time tests in gas motor level by assembling the bearings without vanes and seals to the gas motor. The gas motor speed is increased above 5000 rpm externally by an electric motor and then allowed to slow down. The time taken by the gas motor speed to drop from 5000 rpm to 1000 rpm is noted, as the run down time. It ensures the health of the bearing system. This

could bring out any dimensions or assembly related problems. The run down time is measured before and after a running the gas motor at 5000 rpm for one hour. After the tests, the bearings are disassembled and inspected at magnification and confirmed to be in good condition.

After implementing the above recommendations, the acceptance tests as per Table 4.1 have been completed satisfactorily on three sets of hardware. The gas motor has been further subjected to rigorous qualification tests, which includes 3 hour cold gas run test (cumulative) followed by 7 minute hot gas test at 75% load (with vibration & thermal acquisition) and 3 minute hot gas performance test. At system level, the gas motor has been assembled with engine gimbal control actuation system and tested for system level control system checks, qualification level vibration test, shock test, post vibration repeat control system checks and Low Speed Dynamometer test (LSD) have been carried out, thus qualifying the bearing for the hydraulic actuator application

4.3 Design robustness testing of gas motor

The functioning of the hydraulic control actuation system and its subsystem of gas motor is explained in Section 4.1 through the Figures 4.1 and 4.2 respectively. The failure mode avoidance strategies of one of the components of the gas motor namely angular contact ball bearing has been addressed in Section 4.2 through the analysis of the bearing failure during the qualification program. This section presents the failure mode avoidance strategies for the gas motor system as a whole with the focus on making the system design robust through testing at high stress levels to induce failures early and then widening the system operating environments through design and process solutions.

The hot gas at 36 bar and 630°C is drawn from the liquid engine turbine inlet manifold, and the temperature is reduced to the required level of 225°C in a thermal regulator illustrated in Figure 4.19. The orifice I reduces the water pressure to 36 bar, and orifice II injects the water into the hot gas to reduce the temperature to 225°C. The gas motor functioning has been explained in Section 4.1. The gas at 225°C enters the vane chamber through a speed regulator, rotates the rotor and exits through the gas motor exit. The gas motor runs at a speed of 4800 rpm and drives the

pump, which sustains the hydraulic oil pressure at 210 bar, at the inlet of the servo actuator.

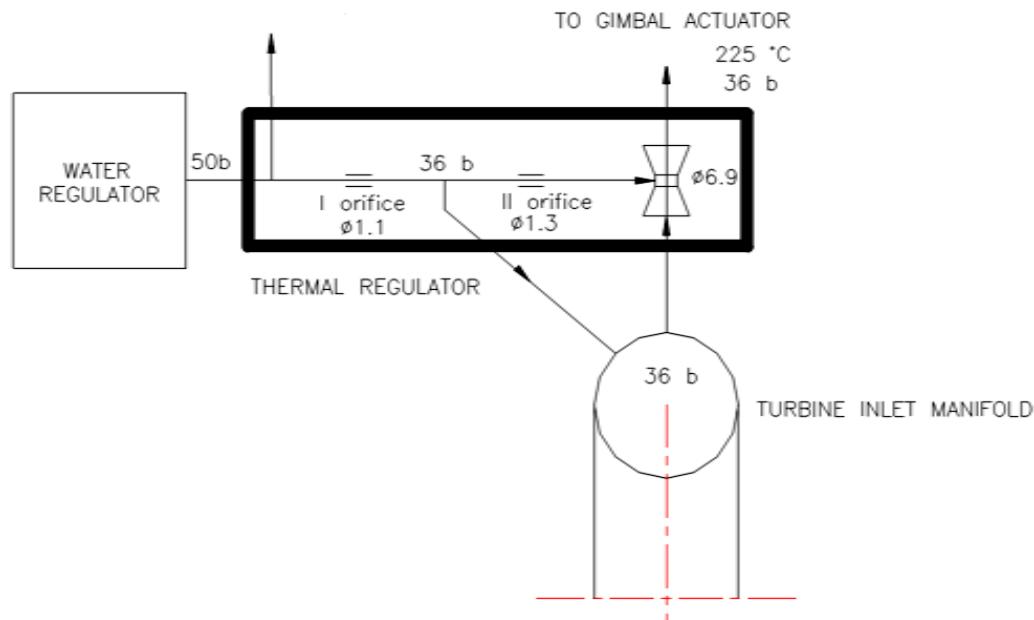


Figure 4.19 Thermal regulator

The normal performance of the electro hydraulic actuation system is illustrated through the system parameters in Figure 4.20. When the actuator is commanded by the control electronics (CMD in Figure 4.20), following sequence of functions take place:

- The oil enters the selected actuator chamber and the piston moves in the desired direction (feedback, FB in Figure 4.20) in accordance with the command.
- As the oil at the high pressure side is used up for the actuation, the system high pressure (P_h) at the outlet of the pump drops. The pump has to supply more oil, which requires higher gas motor output torque.
- Since the torque requirement is high, gas motor speed decreases, causing regulator gap to increase.
- Regulated pressure (P_r), the pressure of hot gas after entry through the inlet nozzle before entry into the vane chamber increases from its nominal value of 4 bar.
- With the increase in the gas regulated pressure, the gas motor speed increases, and system high pressure is regained to the nominal value.

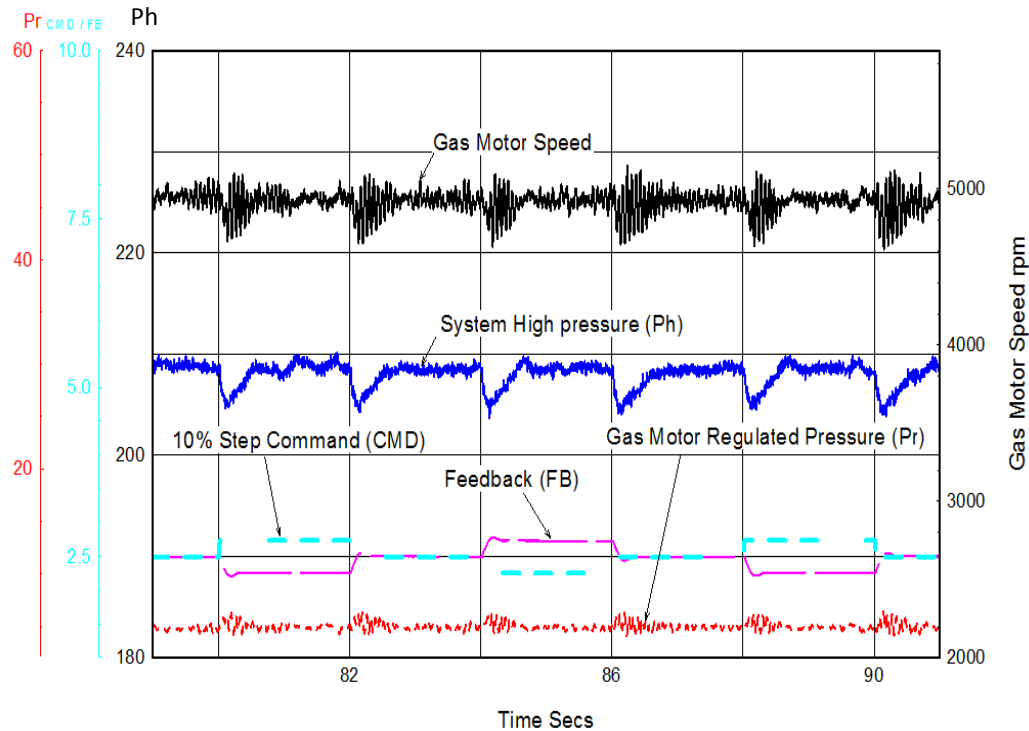


Figure 4.20 Functioning of control actuation system

Many launch vehicle systems, which give a very good functional performance in the ground testing, encounter catastrophic failures in the flight, because of unforeseen environments. The problem is compounded by the variations in the quality of the system hardware. To take care of these uncertainties design is made with a factor of safety, as defined by the applicable standards. A good system design shall ensure adequate design margins through analysis and testing. The loads and durations of the tests for qualification shall be higher than the flight loads and duration (NASA SP 8044, 1970). Therefore, identification of the critical components and environments are essential and this is obtained by doing a detailed FMEA of the system. This forms the basis for a systematic approach towards failure prevention (Samira Abbasgholizadeh Rahimi et al., 2013).

The critical components, single point failure modes and the vital environments for the gas motor system, brought out by the FMEA are given in Table 4.4. The literature also addresses failures of similar hot gas vane motors for aircraft applications and the critical issues such as vane breakage, operation over a wide speed range, high friction forces, leakage at interfaces due to thermal transients, and bearing life (Dussenberry and Carlson, 1986).

Table 4.4 Critical components, failure modes, and environments of the gas motor

Sl. No.	Critical components	Critical Environments	Critical failure modes
1.	Vanes	High temperature High speed Speed oscillations Wetness of the inlet gas Vibration	Vane wear, Vane edges damages, mechanical failure resulting in debris and gas motor stoppage.
2.	Seals	High temperature Vibration	Leak through joints Inadequate output torque
3.	Bearings	High temperature High speed Vibration	Rotor seizure due to bearing failure,
4.	Springs	High temperature Speed oscillations	Loss of stiffness, Fatigue failure, Uncontrolled speed.
5	Rotor and Stator	Structural loads	Stresses exceeding the strength of the material

The design involves system engineering, finalising loads & environments, and finalising the materials & dimensioning. Carbon-carbon is selected as material for vane, considering the requirements of high strength, ability to withstand high temperature and requirement of low density. The stresses on critical elements such as stator, rotor, vanes and bearings have been analysed for the operating environments such as thermal, pressure, vehicle acceleration, centrifugal forces, and vibration loads and positive margins ensured. Based on the output of FMEA and the design analysis, the qualification test requirements have been identified as given in Table 4.5.

In the gas motor the cause for torque losses are due to bearing friction and vane friction (Otmar Teichmann, 1966). The vane friction is controlled by applying vane grease during the assembly, thereby reducing the coefficient of friction between vane sliding surfaces. The bearing friction is also controlled by proper lubrication. The friction is also evaluated by acceptance tests.

Table 4.5 Qualification test requirements of gas motor system

Sl. No.	Environment	Flight Environment	Qualification
1	Temperature, K	225°C to 275°C	300°C
2	Wetness of hot gas, % age	<10%	Functional evaluation simulating flight environment in different hardware
3	Speed, rpm	4000 to 5500	
4	Speed Oscillations, rpm peak to peak	1000 rpm peak to peak	
5	Vibration, g _{rms}	3 g _{rms}	13.5 g _{rms}

Higher temperature is identified as one of the most critical environments, as it could affect the functional performance of all the critical components such as vanes, bearings, seals and the speed regulator. As compared to the nominal specified 225°C, maximum expected temperature at + 3 Sigma level is 275°C. The qualification level is finalised, with an additional temperature margin of 25°C, at 300°C. Failure mode avoidance in a system is addressed by two significant strategies. The first one is by testing the design robustness of the gas motor by subjecting it to more severe environments than the qualification levels, and strengthening the design against the encountered failure modes. The second is by controlling the variations in the key functional parameters and realization of systems as designed.

The process diagram of the gas motor system is given in Figure 4.21. The input to the system is the hot gas from gas generator at specified pressure and temperature. The output is the torque delivered at the output shaft at the specified rotor speed. The system output is influenced by various control factors and noise factors. The control factors of the system are design parameters like the materials, dimensioning of parts, speed setting, and manufacturing related parameters such as process parameters, the sliding clearances, and the assembly process. The noise factors such as unforeseen environments, non-conformance in the input variables and system hardware, assembly deviations, human error, contamination etc., can cause the system to go to the error state namely rotor stoppage or a runaway condition.

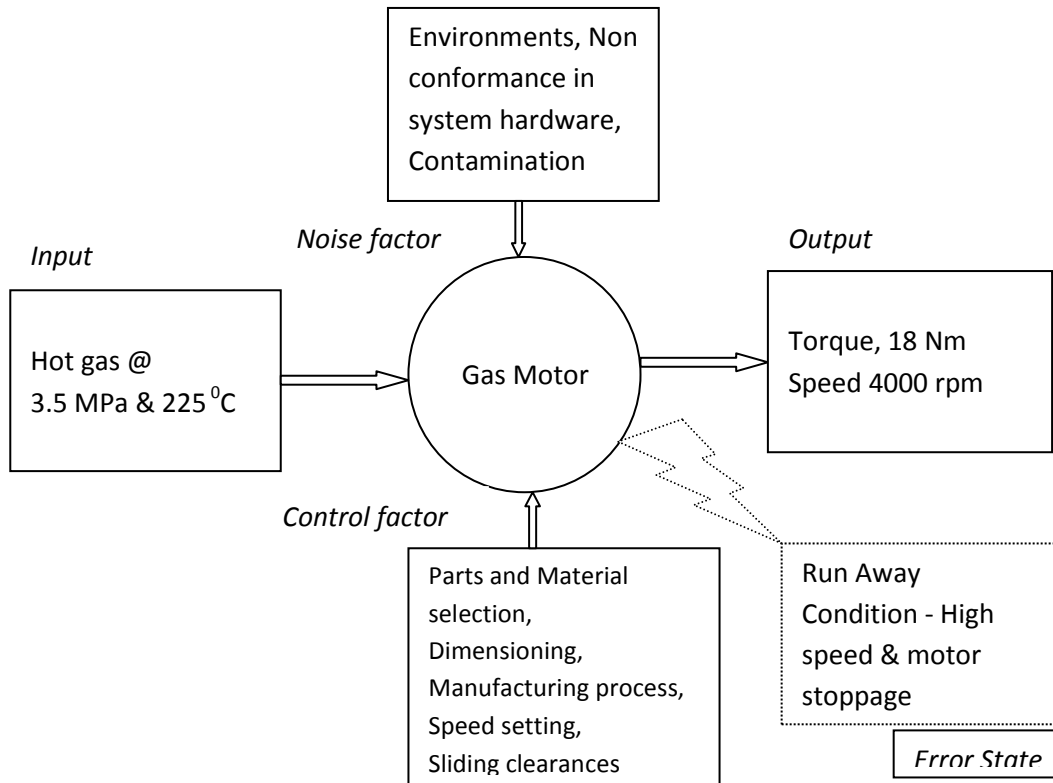


Figure 4.21 The process diagram of the gas motor

The design robustness could be achieved by “operating window methods” approach wherein the value of noise factors is increased to induce the failures, the failure mechanisms are understood, and the control factors or design parameters modified to obtain a broader operating window (Don Clausing and Daniel Frey, 2005). Accordingly, various environmental tests simulating environments much higher than the qualification level such as high temperature tests with hot gas and with wet steam, high speed test, speed oscillation test, and vibration test are additionally identified which is not part of the qualification program. The tests carried out, failure modes and mechanisms brought out by the tests, and corrective actions taken in design to reduce critical stress levels to widen the operating environments of the subsystems are addressed in Sections 4.3.1 to 4.3.5..

4.3.1 Tests with hot gas at 315 °C

The nominal inlet gas temperature is 225°C with an upper bound specification of 275°C (+3 Sigma level). The gas motor, after acceptance testing at nominal inlet gas temperature of 225°C and qualification at upper bound specification of 300°C, is subjected to severe environmental test with inlet gas at a temperature of 315°C (+5

Sigma level) for a duration of 200 s. The test is carried out in an integrated control actuator in flight configuration with temperature monitoring at critical locations of gas motor such as gas motor inlet, near ball and roller bearings and regulator cover. The control system performance is found to be normal, with the feedback following the command. The temperature at filter cover and regulator cover, critical for the effective performance of elastomeric O-ring seals, and at the bearing locations are given in Table 4.6, with a maximum temperature of 257°C at inlet filter cover.

Table 4.6 Temperature measured at critical locations during hot gas test at **315°C**

Sl No.	Location	Peak temperature, °C	Remarks
1	Filter cover	257	Critical for seal functioning
2	Regulator cover	245	
3	Ball bearing	242	Critical for bearing grease and cage
4	Roller bearing	171	



Figure 4.22 Bearing polyamide cage material damage during hot test at 315°C

The seals have been found to be in good condition after the test. But severe degradation is seen in the bearing cage made of polyamide material in the angular contact ball bearing as shown in Figure 4.22. The design is modified with metallic cage with AISI 304 stainless steel material, making the bearing system operational under a wider temperature range.

4.3.2 Tests with hot gas at 390 °C

The design changes in the bearing, made after the high temperature tests at 315°C, brought sufficient robustness in the system design. The tests have been repeated with a higher hot gas temperature of 390°C for a duration of 200 s to find out the fragility limit of various components of the system. The functional performance of control system has been satisfactory, even at these extremely high temperatures. The temperature measured on the critical components is mapped in Figure 4.23. The gas motor is disassembled and all the subsystems have been critically inspected.

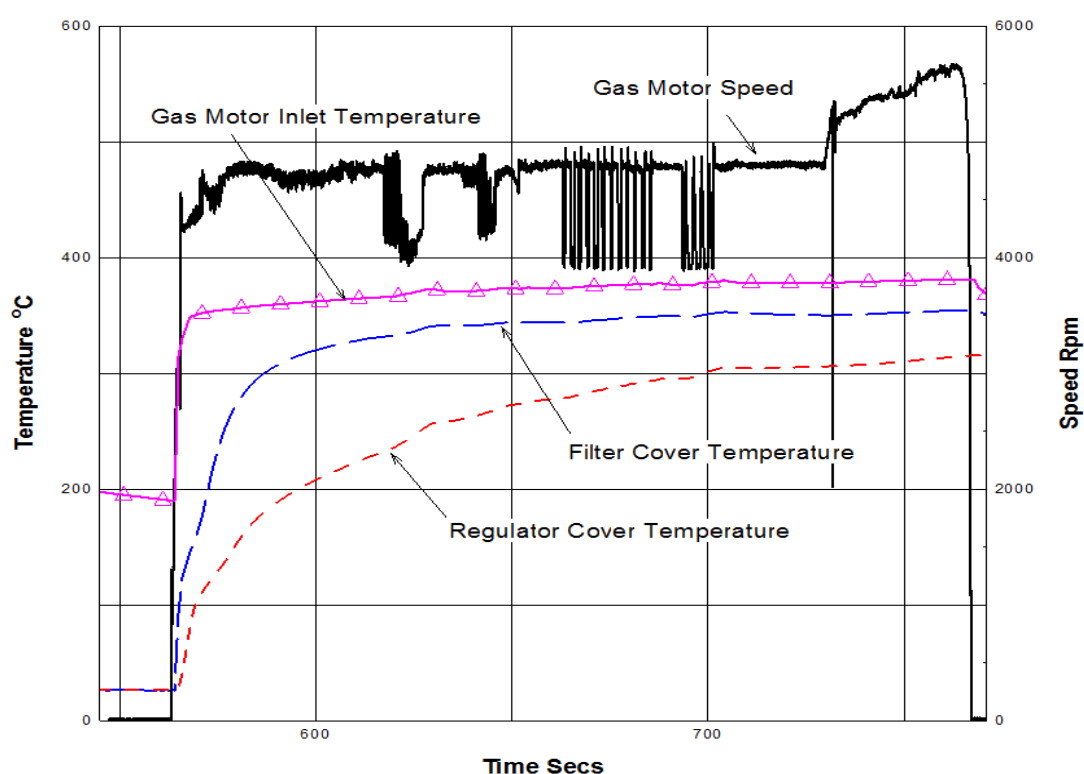


Figure 4.23 Temperature data and observation on regulator O-rings during 390°C test

The temperature measured at O-ring location is 360°C and found exceeding its capability. Gas motor O-ring at the inlet filter cover is found damaged as shown in Figure 4.24. The speed of the rotor has increased after 165 s onwards due to O-ring failure. The leak of gas at the filter cover interface has led to ineffectiveness of speed regulator, causing speed to increase. The temperature measured at ball bearing location and roller bearing location are 280°C and 200°C respectively. With modified bearing design, higher temperature is not a concern for the bearing. However, bearing grease at ball bearing has shown deterioration in high temperature test. The bearing run down time is also found reduced, with degraded grease. Based on the above

observations, temperature of the inlet gas is identified as a critical functional parameter.



Figure 4.24 Observation on regulator O-rings during 390 °C test

The temperature of the inlet hot gas (TGM) for the gas motor is reduced by a thermal regulator, from 630°C to 225°C as explained earlier in Figure 4.19. The temperature is a function of the thermal regulator functioning and the hot gas mass flow rate through the gas motor. Stringent calibration of the thermal regulator with and without the back pressure and fine tuning of the orifice have been implemented. The mass flow rate through the gas motor also is identified as a critical functional parameter and measured and controlled as part of gas motor acceptance tests. These measures effectively controlled the temperature of the hot gas within a narrow band. In addition, considering the failure of the O-ring, the O-ring material has been changed to special grade high temperature resistant silicone O-ring.

4.3.3 Wet steam test:

In flight, the gas motor is run by combustion products from gas generator and because of injection of water for thermal regulation the wetness of the gas can go upto 10% maximum. Wetness in the hot gas, causes two phase flow, liquid and gas, and this combination during expansion in the vane chambers, cause pressure pulsation and speed oscillations. These speed oscillations could be critical for the gas motor elements such as vanes, speed regulator and bearings. This aspect is addressed by a survivability test in the flight configuration on different gas motor hardware with the hot gas from the liquid engine through a number of engine and stage level hot tests. This gives good confidence in the system functioning for flight environments but does

not demonstrate the margins. Furthermore, the gas motor is tested with inlet gas wetness of 20% as compared to about 10% maximum expected in flight. The performance of the system is normal as shown in Figure 4.25, with respect to command, feedback and the system pressures.

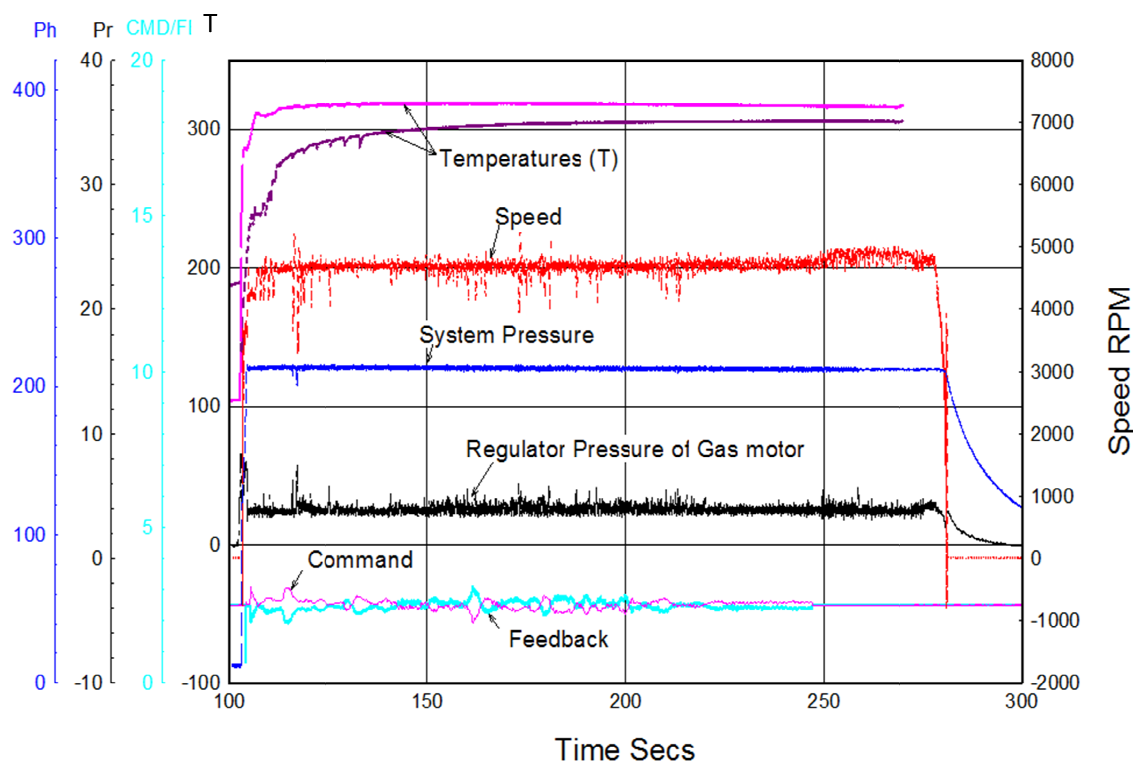


Figure 4.25 Performance of control actuation system during wetness tests

Although, higher wetness is not affecting the functional performance of the actuator, the gas motor speed oscillation is higher in the order of 2000 rpm with a peak speed of 5500 rpm. The test has demonstrated the performance of the gas motor system for the severe speed oscillations.

4.3.4 High speed test:

The inlet gas wetness conditions are found to have an effect on speed and its oscillations. The speed is found to go up to 5500 rpm. Testing the gas motor for higher speeds with speed regulator in place is not feasible, as the regulator would keep the speed within the bounds. In order to demonstrate the performance of the gas motor at very high speeds the gas motor is run, deliberately making the speed regulator ineffective, by permanently keeping the flow opening larger. The test is carried out simulating the engine inertia and with flight profile commands of the control actuator,

simulating speeds of 8600 rpm and 10730 rpm. In the 8600 rpm test, system performance has been found normal.

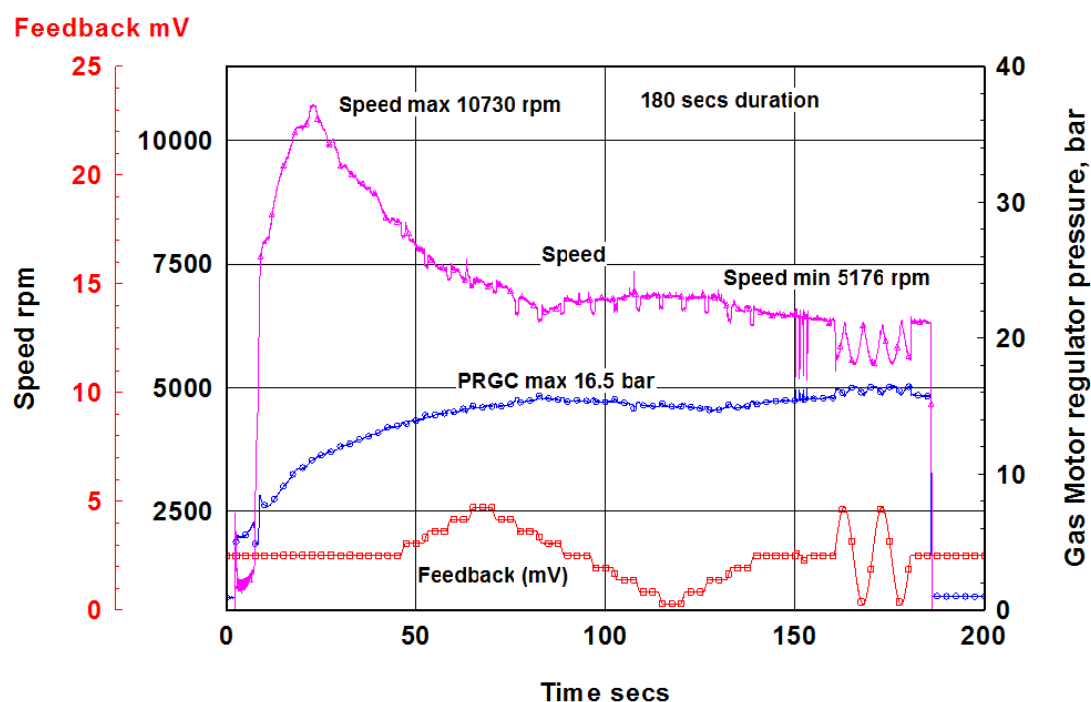


Figure 4.26 Performance of actuator during high speed test

In the 10730 rpm test, the speed after reaching 10730 rpm, has gradually dropped to 6500 rpm with a speed oscillation of 2000 rpm as given in Figure 4.26. On disassembly, the vanes are found to have de-laminations. The speed decrease and vane de-lamination are due to increased friction between the vanes and its rubbing surfaces and degradation of grease. The acceptance test procedures of the vanes have been strengthened based on the observation. The performance of the actuator during this test is found to be normal with respect to control system performance.

4.3.5 Vibration test

The launch vehicle systems experience severe vibration environments due to the lift off noise and aerodynamic noise. In addition to this acoustic noise, the liquid engine operation also causes severe vibration of the systems. The gas motor assembled with actuator has been tested as part of qualification up to 13.5 g_{rms} , as compared to about 3 g_{rms} seen in flight. The system is further tested to a more severe vibration level of 23 g_{rms} as part of the design robustness testing. The gas motor performance is found to be normal and post test inspection of all critical components indicated normalcy.

4.4 FMA concepts based on the failure mode investigations

The analysis and experimentation carried out to investigate the failure modes and failure mechanisms of angular contact ball bearing and gas motor system has brought out a number of general failure mode avoidance strategies applicable to launch vehicle systems, and is discussed in Sections 4.4.1 to 4.4.3.

4.4.1 Configuration control and quality control

The investigation on the angular contact ball bearing has clearly brought out that the failure of the bearing has happened as a result of the combination of factors such as the design error in specifying the fillet radius at the shaft shoulder, the manufacturing process error leading to high interference at the shaft-bearing interface, inspection error in not bringing out the non conformances in the salient features of the geometry, assembly error in pressing the bearing with extra force to seat the bearing, and absence of comprehensive screening procedures for the bearings. The failure modes and failure mechanisms identified lead to following failure avoidance concepts:

- Configuration control of the systems addressing finer design details, particularly at the interfaces has to be carried out through comprehensive reviews involving all the interfacing system agencies.
- The manufacturing process error led to high interference at the shaft-bearing interface. The errors in inspection resulted in not addressing the non conformance in the salient features of the geometry. Manufacturing process review, comprehensive process documents with detailed QC checks, and stage clearance by quality agencies are identified as effective tools for FMA.
- The process deviations are often the cause of failures as brought out by the failure mechanisms identified in the analysis. Identification of Functionally Critical Dimensions (FCD), like the bearing interface dimensions, and re-measurement on receipt from industry, to ensure that critical dimensions are not having any non conformances is essential for an effective FMA.
- Computation of critical interface clearances and ensuring conformance to the specifications, to avoid higher friction/higher vibration of the assemblies help in avoiding inadvertent failures.
- The bearing has been assembled with extra force without alerting the high interference. Also, the 10 μm step has been missed by the inspection team.

Imparting adequate training to the operation team to identify the faults during the inspection and assembly operations, and detailed assembly operation documents with quality control checks to ensure flight assembly without any defects are essential to avoid process errors.

- Enhancing testability of systems at all phases of integration and system health monitoring till the launch time, to screen defects if any, is very important to ensure the flightworthiness of systems.

4.4.2 Design robustness

Severe environmental stress tests have been carried out to test for the design robustness of the gas motor system. Though there have been a few unforeseen failures, on detailed analysis of the observations and test data, the failure mechanisms could be understood which enabled taking suitable corrective actions to ensure satisfactory system performance at a wide range of operating conditions.

The marginality in the polyamide bearing cage has been brought out by the high temperature test and design modified to withstand higher temperature. Marginality in O-ring material with respect to high temperature is brought out, and recommended to change to a high temperature resistant silicone rubber material to extend the operating range. Adequate design margins have been established for the critical parts like carbon-carbon vanes, bearings and speed regulator, for high speeds and vibration levels, demonstrating the robustness of the system.

Though the performance of the system has been normal up to 300°C, the tests brought out the need for controlling the inlet hot gas temperature and thermal regulator has been identified as a very sensitive subsystem. Thermal regulator design, manufacture and acceptance test procedures have been tightened to limit the variations in the hot gas temperature within a narrow band around the nominal specified 225°C. The performance depends on precision manufacturing meeting stringent tolerance requirements. Testability of subsystems is the strength to ensure reliable performance of space systems and thermal regulator calibration with and without back pressure is introduced to ensure the functional performance of the system. Considering the observations during the test, strict process control, inspection procedures, and a comprehensive process and batch qualification plan for the vanes have been evolved and implemented.

The study brings out the requirements of high stress testing to identify the design weaknesses and failure mechanisms of the system, leading to identification of design corrections to make the system design robust. This also helps in identifying the critical parts, dimensions and parameters for the functioning of the system, which could be monitored and controlled to avoid failures.

4.4.3 System hardware certification

Quality of the flight system hardware is critical to the successful functioning of a system, even when the design is robust. Hence, controlling the variations in the product parameters and realization of the systems as designed becomes very important. The manufacturing processes shall be reviewed to meet the design specifications and a detailed process document made for each part to ensure consistency in production, with a focussed attention on critical parts. In a dynamic subsystem such as a gas motor, the critical parts move relative to each other. Vanes move inward and outward within the rotor slot and also rub against stator surface. The bearings interface with the rotor and the bearing housings has been found critical for system performance. If the clearances are too low or negative in these interfaces, it can lead to forced assembly and subsequent jamming of components. If the clearances are more it results in higher play between the mating parts, higher vibration and noise during operation. Surface finish of the mating parts is also important. Hence, it is important to identify critical dimensions and parameters for the functional performance of the system known as Functionally Critical Dimensions (FCDs) and Critical Functional Parameters (CFP) and ensure them within specifications in the flight system. The FCDs have to be confirmed by re measuring to the desired level of accuracy, in the presence of identified Quality Control (QC) personnel, to ensure their correctness beyond doubt. The FCDs also include form tolerances like perpendicularity, parallelism and flatness. The critical sliding clearances and critical parameters such as O-ring squeeze, stretch and fill are also separately computed and ensured within the specifications, preferably towards the nominal value.

Since any contaminant within the system can cause catastrophic failures in such dynamic systems, contamination and cleanliness control is of utmost importance in the system preparation. All the parts used must be cleaned using ultrasonic technique to remove burrs and foreign particles from surface. All the assembly operations shall be done in a clean room of specified class to prevent contamination. The assembly

operations have to be carried out as per written down procedures in a standard operation document format, with detailed step by step procedure and verification of identified check points. The operation team have to be given adequate training in the assembly operations and also various quality control techniques.

The experiments have brought out another important aspect in the reliability assurance of the launch vehicle systems, namely testability of systems. The critical components, identified by the FMEA undergo extensive acceptance testing. Vanes are visually inspected under 10X magnification and Ultrasonic Testing is done for identifying delamination, if any, and edge chipping. Vanes shall have sufficient mechanical strength stipulated by the design to ensure reliable performance, and this is verified by testing for inter laminar shear strength, flexural strength, tensile strength, compressive strength and Barcol hardness on adequate number of specimens. The vanes manufacturing process is qualified through extended period of running at gas motor level, with cold gas as well as hot gas. The gas motor system undergoes vibration and shock test and post test inspection is done to confirm that there is no degradation in the vane. Subsequent to the qualification, when new batches of vanes are realised they undergo the identified batch qualification tests, running with cold gas and hot gas, which is a subset of the process qualification procedure. Flight gas Motor hardware is prepared by running the motor with run in vanes. Subsequently it is assembled with flight vanes and characterized for speed-torque relationship, power output and air consumption rate. Wear of vanes are measured at different stages of testing and ensured within the specifications. The failure modes captured by experimentation also brings out the requirement of enhancing the testability of systems at all phases of system realisation until the launch.

The failure mode avoidance concepts, methods and strategies for space systems are brought out through the analysis and experimentation. The FMA concepts brought out and implemented resulting in flawless performance of systems, validating the effectiveness of the FMA strategy.

CHAPTER 5

FAILURE PREVENTION IN PLUMBING AND HOSES OF HYDRAULIC CONTROL ACTUATION SYSTEMS

5.1 Introduction

Electro hydraulic actuators are used for steering the launch vehicle in the designed trajectory. The main advantages of electro hydraulic actuators are higher torque to mass ratio, ease of installation and the capability to transmit the forces to actuators at different locations through the hydraulic plumbing. Depending on the system requirements, the plumbing can be made in different segments connecting the subsystems like the pump, reservoir, accumulator, manifolds, valves and regulators. In Chapter 4, the failure mode avoidance strategies for a dynamic subsystem of the Control Actuation System (CAS) namely gas motor and its critical parts are addressed. This chapter presents the failure modes of the flexible hoses and the hydraulic plumbing in a CAS, for the service load as well as environmental conditions. The failure prevention strategies are also addressed.

The reliable functioning of an electro hydraulic actuation system depends on the satisfactory performance of the static and dynamic seals in the system. It also depends on the leak tightness of its hydraulic plumbing, flexible hoses and associated joints under the pressure loads and the environmental conditions. The Section 5.2 presents the fatigue life estimation and reliability analysis of a hydraulic plumbing when subjected to severe vibrations. The Section 5.3 presents a detailed failure analysis, root cause identification and the failure prevention strategies adopted during the manufacturing and testing of the flexible hydraulic hose.

5.2 Fatigue life estimation and reliability analysis of hydraulic plumbing

The reliable functioning of hydraulic plumbing and its joints under the pressure load and the environmental conditions is of paramount importance for the successful operation of the mission critical electro hydraulic control actuation systems. Fatigue

fracture is one of the most common failure mechanism in space systems because of the repetitive harmonic loads during launch phase. It is characterised by incremental propagation of cracks until cross section is reduced to the point of failure (Gordon Powel, 1986; Saeed Kiad et al., 2016). John Miles (1954) identifies the fluctuating loads along with static load as the cause of fatigue failure of structural components and joints. Fatigue design of components in mechanical, aeronautical and civil engineering is complicated by the random nature of the input loads. Fatigue life has to be verified at all instances of time when designing systems subjected to loads variable in time (Przemyslaw Strzelecki and Tomasz Tomaszewski, 2017; Yang and Trapp, 1974). The fatigue strength properties and the time of initiation of crack are random in nature. The variations in fatigue strength of the flared tubing are also high due to cold working, and inherent scatter associated with fatigue strength. The dynamic response of the structure is the foundation for the fatigue life analysis. It involves the model, material, boundary condition, results and analysis (Du Zhong lei and Liao Ri dong, 2016; Yang and Trapp, 1974). Fatigue life assessment can be made using global approach such as stress life method or local approach such as elastic-plastic notch base concept. The local approach may require complex nonlinear calculations for each load step of the load-time history. The global approach uses the hypothesis proposed by Palmgren and Miner, based on the assumption that the damage evolution is linear (Antoinne Fissolo, 2015; Matthias Hell et al., 2015). The fatigue damage assessment using the Goodman diagram and damage accumulation law of Palmgren and Miner are addressed in the works of Jiahao Zheng and Jianming Yang (2016). The Palmgren-Miner rule is widely used for design purposes, though it does not consider the effect of loading sequence (Pereira et al., 2009; Risitano et al., 2012).

In the work of Hui Lv et al (2011), severe vibration problem in the aircraft plumbing, under time varying loads due to pump operation is discussed. The hydraulic plumbing vibrates at the same frequency of fluid pressure pulsation, with the amplitude varying with its location on the plumbing. Abhay Jha et al. (2013) has carried out a detailed metallurgical investigation of an AISI 304L stainless steel plumbing used in an electro hydraulic control system, and based on the findings concludes that the cracking is due to fatigue loading induced by vibration during liquid engine operation. Sushant et al. (2015) in another case study, concludes that the failure of stainless steel plumbing in a pressurisation line of a liquid engine as vibration induced fatigue. Therefore, fatigue

failure of the plumbing and its joints due to a combination of the pressure and vibration loading is identified as one of the single point failure mode of the electro hydraulic control actuation system. The fatigue life of aircraft structural elements has a large variability due to the variations in the strength and load spectrum. Therefore, there is a need to assess these variations and assess the reliability to ensure the safety of these structures (Xiaofan He et al., 2013). In the present study, the fatigue behavior of the hydraulic plumbing lines and the flare type fitting, under the fluctuating stresses caused by vibration and static stress due to high pressure loading is addressed. The study has been carried out using analytical and experimental methods, and brings out fatigue life cycle estimate and the reliability of the hydraulic actuation system plumbing and the joints subjected to fatigue loading.

5.2.1 System description and the failure mode study

The functioning of pump fed hydraulic Control Actuation System (CAS) has been discussed in Chapter 4 with the help of Figure 4.1. The hot gas from the gas generator of the liquid engine is used to drive the gas motor, which in turn drives the pump. The hydraulic pump is an axial piston reciprocating pump with rotating pistons. The rotational speed of the pump is 4800 rpm. The hydraulic pump delivers the oil stored at a low pressure of 1.1 MPa to the high pressure side of the hydraulic circuit at 21 MPa. It draws the oil during the pull (retraction) stroke and expels oil during the push (forward) stroke. An accumulator is connected to the pump outlet to suppress the pressure pulsations and to supply oil during peak demands. The flow and direction of oil to the hydraulic ram of the actuator is controlled by a servo valve. The spent oil from the actuator is fed back to the reservoir through the servo valve. The subsystems like the pump, reservoir, accumulator and the hydraulic ram are connected by stainless steel plumbing.

Austenitic stainless steels are used for the pressurization lines in liquid engines owing to their excellent corrosion resistance, and its ability to be formed and welded (Smith, 1993; Kutz, 2002). Accordingly, AISI 304L stainless steel tubing is used for connecting the reservoir to the pump through a suction line 'A' and the pump outlet to the actuator by a delivery line 'B' as shown in Figure 4.1. Figure 5.1 shows the location of the delivery line plumbing in the actuator. The plumbing is flared at the end, and assembled to the adapter in the pump using a flared tube coupling joint as

shown in Figure 5.2. The flare type fittings with ferrule joint are recommended for high pressure joints considering their higher strength, vibration resistance and capability for repeated use (Hugo Buchter, 1979). The oil sealing is achieved by tightening the nut which presses the wedge shaped ferrule against the flared tube, and creates a flare type enlargement on the tube end. The flared joints are developed for aircraft hydraulic systems and later used in launch vehicle applications (NASA SP-8119, 1976).

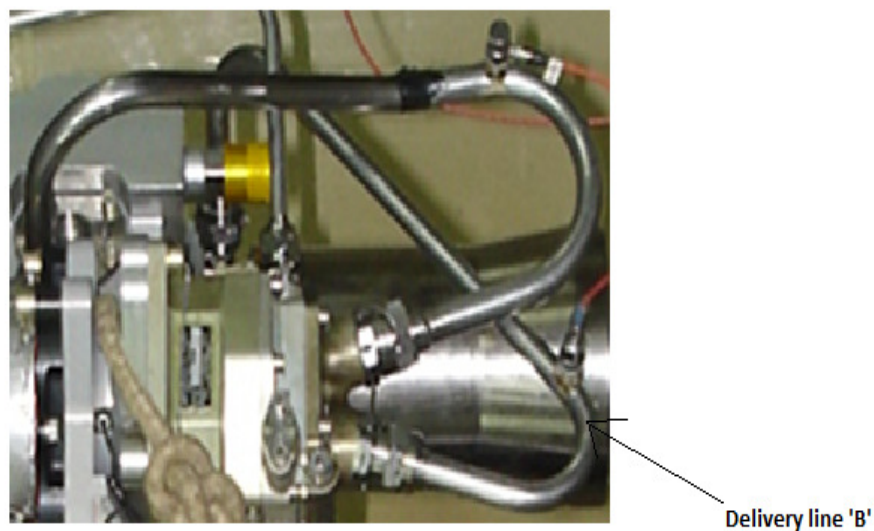


Figure 5.1 Delivery line plumbing in the actuator assembly

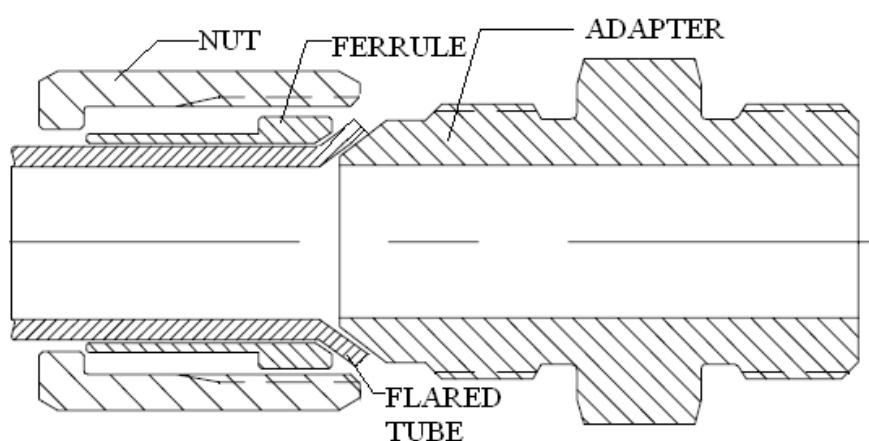


Figure 5.2 Delivery line plumbing flared tube coupling joint with ferrule

Pressure pulsations occur at the pump outlet as a result of alternating suction and delivery strokes. This pressure pulsations cause dynamic pressure variations at a

frequency corresponding to the pump rotation. The pressure pulsations in the hydraulic oil due to cyclic discharge can cause excessive vibration in the plumbing and its joints leading to fatigue failures (Anthony Sofranas, 2012). Fatigue is the result of different types of cyclic stresses forced on the component which leads to the initiation of microscopic cracks (Anthony Sofranas, 2012; Marco Dourado and Delfim Sioares, 2014). The micro cracks subsequently propagate to visible cracks, leading to failure. Anthony Sofranas (2012) stresses the need to consider fatigue as a primary factor in assessing the reliability of such structural elements. Failure of the plumbing or the joints due to vibration results in a leak in the hydraulic system and can lead to catastrophic failure of the launch vehicle mission. This chapter presents a detailed study carried out on the fatigue behavior of the hydraulic plumbing and the joints, critical for reliable performance of the system. The study also suggests actions to make the design robust with respect to the fatigue failure mode. In the hydraulic plumbing of CAS, vibration generated due to the pump pressure pulsation is found to be significant. Dynamic characterization of the plumbing, finite element modeling, numerical simulation of dynamic responses, and detailed stress-strength analysis considering both static and dynamic stress have been carried out for fatigue analysis. The fatigue life cycle estimation and reliability assessment of the plumbing joints have been carried out to ascertain flight worthiness.

5.2.2 Experimentation

Detailed experimentation is carried out to study the dynamics of the pump system and vibration induced on the plumbing by the pump operation

Pump pulsation test

The alternate pistons of the axial piston reciprocating pump, functions to deliver the high pressure oil at the required flow rate. This causes corresponding pressure pulsation at the pump outlet. The pump is rotating at a speed of 4800 rpm and has nine rotating pistons. The outlet pressure pulsation frequency is given by the following equation:

$$\text{Frequency, } f = \frac{nZ}{60} = \frac{4800 \times 9}{60} = 720 \text{ Hz.} \quad (5.1)$$

where n is the rotational speed of the pump in rpm and Z is the number of pistons.

The pressure pulsation test of the hydraulic pump is carried out by mounting the pump in a test set up as shown in Figure 5.3. The pump is run at the specified speed by an electric motor. The pump outlet pressure is controlled by a valve at the outlet. The outlet pressure is monitored using a pressure transducer. The valve is regulated to get the operating pressure of about 21 MPa and a flow rate of 18 lpm, and the pressure pulsation data is recorded by the pressure transducer. The measured pressure pulsation of the hydraulic pump is given in Figure 5.4. The pulsation frequency is 700 Hz with an amplitude of 1 to 2 MPa.

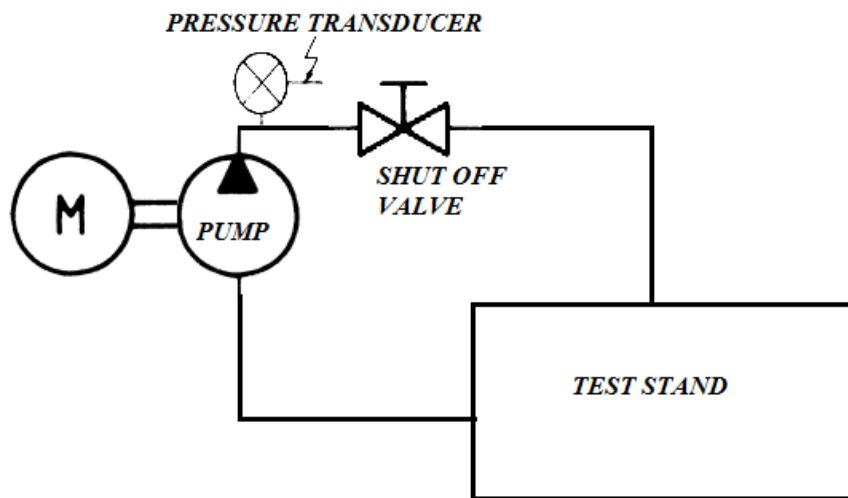
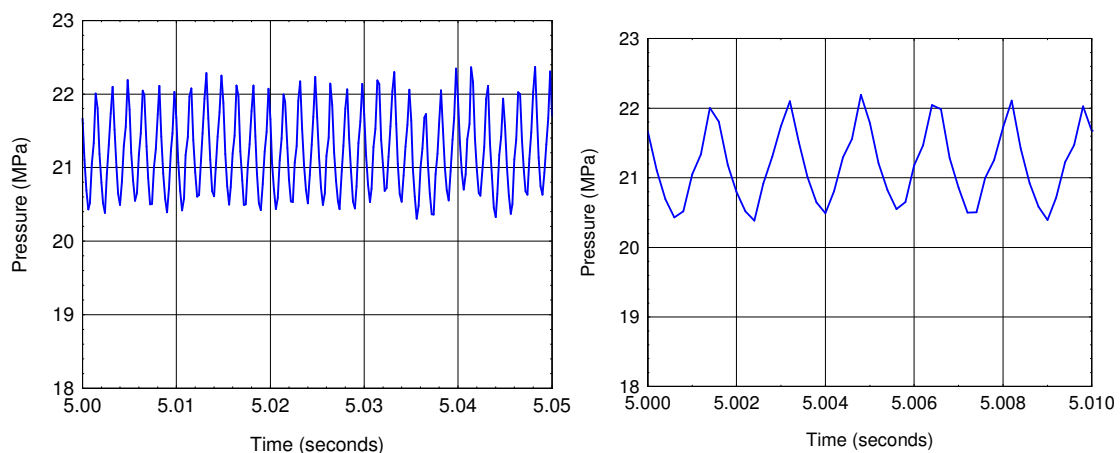


Figure 5.3 Test set up for measurement of pressure pulsation at pump outlet



a. Pump pressure pulsation

b. Zoomed view of pressure pulsation

Figure 5.4 Pressure pulsation measured at pump outlet

Dynamic characterization study of the plumbing

All the hydraulic plumbing of the pump such as the suction, delivery and case drain lines have been assessed for vibration responses induced by different excitations. The vibration response on the actuator due to jet noise, aerodynamic noise and liquid engine functioning have been found to be very benign. However, the vibration generated by the actuation system itself, due to the pump pressure pulsations is found to be significantly high. The system level characterization tests have been carried out to assess the magnitude of these vibrations, in a moment of inertia simulated liquid engine test set up as shown in Figure 5.5.

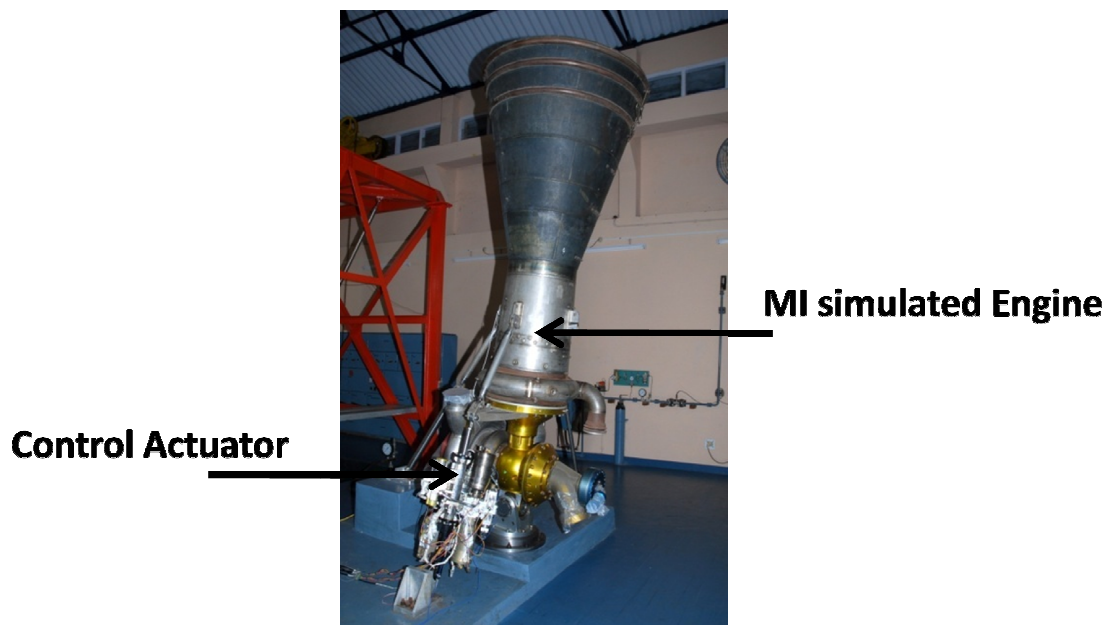


Figure 5.5 Test setup of the actuator simulating the engine inertia

The tests include frequency response (FR) tests at 10%, 5%, 2%, 1% and 0.5 % of the maximum displacement of the actuator for control system performance evaluation, and also the simulation of flight commands. The tests have been carried out in three sets of control actuators, to obtain the dispersions in stress levels due to variations in system hardware. The vibration response has been measured on the delivery line plumbing at two locations, 50 mm and 150 mm away from the pump outlet joint, to validate the dynamic response analysis results obtained from the finite element model. The locations are selected, as the 50 mm location is very near to the pump inlet and measures the excitations from the pump pressure pulsation. The second location of 150 mm has been arrived at based on a number of trial tests, to get the maximum

vibration response. The vibration response measured at 50 mm location is used as the input excitation to the delivery plumbing in the FE model for the random vibration response analysis. The response at 150 mm location from the analysis is then compared with the test results to validate the FE model. Though the control system performance has been satisfactory during all the tests, the vibration response measured on the delivery line plumbing is found to be high in general. In one of the test runs, the measured response at 150 mm from the joint is found to go as high as $1208 \text{ g}^2/\text{Hz}$ at 703 Hz as shown in Figure 5.6. The peak power spectral density (PSD) is close to the pump pulsation frequency of 720 Hz. Assessment of the dynamic stresses due to the observed higher vibration response has been carried out by a detailed dynamic vibration response analysis.

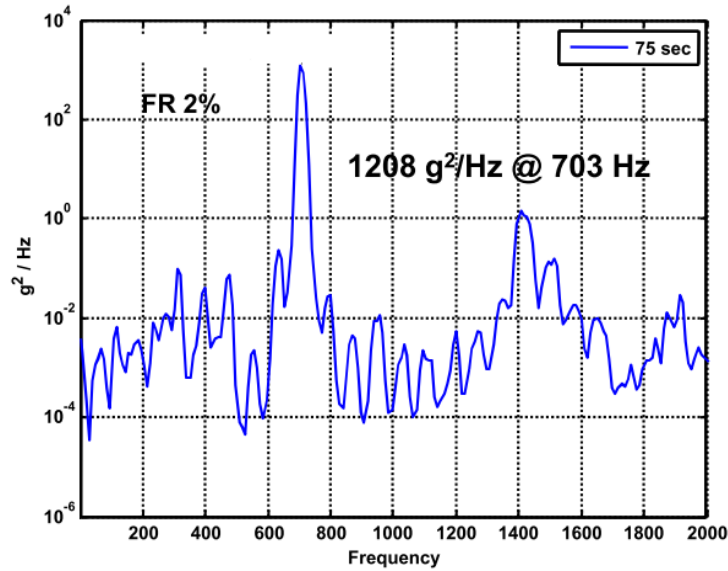


Figure 5.6 Peak response measured on the delivery plumbing

5.2.3 Dynamic vibration response analysis

Dave Steinberg (2010) discusses the traditional method of dynamic response analysis using the Miles equation. The RMS acceleration response is obtained for a given input, and can be converted into an equivalent static load. The Mile's equation is,

$$\text{Response in } G_{\text{rms}} = \sqrt{\left\{\frac{\pi}{2}\right\} * f_n * Q * \{\text{PSD input}\}} \quad (5.2)$$

where G_{rms} is root mean square acceleration in g_{rms} , f_n = Natural frequency in Hz, $Q = 1/2\zeta$ = Amplification at resonance, ζ is the critical damping ratio, and 'PSD input' is

the input Power spectral density in g^2/Hz . However, this method cannot capture the response of multi degrees of freedom systems and is not applicable for stepped or changing input spectra.

As the plumbing system has multiple degrees of freedom and the input vibration has varying PSD at different frequencies, FE random vibration response analysis has been carried out. The analysis has several advantages over traditional methods. The full distribution of stress and rms acceleration can be obtained for all spatial locations. All three axis excitation can be given simultaneously. Mode shapes are taken into account for obtaining acceleration and stress distribution, unlike other analytical methods. Stepped power spectral density input and modal mass participation factor are also considered in the analysis. Random response linear dynamic analysis is used to predict the response of a structure subjected to a nondeterministic continuous excitation that is expressed in a statistical sense by a cross spectral density matrix. The input random loads or base motions are characterized in the frequency domain by a matrix of cross spectral density functions, which links all loaded degrees of freedom.

The finite element model of the delivery plumbing is shown in Figure 5.7. The plumbing is idealized with shell element as per geometry. The diameter and thickness of the pipe are 12 mm and 1.24 mm respectively. The pipe has flared region on its both ends. All six degrees of freedom are constrained at both ends of the pipe. Free vibration analysis is carried out with and without oil in the delivery line. The entire circuit is completely filled with oil by vacuumising, and is pressurized to 1.1 MPa through the piston type reservoir system with nitrogen gas. The vacuumising, oil filling and pressurizing the oil ensure that no air bubble is inside the plumbing, and hence the oil always flows full in the hydraulic plumbing. Hence assumption of smearing the oil mass is a good approximation.

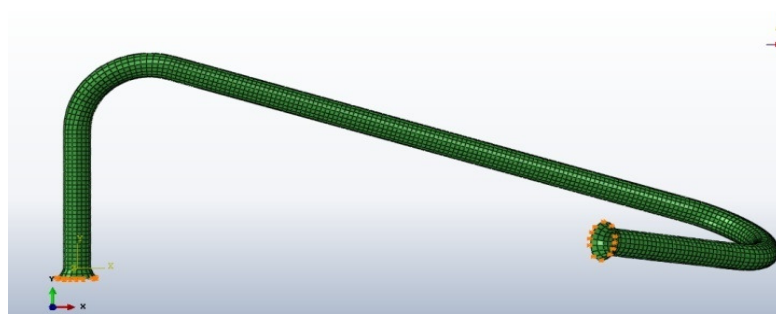


Figure 5.7 FE model of the plumbing

The frequencies of the plumbing, obtained from the model simulating the oil mass smeared over the metallic shell elements, matched well with the experimental results. The analytical frequency of the plumbing with and without oil is compared and is given in Table 5.1. The fourth mode of the plumbing with a frequency of 709 Hz, is shown in Figure 5.8. This matches well with the experimental result of 703 Hz.

Table 5.1 FE analysis results for plumbing, with and without oil

Mode	Plumbing without oil (Hz)	Plumbing with oil (Hz)
I	330	301
II	437	400
III	495	453
IV	776	709
V	834	763
VI	1569	1434
VII	1700	1554

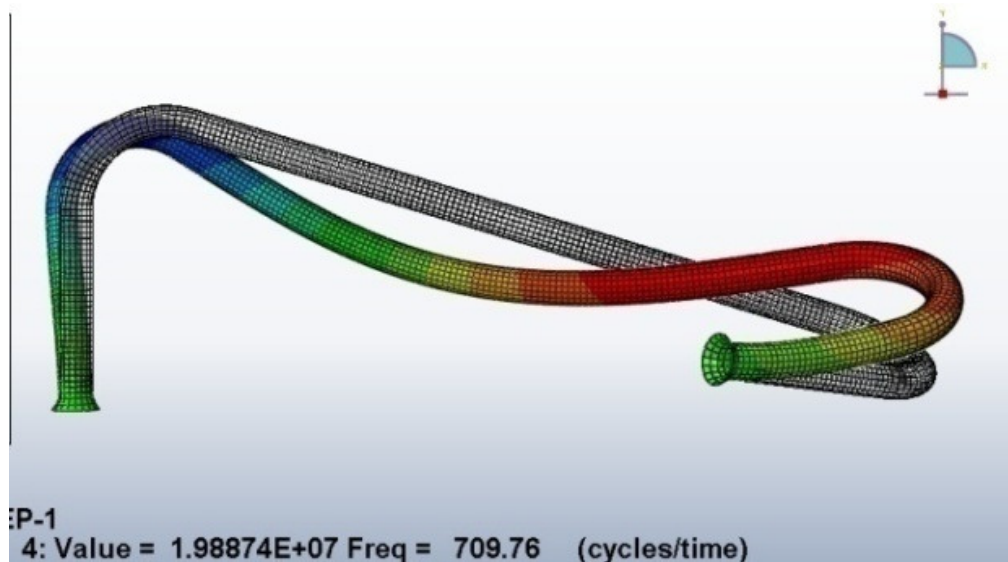


Figure 5.8 Fourth mode shape of the plumbing at 709 Hz (Analytical)

Random vibration analysis is carried out by using the finite element model, exciting the plumbing at 50 mm from the pump outlet with the vibration response measured at this location during the dynamic characterisation tests. A damping of 1% is

considered for the study. The response at 150 mm from the pump outlet, obtained from the dynamic response analysis is found to be 102 g_{rms} as compared to 108 g_{rms} . The vibration spectrum in terms of PSD vs frequency also has been found to have a good match as shown in Figure 5.9. The dynamic stress analysis on the plumbing and the joint, has been carried out with this validated FE model.

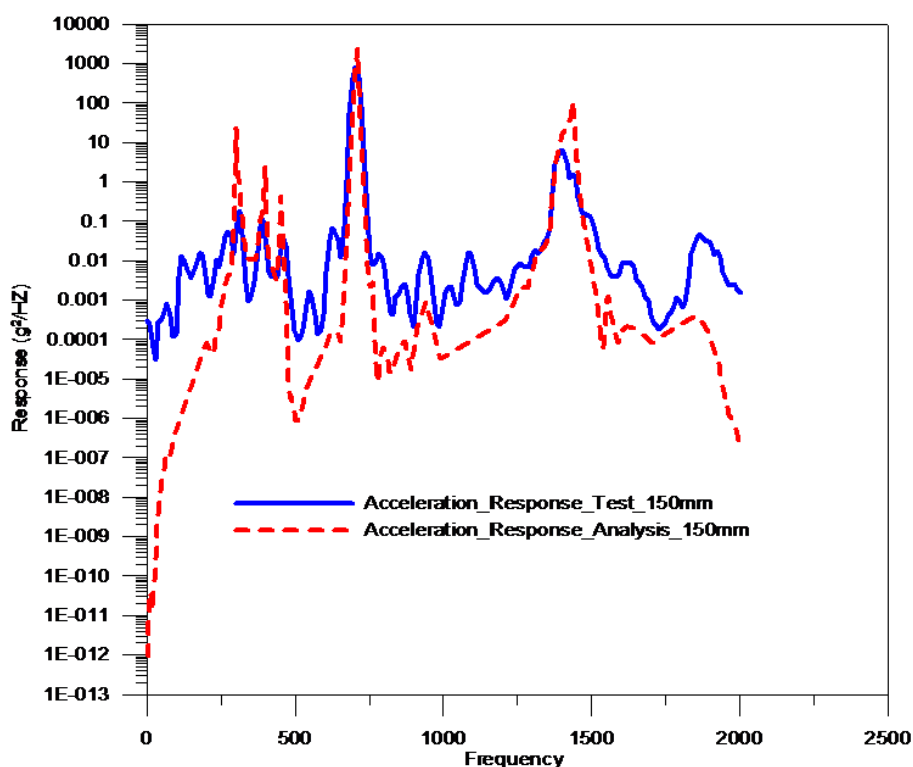


Figure 5.9 Comparison of vibration response - experimental vs analytical

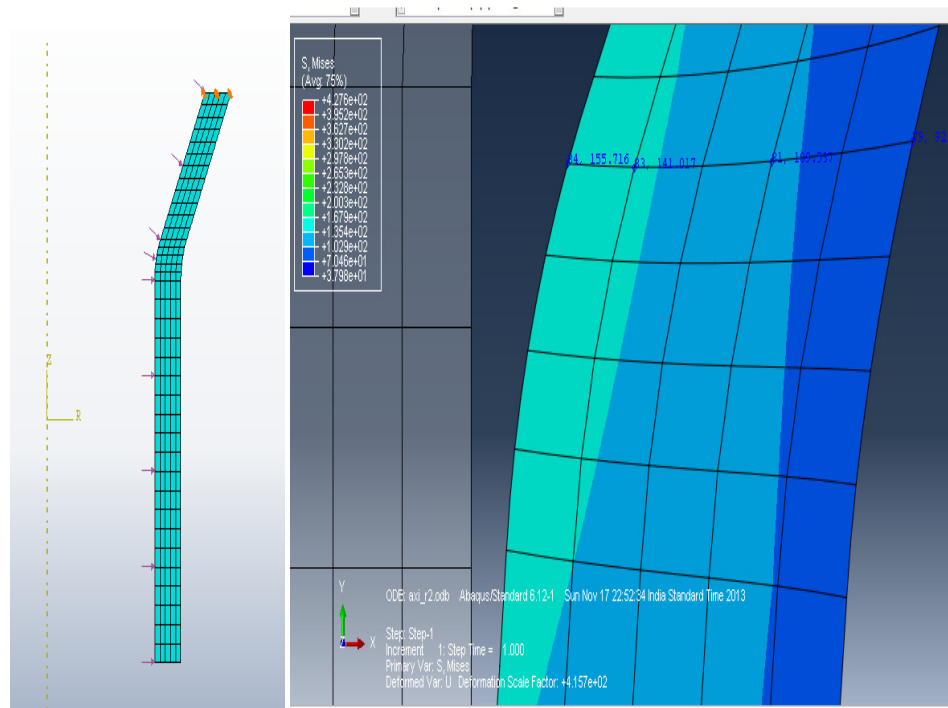
5.2.4 Stress analysis of plumbing flared joint

Accurate estimation of the service fatigue loads is one of the major problems facing the structural engineer and the assumed load spectrum has a large influence on the fatigue life prediction (Dave Steinberg, 2010). Hence in this analysis, a conservative approach is followed to estimate stresses at critical locations with an adequate factor of safety. Structural analysis of delivery plumbing is carried out for pressure and random vibration load. Maximum dynamic rms stress and pressure induced stress are seen at the flared zone of the plumbing.

Static stress

Axi symmetric finite element model of the plumbing is shown in Figure 5.10a. The model is used for the static analysis, to assess the static stresses induced by the

internal pressure. The flared region along with a small length of the cylindrical portion of the plumbing are modelled. Axial and radial degrees of freedom are constrained at one end of the delivery line. The analysis of delivery plumbing is carried out for an internal pressure of 21 MPa. The stress distribution is shown in Figure 5.10b. The von Mises stress is found to be 155.7 MPa at the inner diameter of the flared portion of the plumbing.



a. FE model

b. von Mises stress on the flared portion of the tube

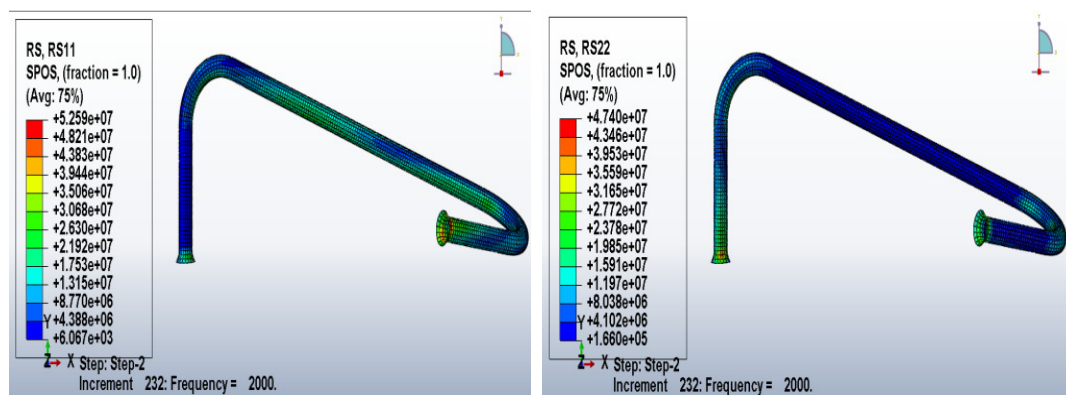
Figure 5.10 Axisymmetric FE model of the delivery plumbing and the stress analysis

Testing has been carried out more than 100 times in a single pump for a duration of 20 hrs. More than 100 pumps have been tested for use in similar applications and found to give consistent output pressure of the pump. This is achieved by pressure compensation setting of the pump. The pump delivery pressure during these tests has not exceeded more than 2.5%. A factor of safety of 1.25 is therefore considered conservative and the corresponding von Mises stress is 195 MPa.

Dynamic stress

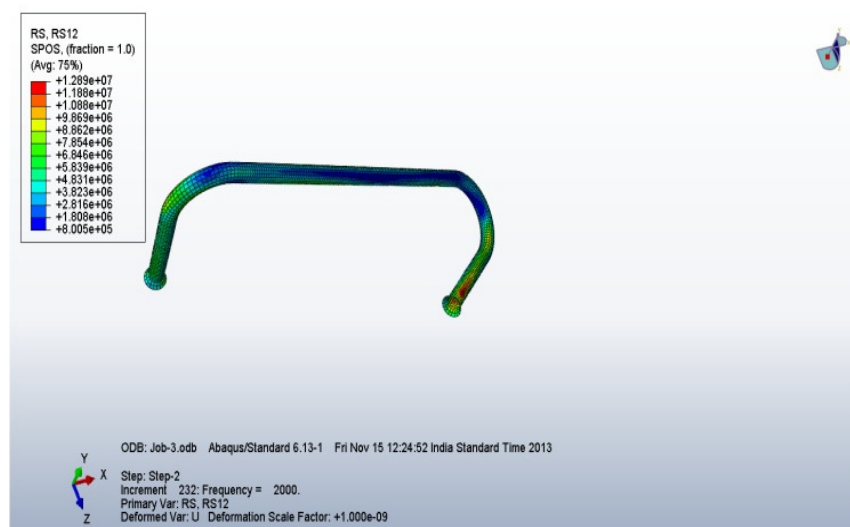
Dynamic stress analysis is carried out using the validated FE model described in Section 5.2.3 on dynamic vibration response analysis. The peak dynamic load occurs

at 703 Hz corresponding to the pump pulsation frequency. The plumbing is excited by the maximum of the vibration spectrum measured at 50 mm location, and the dynamic stresses are obtained from the model. The root mean square (rms) stress distributions upto 2000 Hz in the hoop, axial and shear directions are shown in Figures 5.11a to 5.11c. The dynamic rms von Mises stress is computed from the hoop, axial and shear stresses and is given in Table 5.2. The peak dynamic rms von Mises stress, with a factor of 1.5, corresponds to the Test no. 1, wherein a peak vibration level of 1208 g^2/Hz is observed at 703 Hz.



a. rms hoop stress distribution

b. rms axial stress distribution



c. rms shear stress distribution

Figure 5.11 The rms stress distribution upto 2000 Hz

Table 5.2 Dynamic stress for different load cases

Test No.	1	2	3	4	5	6	7	8	9	10	11	12	13
Frequency (Hz)	703	703	703	712	722	712	722	722	693	683	713	703	693
Peak vibration level (g ² /Hz)	1208	88	59	118	5	70	45	55	315	212	18	177	144
Dynamic stress with a factor of 1.5 (MPa)	211.5	27.5	51	24	11	29	62	35	92	96	21.6	95	56.7

Note: Maximum vibration response 1208 g²/Hz at 703 Hz and corresponding dynamic stress with a factor of 1.5 is 211.5 MPa

Table 5.3 Strength properties at the flared portion, from sample test results

Sample No.	1	2	3	4	5	6	7	8	9	10	11	12	13	14
UTS, MPa	960	965	930	1151	870	854	870	1034	965	896	917	854	870	890
Endurance strength, MPa	432	434	419	518	392	384	392	465	434	403	413	384	392	401

Note: Minimum UTS. $S_u = 854$ MPa and minimum endurance strength = 384 MPa

5.2.5 Strength distribution of plumbing and joints

The flaring operation carried out on the ends of the SS tubing results in cold working, and causes the strength in this region to increase. Since, the stresses are maximum at this location, the phenomenon is studied by preparing samples of the flared region. The micro hardness of the tube material after the flaring operation has been measured at high stress locations for 14 specimens and data converted to the ultimate tensile strength S_u (UTS). The endurance strength S_e is computed as 45 percent of the UTS. The data is given in Table 5.3. The minimum UTS and the endurance strength of the material at flared portion are 854 MPa and 384 MPa respectively. The specimens have been prepared from the flared tubing with conventional metallographic techniques using different grades of emery papers and final polishing with one micron diamond paste. After etching, microstructure at the flared region is observed. The microstructure consisted of equiaxed austenitic grain structure typical of AISI 304L steel, and a large number of slip bands have been observed within the grains, as shown in Figure 5.12, indicative of extensive deformation due to cold working, which corroborates with the measured hardness increase.

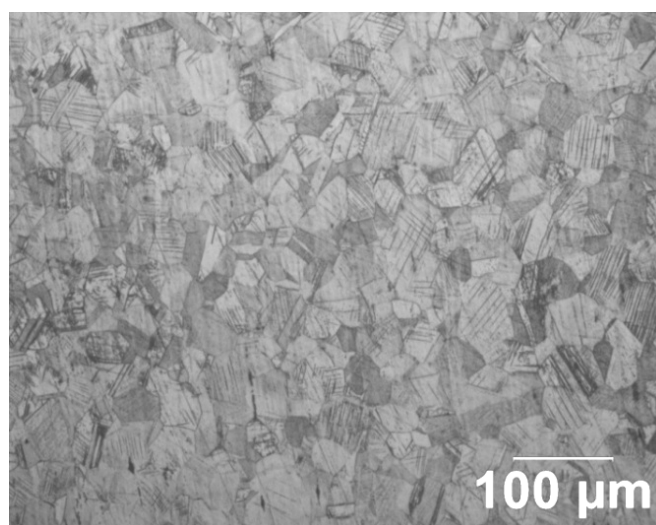


Figure 5.12 Microstructure of the flared tube

5.2.6 Fatigue analysis of plumbing joint

Fatigue life estimation and margin assessment are carried out by using the stress and strength data from the above analysis through traditional stress life method, based on modified Goodman diagram as well as Palmgren - Miner rule. The advantages with these methods are availability of data, easiness of implementation and ability to

represent the high cycle fatigue adequately (Richard Budynas and Keith Nisbett, 2011). Reliability of the plumbing system is assessed by using statistical distributions of endurance stress and strength.

Fatigue life using Goodman diagram

Fatigue load cycles are defined by alternating stress amplitude (S_a) and mean stress (S_m), or by the stress ratio R (S_{\max}/S_{\min}) and stress range ($2S_a$). The S-N curves are obtained for different values of mean stress. For the analysis of S-N diagram, the preferred formulation is Goodman diagram (Herbert Sutherland and John Mandell, 2005). As the mean stress increases, the fatigue strength decreases. From these plots, a fatigue diagram for constant fatigue life with S_m in X axis and S_a in Y axis can be obtained. In the Goodman diagram ABCF, when $S_m = 0$, the allowable alternating stress $S_a = S_e$, the endurance limit. When $S_a = 0$, the allowable mean stress $S_m = S_u$, the ultimate tensile strength. The Goodman diagram assumes a linear decrease of the fatigue strength for an increasing S_m . It is the best known and most commonly used method for the fatigue analysis of metallic structures (Westphal and Nijssen, 2014). The governing equation for the Goodman diagram is

$$\frac{S_a}{S_e} + \frac{S_m}{S_u} = 1 \quad (5.3)$$

The Goodman diagram approach is conservative for fatigue analysis of most metallic structures except for high strength alloys with a low ductility such as AISI 4340 steel, heat treated to a very high S_u value of 1830 MPa, where the fatigue strength drops more (Jeap Schijve, 2009). This approach is used to assess the life cycle estimation and reliability of the system. Since the worst case 3σ alternating stress with an adequate factor of safety is considered to act in each cycle, the approach is very conservative.

The structural margin of the flared region of the plumbing is studied by drawing Goodman diagram, considering the lowest measured local UTS of 854 MPa, the corresponding yield strength of 690 MPa and endurance strength of 384 MPa. The local stress point corresponding to a mean tensile stress of 195 MPa and alternating stress of 211.5 MPa (Point G) is well within the Goodman line ABCD as shown in Figure 5.13. This ensures that no yielding occurs on the critical flared portion of plumbing and it can withstand more than 10^6 number of cycles.

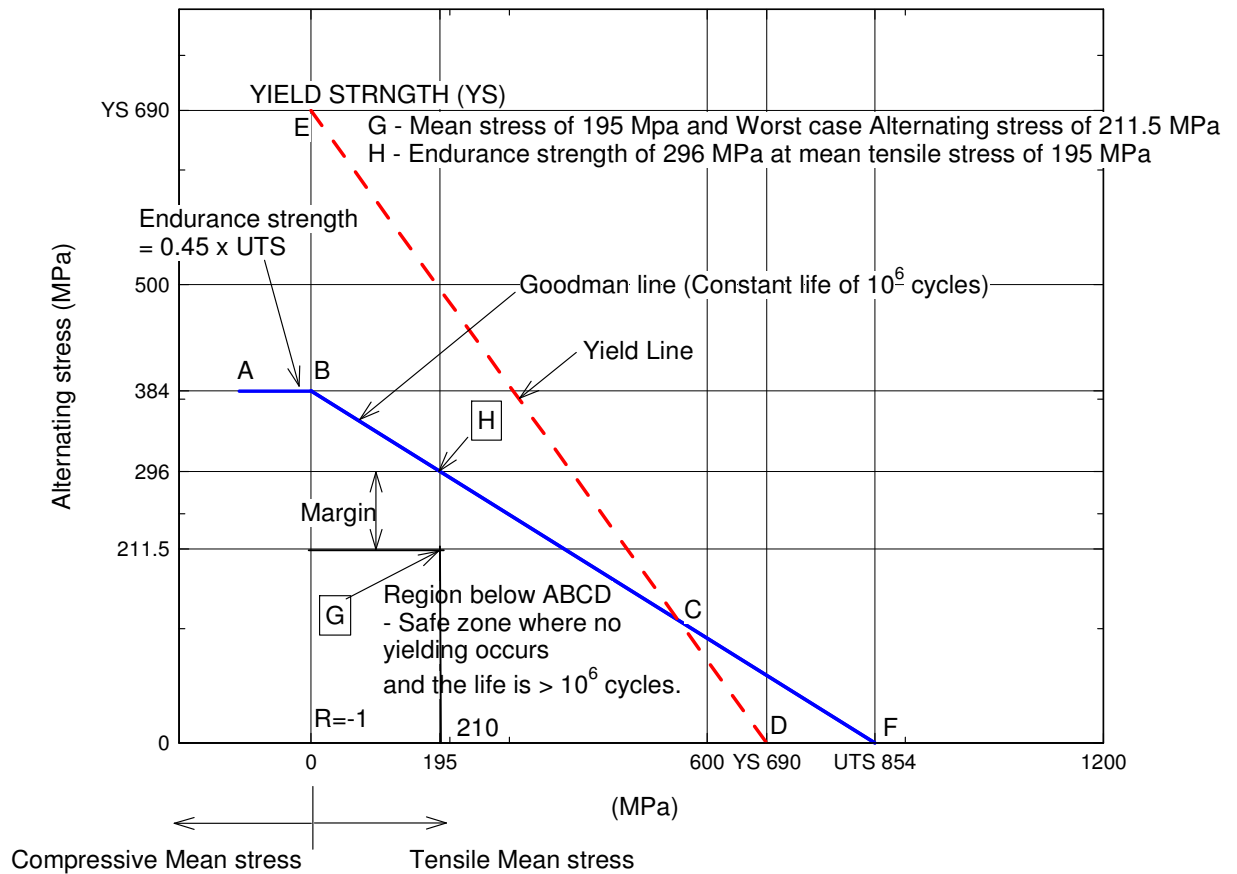


Figure 5.13 Goodman diagram with minimum strength and maximum stress

The maximum allowable alternating stress corresponding to a mean tensile stress of 195 MPa is 296 MPa, point H in Figure 5.13. Hence a margin of 0.52 exists against the endurance strength. Since the peak vibration response occurs at about 700 Hz, the number of cycles experienced at this stress level for 150 s of flight duration is 105000 cycles whereas the joint can withstand 10^6 number of cycles without yielding. Thus, the fatigue life estimate for the plumbing is one order higher than the requirement.

Reliability Analysis based on modified Goodman diagram

In general, a large scatter is observed in the fatigue strength of materials. Tiiu Kutt and Bieniek (1988) highlight the importance of the stochastic models that take into account this randomness and predict the probability of failure as a function of expected number of cycles of loads. The stress and strength estimates are point estimations of the mean, maximum or minimum values, with the corresponding measure of dispersion. When stress and strength are statistically distributed with the probability distribution functions $f_s(s)$ and $f_S(s)$ respectively, reliability is the

probability that strength value will exceed stress value and is given by the Equation (5.4) (William Wessels, 2010).

$$\text{Reliability, } R = \int f_S(s) [\int f_s(s) ds] ds \quad (5.4)$$

The probability density functions of stress and strength have an overlap in the stress-strength axis, which characterises failure probability (William Wessels, 2010). In the case of normal stress-normal strength distribution, with a mean strength μ_s and a standard deviation of σ_s , and a mean stress μ_s with a standard deviation of σ_s , the z-statistic for stress-strength interference is computed as

$$\text{z-statistic} = \frac{\mu_S - \mu_s}{\sqrt{\sigma_S^2 + \sigma_s^2}} \quad (5.5)$$

The interference regime or the unreliability U, and the reliability R are given by

$$U = \Phi(-z) \quad (5.6)$$

$$R = 1 - \Phi(-z) \quad (5.7)$$

The reliability analysis of the joint is estimated based on the alternating stress-endurance strength interference. The alternating stress and endurance strength data are given in Tables 5.2 and 5.3 respectively. The statistical parameters of the data are given in Table 5.4.

Table 5.4 Statistical distribution of stress and strength

Sl No.	Stress	Mean (μ)	Standard deviation (σ)
1	Dynamic (Alternating) stress (s), MPa	62.5	53.5
2	Endurance Strength (S), MPa	331	29.25

The goodness of fit test for normal distribution has been conducted using Kolmogorov-Smirnov test with a null hypothesis H_0 : Data follows a normal distribution and H_1 : Data does not follow a normal distribution. In this test, the

cumulative distribution function (cdf) for the data points is compared with cdf data of a perfect normal curve. The maximum difference between the cdf of the data points and its expected cdf is compared with the critical value corresponding to the sample size at a defined significance level. The test has been conducted at a significance level of 0.05, and the results are tabulated for both stress and strength in Table 5.5. As the maximum difference has been less than the critical value for stress and strength data, the null hypothesis that the data follows normal distribution is accepted.

Table 5.5 Results of Kolmogorov-Smirnov test for normal distribution at a level of significance of $\alpha = 0.05$

Sl No.	Data set	Sample size	Critical value	Max. difference b/w expected & actual CDF	Null hypotheses	Result
1	Dynamic Stress	13	0.23	0.196	Accepted	Fitting to Normal
2	Endurance Strength	14	0.23	0.198	Accepted	Fitting to Normal

From the data given in Table 5.4, the alternating stress due to dynamic load has a mean of 62.5 MPa, with a standard deviation of 53.5 MPa. As the margin and reliability are assessed by the interference theory, the Goodman diagram is redrawn with the mean strength properties namely, UTS of 930.4 MPa, yield strength of 738 MPa and endurance strength of 418.7 MPa, as shown in Figure 5.14. As the system pressure is deterministic and a conservative safety factor of 1.25 is applied, the mean tensile stress of 195 MPa is considered static without random variation. The corresponding endurance strength from the Goodman diagram is 331 MPa, and assuming the same coefficient of variation as that of the UTS, the standard deviation is 29.25 MPa, as shown in Table 5.4.

So, from the above data, the mean strength is $\mu_S = 331$ MPa with a standard deviation of $\sigma_S = 29.25$ MPa, and the mean stress $\mu_L = 62.5$ MPa with a standard deviation of $\sigma_L = 53.5$ MPa.

The z-statistic for load (stress)-strength interference from Equation (5.5),

$$z\text{-statistic} = \frac{\mu_S - \mu_s}{\sqrt{\sigma_S^2 + \sigma_s^2}} = 4.4 \quad (5.8)$$

$$\text{Reliability } R = 1 - \Phi(-z) = 1 - \Phi(-4.4) = 1 - 0.00000541 = 0.999995 \quad (5.9)$$

Hence, a high joint reliability of 0.999995 is established for the plumbing system.

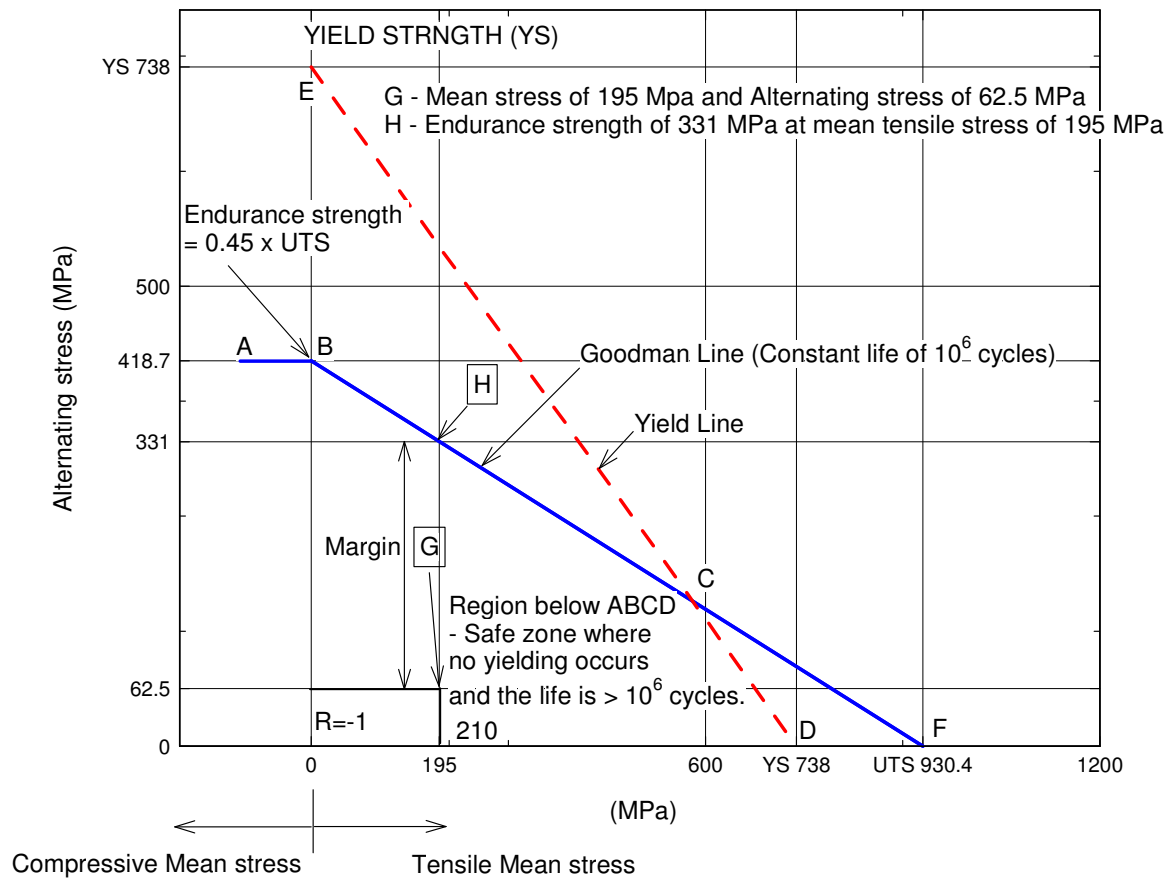


Figure 5.14 Goodman diagram with mean strength and mean stress

Life cycle estimation using Miner's rule

The loading and the stress history are random in nature for structures subjected to vibration, and the Palmgren-Miner rule of cumulative damage is the most suitable method for fatigue analysis in such cases (Fatemi and Yangt, 1998; Tiiu Kutt and Bieniek, 1988; Walter Schutz, 1979). The cyclic loads cause a certain amount of fatigue damage in each cycle and when the total damage accumulates to a certain threshold, failure takes place (Chen Hongxia et al., 2014). For such loadings, the

models for the cumulative fatigue damage are deterministic and extremely simple, employing the Palmgren-Miner rule (Jeap Schijve, 2009; Walter Schutz, 1979). Miner first represented the linear damage concept in the mathematical form. If n_1 is the number of cycles experienced by a system at constant stress amplitude S_{a1} , and the fatigue life at this stress level is N_1 cycles, it is equivalent to consuming n_1/N_1 percentage of its fatigue resistance. Generalising this, if n_i number of cycles are experienced at a stress magnitude of S_{ai} by a system, which has a fatigue life of N_i cycles at this stress level, then the failure occurs if the fatigue resistance is fully consumed i.e.,

$$\sum \frac{n_i}{N_i} = 1 \quad (5.10)$$

Walter Schutz (1979) considered the un-conservative prediction of the Miner rule and accounted for the same by making it conservative by a “relative Miner rule”,

$$\sum \frac{n_i}{N_i} = q, \text{ with } q < 1 \quad (5.11)$$

where the value of q has to be selected from variable amplitude test data with similar load-time histories.

In the Goodman diagram approach, it is assumed that the plumbing is subjected to the peak dynamic loading in every cycle of loading, which is very conservative as the vibration response is random and peak does not occur in every cycle. A more practical approach for life cycle estimation would be through Miner’s rule taking into consideration of the stochastic nature of the load application. Maximum dynamic rms stress with a factor of 1.5 is found to be 70.5 MPa, from the FE random response analysis discussed earlier.

Miner’s rule, based on the number of cycles in 1σ , 2σ , 3σ and 4σ stress levels and the corresponding fatigue limit from S-N curve is used to obtain the life cycle estimation. The number of cycles (n_i) experienced at 1σ , 2σ , 3σ and 4σ stress levels will be 68 %, (95-68) %, (99.73-95) %, and (100-99.73) % of total cycles respectively. As the flight duration is 150 s and the frequency of system is around 700 Hz, the total number of cycles is 105000. Therefore the total number of cycles (n_i) at 1σ , 2σ , 3σ and 4σ stress levels is 71400, 28350, 4967, and 284 respectively as shown in Table 5.6

Table 5.6 Flight number of cycles and fatigue life at different stress levels

Sl. No.	Alternating Stress, MPa		Mean stress, S_m , MPa	Effective alternating stress, S_{ea} in MPa	No. of cycles experienced by system (n)	Fatigue life at the stress level S_m and S_{ea} (N)	Ratio $\{n/N\} \times 4$
	Stress level	Stress value S_a					
1	1 σ	71	195	92	71400	Infinite	-
2	2 σ	141	195	183	28350	Infinite	-
3	3 σ	212	195	275	5250	Infinite	-
4	4 σ	282	195	365	284	$>>10^6$	0.001136

In order to estimate fatigue life using the Miner's rule, it is necessary to compute the number of cycles the system can withstand at each stress level. For a given mean stress S_m and alternating stress S_a , the corresponding equivalent fully reversible alternating stress S_{ea} (with $S_m = 0$) can be obtained from the Goodman relation.

$$\frac{S_a}{S_{ea}} + \frac{S_m}{S_u} = 1, \text{ and so, } S_{ea} = \frac{S_a}{\left[1 - \frac{S_m}{S_u}\right]}. \quad (5.12)$$

Effective alternating stress, S_{ea} , is computed with a mean stress of 195 MPa for different alternating stresses at 1 σ , 2 σ , 3 σ and 4 σ stress levels. The effective alternating stresses thus computed are 92, 183, 275 and 365 MPa respectively. As these stress levels are less than endurance limit (S_e) of 384 MPa, the system can withstand infinitely large number of cycles at these stress levels. Although the 4 σ level of effective alternating stress of 365 MPa is less, it is close to the endurance limit of 384 MPa. Therefore, conservatively, the system is assumed to have only a life of 10^6 cycles at the 4 σ stress level of 365 MPa, corresponding to the endurance strength. Table 5.6 gives the dynamic stress levels at 1 σ , 2 σ , 3 σ and 4 σ levels, corresponding effective alternating stresses with mean stress of 195 MPa, and the

number of cycles experienced by the system at these stress levels, and the fatigue life of the system at these stress levels.

The margins are assessed with a factor of safety of 4 to account for scatter (Chen Hongxia et al., 2014). Applying the Miner's rule discussed in Section 4.2,

$$\text{Margin of safety} = \frac{1}{4 \times \left[\left(\frac{n_1}{N_1} \right) + \left(\frac{n_2}{N_2} \right) + \left(\frac{n_3}{N_3} \right) + \left(\frac{n_4}{N_4} \right) \right]} - 1 \quad (5.13)$$

As N_1, N_2, N_3 , are infinitely large number of cycles, the equation becomes

$$\text{Margin of safety} = \frac{1}{4 \times \left[\left(\frac{n_4}{N_4} \right) \right]} - 1 \quad (5.14)$$

The system is found to have adequate margins against fatigue failure.

5.2.7 Fatigue analysis results and improvement in system design

The critical fatigue failure mode of the hydraulic plumbing flared tube joint in an electro hydraulic actuator has been identified. Experiments have been carried out to assess the vibration responses on the hydraulic plumbing. System level actuation tests are performed in the flight configuration with mass and moment of inertia simulated liquid engine. The actuation is done with frequency response commands and by simulating the flight commands. During the system level tests, vibration response on the delivery plumbing is found to be high in general, and a maximum response of $1208 \text{ g}^2/\text{Hz}$ at 703 Hz is observed in one of the test runs. The analysis is done with a conservative approach, for the maximum observed vibration response of the plumbing and minimum of the measured strength properties.

A finite element model of the delivery plumbing is made, free vibration analysis is carried out, and the plumbing frequencies have been obtained. The root cause of the higher vibration is identified as the pump pressure pulsation frequency of 720 Hz coinciding with the fourth mode frequency of 709 Hz of the plumbing. The FE model is validated with the experimental results by obtaining the response at 150 mm location analytically, for a test measured spectrum given as input at 50 mm location. A good match of the frequencies and the PSD spectrum is seen. The model, after this verification, is used for dynamic stress analysis for the worst case test measured input spectrum. The static analysis is carried using an axisymmetric model for the system

internal pressure of 21 MPa and static stress values have been obtained. A factor of safety of 1.5 and 1.25 are applied on the dynamic and static stresses, thus making the fatigue analysis more conservative.

The margins on the life cycle and fatigue strength are estimated using the Goodman diagram and adequate margins have been established with respect to dynamic stress and fatigue life cycle. Stress and strength data are checked for its goodness of fit for normal distribution. Reliability of the joint using stress-strength interference theory is estimated at 0.999995. This approach is very conservative as it assumes that the system is subjected to peak stress in every cycle, whereas the dynamic loading is random in nature and the system is subjected to the peak stress only in a few cycles. Therefore, the margin on the life cycle has been computed more pragmatically by using the relative Miner's rule. A conservative factor of 4 is considered to account for the scatter reported in the literature on the fatigue strength. A very high margin of safety is established, even with this conservative factor of safety.

Thus, through different approaches, the system reliability and life cycle estimates are assessed, and the system is found safe to fly in the launch vehicle. However, for launch vehicle applications, the system has to be made as much robust as possible, attempting all the possible improvements in system design. In accordance with this principle, the following design solutions have been considered:

- Change in the pipe configuration so that the frequency of the pipe can be kept away from the pump frequency of 720 Hz. Pipe frequencies in all the modes have to be outside the frequency band of 510-1020 Hz.
- Change in the operating speed of the pump to keep the pump pulsation frequency away from the frequency of the plumbing.
- Change in the number of pistons of the axial piston reciprocating pump from nine to seven and making the pump frequency to 560 Hz from the earlier 720 Hz. The pump frequency of 560 Hz can be kept away from the plumbing frequencies.

As the first two solutions have deleterious effects on the system from the envelope point of view and the functional performance respectively, the third solution has been finalised. With seven piston configuration, the maximum vibration response is found to be $1 \text{ g}^2/\text{Hz}$ at 560 Hz. The peak response observed is found to vary from 27 to 32

g^2/Hz at 1680 Hz. The vibration responses have been found to be very benign at the critical frequency and the system design is found very robust for the fatigue failure mode.

5.3 Failure analysis of a flexible hose

The control surfaces of a reusable launch vehicle on the winged body and the fins on the first stage solid rocket are actuated by a single hydraulic power source located at the fore end of the vehicle. The systems like pump, reservoir, accumulator, manifolds, valves, and regulators are connected by both rigid plumbing and flexible hoses as per the functional needs. Flexible hoses are necessary to make connections between different subsystems located within a complex sub-assembly, where relative motions are involved and where high vibrations are expected. PTFE hose with stainless steel braid as reinforcement has been selected as the flexible hose for the application. These hoses are swaged with the end adapters with metal to metal sealing interface for making further connections. This section of the chapter brings out details of the failure that occurred in the swaged joint during the process of qualification of the hoses, identification of root cause and actions taken to avoid similar failures.

5.3.1 System description

The flexible hoses used in the hydraulic CAS shall be capable of withstanding high pressure and temperature and shall provide high degree of cleanliness for the hydraulic oil. Considering these requirements PTFE hose with stainless steel braid as back up is chosen for the application. The interface of the hose with the end adapter is shown in Figure 5.15. The failure of basic hose or the swaged joint with adapter is a single point failure mode for the hose as well as the control system.

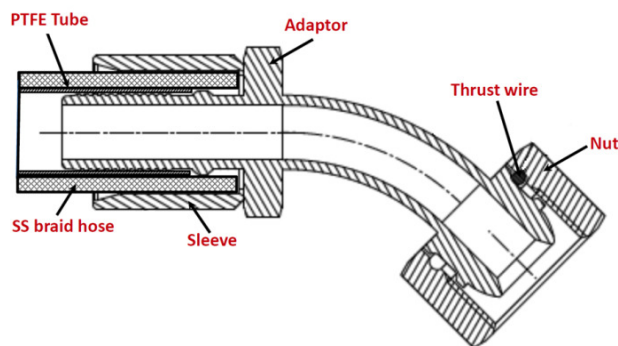


Figure 5.15 Schematic showing the swaged joint interface of hose assembly

The swaging operation is carried out at room temperature using hydraulically operated swaging machine as shown in Figure 5.16. The swage assembly with the AISI 304 stainless steel sleeve is pushed through a fixed swaging die. The OD of sleeve gets reduced from one end to the other, and in the process develops a compressive force which grips the hose against the serrations provided in the adapter, making a permanent joint. To avoid failures in the swaged joint, it is important to control key parameters that affect the gripping force of the joint. Towards this, all aspects related to the process like strict adherence to the standards, control of critical interface dimensions, controlled compression for the swaged joint, alignment of the hose with respect to swaging die, end preparations of the hose and the process parameters of the swaging machine are addressed and finalised.

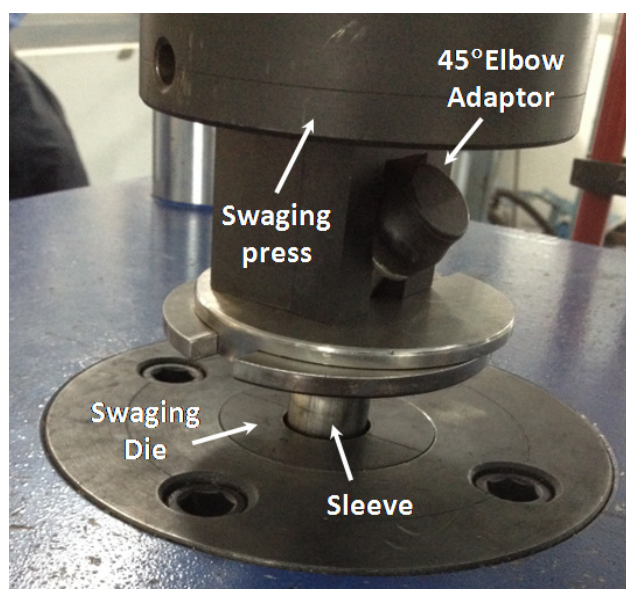


Figure 5.16 Digital photograph showing the swaging process

5.3.2 Qualification procedure for flexible hose system

Considering wide variations that can result during the manufacturing of the hose, adapter, swaging process and overall system integrity, a detailed design/process verification plan has been made in terms of qualification and acceptance test procedures. The qualification plan includes leak checks with pneumatic pressure testing up to 1 MPa, hydraulic pressure testing at working pressure 22 MPa and proof pressure at 33 MPa, low and high temperature tests followed by proof pressure tests, impulse pressure test, burst test at 44 MPa and system level vibration test, as shown in Table 5.7.

5.3.3 Background to failure

The flexible hoses have been prepared strictly following the component acceptance procedures and the swaging process parameters. The hoses after preparation have been taken up for qualification testing. The system has been subjected to initial pneumatic pressure testing up to 1 MPa for 1 minute duration for verifying leak tightness of the hose and joints before going for high pressure hydraulic tests. The hose withstood the pneumatic pressure test. A crack has been observed on the hose sleeve made of AISI 304 when assembly was being prepared for pressure testing in hydraulic pressure test set up. The hose has been removed from the set up and kept aside. The crack has grown after the removal from the test set-up and completely opened up by about 2 hr. Time.

Table 5.7 Details of the qualification tests for the flexible hose assembly

Sl. No.	Qualification tests	Remarks
1.	Dye penetration test on swaged area	To detect surface cracks on swaged surface
2.	Pneumatic pressure test	For joint leak tightness under pneumatic pressure of 1 MPa
4.	Working pressure & proof pressure test	Verifying integrity and leak tightness @ 22MPa and 33 MPa
5.	High temperature test followed by proof pressure test	Soak at 260°C for 3 hour
6.	Low temperature test followed by proof pressure test	Soak at - 45°C for 3 hour
7.	Pressure hold test for 24 hrs.	@operating pressure 22MPa
8.	Impulse pressure test	Verification for fatigue failures, cycling @ the rate of 9 cycles /20 s for 5000 cycles between 0MPa and 33MPa
9.	Burst pressure test	@44MPa pressure
10.	Pneumatic pressure test (Post)	For joint leak tightness under pneumatic pressure of 1MPa
11	Vibration test at assembly level	Verification for fatigue failures

The cracked sleeve has been examined visually and observations are recorded using digital camera. The crack when noticed during the preparation of hydraulic pressure testing is shown in Figure 5.17a. The crack propagation leading to complete opening of the crack after removal from the test set up is shown in Figure 5.17b.

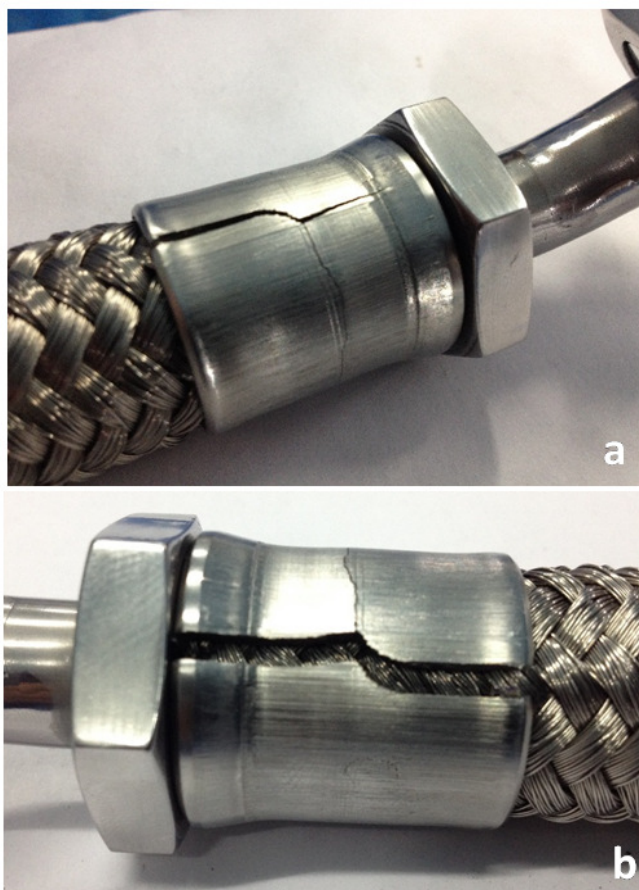


Figure 5.17 Digital photograph showing the cracking of sleeve in hydraulic pressure set up (a), and after removal from the set up (b)

5.3.4 Failure analysis procedure

Detailed metallurgical analysis is carried out on the cracked sleeve to find out the reasons for cracking.

The fracture surface, surface of the sleeves and metallographically prepared specimens have been examined under Carl Zeiss EVO-50 Scanning Electron Microscope (SEM). The chemical composition of the micro constituents is obtained using Oxford-INCA Energy dispersive X-ray spectroscope (EDS) attached with the SEM. The sleeve is sectioned longitudinally and has been metallographically polished with a series of

silicon carbide emery papers and final polishing has been conducted with alumina suspension and one micron diamond lapping compound.

The specimens have been etched with acetic glyceric acid reagent (HCl-15 ml, HNO₃-10 ml, acetic acid-10 ml and Glycerol-5 ml) to reveal the microstructural features. Microstructural observations have been made using an Olympus GX-71 optical microscope and microphotographs recorded. Microhardness measurements have been carried out using Wilson Tukon microhardness tester using Vickers indenter at 100 gf load.

5.3.5 Results of the failure analysis

Visual observations of the cracked sleeve revealed rough surface with die mark lines along the length of the sleeve as shown in Figure 5.18. The primary crack is found to have initiated from OD of the tubular sleeve. The primary crack has been circumferential and deviated along the length during propagation causing complete separation of longitudinal crack as shown in Figures 5.17 & 5.18.

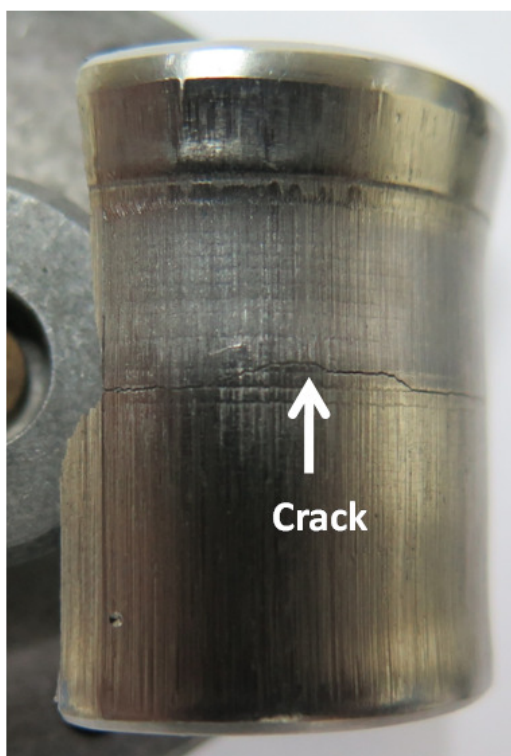


Figure 5.18 Photograph showing the circumferential crack on the sleeve.

SEM observations on the surface of the sleeve near to crack location revealed circumferential micro cracks near to the primary crack as shown in Figure 5.19. Figure 5.19a shows the primary crack indicated by white arrows. Figure 5.19b shows the primary crack at top of the image and two micro cracks below the primary crack. Figure 5.19c shows the higher magnification view of the two micro cracks shown in Figure 5.17b. Figure 5.19d shows micrograph of numerous fine micro cracks on the surface.

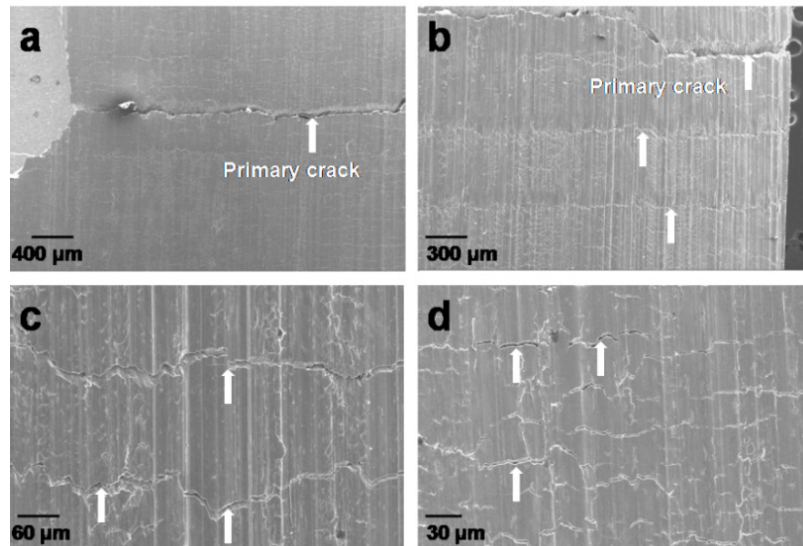


Figure 5.19 SEM image of circumferential micro cracks near to the primary crack.

The fracture surface of the deviated crack which has opened up and separated into two parts has been observed under SEM. Figure 5.20 shows the full view of fracture surface covering the complete thickness of the sleeve. It also shows the location of crack path deviation from circumferential crack to the longitudinal crack.



Figure 5.20 SEM image showing a full view of fracture surface covering complete thickness of the sleeve.

At the location of crack path deviation, a large size silicate inclusion stringer and uniformly distributed sulphide stringers have been observed as shown in Figure 5.21.

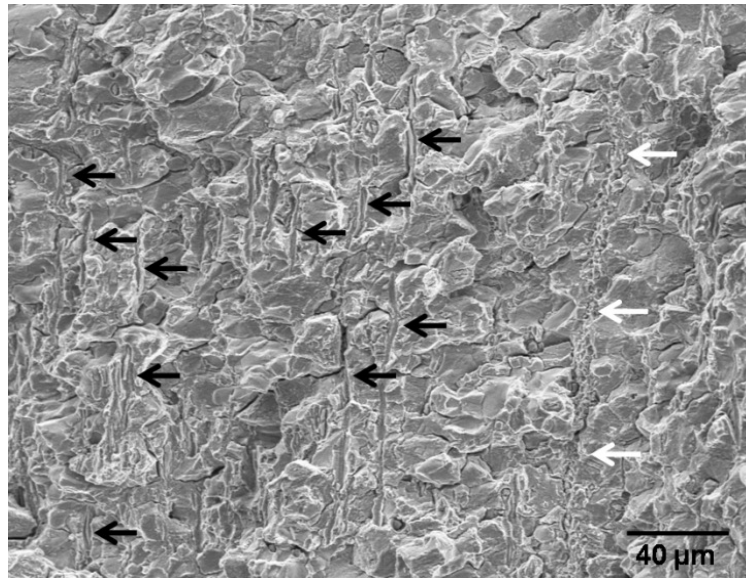


Figure 5.21 SEM image showing isolated large size silicate inclusion (indicated by white arrows) and uniformly distributed sulphide inclusion stringers (indicated by black arrows) at the location of crack path deviation.

The high magnification view of the large size silicate stringer and sulphide stringers are shown in Figures 5.22 and 5.23 respectively. The fracture surface has shown predominantly intergranular mode of failure as shown in Figure 5.24.

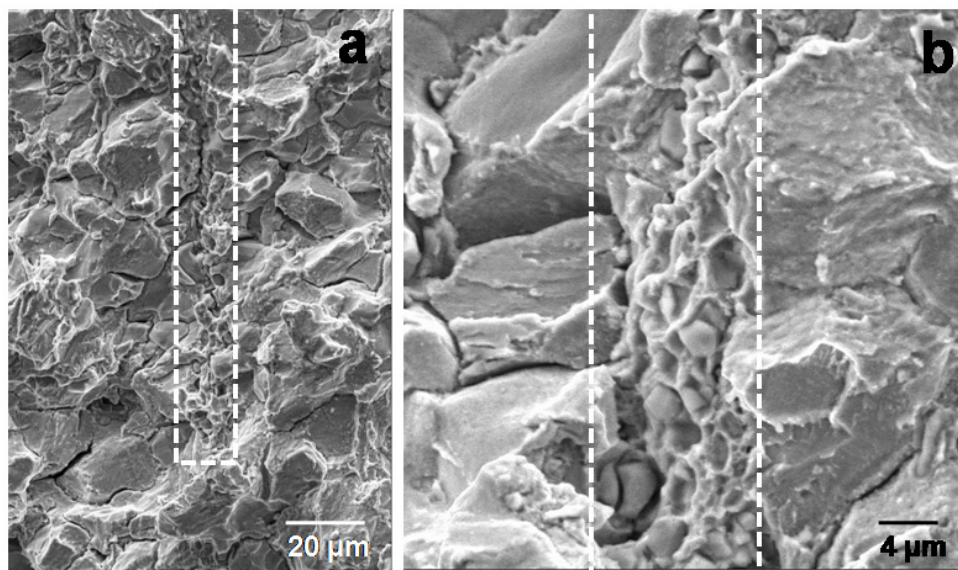


Figure 5.22 High magnification SEM images showing isolated large size silicate stringer on the fracture surface

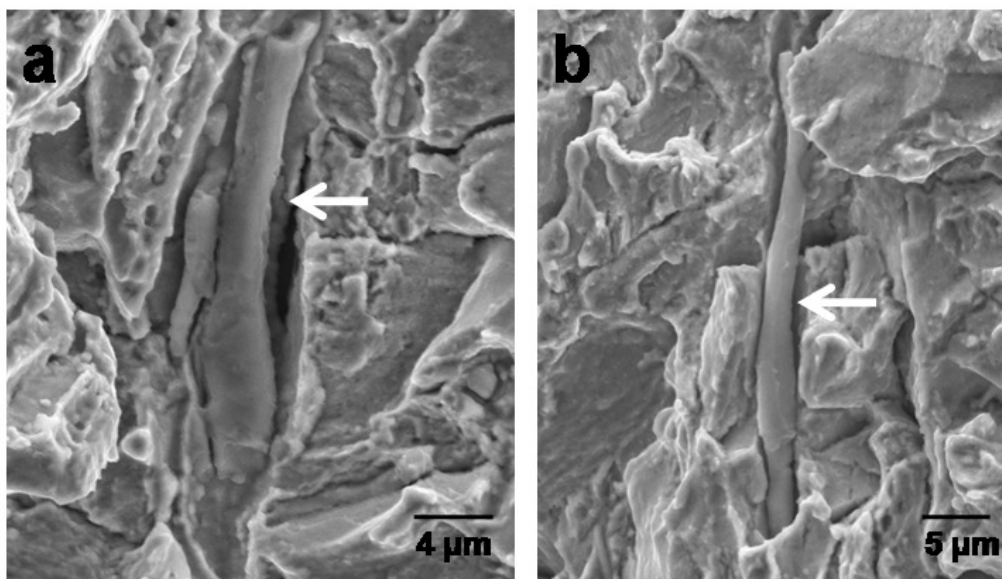


Figure 5.23 High magnification SEM images showing sulphide inclusion stringers on the fracture surface

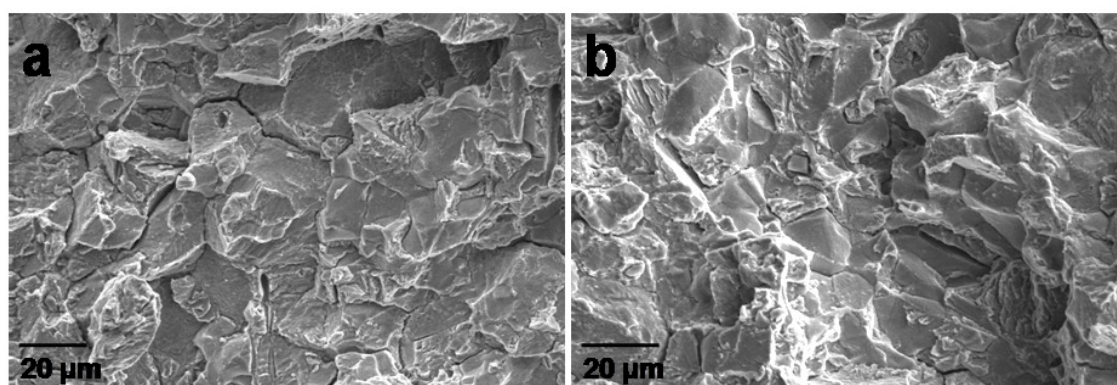


Figure 5.24 SEM images on the fracture surface showing inter granular mode of cracking

Metallographically prepared specimens have been observed under optical microscope for inclusion content. The observations revealed the presence of uniformly distributed sulphide inclusions and oxide inclusion in the material as shown in Figure 5.23a. Isolated long silicate inclusion stringers are also present in the material as shown in Figures 5.25b-d. Very long silicate inclusion stringers of size 2.2 mm and 1.16 mm size have been also observed in the microstructure and are shown in Figure 5.26a and Figure 5.26b respectively.

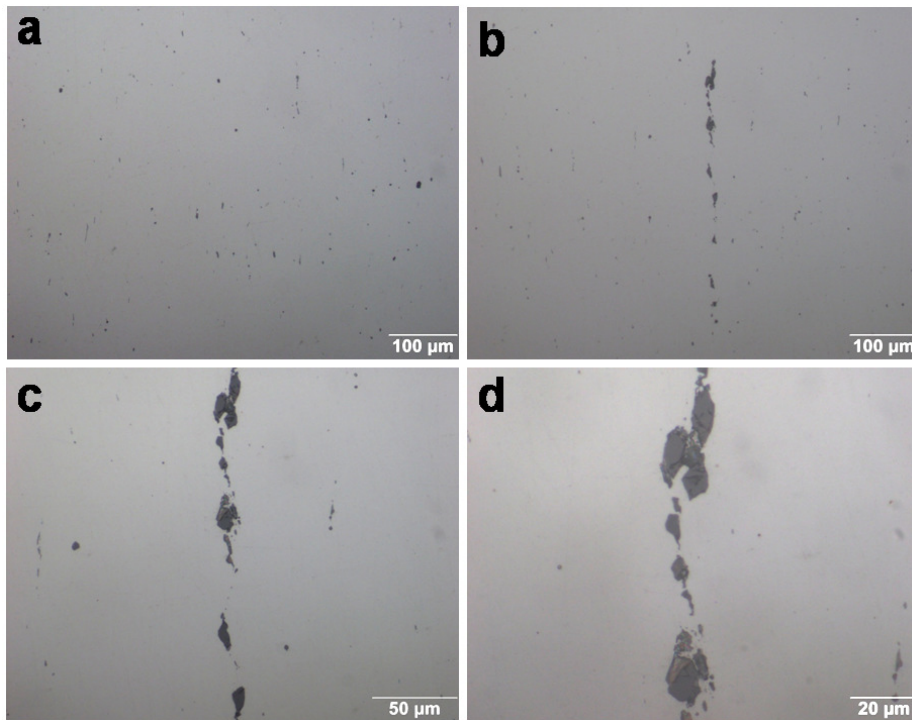


Figure 5.25 Optical micrographs in un etched condition showing (a) sulphide and oxide inclusions, (b) silicate inclusion stringer, (c & d) silicate inclusion stringers at high magnification

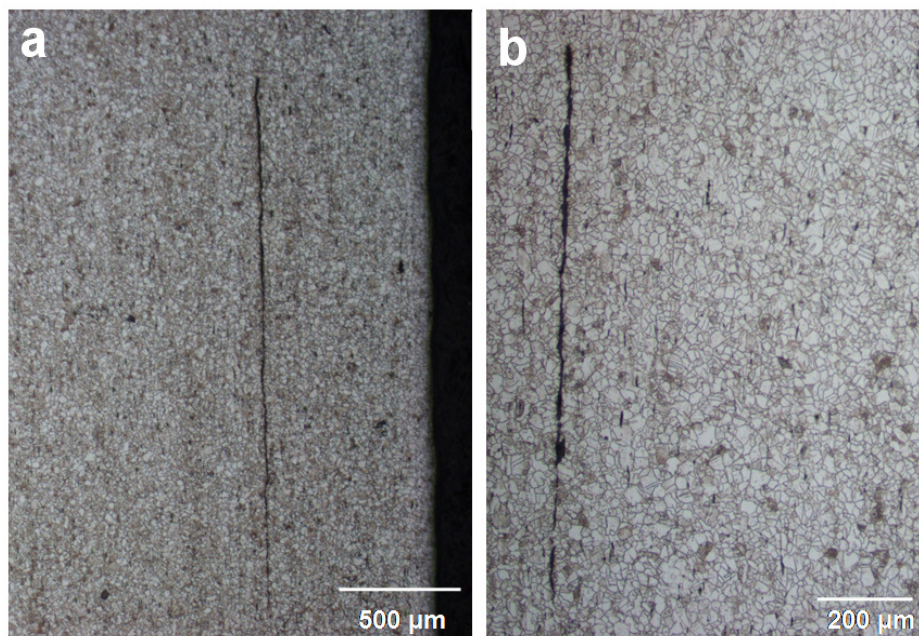


Figure 5.26 Optical micrographs showing very long silicate inclusions.

Micro structural observations at the crack location revealed that the crack originated from the OD of the sleeve and propagated inwards. Two micro cracks of 250 μm and

400 μm size originating from OD are also observed near to the primary crack as shown in Figures 5.27a. Small deviation of the primary crack is noticed at the intersection of crack path with silicate inclusion stringer as shown in Figures 5.27a & b. Very fine micro cracks of 20-30 μm are noticed at the outer edge of sleeve at higher magnification. Deformed and elongated grains have been noticed at the OD edge upto approximately 400 μm from the surface. Equiaxed grains have been observed at the interior of the sleeve as shown in Figure 5.28. Cracking has been completely along the grain boundaries throughout the crack path as shown in Figure 5.29a. The grain boundaries have been decorated with chromium carbide particles as shown in Figure 5.29c. Micro hardness measurements indicated hardness of 470 VPN at outer edge and 340 VPN at the middle of the sleeve.

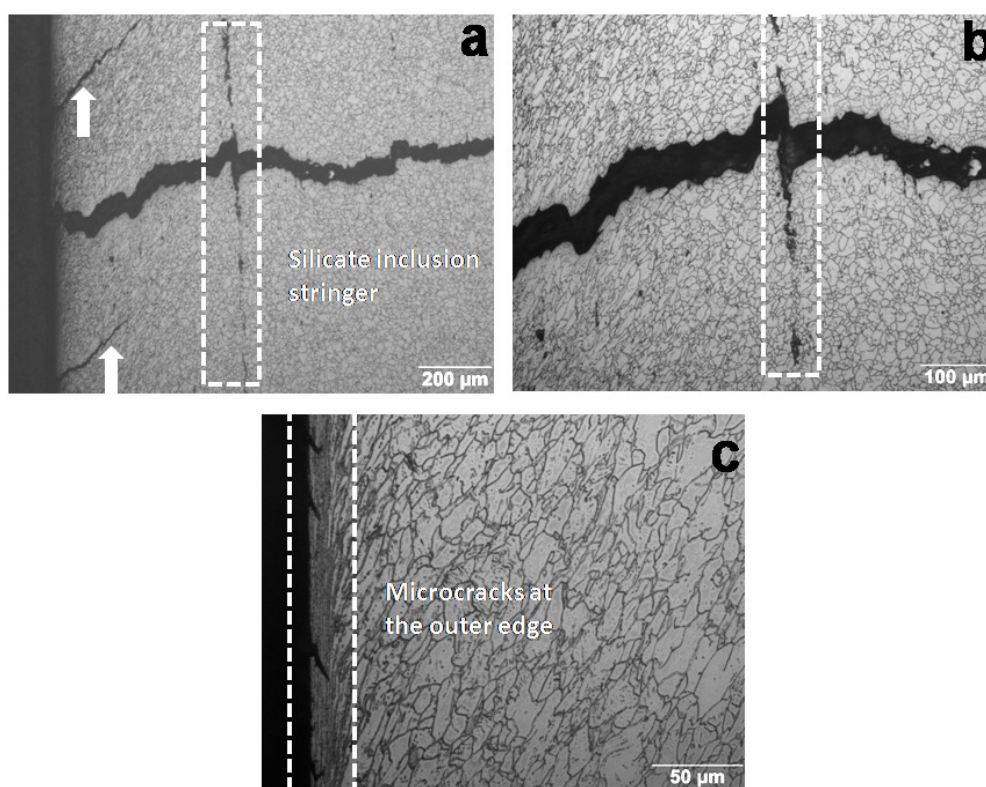


Figure 5.27 Optical micrographs showing (a) two micro cracks of size 250 μm and 400 μm indicated by arrows near to the primary crack and silicate inclusion stringer along the crack path, (b) little deviation of the crack at the intersection with silicate inclusion stringer, (c) numerous small size micro cracks of size 20-30 μm at outer edge of the sleeve.

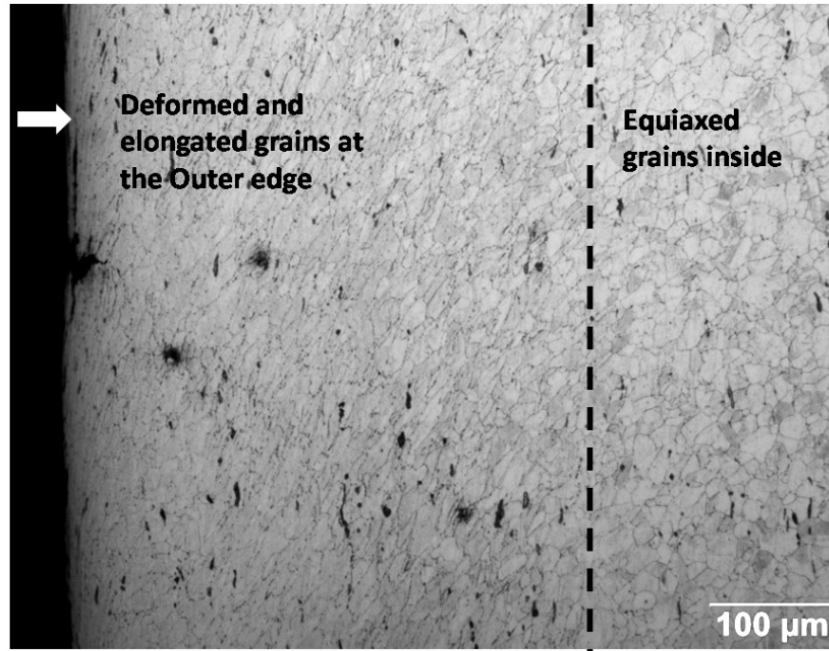


Figure 5.28 Optical micrographs showing deformed and elongated grains at the outer diameter up to approximately 400 μm inside and equiaxed grains at interior of the sleeve.

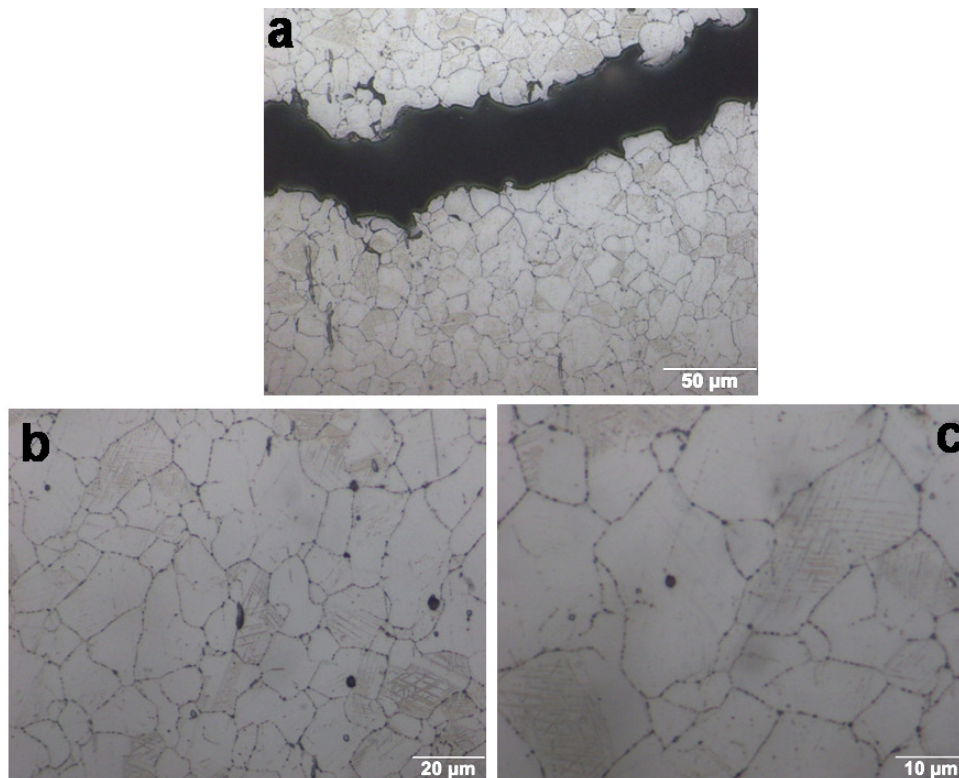


Figure 5.29 Optical micrographs showing (a) cracking along the grain boundaries, (b) & c) chromium carbide precipitation at the grain boundaries.

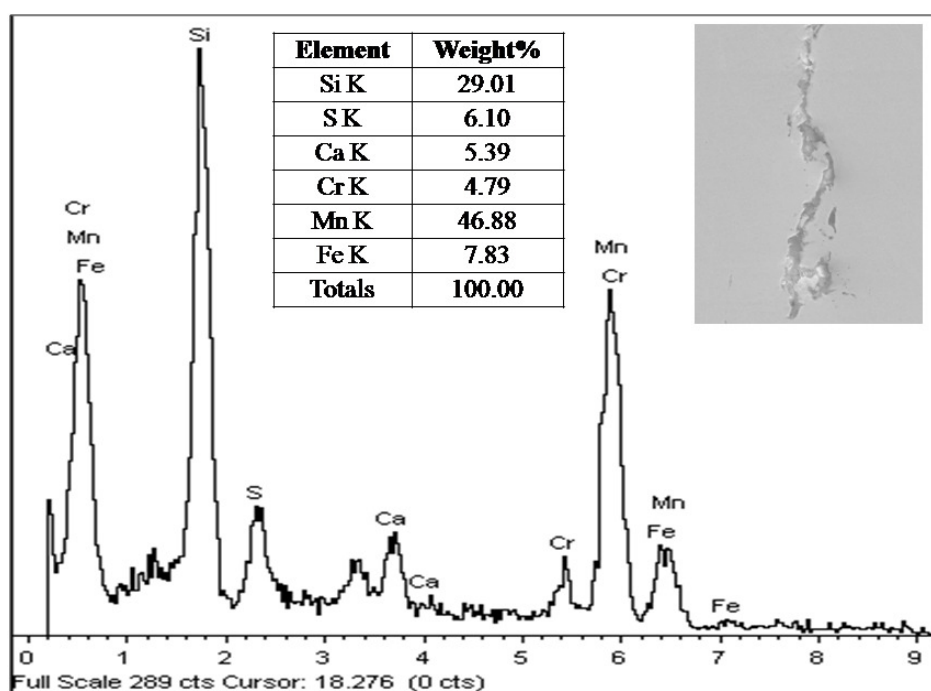


Figure 5.30 EDS spectrum showing chemical composition of silicate inclusion.

EDS analysis on the silicate inclusion stringers revealed presence of calcium-silicates along with manganese sulphide as shown in Figure 5.30. The sulphide inclusions have been confirmed to be MnS composition as shown in Figure 5.31.

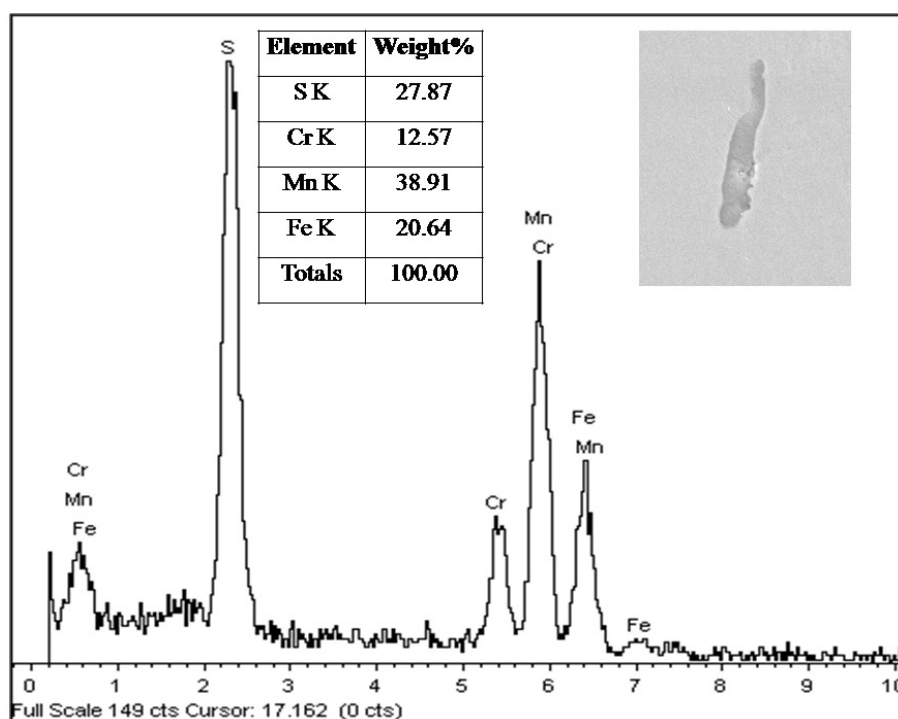


Figure 5.31 EDS spectrum showing chemical composition of sulphide inclusion

The precipitates at grain boundaries have been confirmed to be chromium carbide precipitates as shown in Figure 5.32.

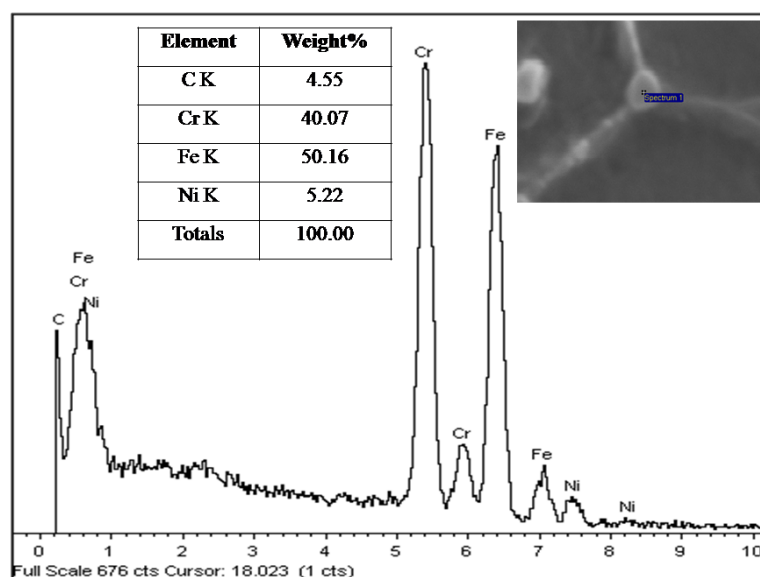


Figure 5.32 EDS spectrum showing chemical composition of chromium carbide precipitation at grain boundaries.

5.3.6 Failure analysis findings

The micro structural observations revealed that the primary circumferential crack has initiated from the OD of the sleeve and propagated inwards. The longitudinal die marks observed on the surface of the sleeve, numerous micro cracks observed near to the primary crack as indicated by SEM observations, and optical microscopic observations at the OD side suggest that they are generated on the surface during swaging operation. The reasons for formation of micro cracks on the surface is attributed to the combined effect of large plastic strain developed on the OD surface of the sleeve and sensitized microstructure of the material. The plastic strain on the surface will be more, if the die used for swaging operation has a rough surface. The rough surface along with longitudinal die marks on the sleeve indicate that the dies used for swaging operation had poor surface finish which introduced large plastic strain on the surface of the sleeve.

The plastic strain on the sleeve is indicated by deformed and elongated grain at outer edge as shown in Figure 5.28. The larger plastic strain and small size micro cracks formed on the OD surface of the sleeve can be seen in Figure 5.27c. Larger plastic

strain at OD surface has also resulted in higher hardness to a magnitude of 470 VPN. The Vickers hardness of AISI 304 steel tends to increase monotonously with increase in cold working as reported by Raghuvir Singh et al. (2003). This indicates that the OD surface of the sleeve has undergone extensive cold reduction on the surface, whereas the extent of cold reduction decreased towards inside the thickness as shown in Figure 5.28. This is reflected as variation in grain elongation and flow from the OD surface to the inside of the sleeve. Microscopic observations indicated that deformed and elongated grains have been present upto 400 μm . It shows that the deformation is not uniform throughout the thickness of the sleeve. The OD surface reveals maximum plastic strain and it reduces gradually towards inside. This results in the generation of residual stresses due to the gradient in the plastic strain along the thickness direction.

Raghuvir Singh et al. (2003) reported that for 80% cold rolling, the hardness was 466 VPN; this indicates that the plastic strain on the outer surface of sleeve has crossed 80% reduction. It was also reported that deformation induced martensite forms with the cold deformation of this steel (Raghuvir Singh et. al., (2003); Arpan Das et al., 2003; Kain et al., 2004). It was reported that at 80% cold reduction, the martensite is a dominant phase in AISI 304 stainless steel. The formation of deformation induced martensite was also corroborated with increase in hardness of cold worked steels (Raghuvir Singh et. al., 2003).

The residual stresses present in the component along with the stresses due to swaging operation are responsible for subsequent growth of micro cracks under no stress condition. The observation of primary circumferential crack near to centre of the sleeve is due to the large stresses at that location. It is also noticed that additional cracks on either side of primary crack has grown upto 250 μm and 400 μm size. The primary circumferential crack encountered the long silicate inclusions aligned in longitudinal direction during the crack propagation leading to deviation in the crack path along longitudinal direction. Microstructure shows uniformly distributed oxide and manganese sulphide inclusions and isolated long silicate stringers. Fractographic observations as shown in Figure 5.21, indicated debonding at the inclusion-matrix interface of manganese sulphide inclusions during crack propagation.

Sulphur is soluble in molten steel, but its solubility in solid steel is very low and hence it is precipitated in the form of sulphides during the solidification of the steel

and its precipitation pattern is influenced by its strong segregation tendency (Roland Kiessling, 1977). Manganese sulphide inclusions are formed during the solidification process. During solidification, the interdendritic liquid gets enriched in the solute content and liquid oxysulphide starts to form. During cooling, iron-manganese oxysulphide remains liquid until the temperature decreases and if sufficient oxygen and sulphur are present in the steel, liquid oxysulphide phase is present at temperature above 900°C depending on manganese content in steel. In steels, the sulphur will be in the form of MnS due to the high solubility product of sulphide and oxysulphide of manganese in liquid iron. It forms only in solute enriched interdendritic liquid during solidification of steel (Turkdogan, 1975). MnS inclusions get deformed and oriented in the direction of thermo-mechanical processing, forming stringers. The elongated MnS stringers present in the steel affect the mechanical properties, notch toughness and ductility (De Ardo and Hamburg, 1975; Kozasu and Tanaka, 1975).

Most silicate inclusions have several oxide components, for example MnO, FeO, CaO, Al₂O₃ and SiO₂. Silicate inclusions have a low index of deformability at lower temperatures and thus brittle at cold working temperature of the steel (Roland Kiessling, 1977). Presence of isolated long silicate stringers up to 2.2 mm size in the sleeve material were more detrimental because they provide very long and continuous weak interface for crack propagation. Isolated long silicate stringers were responsible for deviation of primary crack and subsequent crack propagation leading to fast fracture. The cracks have propagated in an intergranular manner due to the hard and brittle continuous chromium carbide precipitation along the grain boundaries and residual stresses present in the component along with assembly stresses.

The chromium carbide precipitation along the grain boundary is caused by the sensitization of the steel. Sensitization is one of the embrittlement (loss of ductility) phenomenon, resulting in the loss of ductility in austenitic stainless steels. In austenitic stainless steels, chromium carbides dissolve completely in the matrix at approximately above 1035°C. When the steel is cooled slowly from these higher temperatures or reheated to the temperature range of 425°C to 815°C, chromium carbides gets precipitated along the grain boundaries. During annealing of austenitic stainless steel, it is cooled rapidly by water quenching to prevent the sensitization. The rate of carbide precipitation varies significantly with the carbon content in the steel. AISI 304 steel containing 0.05% carbon can be free of sensitization under the cooling conditions

which produced heavy sensitization in the same alloy with 0.08% carbon (Joseph Davis, 1998). Hence to avoid the problem of sensitization, extra low carbon stainless steel AISI 304L is commonly used. AISI 304L grade steel has carbon content of 0.03% compared to 0.08% carbon present in normal AISI 304 steel (AMS-5647H, 2007; AMS-5639H, 2007).

Based on the above observations and discussion, the failure of AISI 304 stainless steel sleeve has been assessed to be due to a combination of factors such as large plastic strain, presence of residual stresses along with assembly stresses and embrittlement caused by sensitized microstructure. The continuous grain boundary network of chromium carbide precipitation has led to cracking of sleeve by brittle intergranular mode. The presence of silicate inclusion stringers has been responsible for easy crack propagation and deviation of the primary crack.

Subsequent to the failure, the material of the sleeve has been changed from AISI 304 to AISI 304L grade material conforming to material acceptance criterion with respect to inclusion rating, microstructure and mechanical properties. The AISI 304L grade steel has very low carbon (0.03%) and hence it is selected to avoid the problem of chromium carbide precipitation at grain boundaries. The swaging procedure has been modified to minimise the strain at the failed location of the sleeve of the hose assembly and surface quality of dies has been ensured. With the change in material grade and modified procedure, hose assembly has passed all the stipulated qualification tests listed in Table 5.7.

5.4 FMA concepts based on the failure mode assessment

The fatigue failure of the hydraulic plumbing and the interface joint of a hydraulic actuator subjected to high pressure and vibration loading is identified as a critical failure mode, and an in-depth analysis is done on the failure mechanisms. The analysis identifies the cause for the higher vibration to be due to pump pulsation frequency coinciding with the fourth mode frequency of the plumbing. Random response linear dynamic analysis is carried out using a FE model and the results have been compared with test results, thereby validating the model. The dynamic stresses are obtained from the model for the input random vibration spectrum. Static stresses are obtained from the axisymmetric FE model. Fatigue analysis of the flared joints of plumbing is carried out using Goodman diagram and relative Miner's rule, for the above static and dynamic

stresses. Life cycle estimation, margin assessment and reliability estimation of the system have been carried out bringing out flight worthiness of the system. As the root cause of the higher vibration response on the shutter has been identified by analysis and experimental test results, a simple and optimal design solution could be arrived at, by changing the pump pulsation frequency away from the plumbing frequencies, making the vibration environment benign.

The study brings to light the requirement of identification of the failure modes and investigation of them through experimentation in the early stages of design, to take appropriate corrective action for the FMA. It also illustrates how failure modes can be introduced when changes are made in complex space systems. A change in the plumbing configuration or change in the pump type, though may meet all the functional requirements of the CAS, it can cause a structural failure, leading to the leakage of oil and consequent mission failure. Therefore, an important FMA strategy from the analysis is that in a working aerospace system, changes shall not be made unless it is backed by strong requirements of improvement of performance. The changes in any subsystem, however minor it may be, have to be studied systematically for its impact on other subsystems, involving all the system agencies.

The analysis also shows the significance of integrated level system testing in identifying the failure modes which otherwise will remain unknown until a costly failure occurs due to marginality. Had the assessment been limited to analysis of system frequencies, the system design would have been cleared on the basis of higher first mode frequency, as this is the general criteria for acceptance. Once the failure modes and its mechanisms are identified, the solutions emerge without difficulty. Similar analysis and experimentation are essential at the integrated system level for all the external environments, to avoid failures.

The metallurgical analysis of the failed AISI 304 sleeve of the flexible hose, identified the propagation of the crack from the OD surface towards ID in an intergranular mode. The intergranular brittle mode of failure is attributed to the embrittlement caused by sensitized microstructure in combination with large plastic strain, and presence of residual and assembly stresses. The sensitized microstructure having continuous grain boundary network of chromium carbide precipitation has helped crack propagation in a brittle intergranular manner. The silicate inclusion stringers are responsible for easy

crack propagation with deviation of the primary crack. It has been recommended to change the sleeve material from AISI 304 to AISI 304L material with lesser carbon content to avoid chromium carbide precipitation at the grain boundaries. The material has been controlled and checked for the inclusions to avoid the problem of chromium carbide precipitation at grain boundaries and inclusion stringers.

The analysis brings out the requirement of having comprehensive guidelines for the material selection, acceptance procedures and the precautions to be followed in the usage of the materials for space applications. With higher strength materials the associated problem is the higher brittleness. The high strength materials are susceptible for hydrogen embrittlement. Many materials are inherently prone for Stress Corrosion Cracking (SCC). Hence while selecting materials for launch vehicle applications, due consideration has to be given for such service related factors including the fatigue aspects. Also, while using SCC prone materials, the designers shall avoid the stress risers in the system hardware design and follow robust corrosion protection measures to avoid inadvertent failures. Good design practices and guidelines for material selection and usage have to be prepared and followed for avoiding such failure modes. The threads have to be made of thread rolling process and stress risers such as under cuts have to be avoided. Identifying potential fracture critical items and adopting a fracture control plan throughout the life of the structural components is an essential FMA strategy. This includes both the design practices as well as inspection strategy. Critical processes such as casting and welding, prone for defects have to be avoided as far as possible by using forgings or milled components, and if adopted due to certain constraints, comprehensive inspection and non destructive test procedures have to be followed to avoid failures

CHAPTER 6

AVOIDANCE OF ENVIRONMENT INDUCED FAILURES IN SPACE SYSTEMS

6.1 Introduction

The launch vehicle and satellite systems are subjected to various environmental conditions during different phases of the system realisation, such as storage, transportation, handling, vehicle integration at launch pad, and during the ascent phases of the launch vehicle. Further, the satellite systems are subjected to the on orbit environments and space capsules to re-entry environments. This chapter presents the strategies for prevention of typical failures in the systems due to various harsh environments during the space flight. The first part of the chapter presents the general qualification requirements at different levels of integration with a focus on FMA for the space based systems. The second part presents a case study of a failure observed during the qualification of a payload cooling umbilical shutter mechanisms and a general approach for failure avoidance in the mechanisms area.

6.2 Qualification of space systems for environments

The space systems shall have the capability of functioning in the harsh environments encountered during launch phase and in outer space. The test and simulation has to envelope all the environments like EMI/EMC, thermal cycling, acoustics, vibration, shock and thermal-vacuum (Nanjundaswamy, 2008). Qualification of the systems by testing is essential to determine whether the system is capable of functioning under the expected range of environments for the expected operating life (Patrick O Conner, 2012). Avionics parts are procured with appropriate quality level and screening tests are carried out to meet the reliability requirements. Military grade parts are used for launch vehicle applications, and space grade parts are used for satellite applications considering the long life requirements. Further the systems are tested at component level [electronic boxes], subsystem level [structure, propulsion, thermal control] and system level [satellite, payload, spacecraft, launch vehicle system like equipment bay] (GSFC-STD-7000, 2015), to qualify for flight environments with adequate margins.

In a typical lunar mission of a mini satellite moon impact probe, the systems have been qualified through EMI/EMC test, radiation test, thermal cycling test, sine vibration test, random vibration test, and thermo vacuum test, with functional testing before and after each of the tests. At the system level, the impact probe is assembled with main orbiter and the integrated proto flight system has been tested for vibration, EMC test, thermal balance test, thermo vacuum test, sine vibration test and acoustic tests. During the radiation test of a standard camera used in a moon impact probe in a lunar mission, an anomaly in the memory device has been observed. The failure occurred at a radiation environment of 5K rad. It has been subsequently hardened by providing a tantalum sheet cover for the memory chip, which made it to work for radiation levels upto 10K rad. The vibration qualification of the structure revealed a failure of the weld and the welding process and inspection procedures have been strengthened to avoid the failure.

The spacecraft mechanisms have parts that have to be held together, until when required for operation in space, and subsequently deploy in space at the required time. The lander of a space mission has to separate from the orbiter, and the deployment mechanisms have to deploy the space probe at the intended time in orbit. In thermovacuum conditions, the parts under clamping forces can get cold welded. In one of the acceptance thermovacuum tests of the system, the clamp band of the separation system had a sluggish separation as the anodisation coating has not been properly applied in the ring. This has been subsequently replaced with rings having proper surface coating and the mission could be accomplished successfully.

In the early design phase, and in many instances even at the time of launch, it is very difficult to predict accurately flight and space environments. Hence, the design and qualification of the system have to be done with higher margins and after obtaining sufficient data, the systems can be optimized resulting in the mass savings. In a typical space capsule recovery experiment (SRE), the heat flux is estimated for the worst case trajectory considering dispersions in mass and drag. The peak heat flux predicted for the re-entry conditions has been in the order of 260 W/cm^2 in the forward nose cap region at stagnation point and 40 W/cm^2 in the silica tile region. This is verified for critical regimes by Computational Fluid Dynamics (CFD) codes and experimentally. Being the first experiment, conservative approach has to be adopted to improve robustness of design. A safety factor of 1.2 has been applied to

compute the heat flux to meet uncertainties in the analysis to compute the heat flux. The silica tile TPS design thickness is augmented by a factor of 1.2 to make the system design robust. The design robustness of the silica tiles has been verified by testing up to 100 W/cm^2 . The silica tiles have been qualified for the heat flux and other environments like aero shear, compression, acoustics and vacuum environments by a combination of tests like kinetic heat simulation test, plasma jet test, high enthalpy test, rocket exhaust test, thermo vacuum test, acoustic test and vibration test. An integrated level qualification test at subscale level has been carried out in a plasma wind tunnel in order to evaluate the performance of aero thermal structure, simulating all the structural joints when subjected to the expected flight environment. Such combination of tests at different level of assembly like a single tile, combination of tiles, and integrated system level tests are essential to identify the failure modes and take appropriate corrective actions before flight.

Considering the uncertainties in the environments, particularly for the first launch, systems have to be designed with adequate margins for all the failure mechanisms of the system. Although analysis is done with the state of art analytical tools, most of the environment induced failure modes can be brought out only by testing. Each of these failure modes need detailed analysis and experimentation and case specific technical solutions have to be implemented for failure mode avoidance. One of the most important environments during a launch is the vibration environment. Failure of systems during the vibration qualification testing are frequently encountered such as malfunction of avionics boxes, failure of propulsion modules, failure of welded brackets, loosening of fasteners, softening of elastomeric isolators, leakage through joints and seals of control systems and propulsion systems. In the following section, a detailed analysis of a failure observed during the qualification of a umbilical shutter mechanism and the actions taken for FMA are presented.

6.3 FMA of umbilical shutter mechanism

The failure mechanisms of vibration induced failures are either the fatigue loading of the parts, or the dynamic stresses and displacements induced by vibratory forces exceeding the capacity of the system. In Chapter 5, the fatigue problem in the hydraulic plumbing due to the pump-induced vibration, and the fatigue life cycle estimation and reliability analysis are presented with the help of detailed analysis and

experimentation. When analyzing the system failures during a vibration test, it is not enough to conclude it qualitatively as due to high cycle fatigue, chatter or wear, but the analysis must relate quantitatively the observed failure to the dynamics of the failed item and its dynamic environment (GSFC-STD-7000, 2015). In this chapter, the vibratory force during vibration qualification of an umbilical shutter causing its inadvertent opening is studied in detail, the failure cause is identified and quantified, and the system reliability is improved by making the system design robust.

6.3.1 System description and failure observed

The spacecraft is assembled over the upperstage of a launch vehicle, through an interface structure called payload adapter. During the atmospheric ascent phase, the spacecraft is protected from the aerodynamic loads and heating by a PayLoad Fairing (PLF). The PLF is separated, when the aerothermal heat flux on the payload is less than 1135 W/cm^2 (Suresh and Sivan, 2015; GSFC-STD-7000, 2015). During the ground operations till lift off, the spacecraft and the vehicle systems are tested for their functional performance. During this phase, the vehicle and spacecraft systems within the PLF get heated up, due to the internal power dissipation of the packages and the atmospheric heating. In order to maintain the system temperatures within their acceptable levels, cool air is supplied from the umbilical tower to the inside of the PLF through an umbilical interface.

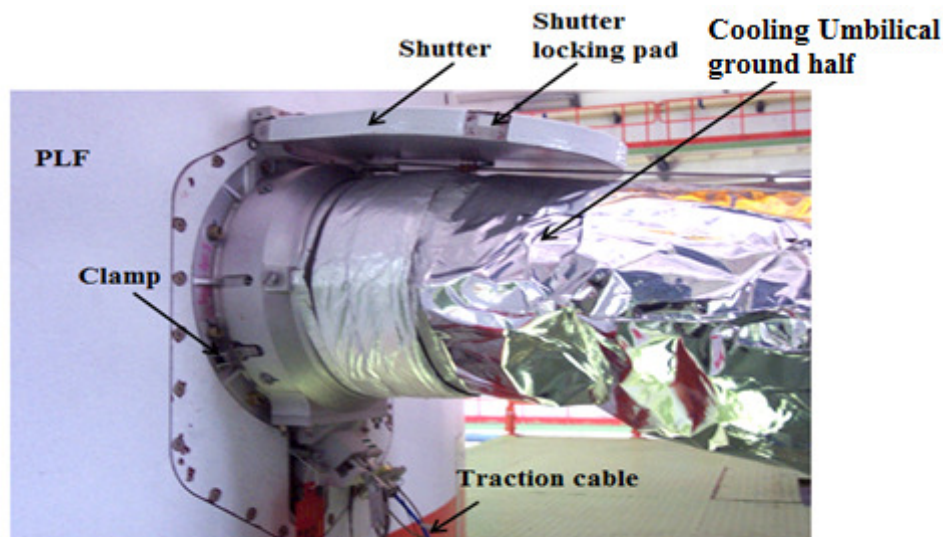
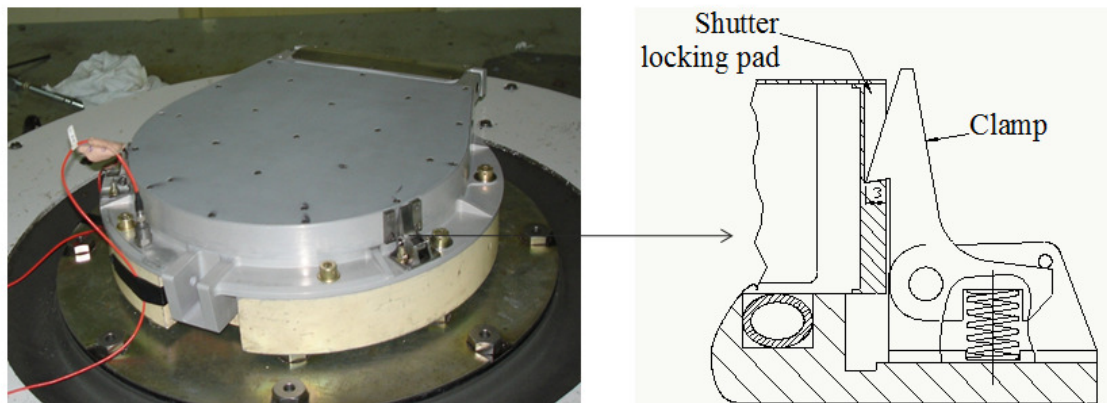


Figure 6.1 Payload cooling umbilical with shutter

The payload cooling umbilical as shown in Figure 6.1 comprises of a ground half and a vehicle half mounted on the cylindrical region of the PLF. The ground half gets separated at lift off by the pull force exerted by a traction lanyard. The vehicle half has a shutter which closes the opening left out by the ground half separation.

The payload fairing is subjected to high external acoustics due to lift off noise by the propulsion system and aerodynamic noise due to turbulent pressure around the vehicle. The Overall Acoustic Sound Pressure Level (OASPL) can go up to 160 dB (Zheng Ling et al., 2016). This acoustic excitation of the PLF manifests as severe vibration of the structure. Therefore, the umbilical shutter along with mechanism is qualified for these vibration inputs simulating the flight configuration as shown in Figure 6.2a.

The rocker clamp mechanism shown in Figure 6.2b, which has to hold the shutter in position failed to do so during the course of testing and resulted in the inadvertent opening of the shutter. This is a critical failure mode as it results in exposure of the spacecraft compartment to external environments. This chapter analyses the above failure of the umbilical shutter mechanism, through analysis and tests. The cause of the failure is identified, and actions have been taken to make the system design robust.



a) Vibration test configuration

b) Shutter rocker clamp mechanism

Figure 6.2 Payload cooling umbilical and its vibration test configuration

The standard practice for qualification of systems for the acoustic environment is to test for the maximum expected acoustic level (acceptance test spectrum) with a margin of +3 dB (GSFC-STD-7000, 2015; NASA-HDBK-7005, 2001; Suresh and

Sivan, 2015). The acceptance acoustic level has been finalised for the umbilical shutter enveloping the maximum predicted acoustic level at boat tail portion, which is 6 dB more compared to the levels at the cylindrical region of the PLF where the shutter is mounted. Though the shutter is far off from the boat tail region, this safe approach is taken partly to account for the structurally transmitted vibration and also to demonstrate the design robustness. This is giving a +6 dB margin in the acceptance level and +9 dB margin in qualification level on the maximum predicted acoustic level at the shutter location.

The acoustic test is done with the shutter in the closed condition, as shown in Figure 6.2a, in the flight configuration. In the acoustic test, an OASPL close to the acceptance test spectrum only could be simulated, due to facility limitations. The random vibration test is a pragmatic test to simulate the vibration induced on the launch vehicle systems by the acoustic excitation. The test is conducted to test the ability of the components and its parts to withstand the dynamic stresses exerted by the vibration in the defined band of frequencies (MIL-STD-202 G, 2002).

The realistic assessment of these vibration levels can be made through dynamic characterisation by subjecting the PLF to an acoustic test with vibration monitoring in the critical subsystems. The umbilical shutter performed satisfactorily during the acoustic test and has been in closed condition. The vibration response has been measured at the base of the shutter during the acoustic test and is extrapolated to the specified acoustic acceptance test spectrum.

The extrapolated vibration response is enveloped to obtain the acceptance vibration test level in terms of the power spectral density (PSD) in g^2/Hz as a function of frequency in Hz. The acceptance vibration test level in g_{rms} , as per standards, is enhanced by a margin of 1.5 times to get the qualification level (GSFC-STD-7000, 2015; NASA-HDBK-7005, 2001; Suresh and Sivan, 2015). This gives a factor of 2.25 in the power spectral density. The measured response, acceptance test level, and qualification test level are derived in accordance with the above procedure and is shown in Figure 6.3.

As part of the qualification, the mechanism is tested first to the acceptance test level in a vibration table and the system withstood the vibration level satisfactorily. When the level is further enhanced to qualification level to complete the qualification testing

of two minutes duration, the shutter got opened during the course of testing. The test has been aborted, and all the parts have been inspected and found in good condition. The failure has been investigated through experimentation results and detailed analysis.

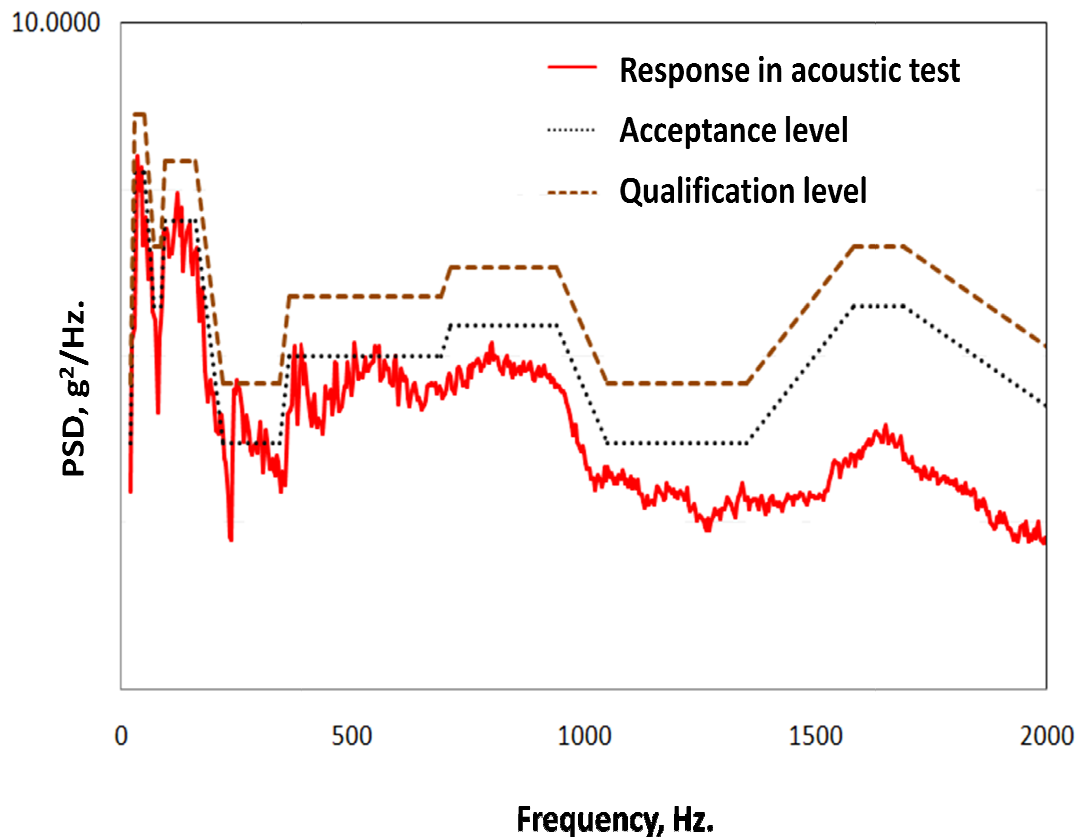


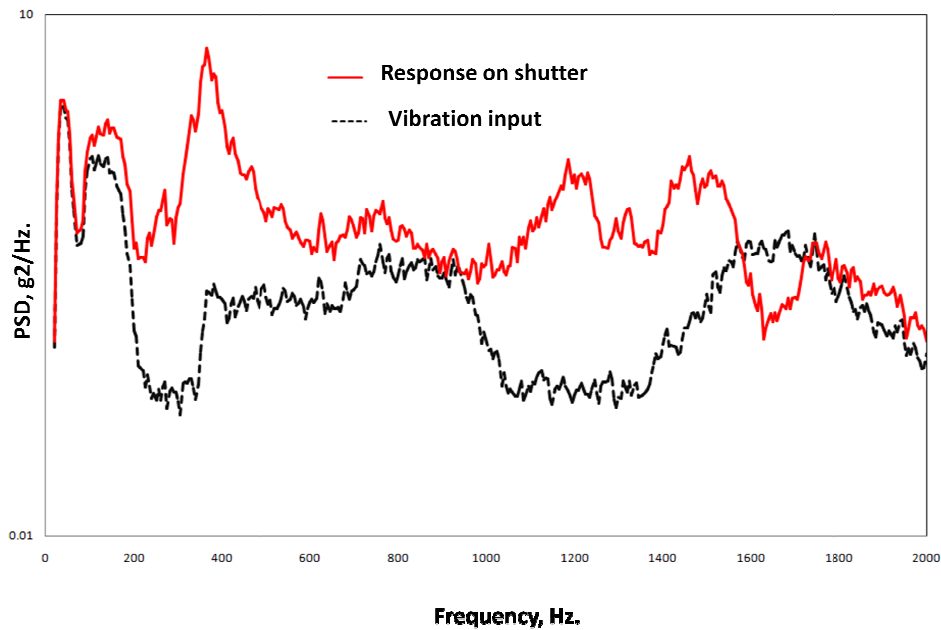
Figure 6.3 Measured vibration response in the acoustic test and extrapolated spectrum for qualification and acceptance vibration tests

6.3.2 Experimentation

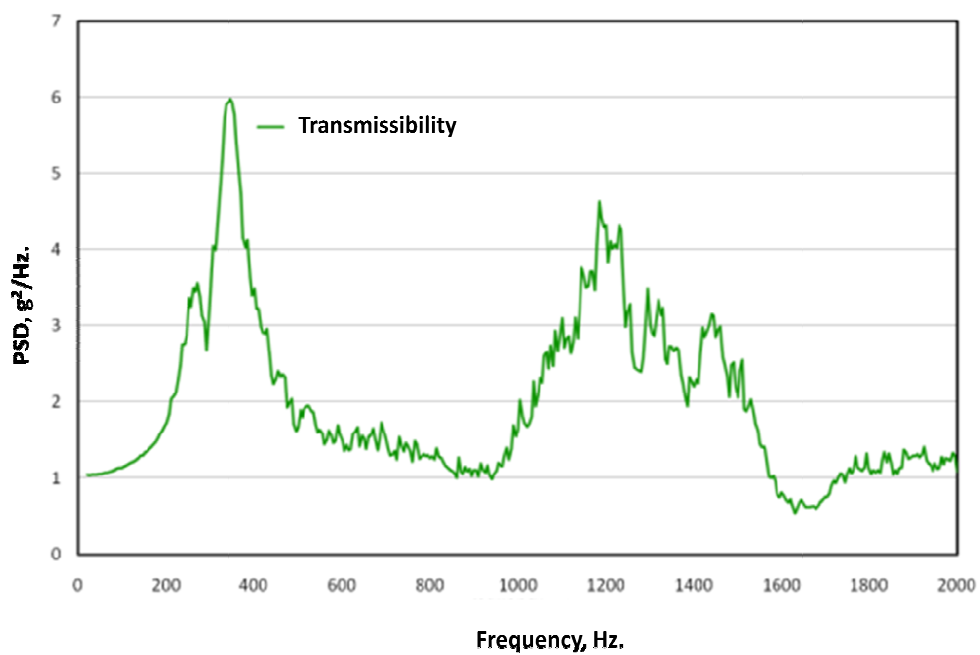
The qualification test of the shutter has been carried out with vibration response monitoring on the shutter. The input PSD and the vibration response monitored on the shutter at the rocker clamp mechanism before the failure are shown in Figure 6.4a. The transmissibility, computed as the square root of the ratio of the response PSD to the input PSD, is given in Figure 6.4b.

The transmissibility curve clearly shows that the umbilical shutter mounting is a two degree of freedom system with widely spaced natural frequencies at 345 Hz and 1200 Hz. The stress responses at higher modes are at least two orders lower compared to

that at the first mode (Ron Li, 2001). This is because of very low amplitudes of vibration at higher frequencies for the same amplitude of responses. Hence, the energy content around the first frequency of 345 Hz is found important. However, the results of these tests have to be corroborated with analysis by assessing the mode shape at this frequency.



a) Vibration response on the shutter and input spectrum



b) Transmissibility curve

Figure 6.4 Vibration response on the shutter, original design

6.3.3 Failure analysis and numerical results

The analysis of failures during vibration, must relate the failure quantitatively to the dynamics of the failed item and its dynamic environment (MIL-STD-810 G, 2002). When the physics of incipient failure of a system is understood unambiguously by analysis and experimentation, it can be effectively used to prevent the particular failure mode (Don Clausing and Daniel Frey, 2005). In the present analysis, dynamics of the system is used to identify the failure mode and failure mechanism, and the dynamic environment defines the failure stresses. The system functioning is studied through detailed FE analysis and the failure mode is identified. The frequencies of the system, the mode shapes, system damping and the dynamic stresses on the system are assessed using the experimental data and correlated with the identified failure mode, fixing the root cause of the failure.

System FE modelling and failure mode identification

The umbilical shutter is made of an isogrid type construction, to meet the required stiffness requirements with reduced mass. It is made of aluminium alloy AA2014 material with 20 mm thickness. The isogrid pockets are covered by a 1 mm thick skin sheet made of AA2014 aluminium alloy and fastened to the top of the shutter at the node of the isogrid pockets. The shutter is hinged at one end and locked by two latches at the other end by a rocker clamp mechanism as shown in Figures 6.2a and 6.2b. The rocker clamp mechanism comprises of a shutter locking pad assembled to the side face of the umbilical shutter. A spring loaded clamp with a 10° taper interface hinged on a bracket is assembled to the shutter mounting ring at two locations, 120° apart. The moment due to the spring force about the hinge holds the shutter in the locked condition when the shutter is closed.

The modal analysis of the shutter is carried out by importing a 3D solid model generated in solid works to the ANSYS work bench. After importing the model to ANSYS, it is meshed with solid 186 3-D 20 node tetrahedral structural solid elements. The element size provided is 3 mm with a minimum edge length of 0.74241 mm. As the shutter is having a hinge with a cylindrical rod at one end, the cylindrical support option is given for the hinge joint and the radial, axial and tangential movements are constrained. An elastic support with a foundation stiffness of 40 N/mm is provided at the latch locations, to simulate the locking force provided by the latches on the

shutter. A modal analysis is carried out to determine the natural frequencies and mode shape of the shutter assembly.

The resonant frequency obtained for the shutter assembly from the modal analysis is 326 Hz, as compared to 345 Hz observed in the test as shown in Figure 6.5 validating the model. The fundamental mode is the cantilever mode with the maximum displacement of the shutter near the shutter to clamp interface which is critical for the mechanism integrity. In this mode, the vibration forces trying to open the shutter, against the holding force exerted by the clamp, will be maximum. The forces due to random vibration cause clockwise moment on the clamp which can result in the opening of the shutter. It is therefore essential to assess the forces and moments on the clamp and address actions for mitigating the opening of the shutter.

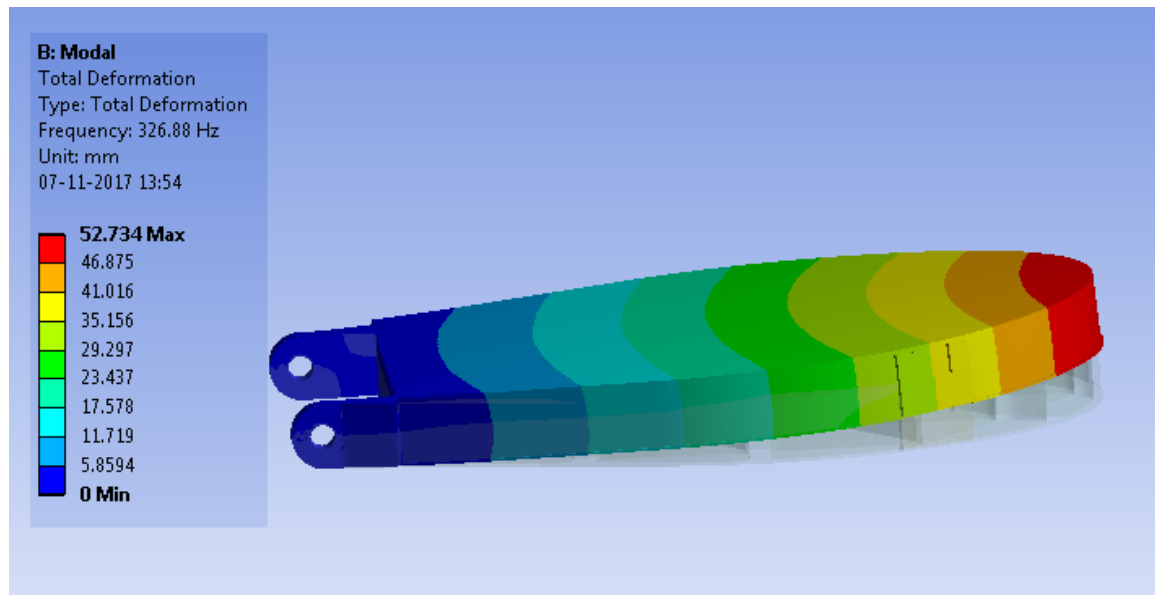


Figure 6.5 First mode of the shutter assembly from the modal analysis

Estimation of the vibratory force

The first two modes of the system are at 345 Hz and 1200 Hz, as seen from the transmissibility curve of Figure 6.4b. The stress responses at higher modes are at least two orders lower compared to that at the first mode (Ron Li, 2001). Moreover, from the first four modes which are studied, the first bending mode is giving the maximum displacement at the shutter location. Considering these points, the vibration forces are estimated for the excitation at first mode with frequency f_n . The half power band width is defined as the bandwidth of frequency in the transmissibility curve where the

transmissibility is greater than $\frac{1}{\sqrt{2}}$ times the peak value, and it is considered a more appropriate measure of energy dissipation in the system around the resonance (Clarence de Silva, 2007). Hence, to get a better picture of the energy content, around the resonance, the amplification factor at resonance ‘Q’ is obtained as $f_n / \delta f_n$, where f_n is the natural frequency, and δf_n is the bandwidth of frequency corresponding to the half power points (Clarence de Silva, 2007). The Q value computed using this procedure from the transmissibility curve shown in Figure 6.4b is 5.75.

The traditional method of dynamic response analysis using Miles equation is a simple and very useful method for obtaining the rms acceleration response for a given input for a single degree of freedom system. The response could be used to obtain the equivalent static load (Dave Steinberg, 2011; Lee, 1993). The Response in g_{rms} , is given by Equation (5.2). Substituting the values,

$$\text{Response, } g_{rms} = \sqrt{\left\{\frac{\pi}{2}\right\} \times 345 \times 5.75 \times \{0.1275\}} = 19.92 \text{ } g_{rms} \quad (6.1)$$

The vibratory force F_{sh} , exerted by the shutter of mass of 1.2 kg on the mechanism clamp is computed for the g_{peak} value, which is obtained by multiplying the g_{rms} value by a crest factor of 3.

$$F_{sh} = 19.92 \times 3 \times 1.2 \times 9.81 = 703 \text{ N} \quad (6.2)$$

As there are two mechanisms, the load per clamp is 352N.

Margin assessment against shutter opening

The random vibration response of the shutter with the mass of 1.2 kg causes the shutter locking pad to exert a force F_{sh} on the clamp as shown in Figure 6.1b. This results in a clockwise moment on the clamp about its hinge on the bracket. This can cause chatter of the clamp, resulting in the opening of the shutter. The opening induced by this clockwise moment is resisted by the anti clockwise moment due to the frictional force F_f and the spring force F_s . The free body diagram of the system with all the forces acting on the clamp is given Figure 6.6.

The vibratory force of the shutter acting normal to the clamp F_{sh} , as computed in the preceding section is 352 N. Considering the clamp wedge angle of 10° , the vertical

component of this force F_v is 346 N ($352 \times \cos 10^\circ$) and the horizontal component F_h is 61 N ($352 \times \sin 10^\circ$). The frictional force F_f at the interface with a coefficient of friction of 0.2 is $0.2 \times 352 = 70 \text{ N}$ and the spring force F_s is 36 N .

Taking the moments about the hinge we get the Clockwise moment M_{CW} ,

$$M_{CW} = F_v \times \text{Moment arm} = 346 \times 5.8 = \mathbf{2006.8 \text{ Nmm}} \quad (6.3)$$

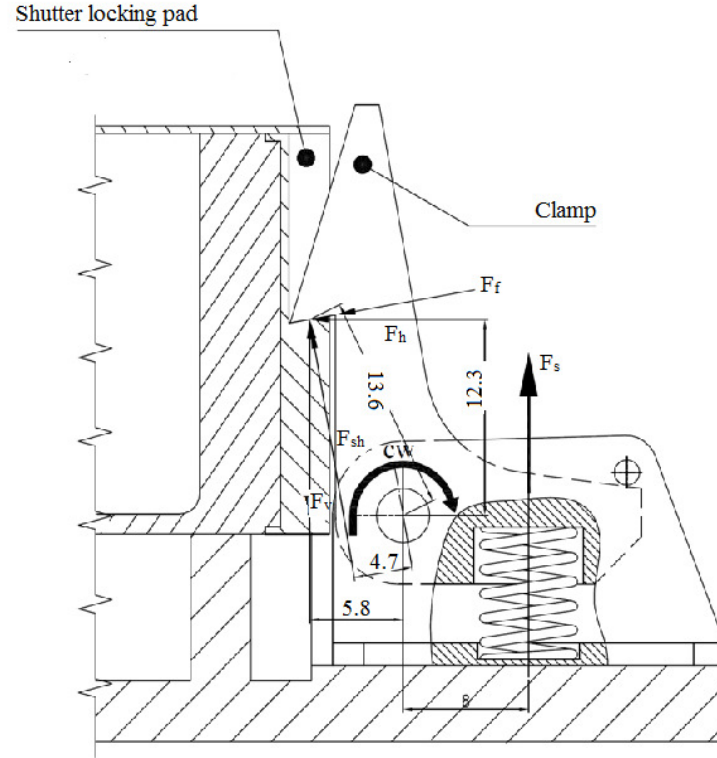


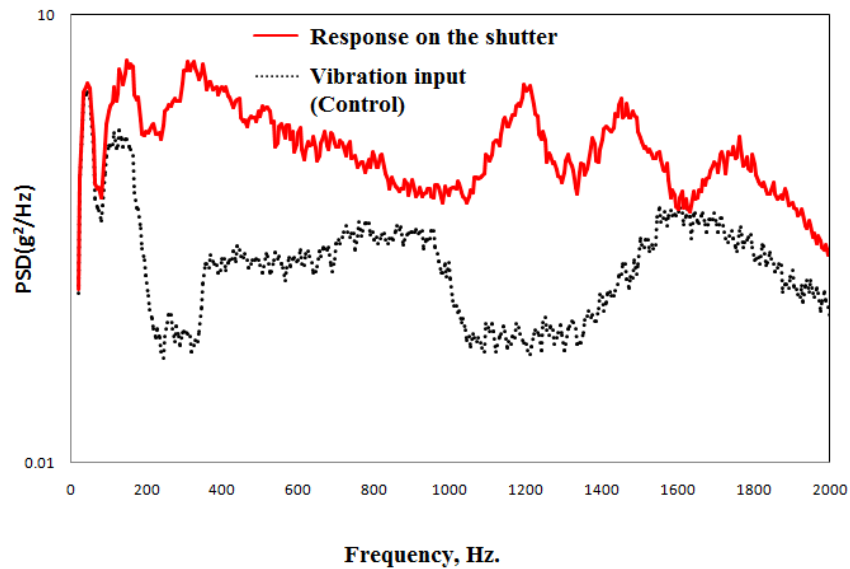
Figure 6.6 Free body diagram of the rocker clamp mechanism, original design

Anticlockwise moment due to the forces F_f , F_h and F_s and their corresponding moment arm is,

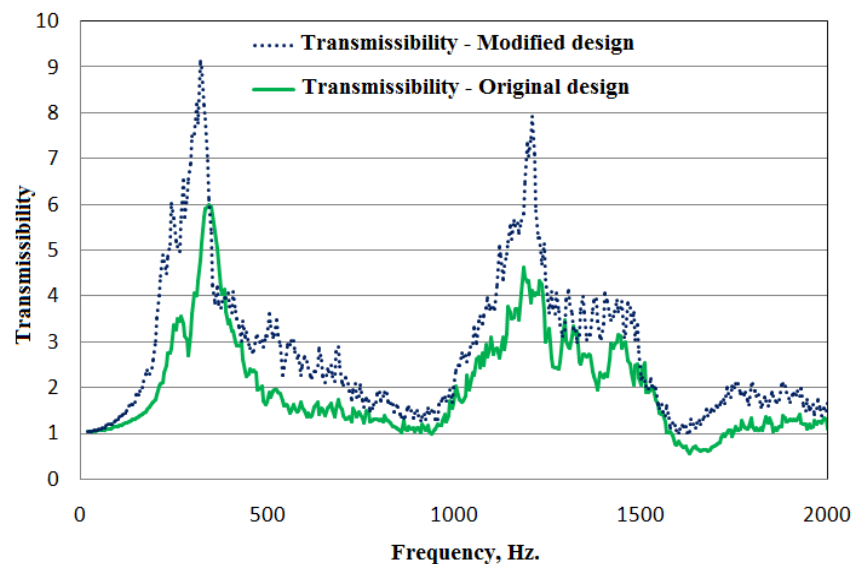
$$\begin{aligned} M_{ACW} &= (F_f \times 13.6 + F_h \times 12.3) + (F_s \times 8) \\ &= (70 \times 13.6 + 61 \times 12.3) + (36 \times 8) = \mathbf{1990.3 \text{ Nmm}} \quad (6.4) \end{aligned}$$

The clockwise moment on the clamp about the hinge tends to open the shutter, while the anticlockwise moment keeps the shutter closed. The analysis shows that the margin against opening is negative $\{(1990.3/2006.8)-1\} = -0.008$. The negative margin points toward design marginality as the cause for the mechanism to open under random vibration. The physics of failure is thus understood to be the clockwise

its transmissibility is computed and compared with that obtained with original design as shown in Figure 6.8b.



a) Input and response on the shutter



b) Transmissibility comparison

Figure 6.8 Vibration response on the shutter with modified design and the transmissibility comparison with original design

The response on the shutter is computed in similar lines of the computation made for the original design. The Q value is 5.92 and the average input PSD around the half power point bandwidth is $0.0711 \text{ g}^2/\text{Hz}$.

$$\text{The response } g_{\text{rms}} = \sqrt{\left\{\frac{\pi}{2}\right\} \times 320 \times 5.92 \times \{0.0711\}} = 14.54 \text{ g}_{\text{rms}} \quad (6.5)$$

$$\text{Force exerted by shutter on the mechanism} = 14.54 \times 3 \times 1.2 \times 9.8 = 513 \text{ N}$$

The load per mechanism is 257 N. Considering the clamp wedge angle of 10° , the vertical force F_v is 253 N and the horizontal force F_h is 44.62 N. The frictional force F_f at the interface with a coefficient of friction of 0.2 is $0.2 \times 257 = 51 \text{ N}$ and the spring force F_s is 36 N. Taking the moments about the hinge, the clockwise moment is 253 Nmm corresponding to a worst case force line offset of 1mm. The anticlockwise moment trying to close the shutter is 1536 Nmm. This gives a margin of 5 against the opening of the shutter in the modified design as compared to a negative margin of 0.008 in the original design. With the modified design, the system has been further tested up to 1.5 times the qualification level to demonstrate the robustness of the system, and the system successfully withstood the vibration loads without opening of the shutter.

6.4 FMA concepts based on the analysis of failures

The satellite systems have to withstand the harsh environments during various phases of its life cycle like launch phase, on-orbit phase, and re entry phase. There are many environment induced failure modes and mechanisms in systems, and demonstrating adequate margin of safety against all these failure modes is vital for ensuring successful performance of systems. Typical failures like vibration induced weld failures, radiation induced failure of memory device in a camera, and cold welding of parts in thermo vacuum conditions are highlighted. It brings out the requirement of qualifying satellite systems for adequate margins for all environments. In the initial flights importance has to be given for robustness in design with higher margins to validate the analysis and simulation results. After obtaining sufficient data from a flight trial, as the environments are fully understood, optimising the system performance can be attempted. This approach which has been followed for

successfully the space capsule recovery experiment mission, is an essential tenet for space systems to avoid failures.

A detailed analysis of a failure observed in the umbilical shutter mechanism during vibration qualification test is presented. The dynamic behaviour of the system has been assessed using the transmissibility curve plotted from the test results, which shows clearly that the system is a two degree of freedom system with frequencies at 345 Hz and 1210 Hz. The FE analysis shows that the 345 Hz content has a cantilever mode aiding the opening of the shutter. The margin of the system against the shutter opening failure mode was obtained using the static equilibrium equations from the free body diagram of the clamp, by comparing the clockwise moment trying to open the shutter with the anticlockwise moment due to frictional and spring forces trying to keep the shutter in closed position. The margin is found to be negative (-0.008) by analysis. The problem could be compounded by the dispersions in the random vibration input, realised hardware dimensions and interface clearances, resulting in the inadvertent opening of the shutter. The failure mechanism has been assessed as the vibratory forces of the shutter causing a clockwise moment on the clamp trying to open the shutter. This marginally exceeds the anticlockwise on the clamp due to spring force. The physics of failure has been effectively used for avoiding this failure mode in the modified design. The clamp is modified to align the vertical component of the vibratory force vector along the hinge so that the clockwise moment trying to open the shutter is avoided.

Building robustness in the design is an important strategy for failure mode avoidance. Hence, it is important to design systems to withstand a wide range of harsh environments and demonstrate it in the ground tests. In accordance with this concept, the vibration qualification level is finalised corresponding to + 9 dB of predicted acoustic spectrum at the cylindrical portion where the shutter is mounted. A positive margin of 5 is established for the DQT vibration levels based on the experimental data and theoretical analysis. The system has been further tested to 1.5 times the qualification vibration levels satisfactorily, thus demonstrating the robustness of the system. Acceptance vibration tests followed by functional tests have been identified as a screening test for aerospace mechanisms to ensure the health of the systems for their strength, stiffness and functional performance.

CHAPTER 7

FAILURE AVOIDANCE IN SOLID ROCKET MOTOR PRESSURE MONITORING JOINT SEALS

7.1 Introduction

This chapter presents the contributions of the thesis in the area of failure mode avoidance and reliability analysis of the seals in the pressure monitoring system joint of Solid propellant Rocket Motors (SRMs). SRMs come in different sizes, propellant loading, and a wide range of thrust from 2 N to 12 million N (George Sutton and Oscar Biblarz, 2010). Taking into advantage of these characteristics, SRMs are being used in launch vehicles for different applications such as main propulsion systems, strap on boosters and as special purpose motors. Simple design coupled with less number of subsystems make the SRMs more reliable compared to liquid rocket engines with more complex, dynamic subsystems. However, being a single shot device its performance cannot be verified by acceptance tests as in the case of the liquid engines. On the contrary, its reliability is assured through adherence to stringent quality standards and procedures throughout the product life cycle and by ensuring adequate design margins. One of the major challenges in the reliability assurance of an SRM is ensuring leak tightness of all the joints under all environmental conditions.

An SRM comprises of factory joints such as weld joints, and field joints like segment joints, and joints for pressure monitoring to evaluate the motor performance. The weld joints are tested at factory for satisfactory performance and are well protected against thermal environments. The field joints such as segment joints are inevitable considering the issues related to casting and transportation of large motors. The motor segment joint has undergone many changes world over, after Space Shuttle Challenger accident, on January 28, 1986, in terms of the seal design and constraining the deformation of the cylindrical sections at seal location through a capture feature making the design robust (Bodekar Dan and Foster Windred, 1998: Rosa Lynn Pinkus at al., 1997). However, the seals used for the pressure monitoring system of the SRMs have not got the due attention in literature. This chapter investigates the failure modes of different sealing joints used in pressure monitoring systems of SRMs, and also

addresses the failure prevention strategies and quantitative assessment of the reliability of these joints.

7.2 System description and design options

A typical satellite launch vehicle with more number of SRMs is shown in Figure 7.1. The launch vehicle comprises of three main SRMs. The first stage comprises of a booster stage with 130 tons of propellant and six number of strapon motors with 12 tons of propellant. The third stage is also an SRM with 7 tons of propellant. The second and fourth stages are powered by liquid propulsion engines. In addition, there are 16 number of special purpose solid rocket motors - four ullage rockets for proper propellant acquisition during the second stage liquid engine ignition and 12 number of retro rockets for collision free separation and jettisoning of first and second stages.



Figure 7.1 A typical launch vehicle with more number of solid rocket motors

The peak pressure, pressure integral, pressure oscillations and the differential pressure between the strapon motors are critical parameters of SRMs affecting the mission performance. Therefore, pressure monitoring of both motors and igniters gains significance and hence minimum two pressure monitoring are essential. The monitoring for the main motors and igniters requires a pressure line conduit so that the pressure sensing diaphragm is not damaged by the high intensity, long duration

heating by the combustion products. The special purpose motors require only one direct mounted pressure pickup considering short duration operation of these motors. Leak tightness of all the pressure monitoring joints is essential for the mission success. Considering the above requirements, a design comprising of PTFE thread sealant and metal to metal contact bull nose seals has been proposed which was successfully flown in earlier launch vehicles. Henceforth in the chapter, this option is addressed as design option 1. Even though the design had heritage, and is a simple working solution, it required skill of the operator and a number of quality control (QC) checkpoints to be ensured at assembly for ensuring its reliable performance. The new launch vehicle, planned as an operational launch vehicle, with increased launch frequency needed a robust design for this critical joint without relying on operator skill. Towards this, various design options and improvements are debated and converged on the configuration with O-ring based shaft seal. Henceforth, this configuration is referred to as design option 2.

Design robustness and the procedures for ensuring quality of system by avoiding mistakes and the non-conformance are the basic requirements for failure prevention (Don Clausing and Daniel Frey, 2005). The methodology to achieve these objectives in the design and realisation phase, and quantitative reliability assessment of the design configurations are addressed in this chapter. Towards this detailed investigative tests have been conducted by varying the design parameters and also with deliberately induced non-conformances in the system. The experimental results provided valuable inputs for the study of failure mechanisms, FMEA and reliability analysis.

7.3 FMEA Procedure

FMEA is an effective tool to design reliability into systems, with a focus on failure prevention. It is a systematic procedure to study the failure modes, its effects on the system, and classify the failure modes based on severity and likelihood of failures. It significantly contributes to improvements in design, processes, process controls and test plans, which in turn prevents the failures or reduces the probability of failure (Carlson, 2012; Mohammed Modarres et al., 2010; Samira Abbasgholizadeh Rahimi, 2015). As per SAE J1739 standard, FMEA is carried out in a spreadsheet format addressing critical components, potential failure modes, its effect on system

performance, failure mechanisms, design controls and recommended actions (Mohammed Modarres et al., 2010). The failure mode is how the failures are revealed, failure mechanisms are what produces the failure mode and failure stresses activates the failure mechanisms (Vincent Lalli, 1994). Each failure mode is rated on a scale of 1 to 10 for severity of failure (S), the probability of occurrence (O), and the possibility of detection (D). The Risk Priority Number (RPN), the product of S, O and D, is used to rank failure modes and prioritize for necessary corrective actions (Mohammed Modarres et al., 2010; Ningcong Xiao et al., 2011; Samira Abbasgholizadeh Rahimi, 2015; Xiaoyan Su et al., 2012).

Severity rating is assigned, from 1 to 10, based on the potential effects of failure [No effect = 1; Hazardous = 10]

Occurrence rating is assigned, from 1 to 10, based on the probability of occurrence of the failure cause [Remote (<1 in 1,50,000) = 1; Very high (>1 in 2) = 10]

Detection ratings are based on design controls to detect the failure cause or failure modes. [almost certain to detect failure mode = 1; uncertain, cannot detect the failure = 10]

RPN is then computed as [Severity \times Occurrence \times Detection]. The rationale for finalising the ratings is given in Appendix D.

Improvements required in the design and the design controls are identified in FMEA. Proper identification of the rating S, O and D are very important and this is done by assessing and judging the failure modes and the sensitivity of the system functioning to the possible process variations. The assessment is dependent on the available test data, engineering judgment and expertise of the assessor, and is adequate to compare the merits and demerits of competing designs. .

7.4 FMEA - Design option 1

The pressure monitoring scheme proposed is detailed in Figure 7.2. It consists of special adapter with an external thread of M18 \times 1.5, on which a few layers of Poly Tetra Fluoro Ethylene (PTFE) tape is wound and then assembled into the female pressure port of the rocket motor or igniter [Joint J1]. The PTFE acts as a thread sealant. Further this adapter has a conical seating at the fore end wherein the bull nose

welded to the plumbing is assembled and tightened by means of a nut, which makes a standard metal to metal seal [Joint J2]. The bull nose to the plumbing weld is the third joint [Joint J3]. Pressure pick up is assembled to the other end of the plumbing through another metal to metal sealing joint [joint J4]. The critical interfaces of the pressure monitoring system are given in Table 7.1.

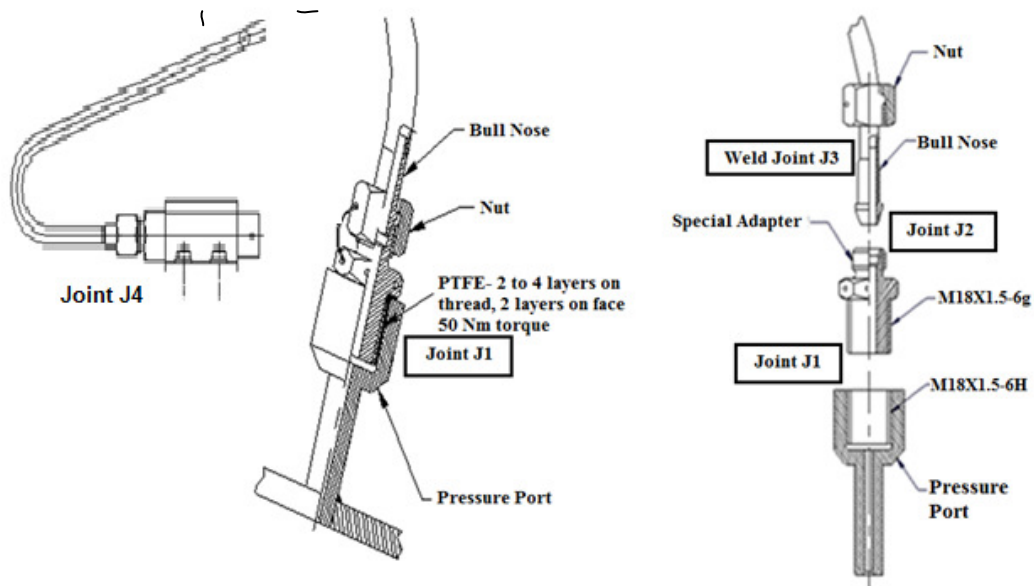


Figure 7.2 Schematic of design option 1 for pressure monitoring

Table 7.1 Critical interface joints of design option 1

Sl. No.	Joint	Interface joint	Type of seal
1	J1	Motor Pressure port - Adapter	Teflon tape sealing
2	J2	Adaptor- Plumbing	Metal to metal sealing
3	J3	Plumbing joints with bull nose.	Weld joint
4	J4	Plumbing- Pr transducer Interface	Metal to metal sealing
5	P1	Pressure transducer	Measurement unit rated for the pressure range of motor.

The system reliability block diagram for the design is given in Figure 7.3. All the four joints J1 to J4 and the pressure pick up P1 should function satisfactorily for the satisfactory performance of the pressure monitoring system. Hence, the system is in series and the reliability of the integrated system is the product of individual reliabilities (John Bentley, 1993)

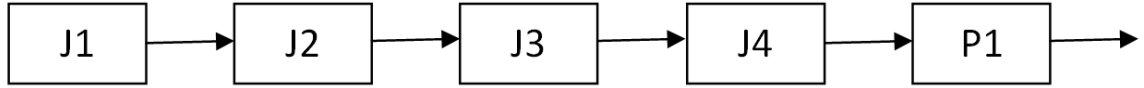


Figure 7.3 System block diagram for the design option1

$$\text{Reliability of pressure monitoring system } R_{pr} = R_{J1} \times R_{J2} \times R_{J3} \times R_{J4} \times R_{P1}. \quad (7.1)$$

All the four joints have to be leak tight for the satisfactory performance of the motor, but pressure sensor failure can be tolerated as it does not affect the motor performance. Therefore, the pressure sensor reliability can be excluded from the SRM reliability.

$$\text{Reliability of solid rocket motor } R_{srm} = R_{J1} \times R_{J2} \times R_{J3} \times R_{J4} \quad (7.2)$$

As the special purpose motors have shorter burn duration, the thermal environment is benign. Hence, a direct pressure monitoring do not affect the sensor performance. Therefore, these motors have a tapped thread interface and pressure pickups are directly assembled, with PTFE as thread sealant, to the pressure port. Hence there is only one joint J1 and reliability of the motor becomes R_{J1} .

The failure mode, its effects, the design & process controls for prevention of failure modes, the probability of occurrence and detection of the deviation in crucial parameters that can lead to failures are given as an FMEA summary sheet in Table 7.2. The rationale for assigning the severity, occurrence and detection ratings are discussed in Sections 7.4.1 to 7.4.3 for the threaded interface with PTFE tape (J1), metal to metal sealing joints (J2 and J4), and the welded joints (J3).

Failure of any one of the joints J1 to J4 results in a catastrophic mission failure and hence severity rating (S) is finalized as 10 or hazardous for all the four joints.

Table 7.2 Failure Modes Effects Analysis (FMEA) of design option 1

Joint	Failure mode	Effect	S	Failure Cause	O	Design Controls	D	RPN SOD	Action
J1	Leak through the PTFE interface	Mission Failure	10	Improper winding of PTFE, adapter not butting	5	Process Control (Not testable)	7	350	Un tested interface. FCD and assembly checks. Higher RPN, Lower Reliability. Use of higher reliable & testable joints
J2	Leak through Metal to metal seal	Mission Failure	10	Improper finish Inadequate torque	4	3D Inspection and Process Control (Not testable)	7	280	
J3	Leak through weld	Mission Failure	10	Quality issues in plumbing, welding	1	Process control, Inspection & testing	1	10	Pressurize the joints in flight configuration and leak testing
J4	Leak through metal to metal seal	Mission Failure	10	Improper Finish Inadequate torque	1	Process Control (Pressure tested)	1	10	
P1	Pressure not sensed	Affects motor performance assessment.	1	Block in Pr pick up line, Pick up failure	2	Sensor level tests	1	2	Pick up failure does not affect motor function
Total RPN { Joints J1 to J4 }								650	

7.4.1 Threaded interface with PTFE tape (J1)

The PTFE tape fills the gap between the male and female threads and also the surface irregularities at the butting interface of the adapter with the pressure port. Experiments have been designed to study the effect of different control parameters and noise factors on the system performance by intentionally varying them. The systems have been realised with the intentional deviations which are beyond acceptable limits and at environments much severe than the specified qualification levels. The failures induced through these tests resulted in better understanding of failure mechanisms and hence enabled taking informed corrective actions.

Tests have been carried out with a varying number of layers of PTFE tape, winding it over the thread alone, over both thread and butting face, and with deliberately induced scratch marks on the mating faces. The results showed that all these parameters affect the system performance. In addition, the skill of the operator has been found to play an important role in system performance. For instance, the operator can wind the tape in the wrong direction or the stretch given to the tape while winding can vary from one assembly to another. Even though the number of layers and thickness of the tape are specified, dispersions in the interface clearance between the mating threads can affect the sealing performance.

Moreover, a leak from the PTFE interface of the adapter caused a special purpose motor failure during a ground static test, revealing the marginality in the design. Also, the joint is not testable being a field joint on the propellant casted rocket motor with nozzle closure. Considering the above points, occasional failure (1 in 400) is likely and a corresponding rating of 5 is chosen for the occurrence.

The system hardware can be inspected for the dimensional and form tolerances of the thread and the mating flanges and assembly process can be controlled with detailed checklists. However, considering that the joint is not testable and there are a number of functionally critical dimensions and process critical parameters, detection rating (D) is very low and a corresponding rating of 7 is given.

7.4.2 Metal to metal seal (J2 and J4)

In a standard metal to metal seal of the bull nose joint, as shown in Figure 7.4, the sealing is achieved by the plastic deformation along the line of contact of the spherical

bull nose with the conical seat of the adapter. Control and maintenance of dimensions, geometry and surface finish of the mating parts, within a close tolerance band is essential for leak tightness. Application of correct tightening torque using calibrated torque wrench is essential for making the required plastic deformation necessary to ensure leak tight joint (Hugo Buchter, 1979; NASA SP-8119, 1976). Pneumatic leak checks have been carried out at 1.5 times the maximum expected operating pressure (MEOP) on the joints. Minor scratch marks on the mating parts that can be caused during handling, have been simulated in the test articles. The joints have been found to leak and efforts to remove the marks locally by emery paper of different grades led to increased leakage, because the profile of mating parts got affected. With increasing torque for the joints, leaks have been found to either decrease or got arrested. However, it is noticed that when the surface roughness with Ra less than $1.6\ \mu\text{m}$ is ensured using high precision lathe at 1000 rpm, the joints became leak tight. With repeated use at same torque level, leaks have been observed in a few cases.

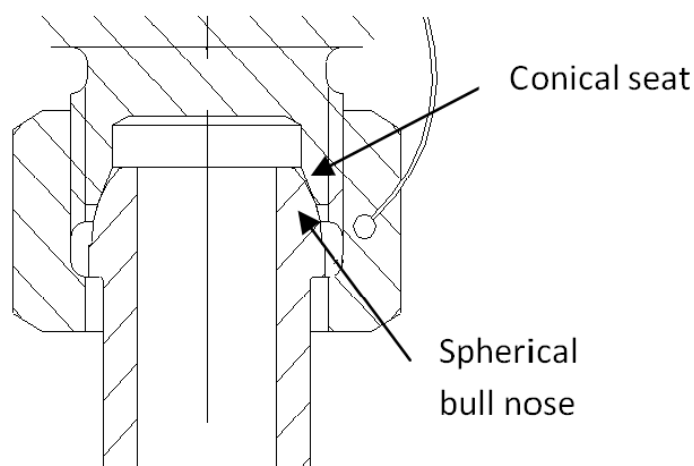


Figure 7.4 Metal to metal sealing joint

The above testing brought out the sensitivity of the metal to metal joint to dimensional and form tolerances of the mating parts and tightening torque. The joint is a standard joint and is reliable if screened by testing. Since the joint J2 is not testable due to configuration constraints and is sensitive to nonconformance, the occurrence rating is 4 or moderate (1 in 2000). The surface finish and tightening torque can be measured and controlled, but joint cannot be tested and hence rating for detection is finalized as 7. However, a metal to metal joint tested and certified is highly reliable. Hence in a testable joint such as J4, ratings for both occurrence (<1 in 1, 50,000) and detection

(almost certain to detect) are 1. It is interesting to note that a testable joint has just an RPN of 10, whereas the same joint when un tested is having a high RPN of 280. This is because with testable joint, defect if any can be detected, and once leak tightness is verified probability of failure of the joint is very low. In the FMEA work sheet, this design control namely acceptance testing requirement is brought out.

7.4.3 Welded joints (J3)

Vibration environment is very critical for the welded joints (NASA SP-8119, 1976). The vibration environments for these joints during launch are very benign, as they are mounted on a stiff motor dome. However, to verify the design and process robustness, the joints have been for one order higher vibration level. Welding is a well established process and quality of weld can be ensured by design, process and quality control. In addition, as the joints are testable through NDT and pressure tests. Hence, the ratings for both occurrence (<1 in 1, 50,000) and detection (almost certain to detect) are assigned as 1. Acceptance testing of the joint is the recommended action from FMEA. FMEA for the design option 1 is given in Table 7.2.

7.4.4 Total RPN for design option 1

From the FMEA, detailed in Table 7.2, total RPN for main propulsion motors pressure monitoring system, with joints J1 to J4, is 650 and RPN for special purpose motors with just one joint J1 is 350. The overall RPN index is 16000 as given in Table 7.3.

Table 7.3 Overall RPN index for design option 1

Type of Motor	RPN for the system (a)	No. of motors (b)	No. of pressure monitoring (c)	Net RPN (a × b × c)
Main propulsion SRMs	650	8	2	10400
Special purpose motors	350	16	1	5600
Overall RPN index				16000

7.5 FMEA - Design option 2

7.5.1 Design considerations

A very high RPN of 16000 highlighted the design weaknesses of design option 1. The number of failure modes with a high probability of occurrence is found to be more in the operating conditions, when the control parameters such as geometrical tolerances, surface finish of components or assembly process had even minor deviations. Hence changes in design are found necessary by physically eliminating the failure modes. However, it has been found very difficult to improve the design with constraints such as a threaded interface on the motor. Different design options for the threaded interface joint with PTFE (J1). A metallic gasket between the pressure port and adapter, two shaft seals (O-rings), and a combination of a shaft seal and a face seal (both O-rings) have been considered.

The metallic gasket option is not considered as it does not remove certain failure modes of un-tested metal to metal sealing joints. The shaft seal is preferred over face seal, as the probability of O-ring mating surface of a face seal on the pressure port getting damaged during handling is more. The final configuration chosen is with two O-rings as shaft seals with a split clamp. In this design, the threaded interface joints J1 and J2 with high RPN and design concerns are replaced by a reliable O-ring joint with seal redundancy as shown in figure 7.5. As the adapter along with the plumbing and pressure pickup, after leak testing of joints, can be inserted into the port and assembled, only O-ring joint J1 is not tested. The O-ring joint, being a standard joint with a proven heritage, is more reliable and robust.

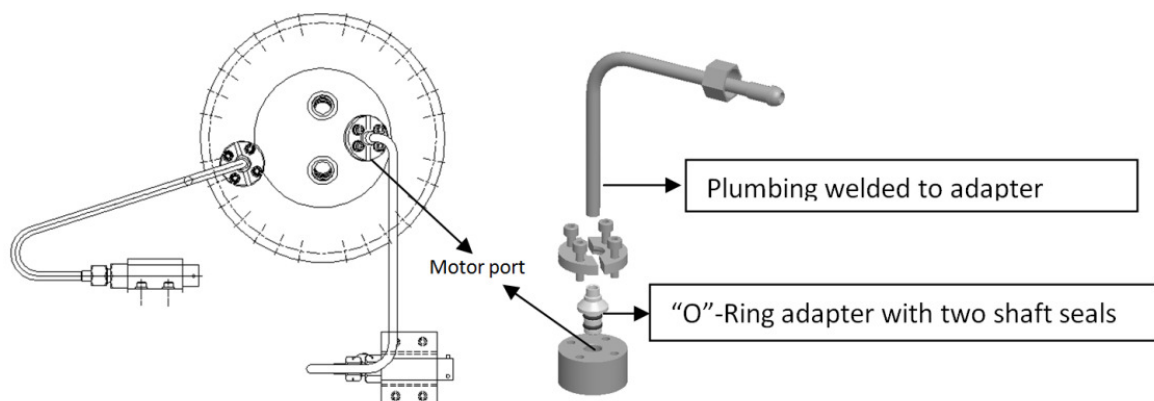


Figure 7.5 Design option 2 with O-ring interface

The shaft seal comprises of two O-ring grooves on the adapter (Male part), assembled with O-rings and inserted into the port as shown in Figure 7.5. The sealing is achieved by the compression of the O-ring and the ring tries to restore the initial cross section, creating a tightening force effect. The elastomer flows and fills all the surface asperities of the contact areas, giving proper seal (Xiaoyan Su et al., 2012; John Bentley, 1993).

Fluorocarbon elastomer with a Shore hardness value of 75 to 85 Shore A is selected as the O-ring material to withstand the envisaged operating pressure and temperature. The O-ring and gland dimensions are selected considering the ISO 3601 series standards and Parker O-ring Handbook (ORD-5700, 2017; ISO3601-1, 2002; ISO3601-2, 2008; ISO3601-3. 2005). The O-ring selected is with Parker size no. 2-011 with an inner diameter of 7.65 mm and cross sectional diameter of 1.78 mm (ORD-5700, 2017). The required compression is ensured for the Maximum Expected Operating Pressure (MEOP) of 9 MPa and the maximum specified stretch value. Other critical requirements for the O-ring joint are the dimensional aspects including the corner radius, the taper angle of the groove, surface finish of the gland; dimensions affecting the squeeze (15% to 30% at assembly), stretch (0 to 5%) and fill of the O-ring (60-95%); and finally the quality of the O-ring and its dimensions. Once these design and quality control requirements of the O-ring and gland are met, the O-ring joint is very reliable and failure chances are very remote. The redundant seal makes the joint highly reliable.

The requirement of pressure monitoring for the special purpose motors is also relaxed to improve the robustness, as accurate pressure data is only a desirable parameter for these motors. Strain monitoring on the motor case is opted to indirectly assess the performance of the special purpose motors.

7.5.2 Study of failure modes and mechanisms

Extensive testing have been carried out to study the failure modes and the failure mechanisms of the design option 2. Testing of more than 200 sample joints and characterization of O-ring material have been carried out to study the failure modes and assess RPN ratings. The selected fluorocarbon rubber has been qualified for continuous exposure at 204°C and is recommended up to 315°C for a short exposure time. Sample joints are heated to 300°C and 400°C and pressurized to 15 MPa for 3

minutes and leak tested, against the expected temperature of less than 200°C and an MEOP of 9 MPa. Thermo gravimetric analysis has been carried out and the data is given in Figure 7.6. No appreciable mass loss is observed in the O-ring material up to 400°C. The thermal and dynamic environments of an SRM have been simulated through testing of the joints in thermal simulation motors, igniters and in static firing tests of SRMs of different propellant loading.

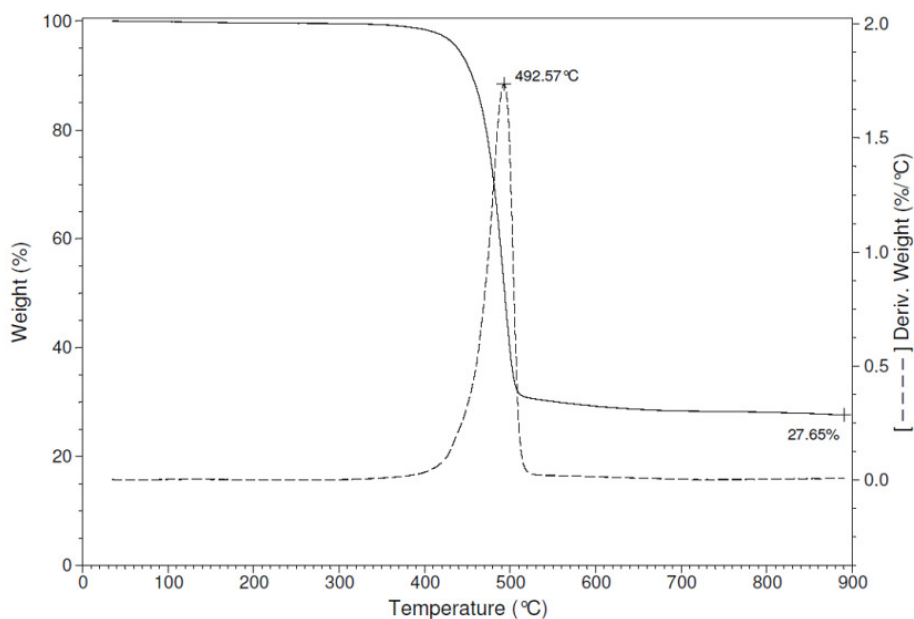


Figure 7.6 Thermo gravimetric analysis data of fluorocarbon O-ring

Apart from testing in the normal configuration, failure mode simulation tests also have been carried out by testing with primary O-ring alone and secondary O-ring alone configurations. A number of joints have been evaluated with deliberately made tool line marks up to 4 µm depth on the pressure port and found to seal effectively even with this deviation. Also, the joint has been qualified for vibration environments in the test set up shown in Figure 7.7. Tests are also done with an improper butting of the pressure pickup adapter, simulating a gap of 0.05 mm between the adapter and the port, to check for certain cases of non conformance in hardware & assembly mistakes, and found to meet the sealing requirements. Tests have been carried out to study the effect of storage under assembled condition and joints have been tested after 18 months of storage and found satisfactory. Guidelines were set to use the O-rings in flight assemblies much prior to the expiry of shelf life stipulated by the manufacturer. The O-rings are also evaluated for the properties periodically to verify their fitness at the time of use. More than 200 joints have been tested and robustness of the joint has

been demonstrated. The joint is also tested in a number of igniter level and motor level static firing tests.

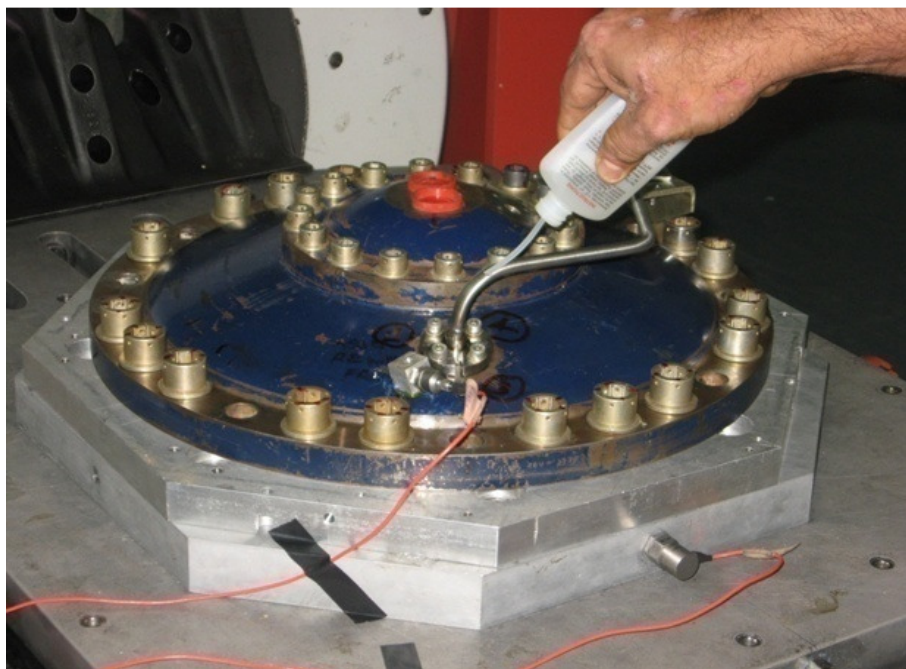


Figure 7.7 Vibration test set up for pressure monitoring system

FMEA for the design option 2 is given in Table 7.4. The failure mode, its effect, design controls to prevent failures are addressed along with RPN numbers. Considering the sensitivity of O-ring joint to parameters such as stretch, squeeze and fill, the dimensions that affect these parameters have been identified as functionally critical dimensions (FCD), as shown in Appendix E.

Failure of any one of the joints results in a mission failure and hence the severity rating is finalized as 10 (Hazardous) for all the joints. NPRD-1995 (1995) gives the failure rate of standard O-ring for airborne application as 2.3873 per 10^6 operating hrs. Considering the good pedigree and high reliability of O-rings as a sealing option, fault tolerance in the design and ability to function under severe environments of the standard O-ring joint, the rating for failure occurrence is assigned as 1.

O-ring damage due to sharp edges at pressure port entry point or a contaminant during assembly is a critical failure mode and hence trial assembly followed by visual inspection of the O-rings is made a mandatory checkpoint. After the trial assembly, the O-rings are inspected and final assembly is carried out with fresh O-rings. Hence detection is rated as high, 3.

Table 7.4 Failure modes effects analysis (FMEA) of design option 2

Joint	Failure mode	Effect	S	Failure cause	O	Design controls	D	RPN S*O*D	Action
J1 and J2	Leak through the O-ring joint (J1 and J2 combined to a single joint)	Mission failure	10	Improper dimension control of mating parts Stretch, squeeze and fill, and faulty installation. Defective O- ring Failure due to higher pressure, temperature, lack of preload, severe vibration	1	Dimension and Process Control O-ring QC checks	3	30	Reconfirmation of FCDs Trial assembly & checks. Qualified for the service environments
J3	Leak	Mission failure	10	Quality issues in plumbing, welding	1	Process control, Inspection & testing	1	10	Pressure testing of the joints.
J4	Leak	Mission failure	10	Improper finish Inadequate torque	1	Process Control, Pressure testing	1	10	
Total RPN								50	

The subassembly comprising of the adapter, the plumbing & the pressure pick up is prepared separately and pneumatically pressure tested to ensure leak tightness of joints J3 and J4. This acceptance testing identified in FMEA, is an important design control, to ensure reliable performance of the joints. Finally, assembly of the adapter with pressure port is completed. Pressure monitoring is not done, and performance of SRM is indirectly assessed through motor case strain monitoring for the special purpose motors. Since the joint is deleted. RPN is Nil.

7.5.3 Total RPN for design option 2

The RPN for main propulsion motor's pressure monitoring system, with joints J1 to J4, is only 50 and RPN for special purpose motors with strain monitoring for assessing motor performance is Nil for the design option 2. The overall RPN index is for the design option 2 is 800 as given in Table 7.5.

Table 7.5 Overall RPN index for design Option 2

Sl. No.	Type of SRM	RPN for pressure monitoring system (a)	No. of motors (b)	No. of pressure monitoring for each motor	Net RPN (a × b × c)
1	Main Propulsion	50	8	2	800
2	Special Purpose Motors	0 (nil)	16	1	0 (nil)
Total RPN					800

7.6 FMA concepts and reliability analysis based on investigation of failure modes

Failure modes are investigated for critical sealing joints of the proposed pressure monitoring systems of SRMs in a typical launch vehicle with 24 number of SRMs. The failure modes, effects and causes are studied in detail by analyzing the physics of failure mechanisms through detailed experiments. The testing with noise factors have been found to bring out the design weaknesses so that proper and actions to mitigate

failure modes could be taken. The joints with higher RPN indices have been identified as areas of concern and different options are studied and a design solution has been obtained by replacing two high risk joints with a simple, standard and reliable O-ring joint with redundancy. Improvements have been made in the design, processes, process controls and test procedures to prevent failures. Because of the design and process improvements, the RPN index improved phenomenally from 16000 to 800. Reliability assessment is made to compare the relative merits of the design options and a quantum jump is seen in the reliability of the final design to 0.999 from the earlier 0.916. The study also enabled design controls towards reliability assurance of the system by identifying functionally critical dimensions, re-confirmation of the same for system hardware and introducing detailed quality control checkpoints for the system assembly and acceptance testing. The actions taken helped in the prevention of failures and ensured reliable performance of the joints. The FMA concepts based on the analysis and the reliability assessments are summarised in Sections 7.6.1 to 7.6.3.

7.6.1 Comparison of RPN for the design options

FMEA of design option 1 (original design), along with improvements in design option 2 (modified design) and the resultant improvements in RPN numbers are illustrated in Table 7.6. In the design option 2, the joint J1 (PTFE sealing) and joint J2 (Untested metal to metal contact seal) are replaced by a single reliable O-ring joint. The major improvements made are (i) avoiding the PTFE sealing which is sensitive to noise parameters like operator skill, number of PTFE layers, thickness of the PTFE tape etc.,; and (ii) deletion of untested metal to metal sealing joint which is a design concern. All the metal to metal sealing joints are testable in the new configuration. A highly reliable O-ring joint is the only untested interface. All the design requirements have been complied to the standards, in the selection of O-ring material, its properties and gland design. The design modification has brought down the RPN from 650 to 50.

Hence for a single pressure monitoring system of the main propulsion SRMs, the design risk index has come down from a high value of 650 to a low value of 50, thus highlighting the quantum improvement in design. Pressure monitoring is replaced by strain monitoring for the SRM performance assessment in the case of special purpose motors, thus removing the failure mode of the pressure monitoring joints, bringing down the RPN from 350 (for joint J1) to Nil.

Table 7.6 Summary of RPN values for design option 2 as compared to design option 1

Item/Function	Design option1					Design option 2				
	Failure mechanism	S	O	D	RPN	Actions taken	S	O	D	RPN
J1	Improper winding of PTFE tape Adapter Butting	10	5	7	350	Changed to O-ring interface for main motors. Strain gauge monitoring for special purpose motors. Pressure monitoring is deleted	10	1	3	30
J2	Improper finish, Inadequate Torque	10	4	7	280	Joint is deleted	-	-	-	-
J3	Quality issues in plumbing, welding	10	1	1	10	Testable joint	10	1	1	10
J4	Improper finish, Inadequate torque	10	1	1	10	Testable joint	10	1	1	10
	Total RPN, design option1				650	Total RPN, design option 2				50

Note: In design option 2, joint J1 and joint J2 are combined in a single joint with two shaft seals (O-rings)

7.6.2 Reliability analysis

The improvements in the design are brought out quantitatively, in the previous section, by one order reduction in RPN number. The reliability of the joint is worked out using the failure probability, identified in FMEA tables. This is illustrated in Table 7.7. This brings out quantitatively the improvements in the design and not the inherent reliability of the system.

Table 7.7 Reliability comparison of design options 1 & 2

Joint	Interface joint	Type of seal		Reliability	
		Design option 1	Design option 2	Design option 1	Design option 2
J1	Motor pressure port/adaptor Interface	PTFE tape Sealing	O-ring joint	0.9975 ^a	0.99999 ^c
J2	Adapter to plumbing joint	Metal-to-metal sealing	Deleted	0.9995 ^b	
J3	Plumbing joints	Weld joints	Weld joints
J4	Plumbing to pressure pick up interface	Metal-to-metal sealing	Metal-to-metal sealing
Net Reliability				0.997	0.99999
Notes:					
...No failure expected in tested and cleared joints J3 & J4; reliability R_{J3} and R_{J4} is close to 1					
^a Occurrence rating 5, failure probability 1 in 400, $R_{J1}=0.9975 \{1-(1/400)\}$					
^b Occurrence rating 4, failure probability 1 in 2000, $R_{J2}=0.9995 \{1-(1/2000)\}$					
Reliability of design option1 = $0.9975 \times 0.9995 = 0.997$					
^c Occurrence rating 1, failure probability <1 in 1,50,000, $R_{J1} \& J2=0.99999 \{1-(1/150000)\}$					

Reliability of design option 1

In the design option 1, for the eight main propulsion motors, each having two pressure monitoring, pressure monitoring is done through 16 pressure ports. The reliability of the pressure monitoring per motor joint is 0.997. Hence, the reliability of all 8 main motors will be $0.997^{16} = 0.953$. There are 16 special purpose motors with a pressure monitoring joint with a reliability of 0.9975 and the net reliability for special purpose motors is $0.9975^{16} = 0.961$. Hence the net reliability is the product of Reliabilities of main and special purpose motors which works out to 0.916.

Reliability of design option 2

In the design option 2, Reliability of a pressure monitoring joint in one motor is 0.99999. So, for the eight main propulsion motors with 16 pressure monitoring the reliability is $0.99999^{16} = 0.999$. In the special purpose motors, the joints are avoided by going for strain based performance monitoring wherein there is no critical failure modes related to motor performance. So, the net reliability of the motor pressure monitoring joints in design option 2 is 0.999. Thus, the Reliability of the modified design is 0.999, which is one order higher compared to 0.916 of the original design.

7.6.3 Significance of quality control checks

The experiments carried out to assess the robustness of joints and the FMEA brought out the failure mechanisms and design concerns, thus enabling focused attention for improving the design and avoiding failures. The analysis brings out the requirement to make the design robust enough without relying on the operator skill. It also emphasise the need for making system simple and more reliable by reducing number of joints. The design option 2 is found to work satisfactorily in the presence of variations in control parameters and harsh environments. Thus, it is found to be highly robust as compared to design option 1. An untested PTFE sealing joint and a metal to metal sealing joint are replaced with a highly robust O-ring joint with redundant seal. The analysis also brings out the importance of QC checks during system realisation, assembly and testing. The O-ring quality is inspected and confirmed for geometrical tolerances as per ISO 3601-3 (2008). The quality requirements of O-rings have to be confirmed through a detailed characterization of its physical and mechanical properties. The O-ring and groove dimensions have to be strictly adhered to

specifications as per standards. Dimensions affecting the functionality of the O-ring joint are identified as Functionally Critical Dimensions (FCD) and re-measured by the assembly team on receipt from the manufacturer. The squeeze and gland fill are computed taking into consideration of the stretch of the O-ring and circularity of interfacing diameters. Any line mark or contaminant is not permitted across the O-ring seating area which can form a leak path. The O-ring grooves have to be critically inspected for this aspect before assembly. Strict adherence to the above has to be enforced by detailed process control, quality control, and assembly operation documents with critical check points for FMA. Acceptance test procedures have to be strengthened to test all the flight joints. Thus, the research and analysis on the failure modes and reliability of systems bring out requirements for a robust design without depending on operator skill and also stringent QC checks during various phases of system realisation to avoid failures.

CHAPTER 8

SUMMARY AND FUTURE SCOPE OF WORK

8.1 Summary of thesis

Considering the high complexity of space systems and the harsh launch and space environments, the probability of failure modes that could be due to design, process or workmanship getting into the flight system, and causing a failure is more. The failure modes have to be avoided to make the systems reliable. Accordingly, the failure mode avoidance concepts have been developed, through the research on failure modes of selected space systems, by analysis and experimentation. The space systems analysed have been diverse in nature with different failure modes like a gas motor subsystem of a control system, an angular contact ball bearing, hydraulic plumbing, flexible hoses, umbilical shutter mechanism and solid rocket motor pressure monitoring joint seals

The evolution of space systems happens in a phased manner, and new designs are generally derived from the pedigree systems. Hence, based on the knowledge and experience with operation of similar systems, considerable confidence exists on the new system. An analytical model for the reliability analysis of newly developed space systems with limited data is formulated which transforms this confidence into a quantitative reliability figure. Following are the salient features of the new analytical model:

- The similarity of the new system with the heritage system is assessed against a number of System Reliability Influencing Factors (SRIFs) by assigning a weighting index for each SRIF.
- Tuning parameters are incorporated in the analytical model to account for various uncertainties affecting reliability such as the complexity of the system, and the limitations in the design analysis and verification carried out for the new system.
- The process and rationale of finalizing the SRIFs, weighting index, and the tuning parameters are defined based on technical evaluation of the systems, which removes subjectivity of the assessment.
- The analytical model has been validated using actual test data of the liquid propellant rocket stages of three typical launch vehicles.

- The method results in a more accurate reliability assessment, where as with earlier approaches reliability estimate has been found to be subjective and inaccurate.
- The proposed model provides a general formalised methodology for the reliability analysis. It overcomes the disadvantages of Bayesian approach, used for assessing reliability with limited test data, namely subjective assessment and not accounting the evolution of different systems.
- The model contributes to savings in cost and schedules, by pragmatically assessing the reliability test requirements.

The failure of a double row angular contact ball bearing in a control actuation system (CAS), has been analysed through analysis and experiments. The analysis identified the cause of the failure as overloading of the bearing, due to a combination of factors. Following failure mode avoidance concepts have emerged based on this analysis:

- The design error in wrongly specifying the fillet radius at the shaft shoulder resulted in the interface issue, causing the bearing misalignment. Configuration control of the systems addressing finer design details, particularly at the interfaces is identified as a FMA strategy.
- The manufacturing process error led to high interference at the shaft-bearing interface. The errors in inspection resulted in not addressing the non conformance in the salient features of the geometry. Manufacturing process review, comprehensive process documents with detailed QC checks and stage clearance by quality agencies are identified as tools for FMA.
- The bearing has been assembled with extra force without alerting the high interference. Imparting adequate training to the operation team to identify the faults during the inspection and assembly operations, detailed assembly operation documents with quality control checks ensure flight assembly without any defects.
- Enhancing testability of systems at all phases of integration and system health monitoring till the launch time, can screen defects if any, and ensures the flightworthiness of systems.

Space systems shall have the capability of functioning under harsh environments without human intervention. The severe environmental stress testing carried out on the gas motor subsystem of CAS and SRM pressure monitoring joint seals has given a better understanding of the of failure mechanisms leading to appropriate design

solutions. The typical environment induced failures and the avoidance of these failures through proper qualification are highlighted with satellite and space capsule related failures. A specific case study of an inadvertent opening of an umbilical shutter mechanism during vibration qualification has been analysed. Through a detailed FE analysis and experimentation, the failure mechanism has been identified, and the design is made robust by simple design solution which emerged on the basis of physics of failure.

- The high stress experimentation with noise factors is found to be an effective FMA strategy to ensure a robust design without depending on operator skill. It has brought out the design weakness in the SRM joint seals, and failure mechanisms of the bearing cage and the elastomeric O-ring seal material.
- The requirement of qualification of systems with adequate margin and establishing robustness in design for the initial missions is brought out. The design optimisation could be attempted after measuring the flight environments in the first mission.
- The experimentation also brought out criticalities of the manufacturing and assembly processes, operating parameters, and dimensions, for reliable system performance. The recommended procedures in this regard like re verification of FCDs and CFPs, could be generalised to avoid faults in any flight system.

The fatigue failure of the hydraulic plumbing and the interface joint of a CAS, which is subjected to high pressure and vibration loading, is identified as a critical failure mode and investigated by exhaustive analysis and experimentation.

- The study brings out the importance of detailed experimentation at the highest level of integration to bring out unanticipated failure modes.
- The analysis also reveals how failure modes can get introduced with changes, bringing the requirement of robust review mechanism to assess changes.

The failure of an AISI 304 stainless steel sleeve in the swaged joint of a flexible hose of a CAS has been analysed through a detailed micro structural analysis. The silicate inclusions and the chromium carbide precipitation along grain boundaries have contributed in the propagation the cracks developed during swaging. The material of the sleeve is changed to AISI 304L with lower carbon content, to reduce the chromium carbide precipitation.

The study brings out the importance of documenting and following good design practices and guidelines for material selection and usage for avoiding material related failure modes such as H₂ embrittlement, SCC, fracture, fatigue, and failures due to defects in the materials.

In summary, the research thesis has significantly contributed in the failure mode avoidance and reliability analysis of launch vehicle and satellite systems. The new analytical model has been found to transform the confidence from the operation of similar proven systems to an accurate reliability figure, by systematic technical evaluation of the systems. The failure mode avoidance concepts are evolved and validated through carefully selected case studies, for achieving reliable space missions. The collection of the case specific solutions evolved through the analysis and experimentation forms the basis for a general failure mode avoidance strategy for the space systems.

8.2 Scope for future work

This research thesis addresses the failure mode avoidance and reliability analysis of integrated space systems like solid rocket motors, liquid rocket engines, and propulsion stages. These systems comprise of primarily mechanical systems. Considering this limitation, the scope for future research in the area of space systems reliability is identified as follows:

- Reliability of integrated avionics systems are substantially lesser compared to the design reliability. Considering this, there is scope for following research works in this area:
 - Development of failure mode avoidance concepts for integrated avionics systems
 - Evaluation of fragility limits of avionics subsystems
 - Innovative methods for reliability estimation of avionics systems addressing the limitations of present methods
- Developing failure mode avoidance strategies for the multidisciplinary systems addressing the interactions among the systems
- Developing reliability models to address the uncertainties in the system interfaces in the multi disciplinary systems including the flight software.

APPENDIX A

Computation of weighting factor for L37.5 stage for reliability assessment of L110 stage

Sl. No.	SRIFs	Similarity Class	w_{ij}	ws_j	Rationale for the Weighting index of L110
Engine Design features					
1	Engine combustion cycles	I	1	0.8	Both engines work with same combustion cycle
2	Engine Start/Shut-off transient hazards	I	1	0.8	The shut off transients are similar, with either command cut off or U- depletion
3	Propellant specific hazards; Engine derating / uprating;	I	1	0.8	Same propellant used. All engines operate at same thrust level.
4	Vehicle and Engine Interface & Interface hazards	II	0.8	0.572	Differences related to twin engine configuration
5	Design Method/ Philosophy	II	0.8	0.572	Engine configuration same. Stage engineered with twin engine, Two independent propellant tanks and double ply throat insert.
6	Environment (Temp, Load, Pressure, Vibration, shock, acoustic etc.)	III	0.4	0.051	Vibration & Acoustic levels are higher for L110. Thermal environment will also be higher as heat radiated by one engine will be seen by other engine in L110.
7	Modelling/Analysis Method	I	1	0.8	Analysis procedure followed is same.
8	Design Margins	I	1	0.8	Minimum margin of safety for structures, flexible hoses, plumbing and engine subsystems are same.
9	Total No. components and subsystems	II	0.8	0.572	Number of feed lines, gas bottles and interface joints are marginally higher.
10	Burn duration	III	0.4	0.051	Engine burn duration is substantially higher at 200 s as compared to 150 s of L37.5 and 160 s of L40

Sl. No.	SRIFs	Similarity Class	w_{ij}	ws_j	Rationale for the Weighting index
11	Overall Dimensional similarity of critical components	III	0.4	0.051	Changes due to stage systems being different and twin engine configuration
Materials and Manufacturing					
12	Materials used	I	1	0.8	Identical
13	Material Property Evaluation Method/Approach	I	1	0.8	Identical
14	Manufacturing Method used	II	0.8	0.572	Minor difference
Quality Aspects					
15	Extent of QA coverage	I	1	0.8	Identical
16	Extent of QC coverage	I	1	0.8	Identical
17	No. of qualification tests conducted	III	0.4	0.051	Lesser
18	Matching of qualification test results with analytical prediction	I	1	0.8	Identical
19	NC management approach	I	1	0.8	Identical
20	No. of major NCs	I	1	0.8	Similar
Sum of values of criticality parameters ($\sum c_j$)		Sum of Weighting Score ($\sum ws_j$)		Weighting factor $wf = (\sum ws_j) / (\sum c_j)$	
20		12.095		0.605	

Note: $c_j=1$, $k_{1j}=0.8$, $k_{2j}=1.2$ and ws_j computed for each SRIF using Equation (3.5)

APPENDIX B

Computation of weighting factor for L40 stage for reliability assessment of L110 stage

Sl. No.	SRIFs	Similarity Class	w_i	ws_j	Rationale for the Weighting index
Engine Design features					
1	Engine combustion cycles	I	1	0.8	Both engines work with same combustion cycle
2	Engine Start/Shut-off transient hazards	I	1	0.8	The shut off transients are similar, with either command cut off or U- depletion
3	Propellant specific hazards; and Engine derating / uprating;	I	1	0.8	Same propellant used. Both engines operate at same thrust level.
4	Vehicle and Engine Interface & Interface hazards	II	0.8	0.572	Differences related to twin engine configuration
5	Design Method/ Philosophy	II	0.8	0.572	Overall engine configuration is same. Stage engineered with twin engine configuration, and double ply throat insert. Design methodology same.
6	Environment (Temp, Load, Pressure, Vibration, shock, acoustic etc.)	I	1	0.8	Environments are likely to be of the same order, as both experience similar lift off environments.
7	Modelling/ Analysis Method	I	1	0.8	Analysis procedure followed is same.
8	Margin of safety	I	1	0.8	Minimum margin of safety for structures, pressure ratings, flexible hoses, plumbing are and other engine subsystems are same.
9	Total No. of subsystems	II	0.8	0.572	No. of components are marginally higher.
10	Burn duration	III	0.4	0.051	Engine burn duration is 200 secs as compared to 160 secs of L40.

Sl. No.	SRIFs	Similarity Class	w_{ij}	ws_j	Rationale for the Weighting index
11	Overall Dimensional similarity of critical components	III	0.4	0.051	Changes due to stage systems being different and twin engine configuration
Materials and Manufacturing					
12	Materials used	I	1	0.8	Identical
13	Material Property Evaluation Method/Approach	I	1	0.8	Identical
14	Manufacturing Method used	II	0.8	0.572	Minor difference
Quality Aspects					
15	Extent of QA coverage	I	1	0.8	Identical
16	Extent of QC coverage	I	1	0.8	Identical
17	No. of qualification tests conducted	I	1	0.8	Comparable
18	Matching of qualification test results with analytical prediction	I	1	0.8	Identical
19	NC management approach	I	1	0.8	Identical
20	No. of major NCs	I	1	0.8	Similar
Sum of values of criticality parameters ($\sum c_j$)		Sum of Weighting Score ($\sum ws_j$)		Weighting factor wf = ($\sum ws_j$) / ($\sum c_j$)	
20		13.592		0.68	

Note: $c_j=1$, $k_{1j}=0.8$, $k_{2j}=1.2$ and ws_j computed for each SRIF using Equation (3.5)

APPENDIX C

Computation of weighting factor for L37.5 for reliability assessment of L40 stage

Sl. No.	SRIFs	Similarity Class	w_{ij}	ws_j	Rationale for the Weighting index
Engine Design features					
1	Engine combustion cycles	I	1	0.8	Both engines work with same combustion cycle
2	Engine Start/Shut-off transients.	I	1	0.8	The transients are similar, command cut off or U- depletion
3	Propellant specific hazards; and Engine derating	I	1	0.8	Same propellant used. Both engines operate at same thrust level.
4	Vehicle and Engine Interface & Interface hazards	II	0.8	0.572	Differences related to stage configuration and separate propellant tanks in place of common bulk head type propellant tank.
5	Design Method/ Philosophy	II	0.8	0.572	Stage engineered with separate propellant tanks for fuel and oxidiser. Design methodology same.
6	Environment (Temp, Load, Pressure, Vibration, shock, acoustic etc.)	III	0.4	0.051	Vibration & Acoustic levels are expected to be higher for L40. Thermal environment also higher due to heat radiated by the firing of core stage and strapon boosters.
7	Modelling/ Analysis method	I	1	0.8	Analysis procedure followed is same.
8	Margin of safety	I	1	0.8	Similar
9	Total No. of components	II	0.8	0.572	Marginally higher
10	Burn duration	III	0.4	0.051	Engine burn duration marginally higher at 160 secs in L40 as compared to 150 secs of PS2.

Sl. No.	SRIFs	Similarity Class	w_{ij}	ws_j	Rationale for the Weighting index
11	Dimensional similarity	III	0.4	0.051	Changes due to stage systems being different
Materials and Manufacturing					
12	Materials used	I	1	0.8	Identical
13	Material Property Evaluation Method/Approach	I	1	0.8	Identical
14	Manufacturing Method used	I	1	0.8	Similar
Quality Aspects					
15	Extent of QA coverage	I	1	0.8	Identical
16	Extent of QC coverage	I	1	0.8	Identical
17	No. of qualification tests conducted	I	1	0.8	Identical
18	Validation of analytical model by experiments	I	1	0.8	Identical
19	NC management approach	I	1	0.8	Identical
20	No. of major NCs	I	1	0.8	Similar
Sum of values of criticality parameters ($\sum c_j$)		Sum of Weighting Score ($\sum ws_j$)		Weighting factor $wf = (\sum ws_j) / (\sum c_j)$	
20		13.071		0.654	

Note: $c_j=1$, $k_{1j}=0.8$, $k_{2j}=1.2$ and ws_j computed for each SRIF using Equation (3.5)

APPENDIX D

Rationale for ratings for RPN

Sl. No.	Rating	Severity of effect	Occurrence Probability	Detection feasibility
1	1	No effect	<1 in 150,000	Almost certain
2	2	Very Minor	1 in 150,000	Very high
3	3	Minor	1 in 15,000	High
4	4	Very low	1 in 2000	Moderately high
5	5	Low	1 in 400	Moderate
6	6	Moderate	1 in 80	Low
7	7	High	1 in 20	Very low
8	8	Very high	1 in 8	Remote
9	9	Serious	1 in 3	Very remote
10	10	Hazardous	>1 in 2	Uncertain

APPENDIX E

Functionally critical dimensions and parameters

Sl. No.	Functionally Critical Dimension and Parameters
1. O-Ring Adapter Gland dimensions	
1.1	O-ring groove diameter
1.1	Adapter outer diameter (Plug diameter)
1.2	Width of the groove
1.3	Entry corner radius
1.4	Groove bottom corner radius
1.5	Surface finish of Groove and mating face
2	Motor pressure port
2.1	Pressure port ID
3	O-ring
3.1	O-ring Inner Diameter
3.2	O-ring cross section
4.	Critical Parameters
4.1	Diametric clearance
4.2	Depth of the groove
4.3	Stretch of the O-ring (0-5%)
4.4	Squeeze of O-ring (15-30%)
4.5	Fill of the O-ring (65-90%)

REFERENCES

1. **Abhay, K. Jha, M. Swathi Kiranmayee, and Sushant K. Manwatkar** (2013). Metallurgical investigation of cracked stainless steel plumbing tubes used in engine gimbal control system of launch vehicle. *Engineering Failure Analysis*, **25**, 225-231.
2. **Ahsan Qamar, Mathew Meinhart, and George Wallay** (2017) Model based systems engineering to support failure mode avoidance for driver-assistance systems. *Aerospace Conference*, IEEE, Big Sky, MT, USA, March, 1-9.
3. **Ake Lonnqvist, and Ida Gremyr** (2008) A note on failure mode avoidance. *11th Quality Management and Organisational Development Conference*, Attaining sustainability from organisational excellence to sustainable excellence, Helsingbore, Sweden, August, 109-116.
4. **AMS-5639H** (2017) *Aerospace Material Specification*. SAE Aerospace.
5. **AMS-5647H** (2017) *Aerospace Material Specification*. SAE Aerospace.
6. **Andrews, J.** (2009) System reliability modelling: The current capability and potential future developments. *Proceedings of the Institution of Mechanical Engineers, Journal of Mechanical Engineering Science*, **223 (C)**, 2881-2895.
7. **Anthony Sofranas** *Case histories in vibration analysis and Metal fatigue for the practicing engineer*. John Wiley & Sons, Hoboken NJ, 2012, 77-98.
8. **Antoinne Fissolo** (2015) Investigations on the cumulative fatigue life for a type 304-L stainless steel used for pressure water reactor. *International Journal of Fatigue*, **77**, 199-215.
9. **Arpan Das, S. Sivaprasad, M. Ghosh, P.C. Chakraborti, and S. Tarafder** (2008) Morphologies and characteristics of deformation induced martensite during tensile deformation of 304 LN stainless steel. *Materials Science and Engineering A*, 283-286.
10. **Ben Evans** *Space Shuttle Challenger: Ten journeys into the unknown*. Praxis Publishing Ltd, Chichester, UK, 2007, 241-272.
11. **Bernard, R.W.A.** (2003) The future of reliability engineering. *International Council on Systems Engineering*. South Africa.

12. **Bernard, R.W.A.** (2004) Reliability engineering: futility and error. *Conference of International Council on Systems Engineering (INCOSE)*, South Africa, August, 1-7.
13. **Bin Wu** *Reliability analysis of dynamic systems: efficient probabilistic methods and aerospace applications*. Elsevier, Waltham, USA, 2013, 1-41.
14. **Bodekar Dan A III., and Foster A. Windred Jr.** (1998) *Structural stiffness characteristics of the Solid Rocket Booster field joint*. NASA/CR-1999-208192, NASA Marshall Space Flight Center, Huntsville, AL United State, 1-13.
15. **Brian D. Allan** (2001) Historical reliability of U.S launch vehicles. *AIAA2001-3874, 37th AIAA/ASME/SAE/ASEE Joint Propulsion Conference and Exhibit*, Salt Lake City, Utah, 1-7.
16. **Bugra H. Ertas, and Hohn M.Vance** (2014) Effect of static and dynamic misalignment on ball bearing radial stiffness. *Journal of Propulsion and Power*, **20(4)**, 234.
17. **Carlson, C. S.** *Case studies, in effective FMEAs: achieving safe, reliable, and economical products and processes using failure mode and effects analysis*. John Wiley & Sons, Hoboken, NJ, 2012, 1-19.
18. **Chen Hongxia, Chen Yunxia, and Yang Zhou** (2014) Coupling damage and reliability model of low-cycle fatigue and high energy impact based on the local stress-strain approach. *Chinese journal of Aeronautics*, 846-855.
19. **Clarence W. de Silva** *Vibration damping, control and design*. CRC Press, Taylor & Francis group, 2007, 1.9–1.31.
20. **Daniele Regazzoni, and Davide Russo** (2011) Triz tools to enhance risk management. *Procedia Engineering*, **9**, 40-51.
21. **Dave S. Steinberg** *Vibration analysis for electronic equipment*. Third edition, John Wiley & sons, 2010, 188-216.
22. **DeArdo, A. J. Jr., and E.G. Hamburg** *Influence of elongated inclusions on the mechanical properties of high strength steel plate*. Sulphide inclusions in steel, ASM, 1975, 309-337.
23. **Dennis Moore, and Willie J. Phelps** (2011) Reusable solid rocket motor-accomplishments, lessons, and a culture success. *AIAA SPACE 2011 Conference and Exposition*, Long Beach, CA, United States, September, 1-22.

24. **Don Clausing**, and **Daniel D. Frey** (2005) Improving system reliability by failure mode avoidance including four concept design strategies. *Systems Engineering*, **8(3)**, 245-261.
25. **Du Zhong-lei**, and **Liao Ri-dong** (2016) Fatigue life prediction and optimization of pipeline under random loads. *International Conference on Mechanics, Materials and Structural Engineering*, Atlantis press, 407-413.
26. **Dussenberry, G.**, and **D. Carlson** (1986) Development of a hot gas vane motor for aircraft starting systems. *Aerospace Technology Conference and Exposition, California*, October, 13-16, 31-38.
27. **Ed Henshalla**, **Felician Campeana**, and **Brian Rutterb** (2017). A systems approach to the development of enhanced learning for engineering systems design analysis. *Procedia CIRP*, **60**, 130-135.
28. **Elisabeth L.M.**, **Joseph R. Fragola**, and **Blake Putney** (2010) Modeling launch vehicle reliability growth as defect elimination. *AIAA Space 2010 Conference & Exposition*, Anaheim, California, August.
29. **Fatemi, A.**, and **L. Yangt** (1998) Cumulative fatigue damage and life prediction theories: a survey of the state of the art for homogeneous materials. *International Journal of Fatigue*, **20(I)**, 9-34.
30. **Federal Aviation Administration** (2005a), *Guide to Reusable Launch and Re-entry Vehicle Reliability Analysis*. Version 1.0, FAA, Washington, 12-20.
31. **Federal Aviation Administration** (2005b), *Guide to probability of failure analysis for new expendable launch vehicles*. Version 1.0, FAA commercial space transportation, 1-11.
32. **Feiyun Cong**, **Jin Chen**, **Guangming Dong**, and **Michael Pecht** (2013) Vibration model of rolling element bearings in a rotor-bearing system for fault diagnosis, *Journal of Sound and Vibration*, **332 (8)**, 2081-2097.
33. **Fox, B.L.** (1966) *A Bayesian approach to reliability assessment*. Memorandum RM-5084- NASA, The Rand Corporation, Santa Monica, California, 1-23.
34. **Frank Corl**, **Phong Do**, and **V. Iyengar** (2014) Reliability products for space launch vehicle safety assessments. *Annual Reliability and Maintainability Symposium (RAMS)*, IEEE, Colorado Springs, CO, USA, 1-4.
35. **Franz Josef Ebert** (2010) Fundamentals of design and technology of rolling element bearings. *Chinese Journal of Aeronautics* **23**, 123-136.

36. **Gaspare Maggio, and Dennis G Pelaccio** (2000) Factors and metrics in establishing reliability goals for next generation launch vehicle liquid propulsion systems. *36th AIAA/ASME/SAE/ASEE joint propulsion conference and Exhibit AIAA 2000-3452*, July.
37. **George P. Sutton, and Oscar Biblarz** *Rocket propulsion elements*. 8th edition, John Wiley & Sons, 2010, 335-350.
38. **Goodland, J., I.F. Campean, A. Counce, J.L. Victory, and M.L. Jupp** (2013) A manufacturing failure mode avoidance for aerospace manufacturing. *Proceedings of the ASME 2013 International Mechanical Engineering Congress and Exposition*, November, 1-9.
39. **Gordon W. Powell** (1986) *Identification of failures*. ASM Hand Book Committee, Failure Analysis and Prevention, Metals Hand book, Vol. 11, Ninth edition, 1986, 490-513.
40. **GSFC-STD-7000** (2015) *Environmental verification standard (GEVS) for GSFC flight programs and projects*. NASA Goddard Space Flight centre, 2.2-1 to 2.2-6.
41. **Gurumoorthy, K., Bradley D. Faye, and Arindham Ghosh** (2013) Handling abuse causes premature bearing failures. *Case studies in Engineering Failure Analysis*, **1**, 235-242.
42. **Hamlin, T.L., Eric Thigpen, Joseph Kahn, and Yunnhon Lo** (2013) Shuttle risk progression: use of the shuttle probabilistic risk assessment (PRA) to show reliability growth. *International Journal of Performability Engineering*, **9(6)**, 633-640.
43. **Hanson John, M. Hill, Ashley D. Beard, and B. Bernard** (2013) *launch vehicle abort analysis for failures leading to loss of control*. Report No. M12-1484, Document ID: 20130001801, available from the NASA server at <https://ntrs.nasa.gov/archive/nasa/casi.ntrs.nasa.gov/20130001801.pdf>.
44. **Herbert J. Sutherland, and John. F Mandell** (2005) Optimised Goodman diagram for the analysis of fibreglass composites used in wind tunnel turbine blades, *43rd AIAA Aerospace Sciences meeting and Exhibit*, Reno, Nevada, January, 1-10.
45. **Hobbs, G.K.** *Accelerated Reliability Engineering: HALT and HASS*. John Wiley & Sons, England, 2000.

46. **Houghton, P.S.** *Ball and roller bearings*. Applied Science Publishers, London, 1976, 1-19.
47. **Howard E. Boyer** (1975) *Failure analysis and prevention*. Metals Hand Book, Vol.10, eighth edition, American Society for Metals, Metals Park Ohio, 1-5, 416-437.
48. **Huairui Guo, Sharon Honecker, Adamantios Mettas, and Doug Ogden** (2010) Reliability estimation for one-shot devices with zero component test failures. *Reliability and Maintainability Symposium (RAMS), 2010 Proceedings*, IEEE, San Jose, CA, USA, 2010.
49. **Hugo Buchter, H.** *Industrial Sealing technology*. John Wiley & sons, 1979, 87-101.
50. **Hui Lv., Yuanying Qiu, and Ying Sheng** (2011) Fatigue analysis of the aircraft's hydraulic pipes based on fluid-structure interaction. *Advanced Materials Research*, **299**, 917-920.
51. **IEEE-STD-1413.1-2002** (2002) *Guide for selecting and using reliability predictions based on IEEE1413*. Institute of Electrical and Electronics Engineers, New York, USA, 1-90.
52. **ISO 3601-1-2002(E)** (2002) *Fluid power systems, O-rings, Part 1: inside diameters, cross sections, tolerances and size identification code*. International organization for standardization, 1.1 to 9.1.
53. **ISO 3601-2-2008 (E)** (2008) *Fluid power systems, O-rings, Part 2: housing dimensions for general applications*. International organization for standardization.
54. **ISO 3601-3-2005 (E)** (2005) *Fluid power systems, O-rings, Part 3: quality acceptance criteria*. International organization for standardization, 2005, 1-11.
55. **James Ekstrom, and Allen Allred** (1991) Verifying reliability of solid rocket motors at minimum cost. *Proceedings of Annual Reliability and Maintainability Symposium*, January, 502-508.
56. **Jaya Balakrishnan, Swapna Surendran, M.N. Nampoodiripad, and Thomas Kurien** (2010) Failure detection schemes in control actuation systems for launch vehicles. *International Journal of Automation and Control*, **4(3)**, 284-297.
57. **Jeap Schijve** *Fatigue of structures and materials*. Springer, Second Edition, 2009.

58. **Jiahao Zheng**, and **Jianming Yang** (2016) Random fatigue analysis of drill-pipe threaded connection. *Int. J. Materials and Structural Integrity*, **10**, 34-51.
59. **John Buzzato** (2015) Independent assessment across the launch vehicle-satellite interface. *AIAA SPACE 2015 Conference and Exposition*, Pasadena, California, August, 1-9.
60. **John W. Miles** (1954) On structural fatigue under random loading. *Journal of the Aeronautical Sciences*, 753-753.
61. **John P. Bentley** Reliability and quality engineering. John Wiley & Sons, Inc, 1993, 31-37.
62. **John G. Elerath**, and **Michael Pecht** (2012) A standard for reliability predictions. *IEEE transactions on reliability*, **61(1)**, 125-129.
63. **Jose Emmanuel**, **Ramirez Marquez**, and **Wei Jiang** (2006) On improved confidence bounds for system reliability. *IEEE transactions on reliability*, **55(1)**, 26-31.
64. **Joseph R. Davis** *Metals Handbook*. Desk edition, ASM International, 1998.
65. **Kain, V.**, **K. Chandra**, **K.N. Adhe**, and **P.K. De** (2004) Effect of cold work on low temperature sensitization behavior of austenitic stainless steels. *Journal of Nuclear Materials*, **334**, 115-132.
66. **Kapur, K.C.**, and **L.R. Lamberson** *Reliability engineering in design*. John Wiley & Sons, New York, 1977.
67. **Keiji Mizuta**, **Takayoshi Inoue**, **Yasuro Takahashi**, **Shuwei Huang**, **Kouji Ueda**, and **Hidefumi Omokawa** (2003) Heat transfer characteristics between inner and outer rings of an angular ball bearing. *Heat Transfer—Asian Research*, **32(1)**, 2003, pp. 42-57.
68. **Kenan Bozkaya.**, **Metin Akkok** and **Alp Esin** (2009) Reliability improvement of a solid rocket motor in early design phases. *Journal of Spacecrafts and Rockets*, **46(4)**, 914-922.
69. **Kozasu, I.**, and **J. Tanaka** *Effects of sulphide inclusions on notch toughness and ductility of structural steels*. Sulphide inclusions in steel, ASM, 1975, 286-308.
70. **Kutz, M.** *Handbook of Materials selection*, John Wiley & Sons, New York, 2002.

71. **Lee H.M.** (1993) *A simplistic look at limit stresses from random loading*. NASA Technical Memorandum – 108427, George C. Marshall Space Flight Centre, October, 1-19.
72. **Levin, M.A., and T.T. Kalal** *Improving product reliability, strategies and implementation*. John Wiley & Sons, England, 2002.
73. **Lisa A. Bloomer** (2004) *Reliability assessment of conceptual launch vehicles*. NASA fellowship program, 1- 5.
74. **Marco Dourado, and Delfim Sioares** (2014) A comparative study of fatigue behavior of MAG and laser welded components using reliability analysis. *Material Science Engineering*, 31-39.
75. **Marshall Space Flight Center** Practice no. PD-ED-1252 *Material selection practices*. NASA preferred reliability practices, 1-5.
76. **Marshall Space Flight Center** Practice no. PD-ED-1257 *Solid rocket motor joint reliability*. NASA preferred reliability practices, 1-5.
77. **Matthias Hell, Rainer Wagener, and Heinz Kaufmann** (2015) Fatigue life design of components under variable amplitude loading with respect to cyclic material behaviour. *Procedia Engineering*, **101**, 194-202.
78. **Michael Stamatelatos, and Homayoon Dezfuli** (2011) *Probabilistic risk assessment procedures*. Guide for NASA Managers and Practitioners, NASA/SP-2011-3421.
79. **Michael G. Lutomski, and Joel Garza** (2011) Estimating the reliability of a crewed spacecraft. Proceedings of the *5th IAASS conference 'A Safer Space for a Safer World'*, Versailles, France, October, 1-7.
80. **Michael, S.H., G. Alyson, C. Wilson, Shane Reese, and Harry F. Martz** *Bayesian reliability*. Springer, New York, 2008.
81. **MIL-HDBK-217 F** (1998) *Reliability prediction of electronic equipment*. Military Handbook, Department of Defence, USA.
82. **MIL HDBK 338 B** (1998) *Electronic reliability design handbook..* Military Handbook, Department of Defence, USA, 2.1-3.20.
83. **MIL-PRF-81322 F** (1998) *Performance specification: grease, aircraft, general purpose, wide temperature range*. Naval Air Warfare Center, Aircraft Division, Lakehurst, NJ.

84. **MIL-STD-202 G** (2002) *Method 214 A, Random vibration, test method for standard electronic and electrical component parts*. Department of Defense test method standard, USA, 1-4.
85. **MIL-STD-810 G** (2008) *Method 527, Multi exciter testing, Environmental Engineering Considerations and Laboratory test*. Department of Defense test method standard, USA, 527-13.
86. **Mohammad Modarres, Mark Kaminskiy, and Vasily Krivtsov** Reliability engineering and risk analysis. CRC Press, 2010.
87. **Mohammed Gharouni, S., Hamid M. Panahiha, and Jafar Eskandari Jam** (2014) Space shuttle SRM field joint. *Metallurgical and Materials Engineering*, **20(3)**, 155-164.
88. **Moss, T.R., and J.D. Andrews** (1996) Reliability assessment of mechanical systems. Proceedings of *Institution of Mechanical Engineers, Part E*, **210**, 205-216.
89. **Nanjundaswamy, T.S., and R.K. Rajangam** (2008) Reliability and quality assurance of space missions-Indian scenario. Proceedings of *TRISMAC 2008*, ESA-ESTEC, Noordwijk, The Netherlands, April, 1-4.
90. **NASA SP 8044** (1970) *Qualification testing*. NASA Space Vehicle Design Criteria, National Aeronautics and Space Administration, 1-11.
91. **NASA SP-8119** (1976) *Liquid rocket disconnects, couplings, fittings, fixed joints and seals*. National Aeronautics and Space Administration, Washington, DC, United States.
92. **NASA-HDBK-7005** (2001) *Dynamic environmental criteria*. NASA Technical Handbook, National Aeronautics and Space Administration, 194-195.
93. **NASA-SP-8048** (1971) *Liquid rocket engine turbo pump bearings*. NASA Space Vehicle Design Criteria, NASA Lewis Research Center; Cleveland, OH, United States.
94. **Ningcong Xiao, Hong Zhong Huang, Yanfeng Li, and Tongdan Jin** (2011) Multiple failure mode analysis and weighted risk priority evaluation in FMEA. *Engineering Failure Analysis*, **18**, 1162-1170.
95. **NPRD-1995** (1995) *Nonelectronic parts reliability data*. Reliability Analysis Centre, Rome Laboratory, Griffis AFB, New York.

96. **NSWC-2010** (2010) *Hand book of reliability prediction procedures for mechanical equipment*. Logistics Technology Support, Naval Surface Warfare Center, West Bethesda, Maryland.
97. **ORD-5700** (2017) *Parker O-ring handbook*. Parker Hannifin Corporation, Cleveland, 1.1 to 9.1.
98. **Otmar E. Teichmann** (1966) *Analysis and design of Air motors*. Hydraulic and Pneumatic Power and Control. McGraw-Hill Book Company, 1966, 256-260.
99. **Patrick D. T. O' Conner** (1995) Quantifying uncertainty in reliability and safety studies. *Microelectronics and Reliability*, **35(9-10)**, 1347 – 1356.
100. **Patrick D. T. O' Conner** (2000) Commentary: reliability-past, present and future. *IEEE Transactions on Reliability*, **49(4)**, 335-340
101. **Patrick D. T. O' Connor**, and **Andre Kleyner** *Practical reliability engineering*. Fifth edition. John Wiley & sons limited, UK, 2012, 363 to 365
102. **Paul. D. Wilde. Elisabeth Morse, Paul Rosati, and Corey Cather** (2013) Probability of failure analysis standards and guidelines for ELVs. *Sixth IAASS conference*, May 2013.
103. **Pereira, H. F. S. G., A. M. P. Jesus, A. S. Ribeiro, and A. A. Fernandes** (2009) Fatigue damage behaviour of structural components under variable amplitude loading. *Mecânica Experimental*, **17**, 75-85.
104. **Przemyslaw Strzelecki, and Tomasz Tomaszewski** (2017) Analytical models of the S-N curve based on the hardness of the material. *Procedia, Structural Integrity*, **5**, 832-839.
105. **Raghuvir Singh, B. Ravikumar, A. Kumar, P.K. Dey, and I. Chattoraj** (2003) The effects of cold working on sensitization and intergranular corrosion behavior of AISI 304 stainless steel. *Metallurgical and Materials Transactions*, **34(A)**, 2441 – 2447.
106. **Richard P. Feynmann** (1986) *Personal observations on the reliability of the Shuttle*. Appendix F, Report of the presidential commission on the Space Shuttle Challenger Accident, 1986.
107. **Richard G. Budynas, and J. Keith Nisbett** (2011) *Shigley's Mechanical engineering design*. Ninth edition, McGraw Hill Education (India) Private Limited, 273-316.

108. **Risitano, A., D. Corallo, and G. Risitano** (2012) Cumulative damage by Miner's rule and by energetic analysis. *Structural Durability and Health Monitoring, Tech Science Press*, **8(2)**, 91-109.
109. **Roger Rivett, Ibrahim Habli, and Tim Kelly** (2015) Automotive functional safety and robustness - never the twain or hand in glove?, *CARS Workshop - Critical Automotive Applications: Robustness & Safety*, Paris, France, September, 1-4.
110. **Roland Kiessling** *Non-metallic inclusions in steel*. Second edition, The Metals Society, 1977.
111. **Ron S. Li** (2001) A methodology for fatigue prediction of electronic components under random vibration load. *Transactions of the ASME*, **123**, 394-400.
112. **Ronald L. Widener** *Failures of rolling element bearings*. ASM Hand Book Committee, Failure Analysis and Prevention, Metals Hand book, Vol. 11, Ninth edition, 1986, 490-513.
113. **Rosa Lynn Pinkus, B., Larry J. Shuman, Norman P. Hummon, and Harvey Wolfe** *Engineering ethics, balancing cost, schedule, and risk- lessons learned from the space shuttle*. Cambridge University Press, 1997, 341-344.
114. **Saeed Kiad, Mohammad Pourgol Mohammad, and Hossein Salimi** (2016) Probabilistic reliability evaluation of space system considering physics of fatigue failure. *Accelerated stress testing and reliability conference (ASTR)*, IEEE, Pensacola Beach, Florida, 1-8.
115. **Samira Abbasgholizadeh Rahimi, Afshin Jamshidi, Daoud Ait Kadi, and Angel Ruiz** (2015) Using fuzzy cost-based FMEA, GRA, and profitability theory for minimizing failures at a healthcare diagnosis service. *Quality and Reliability Engineering International*, **31(4)**, 601-615.
116. **Saxena, A., T. Davis, and J.A. Jones** (2015) A failure mode avoidance approach to reliability. *Reliability and Maintainability Symposium*, Palm Harbor, January, 1-6.
117. **Sergio Guarro** (2015) On the estimation of space launch vehicle reliability. *International Journal of Performability Engineering*, **9(6)**, 619-631.
118. **Seth D. Guikema, and Elisabeth Pate-Cornell** (2004) Bayesian Analysis of launch vehicle success rates. *Journal of Spacecrafts and Rockets*, **41(1)**, 93-102.

119. **Shih Chang, I.** (1996) Investigation of space launch vehicle catastrophic failures. *Journal of Spacecraft and Rockets*. **33(2)**, 198-205.
120. **Smith, W.F.** (1993) *Structure and properties of engineering alloys*. Second edition, McGraw Hill Inc, New York, 1993, 313-322.
121. **Sojourner, T.S., D. E. Richardson, B. D. Allen, K. S. McHenry, and B. E. Goldberg** (2015) Solid rocket booster reliability and historical failure modes review. *51st AIAA/SAE/ASEE Joint Propulsion Conference*, Orlando, FL, 1-17.
122. **Steven S. Lee** (2001) *Reliability Drivers for advanced space vehicles*. AE8900 Special Project Report, Space Systems Design Laboratory, Georgia Institute of Technology, 20001, 1-26.
123. **Suresh. B.N., and K. Sivan** *Integrated design for Space Transportation*. Springer, New York, 2015.
124. **Sushant, K. M., S.K. Kailas, S.V.S. Narayana Murty, and P. Ramesh Narayanan** (2015), Metallurgical analysis of failed AISI 304L stainless steel tubes used in launch vehicle applications. *Metallographic and Micro Structural Analysis*, **4(6)**, 497-505.
125. **Susie Go, Scott L. Lawrence, Donovan L. Mathias, Moffett Field, and Ryann Powell** (2017) *Mission success of US launch vehicle flights from a propulsion stage-based perspective*. NASA Report, NASA/TM-2017-219497. 1-73.
126. **Tapan, P. Bagchi** *Taguchi methods explained, practical steps to robust design*. Prentice Hall of India Private Limited, New Delhi, 1993, 14-17.
127. **Tedric A. Harris, and Michael N. Kotzalas** *Advanced concepts of bearing technology, Fifth edition*. CRC press, Taylor & Francis, Boca Raton, 2007a.
128. **Tedric A. Harris, and Michael N. Kotzalas** *Essential concepts of bearing technology, Fifth edition*, CRC press, Taylor & Francis, Boca Raton, 2007b.
129. **Thomas A. Ward** *Aerospace propulsion systems*. John Wiley & Sons (Asia) Pte Ltd, 141-142, 2010.
130. **Tiiu V. Kutt, and M.P. Bieniek** (1988) Cumulative damage and fatigue life prediction. *American Institute of Aeronautics and Astronautics Journal*, **26(2)**, 213-219.
131. **Turkdogan, E.T.** *Theoretical aspects of sulphide formation in steel*. Sulphide inclusions in steel, ASM, 1975, 1-22.

132. **Upadhyay. R.K., L.A. Kumaraswamidas, and Md. SikandarAzam** (2013) Rolling element bearing failure analysis. *Case Studies in Engineering Failure Analysis*, 15-17.
133. **Videira, E., C. Lebreton, S.D. Lewis, and L. Gaillard** (2013) Design, assembly and preloading of ball bearings for space applications - Lessons learned and guidelines for future success. *15th European Space Mechanisms and Tribology Symposium-ESMATS*, Noordwijk, Netherlands, September.
134. **Vincent R. Lalli** (1994) Design for reliability; NASA preferred practices for design and test. NASA TM 106313, *Reliability and Maintainability Symposium*, California, January, 1-24.
135. **Vintr, M.** (2007) Reliability assessment for components of complex mechanisms and machines. *12th IFToMM World Congress*, Besançon, France, June.
136. **Walter Schutz** (1979) The prediction of fatigue life in crack initiation and propagation stages, A state of the art survey. *Engineering Fracture Mechanics*, **11**(2), 405-421.
137. **Westphal, T., and R.P.L. Nijssen** (2014), Fatigue life prediction of rotor blade composites, validation of constant amplitude formulations with variable amplitude experiments. *Journal of Physics Conference series*, **555**, 1-11.
138. **Wiley J. Larson, and James R. Wertz** *Space mission analysis and design*. Third Edition, Microcosm Press, California and Kluwer Academic Publishers, Netherlands, 2005, 1-7.
139. **William R. Wessels** *Practical reliability engineering and analysis for system design and life-cycle sustainment*. CRC press, Boca Raton, 2010, 235-293.
140. **Xiaofan He, Fucheng Sui, Bin Zhai and Wenting Liu** (2013). Probabilistic and testing analysis for the variability of load spectrum damage in a fleet. *Engineering Failure Analysis*, **33**, 419-429, 2013.
141. **Xiaoyan Su, Yong Deng, Sankaran Mahadevan, and Qilian Bao** (2012) An improved method for risk evaluation in failure modes and effects analysis of Aircraft engine rotor blades. *Engineering Failure Analysis*, **26**, 164-174.
142. **Yang, J.N., and W.J. Trapp** (1974) Reliability analysis of aircraft structures under random loading and periodic inspection. *American Institute of Aeronautics and Astronautics Journal*, **12**(12), 1623-1630.

143. **Yung-Li Lee, Sandeep Makam, and Sean McKelveya Ming-Wei Lu** (2015) Durability reliability demonstration test methods. *Procedia Engineering*, **133**, 31 – 59.
144. **Zhaofeng Huang, Jerry A. Fint, and Frederick M. Kuck** (2005) Key Reliability drivers of Liquid Propulsion engines and a Reliability model for sensitivity analysis. *41st AIAA/ASME/SAE/ASEE joint propulsion conference and Exhibit*, AIAA2005-4436, July, 1-12.
145. **Zhaogfeng Huang** (2014) Design for reliability considerations and modeling for Liquid Propulsion engines starting from conceptual design. *50th AIAA/ASME/SAE/ASEE Joint Propulsion Conference*, AIAA-2014-3879, July, 1-10.
146. **Zhaogfeng Huang** (2015) False positive and false negative analysis for enhancing liquid propulsion system reliability and safety. *51st AIAA/ASME/SAE/ASEE Joint Propulsion Conference*, AIAA-2015-4064, July, 1-8.
147. **Zheng Ling, Wei Jinbo., and Chen Yuanyuan** (2016) Noise control of a payload fairing through layout of acoustic blanket. *23rd International Congress on Sound and Vibration*, ICSV 23, Athens, Greece, 1-8.

LIST OF PAPERS BASED ON THESIS

I. Standard refereed journals

1. **Murugesan, V., P.S. Sreejith, A.K. Anilkumar, and V. Kishorenath** (2017) Failure mode avoidance of solid rocket motor pressure monitoring joint Seals. *Journal of Failure Analysis and Prevention*, Springer, **17(6)**, 1191-1201.

DOI: <https://doi.org/10.1007/s11668-017-0356-6>.
2. **Murugesan, V., P.S. Sreejith, Sushant K. Manwatkar, S. Sankar Narayan, S. V. S. Narayana Murty, and P. Ramesh Narayanan** (2017) Failure analysis of AISI 304 stainless steel sleeve used in high-pressure hose assembly of actuation system of a satellite launch vehicle. *Journal of Failure Analysis and Prevention*, Springer, **17(2)**, 178-188,

DOI: <https://doi.org/10.1007/s11668-016-0232-9>.
3. **Murugesan, V., P.S. Sreejith, P. B. Sundaresan, and V. Ramasubramanian** (2018) Analysis of an angular contact ball bearing failure and strategies for failure prevention. *Journal of Failure Analysis and Prevention*, Springer, **18 (3)**, 471-485.

DOI: <https://doi.org/10.1007/s11668-018-0441-5>.
4. **Murugesan, V., P.S. Sreejith, M. Gopakumar, P. Damodaran, and M. Premdas** (2018) Failure analysis of a launch vehicle umbilical shutter mechanism during vibration qualification. *Journal of Failure Analysis and Prevention*, **18 (3)**, 457-464.

DOI: <https://doi.org/10.1007/s11668-018-0442-4>.
5. **Murugesan, V., P.S. Sreejith, Shashi Bhushan Tiwari, and K. Kumar** (2018) Fatigue life cycle estimation and reliability analysis of hydraulic plumbing of a launch vehicle control actuator. *International Journal of Materials and Structural Integrity*, Inderscience (Accepted).

6. **Murugesan, V., P.S. Sreejith, V.J. Saji, and S.S. Maruthi** (2018) A new analytical model for reliability analysis of a launch vehicle system with limited test data. *Proceedings of the Institution of Mechanical Engineers, Part G: Journal of Aerospace Engineering*. (Submitted on 08-06-2018, under review).
7. **Murugesan, V., P.S. Sreejith, V.Sajiv, A.K. Anilkumar** Strategies for failure prevention in a gas motor of a launch vehicle control actuation system. Submitted to *International Journal of Quality Engineering and Technology*, Inderscience (Submitted on 09-09-2017, under review.).

II. Presentation to international conferences

1. **Murugesan, V., P.S. Sreejith, V. Sajiv, A.K. Anilkumar.** Failure mode avoidance through high stress testing – case study with gas motor of electro hydraulic actuator. *International Reliability Symposium ARS -2016*, Bangalore, August 2016.
2. **Murugesan, V., P.S. Sreejith, Immanuel Inbaraj, P. Renish, M. Sunoj.** Qualification and certification of thermal protection systems for re-entry missions. *ICETIME international conference*, CUSAT, Kochi, December 2015.

CURRICULAM VITAE

1. **Name** : MURUGESAN V.

2. **Date of Birth** : 20-02-1962

3. **Educational qualifications**

1984 Bachelor of Technology (B.Tech)

Institute : NSS college of Engineering, Calicut University

Specialisation : Mechanical Engineering

1990 Master of Technology (M.Tech)

Institute : Indian Institute of Technology, Madras, Chennai

Specialisation : Manufacturing Engineering

Ph.D Registered on 17-10-2014

Institute : Cochin University of Science and Technology, Kochi.

4. **Work experience and awards**

November 1984 to April 1985 : Teaching Assistant

Institute : Regional Engineering College, Calicut

April 1985 to till date : Scientist/Engineer

Institute : Vikram Sarabhai Space Centre, ISRO, Trivandrum

Nature of job : Quality Assurance of launch vehicle mechanical systems and environmental testing.

Recipient of three ISRO team excellence awards in recognition of the contributions to the successful accomplishment of

- (i) Space capsule Recovery Experiment Mission (2006)
- (ii) Chandrayaan-1 Spacecraft including Moon Impact Probe (2008)
- (iii) GSLV Mk-III Mock- up vehicle and Integration Simulation at Launch Complex (2011)